INVESTIGATION OF CODING AND EQUALIZATION FOR THE DIGITAL HDTV TERRESTRIAL BROADCAST CHANNEL

by

JULIEN J. NICOLAS

Diplôme d'Ingénieur, Ecole Centrale de Paris, France (1981)
S.M., Massachusetts Institute of Technology (1982)

Submitted to the
Department of Electrical Engineering and Computer Science
in Partial Fulfillment of the Requirements for the degree of

Doctor of Science

at the
MASSACHUSETTS INSTITUTE OF TECHNOLOGY

September 1994

Author _____
Department of Electrical Engineering and Computer Science
September 1, 1994

Certified by _____
Jae S. Lim
Professor of Electrical Engineering
Thesis Supervisor

Accepted by _____
Frederic R. Morgenthaler
Chairman, Committee on Graduate Students

INVESTIGATION OF CODING AND EQUALIZATION FOR THE DIGITAL HDTV TERRESTRIAL BROADCAST CHANNEL

by

JULIEN J. NICOLAS

Submitted to the Department of Electrical Engineering and Computer Science
on September 1, 1994, in partial fulfillment of the
requirements for the degree of
Doctor of Science

Abstract

Bandwidth and power constraints, as well as compatibility considerations, limit the amount of information that can be conveyed over the high definition television (HDTV) terrestrial broadcast channel. As a consequence, elaborate source and channel coding techniques must be employed in order to use the limited channel resources efficiently.

This thesis explores several ways of improving the performance of digital HDTV transmission systems: by increasing the efficiency of single-rate schemes; by providing multiple rates to different receivers; and, by combining equalization and coding.

The thesis first examines several single-rate coded modulation schemes appropriate for HDTV. It is shown that the concatenation of powerful inner trellis codes and outer block codes provides a good performance-complexity tradeoff.

The thesis then examines methods for providing a multiplicity of data rates and signal-to-noise ratios, thus making a better use of the inherent variable capacity of the broadcast channel. Among the several possible coding schemes examined, multiresolution coded modulation schemes seem particularly appealing. A practical multilevel coded scheme is proposed which is capable of achieving a variety of rates and performances, at about the same complexity as single-resolution schemes.

The compensation of multipath and NTSC co-channel interference, a major cause of performance degradation for HDTV, is then investigated. Current schemes have addressed this problem in ways that compromise the performance and the efficiency of the transmission system. Here, receiver structures which do not compromise the bandwidth and power gains achievable on more ideal channels are proposed. In particular, a scheme combining interference rejection and coded modulation is put forward. The scheme is based on a reduced-state sequence estimation (RSSE) approach.

Finally, the topic of equalization and coding is investigated further, in the context of multicarrier modulation. Analysis and simulations are carried out to ascertain whether multicarrier modulation could advantageously replace the single carrier schemes currently proposed in the US for terrestrial broadcasting. It is shown that, from a theoretical standpoint, multicarrier modulation is not superior to single carrier modulation for combatting static multipath but that it may be a good solution for dynamic multipath impairments.

Thesis Supervisor: Jae S. Lim
Title: Professor of Electrical Engineering

Acknowledgments

I would like to express my thanks to Professor Jae Lim who has supported this research and guided the development of the subject matter. I am also indebted to Dr. David Forney, whose thought-provoking discussions and knowledgeable review of the material, has benefited this thesis greatly; to Dr. Vedat Eyuboğlu for a number of discussions on coding and equalization; and to Professor Staelin for his thorough review of this work.

There are also a number of people who helped in the development of this thesis who I would like to thank: Professor William Schreiber for his interest in the topic and global perspective on the issues; Tony Uyttendaele of ABC/Capital Cities, for his interest in multicarrier modulation; Norman Parker of Motorola for an early discussion on NTSC and HDTV broadcast; Dr. Woo Paik and Scott Levy from General Instrument for discussions on the DigiCipher HDTV system; and finally Dr. Josko Catipovic of WHOI for his support and interest in low-bit-rate video coding.

Thanks also to my friends and colleagues in the laboratory for Advanced Television Research. And thanks to the Consortium for Advanced Television Studies whose generous support of our laboratory has enabled our group to be on the cutting edge of television research.

Finally, special thanks to my wife Breda for reasons too numerous to list here (and USAir who kept us together).

Contents

1 Introduction 15

1.1 Digital communications 15

1.2 Digital terrestrial television broadcasting 18

1.3 Goals and motivation of the dissertation 19

1.4 Dissertation organization 20

1.5 Summary of contributions 21

2 Overview of digital terrestrial television broadcasting 23

2.1 Introduction 23

2.2 General features of video coding for broadcast HDTV 24

2.2.1 Signal capture 25

2.2.2 Data reduction 26

2.2.3 Data compaction 28

2.2.4 Encoder for video processing 28

2.3 The HDTV broadcast channel 29

2.3.1 Policy constraints 30

2.3.2 Interference mechanisms 31

2.3.3 Medium and receiver limitations 33

2.3.4 Implications for the HDTV service 35

2.4 Transmission systems for HDTV 35

2.4.1 Major functions 35

2.4.2 High-level block diagram 36

2.4.3 Error control 38

2.4.4 Modulation and pulse shaping 39

2.4.5 Equalization 41

2.4.6 Synchronization 46

2.4.7 High-power amplification 49

2.5 Conclusion 50

3 Modeling channel distortion **51**

3.1 Introduction 51

3.2 Bandwidth constraint 51

3.3 Multipath impairments 52

3.4 Fading impairments 55

3.4.1 Coherence bandwidth 55

3.4.2 Coherence time 56

3.4.3 Receiver performance 56

3.5 Interference impairments 57

3.5.1 NTSC co-channel interference 57

3.5.2 NTSC signal format 58

3.5.3 Luminance signal models 61

3.6 Conclusion 66

4 Channel coding for the HDTV Gaussian channel **67**

4.1 Introduction 67

4.2 Channel capacity and normalized SNR 68

4.2.1 The bandlimited Gaussian channel 68

4.2.2 Channel capacity 69

4.2.3 Normalized signal-to-noise ratio 71

4.3 Combined modulation and coding 73

4.3.1 Trellis-coded modulation 75

4.3.2 Signal-space codes 79

4.3.3 Performance of selected trellis codes 83

4.4 Concatenated coded modulation 99

4.5 Conclusion 110

5 Multi-rate channel coding for the HDTV broadcast channel **111**

5.1 Introduction 111

5.2 The memoryless Gaussian broadcast channel 114

5.2.1 Maximin approach 114

5.2.2 Multiplexing approach 115

5.2.3 Superposition approach 116

5.3 Simple embedded constellations 117
5.4 Unequal error protection coding 124
5.4.1 Coded modulation with time-multiplexing 127
5.4.2 Coded modulation with unequal constellations 128
5.4.3 A practical coding scheme for a 3-resolution system 130
5.5 Conclusion 131

6 Equalization and interference rejection with uncoded modulation 134
6.1 Introduction 134
6.1.1 Notations and definitions 135
6.2 General performance bounds 137
6.2.1 System model 137
6.2.2 Matched filter (MF) front end 138
6.2.3 Performance bounds: the MFB and the MLSE 140
6.3 Linear equalization: ZF and MSE 143
6.3.1 Zero-forcing linear equalizer 144
6.3.2 Mean-square error linear equalizer 146
6.4 Decision-feedback equalization: ZF and MSE 148
6.4.1 DFE-ZF 148
6.4.2 DFE-MSE 150
6.4.3 Tomlinson-Harashima precoding 152
6.5 Application to the NTSC co-channel interference problem 155
6.5.1 Previous NTSC interference reduction methods 155
6.5.2 New receiver structures 158
6.5.3 Performance evaluation 160
6.5.4 Improved interference rejection approach 190
6.5.5 Joint multipath and interference reduction 191
6.6 Conclusion 193

7 Equalization and interference rejection with coded modulation 194
7.1 Introduction 194
7.2 Conventional approach 196
7.3 Decision-feedback equalization with coded modulation 199
7.3.1 Decision-feedback equalization with a decoding delay 201

7.4 Interference rejection scheme with improved performance 204
7.4.1 Reduced-state sequence estimation 204
7.4.2 New interference rejection scheme with improved performance 206
7.5 Conclusion 208

8 Equalization and multicarrier modulation **211**
8.1 Introduction 211
8.2 Overview of MCM 212
8.2.1 MCM for the Gaussian channel 212
8.2.2 MCM for the broadcast channel 214
8.3 General principles of MCM 215
8.4 Performance of MCM in the presence of multipath 218
8.4.1 Guard interval 218
8.4.2 Discrete-time models for the HDTV channel 219
8.4.3 Performance analysis 220
8.4.4 Simulation results 222
8.5 Comparison with single-carrier modulation 226
8.6 Conclusion 226

9 Conclusion **228**

A NTSC planning factors **230**
A.1 NTSC service contours 230
A.2 NTSC receiver SNR 232
A.3 NTSC channel separations 232

B Symbol, bit and block error rate calculations **234**

C Estimating the probability of error by the Monte Carlo method **238**

List of Figures

2-1 High-level view of a video encoder. 25
2-2 Video encoder using motion-compensated prediction. 29
2-3 High-level view of a transmission system. 36
2-4 Block diagram of a generic HDTV transmission system. 37
2-5 Raised cosine pulse 40
2-6 Folded spectrum for Nyquist channel. 42
2-7 Baseband linear equalizer for QAM. 42
2-8 Decision-feedback equalizer. 43
2-9 Discrete-time linear equalizer. 45
2-10 Joint carrier recovery and equalization. 48
2-11 Simplified timing recovery loop. 48
2-12 Transfer functions of an envelope nonlinearity. 50

3-1 Discrete multipath model. 53
3-2 NTSC co-channel interference from spatially adjacent transmitter. 57
3-3 NTSC composite video signal. 58
3-4 Idealized spectrum of transmitted NTSC signal. 59
3-5 Amplitude spectrum of a typical NTSC program. 61
3-6 Spectrum of a raster-scanned video signal. 62
3-7 Spectrum of luminance signal near DC (simulation). 63
3-8 Two-dimensional prediction. 64
3-9 Normalized ACF for NTSC interference model. 66

4-1 The bandlimited Gaussian channel model. 68
4-2 Determination of the capacity-achieving spectrum. 70
4-3 Discrete-time bandlimited Gaussian channel. 70
4-4 Universal performance curve for QAM. 73
4-5 Channel capacity of bandlimited Gaussian channels. 75

4-6 Block diagram of an Ungerboeck encoder/modulator for trellis-coded modulation. 76
4-7 Set partitioning of a 32QAM constellation. 77
4-8 8-state code and trellis for 32QAM. 78
4-9 Encoder for a signal space code. 80
4-10 Lattice $\Lambda = \mathbb{Z}^2 + (1/2, 1/2)$ and its sublattices. 82
4-11 Performance of 8 and 64-state 2-dimensional Ungerboeck trellis codes. 85
4-12 Performance of 4D 16-state Wei code. 86
4-13 Code performance versus normalized SNR. 87
4-14 Constellation mappings. 90
4-15 Detail of the 32QAM constellation mapping. 91
4-16 Performance based on union bound. 97
4-17 Union bound performance for 32QAM 8 states. 98
4-18 Union bound performance for 32QAM 64 states. 98
4-19 Concatenated coding using trellis coding. 100
4-20 P_{bit} versus P_{in} for t-error-correcting RS code $(256, 256 - 2t)$ over GF(2^8). 102
4-21 Performance of concatenated scheme based on inner 4-state 32QAM trellis. . . . 105
4-22 SNR_{norm} vs. code rate for concatenated scheme with 4-state 32QAM trellis code. 105
4-23 Concatenated code performance as a function of 16QAM inner code states. . . . 107
4-24 SNR_{norm} vs. code rate for concatenated scheme with 16QAM trellis code 107
4-25 Concatenated code performance as a function of 32QAM inner code states. . . . 108
4-26 SNR_{norm} vs. code rate for concatenated scheme with 32QAM trellis code 108
4-27 Concatenated code performance as a function of 8PAM inner code states. 109
4-28 SNR_{norm} vs. code rate for concatenated scheme with 8PAM trellis code 109

5-1 Television broadcast channel. 111
5-2 Broadcast channel. 114
5-3 Minimax and multiplexing achievable rates 115
5-4 Achievable rates for the Gaussian broadcast channel. 116
5-5 Superposition coding in the two-receiver case. 117
5-6 Embedded QAM constellations. 118
5-7 Information rate for non-uniform 16QAM constellation. 119
5-8 Achievable transmission rates for two-resolution system. 121
5-9 Required SNR for non-uniform constellations. 122
5-10 Non-uniform 64QAM constellation. 123

5-11 Performance of non-uniform 64QAM constellation (1). 125
5-12 Performance of non-uniform 64QAM constellation (2). 126
5-13 Encoder for trellis-coded time-multiplexing. 127
5-14 Coded modulation and non-uniform constellations. 128
5-15 Multilevel coding and non-uniform constellations. 131
5-16 Performance of coded non-uniform 64QAM constellation. 132

6-1 System model. 138
6-2 White noise channel model. 138
6-3 Nonwhite noise channel model. 139
6-4 Sampled matched filter. 139
6-5 Whitened matched filter. 139
6-6 Discrete-time model with WMF receiver 140
6-7 MLSE applied to the output of the WMF. 142
6-8 Discrete-time channel with linear equalizer. 143
6-9 Equivalent discrete-time LE-ZF. 144
6-10 Generalized LE-ZF. 145
6-11 Linear equalizer with MSE criterion. 147
6-12 Zero-forcing decision-feedback equalization. 148
6-13 Generalized zero-forcing DFE 149
6-14 Generalized MSE DFE. 151
6-15 Tomlinson-Harashima precoding. 152
6-16 Equivalent transmitter precoder for M-PAM signaling. 153
6-17 TH precoding signal sets for 8-PAM modulation. 154
6-18 Modified TH precoding for 8-PAM modulation. 154
6-19 Modified TH precoding signal sets for 8-PAM modulation. 155
6-20 Precoding/comb filtering method. 156
6-21 Interference rejection with narrowband filters. 157
6-22 Co-Channel interference rejection. 159
6-23 Discrete-time NTSC interference model. 161
6-24 Performance of 16QAM with LE and DFE (1). 165
6-25 Performance of 16QAM with LE and DFE (2). 165
6-26 LE-MSE tap settings vs. SIR for first order interference model. 166
6-27 DFE-MSE tap settings vs. SIR for first order interference model. 167

6-28 Performance of 16QAM with LE and DFE (3). 171
6-29 Performance of 16QAM with LE and DFE (4). 171
6-30 LE-MSE tap settings vs. SIR for third-order interference model. 172
6-31 DFE-MSE tap settings vs. SIR for third-order interference model. 173
6-32 SNR gain for finite-length LE-MSE. 176
6-33 SNR gain vs. number of taps for finite-length LE-MSE. 176
6-34 Noise-predictive DFE. 178
6-35 SNR gain for finite-length DFE-MSE. 180
6-36 Performance of reduced-complexity interference rejection scheme (1). 183
6-37 Performance of reduced-complexity interference rejection scheme (2). 183
6-38 Performance of reduced-complexity LE. 184
6-39 Performance of reduced-complexity DFE. 184
6-40 Co-channel interference rejection (1). 186
6-41 Co-channel interference rejection (2). 186
6-42 Co-channel interference rejection (3). 189
6-43 Interference rejection based on RSSE. 192
6-44 Reduced-state sequence estimation. 192

7-1 LE-MSE based interference rejection with coding. 197
7-2 Performance of combined linear filtering and trellis coding approach. 198
7-3 Noise predictive DFE with decoding delay and coding. 200
7-4 Noise predictive DFE with decoding delay and convolutional interleaving. 200
7-5 DFE-based interference rejection with decoding delay. 201
7-6 Performance of interference rejection scheme with decoding delay. 203
7-7 RSSE-based interference rejection. 207
7-8 Performance of interference rejection scheme (1). 209
7-9 Performance of interference rejection scheme (2). 210

8-1 MCM signal synthesis. 216
8-2 Example of power spectral density of MCM signal. 216
8-3 Demodulation of an MCM signal. 217
8-4 Discrete-time multicarrier transmission. 217
8-5 Equivalent discrete-time channel model. 219
8-6 Simulation results for uncoded MCM over static multipath channel. 224

8-7 Simulation results for uncoded MCM over dynamic multipath channel. 224
8-8 Simulation results for coded MCM over static multipath channel. 225
8-9 Simulation results for coded MCM over dynamic multipath channel. 225

A-1 NTSC field strength as a function of distance. 231

C-1 Generic system model. 239
C-2 Confidence intervals for Monte Carlo simulations. 240

1

Introduction

1.1 Digital communications

Perhaps Shannon's most important and surprising contributions to the theory of communications were to establish that the probability of error over a communication channel could be made arbitrarily small so long as the information rate was smaller than a fundamental quantity known as the channel capacity, and to recognize that the task of transferring information between points could be partitioned into two separate processes - the process of finding a good representation for the source with the minimum number of units of information or "nats" possible, and the process of transmitting this representation in the most reliable and efficient manner. The first process is known in information theory as the source coding problem; the second, as the channel coding problem.

The power of the principle of separation of source coding and channel coding lies in its generality and abstraction. This says that, regardless of whether the signals or channels are analog or digital, one can always define a bit stream as the interface between the source of information and the transmission system. Of course, it is only natural to use digital communication techniques to transmit digitally-originated data (e.g. computer data). It is somewhat more surprising to realize that nothing need be lost by sampling and digitizing an analog source, for example a continuous time signal such as a video, image or voice signal, and transmitting the digital data using digital transmission techniques, provided both the task of forming a representation of the source and the task of transmitting the information are performed in an optimal fashion. By this, we mean that the transmission system is able to operate at its ultimate transmission rate, known in information theory as the channel capacity, and the source coder is able to represent the signal by the available data rate in some optimal way. If this is not the case, penalties such as increased bandwidth and power may be incurred, which may make a digital implementation less attractive than an analog one.

In the real world, many channels are fundamentally analog in nature, in that they transmit waveforms rather than bits, and digital data must be modulated onto waveforms in order to be transmitted. This is true of wire pair or coaxial cable channels, composite voiceband telephone channels, and radio frequency channels - satellite, point to point, mobile radio, "over-the-air" broadcast television, etc. In many cases, the source provides the information in analog form, and the destination ultimately requires analog data, for example for display. Why then use digital communications to transmit the information? It may, indeed, seem counter-productive to convert between analog and digital formats repeatedly along the data path since these operations are not simple, may be costly and may not be required. The answer however is simple: there is no guarantee that in an analog system, in the absence of some sophisticated and costly analog processing, the waveforms produced by the source will be matched in any way to the characteristics of the transmission channel.

One obvious advantage of the digital approach is that it is possible to carefully tailor the transmitted waveforms to the characteristics of the channel. There is much flexibility in designing such waveforms for digital communications. Redundancy can be included in the data stream or in the signal stream in order to make the data more tolerant of the channel imperfections, and to detect, correct or prevent errors so that the reliable flow of information through the channel is ensured. It is possible to perform operations such as time, frequency and code division multiplexing with great flexibility, and at a much lower cost than with analog systems.

A number of other benefits ensue from the ability to carefully control the waveforms used to convey information. For instance, techniques such as decision-directed carrier recovery and decision-feedback equalization make it possible to, at least partially, remove impairments due to linear distortions and noise. Such techniques cannot be used in analog communications, since there are no fixed references against which the received signal can be compared. Ghost canceling techniques in analog television, for instance, must rely on the presence of a test signal (ghost canceling reference or GCR) to estimate the channel characteristics and can suffer from severe noise enhancement problems in the case of strong multipath signals. Digital signals are more effective at mitigating these impairments.

In general, analog transmission schemes such as those used in practice for the transmission of voice over analog lines, and radio and television over cable and terrestrial broadcast channels, make only relatively superficial changes to the signal in order to get it through the channel. In many cases, there is a simple relationship between the source signal and the modulated waveform that is transmitted over the channel. While this may seem an advantage, it is in fact a drawback because it limits the type of processing that can be applied to the source signal, and this implies that channel imperfections will affect the source in some more or less direct fashion.

A case to point is the National Television Systems Committee (NTSC) transmission standard. Here channel impairments may translate into a wide variety of source impairments which may include: decreased signal-to-noise ratios; perceptible echoes or ghosts on a television display tube; third-order intermodulation products caused by transmitter or receiver nonlinearities, resulting in shadow images; cross-color distortion caused by linear channel distortions; luminance-chrominance distortions caused by imperfect separation between the luminance and chrominance spectra; and many others.

Digital communication systems, on the other hand, are able to abstract the source signal from the channel impairments. It is argued that digital transmission eliminates ghosts and channel noise in television broadcast, and this is true. In a digital system, impairments such as noise, multipath, nonlinearities and other channel distortions do not affect the source directly, but rather the interface, namely the data stream. Because the interface is digital, the number of problems that these impairments may cause is limited. Problems such as increased error rates and increased decoding delays may result from transmission impairments, and these may indeed require that the data rate be reduced. It is easier, however, to design a source coding scheme tolerant of a limited number of defects than to design a system which must take into account all aspects of the source and channel coding problems together. Error concealment techniques are an example of how to deal with uncorrectable errors.

In the early days of communication theory, it was thought that analog communications were more conservative of bandwidth than their digital counterparts, but this argument is rapidly losing its legitimacy. The tradeoffs between bandwidth and power, and between error rate and signal to noise ratio are now well understood, and very efficient multilevel/multiphase coded modulation techniques have been developed that now approach channel capacity within a few decibels.

A disadvantage of digital systems sometimes mentioned is that of quantization noise. Quantization noise, however, is completely under the control of the designer of the source coding scheme, and will be the only important source of noise in the signal received by the user. Digital source coding techniques have now improved to such an extent, that it is no longer possible to argue that channel noise is preferable to quantization noise. In a well designed source and channel coding system, the quantization noise is far smaller than the channel noise it replaces, and is bound to decrease still further as the psychophysical effects of this noise on the ultimate target (e.g. the viewer, the listener) are better understood.

An important side effect of the absence of channel noise in the received signal is the ability to regenerate the data stream almost perfectly even after a large number of passages through the channel. Consider for example, a post-production video processing application where multiple storage and retrieval operations are required before obtaining the final product. In

the absence of channel errors, the final material would be identical to the original. In the more realistic situation where there is a small probability of error at each storage and retrieval operation, m storage and retrieval operations would result in m times the probability of error of a single operation. This is in stark contrast to analog storage and retrieval, where noise is amplified at each stage of the process.

1.2 Digital terrestrial television broadcasting

There is now a steady and global trend towards conversion to digital source coding and digital channel coding. For example, the well known integrated service digital network (ISDN) concept proposes to upgrade most of the existing analog communication system into universal digital information channels. Data, voice, text and images would be transferred along copper wires, satellite, fiber and microwave links. Even more ambitious plans have been recently proposed for the development of a National Information Infrastructure (NII). Digital high-definition television (HDTV) for terrestrial, cable, fiber and satellite broadcast as well as for multimedia and telecommunications applications is part of this global evolution. Earlier efforts in Japan (MUSE) and in Europe (HD-MAC) to develop HDTV systems based on a mix of analog and digital technology have largely succeeded but there is a realization that a totally digital television environment is now possible, and that it would present many advantages over a mixed environment.

Digital terrestrial broadcast HDTV is presently acting as the catalyst for the transition to an all digital high-definition television environment. In the United States, jurisdiction over terrestrial broadcasting is exercised by the Federal Communications Commission (FCC). A special committee, the FCC Advisory Committee on Advanced Television Systems (ACATS) is in the process of examining different HDTV systems for possible adoption as the United States standard for the digital terrestrial broadcast of HDTV. In the US as elsewhere, there is a general shortage of RF spectrum and there is increasing pressure to free more spectrum for non-broadcast use. Decisions were made early on in the FCC process to maintain the existing frequency spectrum for both the current NTSC service and the upcoming HDTV service and this requires that the new HDTV service be capable of being transmitted via the same 6 MHz terrestrial RF channels as the existing analog NTSC service. Furthermore, in the interest of protecting the enormous existing NTSC customer base during a transition period from NTSC to HDTV, it was deemed necessary to maintain service to existing NTSC receivers for at least a number of years.

In order to offer a wide-screen high definition television service, state-of-the-art source coding techniques require 15-20 Mb/s, for roughly twice the horizontal and vertical resolution of the current NTSC standard. The problem of designing a transmission system for a high

definition television system is therefore both multifaceted and highly constrained and was deemed by many at first to be a technical impossibility. The major constraints are: minimal impact on current NTSC coverage areas; robustness to NTSC interference, particularly co-channel interference; immunity to multipath propagation; low transmitter power relative to NTSC; fixed bandwidth of 6 MHz; efficient use of the radio spectrum; and, transmission in the so-called taboo channels because no additional radio spectrum will be allocated for the new service. These constraints will require that the new systems be able to operate at significantly reduced co-channel spacings, with powers 10-15 dB below the current NTSC transmitters.

1.3 Goals and motivation of the dissertation

During the last several years, understanding of the requirements for high-definition television broadcasting has greatly progressed and a significant number of milestones have been achieved. There remains, however, particularly in the area of digital transmission, a number of important issues that still have not received satisfactory answers, and a number of problems that still have not been clearly posed.

The goal of this thesis is to attempt to clearly identify and discuss the most pressing of these unresolved issues. Three areas have been identified as particularly important: efficient use of channel capacity; combined equalization and coding; and, performance of multicarrier modulation transmission in HDTV applications.

The thesis first discusses the issue of using the inherently variable broadcast channel capacity more efficiently than is now the case. While there is a large body of literature on practical ways of achieving some form of variable transmission rate [26, 77, 88, 91], there appears to be little critical discussion of the theoretical justification for such approaches. In this thesis, we will provide some additional insights into the advantages and disadvantages of multiple-rate transmission systems.

The thesis then discusses the issue of equalization and interference reduction. Some of the concepts presented here have been treated in different areas [17, 28, 32, 35, 67, 76, 85]. However, we are unaware of any prior discussion that directly addresses the terrestrial broadcast situation. In this dissertation, we examine various schemes to reduce the impact of multipath and co-channel interference on broadcast channels. As will later become clear, these are the major sources of linear distortions in digital television terrestrial broadcasting.

Finally, the thesis examines multicarrier modulation in the context of broadcast HDTV. This transmission technique, which was originally developed for digital audio broadcasting as a means of delivering a low data rate to mobile receivers in a reliable and robust fashion, has generated considerable debate as to its applicability to the transmission of high data rate

television signals [2, 8, 21, 53, 60, 92]. Multicarrier modulation has been touted as the means to achieve higher spectral efficiency through the use of Single Frequency Networks (SFN). This concept, initially proposed for low-rate transmission to mobile receivers, consists of providing service by using a collection of low-power transmitters rather than single, centralized, high-power transmitters. We attempt to discuss and clarify these issues and provide a comparison with the single carrier transmission schemes currently proposed for digital HDTV transmission.

1.4 Dissertation organization

Chapter 2 is an overview of digital HDTV, both from the source coding aspect and from the channel coding aspect. Most of the emphasis of this chapter is on the channel coding problem. It lays the foundations for further discussion of this problem in the main body of the thesis.

In Chapter 3, models for the HDTV channel are proposed. The goal of this chapter is to clearly define the characteristics of the terrestrial broadcast channel, in order to allow for more rigorous discussion in the following chapters.

Chapter 4 discusses various concepts that are of particular importance in designing a transmission system for HDTV. In particular, issues relating to spectrum efficiency are emphasized. Different coded modulation schemes are evaluated by computer simulation and analysis. The use of concatenated coded modulation schemes is investigated. New results concerning the optimization of concatenated coded modulation are presented.

Chapter 5 looks at the problem of coding as it relates to the variable capacity of the broadcast channel. Several techniques are reviewed and a practical technique based on multilevel coding is proposed.

Chapters 6 and 7 describe specific techniques for combatting intersymbol interference and co-channel interference, without and with coded modulation respectively. An improvement is proposed on existing methods, using a practical and cost-effective way of combining the benefits of high coding efficiency and good interference rejection. The performance of this method is compared with a variety of other methods proposed in the context of the present HDTV competition.

Chapter 8 describes the general principles of multicarrier modulation and examines a specific issue: the performance of multicarrier modulation in a multipath, co-channel interference limited environment. Comparisons between single carrier and multicarrier modulation are provided.

Chapter 9 presents conclusions and outlines directions for future research.

1.5 Summary of contributions

The following contributions have been made in this thesis:

- A unified presentation of modulation and coding for the broadcast channel is provided. Several candidate coded modulation schemes for HDTV broadcasting are compared and evaluated by simulation as well as by analytical means. The precise weight distribution of a number of trellis codes is computed and is used to explain some of the observed code characteristics. An investigation of concatenated coded modulation is carried out, where it is shown that performance improvements can be achieved by using sufficiently powerful inner codes, a conclusion that runs contrary to the current practice in digital HDTV.

- An analysis of the performance of non-uniform constellations has been carried out, to assess the efficiency of multiresolution signaling schemes. While such schemes have been proposed by many as a means of achieving the goal of graceful degradation as a function of distance from the transmitter, little work appears to have been done on a precise characterization of the tradeoffs. Simulations have been carried out to quantify the performance of unequal error protection schemes. The results suggest that the main benefit of superposition for broadcasting purposes may be for the case when one wants to add a low-power high-rate signal to the basic signal. The thesis also examines the case where multiresolution modulation is used in conjunction with coding. It is demonstrated that coding can be integrated into a multiresolution system to achieve higher coding efficiency. A practical multilevel coded scheme is proposed which is capable of achieving a variety of rates and performances, at about the same complexity as single-resolution schemes.

- Rather than propose ad hoc methods for reducing the effects of multipath and interference, we have chosen to rigorously derive estimates of the performance of different receiver structures. We have clearly demonstrated the relationship between equalization and interference rejection for HDTV. We have shown that decision-feedback equalization (DFE) is in general far superior to linear equalization (LE) for interference rejection. We have found that these structures can be simplified by taking advantage of the known characteristics of the interference. Furthermore, we have proposed an improved interference rejection scheme based on a reduced-state sequence estimation (RSSE) approach. A gain of close to 2 dB at an error rate of 10^{-6} was demonstrated by simulation.

- A problem exists when one wants to combine equalization with power efficient coding techniques. This problem has been addressed and specific receiver structures have been

proposed. In particular, two schemes combining trellis coded modulation and equalization have been suggested. The first uses a DFE with delayed decisions to partially cancel the co-channel interference. The second uses DFE in combination with RSSE to achieve improved performance. Simulations have been carried out to evaluate these schemes. The advantages and drawbacks, both theoretical and practical, of the different receiver structures have been discussed.

- The all-important topic of equalization and coding has been investigated further, in the context of multicarrier modulation. Analysis and simulations were used to ascertain whether multicarrier modulation could advantageously replace the single carrier schemes currently proposed in the US for terrestrial broadcasting. The performance of multicarrier modulation under assumptions similar to those used for single carrier modulation has been formulated and contrasted with the performance of single carrier modulation. In particular, the performance of multicarrier modulation in the presence of static and dynamic multipath has been obtained. It was shown that, from a theoretical standpoint, multicarrier modulation is not superior to single carrier modulation for combatting static multipath but that it may be a good solution for dynamic multipath impairments.

2

Overview of digital terrestrial television broadcasting

2.1 Introduction

When a color television broadcasting standard was approved by the FCC in 1953, it could not have been foreseen that it would survive well into the last decade of this century. The success beyond expectations of the NTSC color television standard in America and Japan, and of the PAL and SECAM systems in Europe, Asia and elsewhere in the ensuing years since 1953 has been the engine of a powerful consumer electronics industry and has enabled the development of new technologies such as videotape and disk recording for the consumer market. Yet, in a curious twist, it is this very success that is making the transition to more sophisticated television systems more problematic. One contributing factor for broadcasters has been the desire to retain the very large existing customer base. Another has been the fact that broadcasters have made large capital investments in current television systems and are not particularly eager to make even larger investments in a technology that, until recently, was perceived as somewhat risky.

Yet there are many factors that make higher definition television systems desirable and in some cases even necessary for the consumer. Steady improvements in large direct-view screens and projection systems have resulted in a greater perception of fine detail by viewers and a demand for an increase in resolution. As well, as screen areas increase, there is a need to increase the width of the screens, in order to provide a greater sense of proportion similar

to that of present-day motion picture theater presentations. There are also new specialized demands for imaging systems with higher temporal or spatial resolutions in fields such as medicine, computer graphics, publishing and archiving, which are driving the search for a higher resolution product.

Because of this consumer demand, there have been intense efforts since the mid-1980s to develop advanced television systems for distribution over a variety of media, including terrestrial broadcast channels, telecommunication networks, and satellite channels. There is also an increasing effort to integrate a variety of services such as voice, data, and video through a single distribution medium called BISDN (broadband integrated services digital network).

Terrestrial broadcast HDTV is, in many ways, acting as the catalyst for a transition to an all-digital high definition television environment. Proposals for digital high definition television broadcast are being examined by the FCC Advisory Committee on Advanced Television Systems (ACATS). These proposals have generally evolved to such an extent that they now share broadly similar characteristics, both in terms of source coding and in terms of channel coding.

In the next sections, we review the key features of HDTV for terrestrial broadcasting with a view to define the constraints of the problem and to outline current achievements. A clear understanding of the constraints of the problem will result in the determination of better overall solutions.

2.2 General features of video coding for broadcast HDTV

What is meant by high-definition television? In many respects, HDTV is defined by what the viewer sees: a "picture" with specified spatial and temporal resolution, intended to be viewed at a given viewing distance on a display with certain aspect ratio (width to height ratio). Although there are variations among HDTV systems, it is fair to say that a number of design characteristics clearly distinguish HDTV from NTSC, PAL or SECAM systems (referred to as conventional systems in this thesis). In the current state of technology, these include a wider aspect ratio than conventional systems (typically 16:9 instead of 4:3), vertical and horizontal spatial resolutions roughly twice that of conventional systems, and temporal resolutions or rates at least as high as the 25-30 frames/s used in conventional systems.

Most HDTV systems intended for terrestrial broadcast are limited to transmitting binary data at rates in the neighborhood of 20 Mb/s, in order to meet coverage and signal strength requirements (the reasons for this will be examined in detail in later sections). Any source coding or compression system must be able to operate within these constraints, yet provide a picture which is substantially better than is achievable with conventional NTSC under similar

transmission conditions. The remainder of this section summarizes the essential features of the compression systems that have so far successfully met this challenge.

A high-level block diagram of the functions performed by a video encoder is shown in Figure 2-1. A video encoder may be viewed as a system performing three major tasks. The

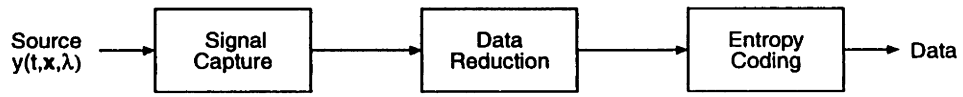

Figure 2-1: A high-level view of a video encoder.

first task, which we call signal capture, involves signal sampling and color separation. The second task is one of data compression or reduction. This task is by far the most complex from a signal processing standpoint and generally includes, as a first step, analog-to-digital conversion followed by some form of spatial and temporal processing. The third and last step, is to pass the data through an entropy coder whose task it is to represent the incoming data concisely but without changing the amount of information in the data stream. These three functions are reviewed in the next sections.

2.2.1 Signal capture

In this first phase, it is convenient to view the input to the video system as a multidimensional intensity signal with time, two-dimensional space, and wavelength as dimensions. Signal capture involves sampling of the source along each of these dimensions. Television relies on the persistence of vision to convey the impression of motion by presenting a rapid succession of slightly different still images ("frames"). Under specific conditions, a difference in the position of an object from one frame to the next is interpreted as motion of that object. Natural and accurate rendition of motion in a scene, without flicker, is an important objective of high definition television. Clearly, the frame display rate must be high enough so that motion in the scene is conveyed smoothly, with no sudden jumps from frame to frame. In addition, the frame rate must be high enough to ensure that the persistence of vision extends over the interval between flashes, thus avoiding a perception of flicker. A tradeoff encountered in HDTV design is the need to reduce the rate at which some of the spatial aspects of the image are reproduced, thus conserving bandwidth, while maintaining temporal integrity, particularly the position and the shape of objects in motion.

2.2.2 Data reduction

The data reduction phase involves applying different types of processing to the different signal dimensions. The main operations are:

Temporal processing: The frame rate to achieve proper motion rendition is usually high enough to result in a great deal of temporal correlation between adjacent frames. This is especially true for natural scenes where much of the variation of intensity from frame to frame can be identified with objects moving with little deformation in the field of view of the camera. By exploiting this redundancy through temporal processing, the amount of data that needs to be sent (after quantization) over the transmission channel can be drastically reduced. A simple way of achieving some data reduction is to exploit the correlation between adjacent frames by encoding their differences. A variation of this idea involves encoding only those regions of each frame that have changed from the preceding frame. Such methods are simple and inexpensive but achieve only modest coding gains and are therefore of limited use for television broadcast applications. Higher coding gains can be achieved by exploiting the notion that adjacent frames or regions of adjacent frames are often related by simple transformations. If regions can be identified with objects in the scene, the mapping between related regions in different frames corresponds to a projection in two dimensions of the three dimensional displacements of the objects during the corresponding time interval. The process of determining such transformations is known as motion estimation (ME). Processing images accounting for the presence of motion is referred to as motion-compensated (MC) processing. Motion estimation is in general a complicated and computationally expensive task. Specific assumptions about the scene illumination, the objects in the scene, the camera model etc. are useful to derive realistic motion parameters. Existing HDTV broadcast systems have, to this day, used fairly simple models of motion, but the situation is likely to change in the near future.

Spatial processing: Even after temporal processing, there is still, in general, a substantial amount of spatial redundancy in the MC prediction error. Spatial redundancy may be present in the form of spatial correlations which are amenable to traditional still image processing techniques. These include transform (e.g. discrete Fourier transform (DFT), discrete cosine transform (DCT), lapped orthogonal transform (LOT), etc.), subband (e.g. quadrature mirror filter banks (QMF)) and multiresolution (e.g. Laplacian pyramid, wavelet) techniques. There is intense ongoing research in this area, particularly in relation to multiresolution, multiscale methods, which, in principle, match more closely the processing of the human visual system (HVS). A large number of video source coders and image coders, including all current digital HDTV proposals, JPEG, H.261, MPEG-1 and MPEG-2, use the block DCT as the spatial processing method. This choice is in part motivated by practical considerations (e.g. hardware availability, "safe and proven" algorithms) and in part by some interesting characteristics of block

transforms. Motion compensation and adaptive quantization on a block basis are easily implemented, prediction errors when they occur tend to be more localized than with multiresolution schemes, and processing can be easily divided among different processing units. The block DCT suffers, however, from an inherent inability to represent edge-like features in images, or to exploit spatial correlations between blocks, and it also exhibits visible blocking artifacts at low coding rates. Yet the block DCT is the spatial processing method of choice for the current generation of HDTV source coders as its advantages outweigh the disadvantages.

Quantization: Temporal and spatial processing may be viewed as methods of changing the representation of the information present in the video signal without changing the amount of information (since both operations are reversible). Quantization is the operation of mapping a real number or a vector of numbers to another number selected from a countable alphabet of numbers. The quantization step is the only operation in the video encoding chain where some intentional distortion (quantization noise) D is introduced in the data so that it can be better compressed.

A fundamental theorem due to Shannon is that a source can be characterized by a rate-distortion function $R(D)$, where R is the number of bits per source symbol required to identify a code sequence. The role of the rate-distortion function in quantization applications parallels that of the channel capacity function in transmission applications. Its significance is that there exist quantization schemes for any $R > R(D)$ that achieve per-symbol distortion no greater than D, and conversely, that there exists no quantization scheme with rate $R < R(D)$ that achieves an average distortion of D or less. Generally, complex codes are required to obtain simultaneously low rate and low distortion, in much the same way as in transmission applications, where complex codes are required to achieve simultaneously high information rate and low SNR. Rate-distortion functions have been derived for a variety of source models. Notwithstanding the fact that real sources rarely obey simple models, the knowledge of the fundamental quantization limits for a given source model does not tell us how to implement a quantizer that approaches that limit. This probably explains why it is at this compression stage that one finds the greatest variety of techniques in the video coding process.

A key consideration in the design of quantization schemes for HDTV is introducing distortion in such a way that it is least perceptible by the human visual system. Basic techniques include: introducing more distortion in the chrominance components while preserving, as much as possible, the accuracy of the luminance component; quantizing high frequency components more coarsely than the perceptually more important low frequency components; and, making the quantization step size a complex function of the quantization history and of the local scene complexity. This last step seeks to exploit a property of the HVS known as spatial masking, which is the reduced capacity of the human eye to see artifacts in a detailed region

of an image as compared to a less detailed region. In MC predictive coding, the complexity of the prediction errors is an increasing function of the complexity of the motion field. Fortunately, the acuity of the HVS is maximum for stationary objects, and it is therefore possible to introduce larger error in the coding of moving areas.

Finding the right performance-complexity tradeoff is particularly important for broadcast HDTV. At the time of writing, most practical quantization schemes for HDTV use the following basic approach: each block of DCT coefficients obtained from the temporal and spatial processing is multiplied by a block-size "weighting matrix" (typically 8x8), and then each coefficient is passed through a scalar quantizer. The weighting matrix is obtained by multiplying a primitive matrix (chosen from a small fixed set), by a scaling factor which is dependent on a number of factors, including perceptual factors (scene complexity), state of the encoder, etc. Therefore, the quantization used is fundamentally a scalar quantization scheme with perceptual weighting.

2.2.3 Data compaction

The last step consists of passing the data stream through an entropy coder whose task it is to represent the incoming data concisely, but without changing the amount of information in the data stream. The data obtained by quantization, a series of indices taken from a set, is typically highly redundant and can be compressed without introducing additional distortions. A data compaction code is used to reduce this redundancy. The lower bound on the rate of the data compaction code is defined by the entropy of the source. In general, to achieve rates close to the entropy limit, complex data compaction codes are required. Finding the right tradeoff between rate and complexity is an important consideration in the design of the entropy coder. One simple and widely used method in video processing is runlength coding followed by Huffman coding. In this method, all the indices are ordered in some manner, and the runs between non-zero indices as well as the non-zero index values are coded with different Huffman codes. A slightly more complex method, not yet used in broadcast applications, is adaptive arithmetic coding.

2.2.4 Encoder for video processing

Finally, to better illustrate the overall encoding process, we show in Figure 2-2 a possible implementation of a video encoder using predictive motion compensation. This is the basic structure of all current HDTV video encoders. The DCT operates on the difference between the original frame and the motion-compensated predicted frame (this difference is sometimes called the

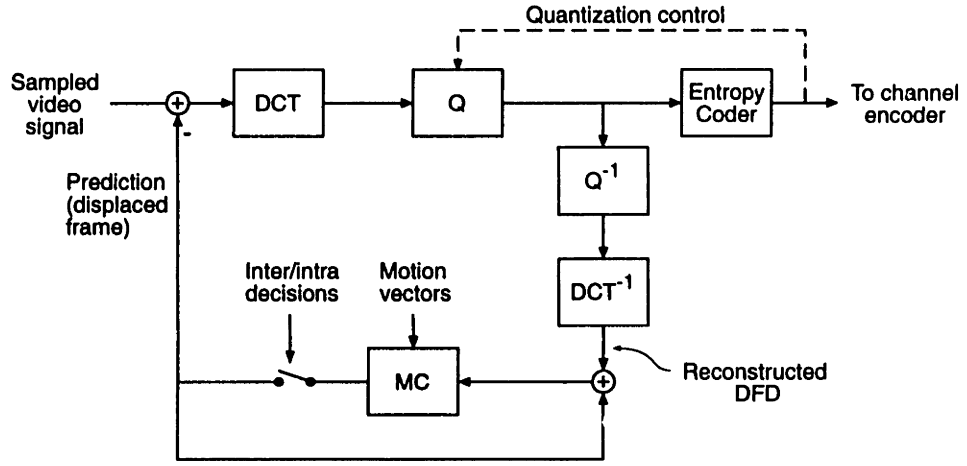

Figure 2-2: Video encoder using motion-compensated prediction.

prediction residual). Clearly, when the block is predictable, very little energy is present in the prediction residual. Thus, the predictive loop is used to remove temporal redundancies in the video signal. The spatial transform (here a DCT) then attempts to concentrate the residual energy in only a few coefficients. Quantization is then performed, thereby reducing the amount of information present in the signal, in a way that is the least visible to the human eye.

2.3 The HDTV broadcast channel

There has been a surprising convergence in the design of video coding for digital HDTV broadcasting applications. All systems to date are based on motion-compensated frame-to-frame prediction and make use of the block DCT (Discrete Cosine Transform) to reduce the correlation between neighboring pixels. They are all designed to yield good quality images for data rates in the range of 20 Mb/s, for roughly twice the horizontal and vertical resolution of the current NTSC standard. By contrast, there has been more variation in the design of the channel coding portion of transmission systems for HDTV broadcasting.

One reason for these differences is the relative novelty of the application of digital transmission techniques in broadcast applications. Another is that the problem of broadcasting digital information at high data rates in an existing network of analog transmitters and receivers is multifaceted and highly constrained. These constraints include: minimal impact on current NTSC coverage areas; robustness to NTSC interference, particularly co-channel interference; immunity to multipath propagation; low transmitter power relative to NTSC; fixed bandwidth of 6 MHz; efficient use of the radio spectrum; and transmission in the so-called taboo channels

because no additional radio spectrum will be allocated for the new service. These constraints will require that the new systems be able to operate at significantly reduced co-channel spacings, with powers 10-15 dB below the current NTSC transmitters. Some of the constraints are due to the characteristics of the transmission medium and receiver characteristics (noise, multipath), others are a matter of policy set forth by the FCC (simulcast transmission, service area requirements), and the remaining are the product of previous decisions or an existing situation (adjacent channel interference). Each of these constraints is reviewed briefly in the following paragraphs.

2.3.1 Policy constraints

2.3.1.1 Spectrum for HDTV

Radio frequency spectrum allocations constitute a highly valuable commodity in limited supply. A wide variety of telecommunication services, including commercial, military, broadcast, relay, point-to-point, fixed stations and mobile services make use of this spectrum. For this reason, the FCC issued a ruling in 1987 stipulating that channel assignments for HDTV terrestrial broadcasting shall be confined to the VHF and UHF bands currently occupied by the NTSC service. These bands extend from about 40 MHz to 200 MHz for VHF and from 470 MHz up to almost 1 GHz for UHF. The VHF band is shared with frequency-modulation broadcasting, while the UHF range contains only television channels (a television channel being defined as a 6 MHz slot), although there are gaps in both ranges that are assigned to other services, such as land-mobile radio. The paucity of channels in the VHF band implies that HDTV broadcast will likely be limited to the UHF band. Unfortunately, UHF transmitters are required to operate at greater powers than their VHF counterparts in order to overcome the greater losses in free-space propagation and in the receiver antenna and tuner subsystems.

2.3.1.2 Simulcast policy

The FCC announced later, in 1990, that it intended to select an approach whereby transmission of NTSC on existing channels would be maintained while HDTV transmission of the same program would use an additional channel of no more than 6 MHz, the channel bandwidth for conventional systems. This approach, which has come to be known as the *simulcast approach*, was recommended at the outcome of a study concerned with the issue of compatibility of HDTV with NTSC. An important consideration was that the NTSC service should be protected at least until the new service establishes its technical and economical viability. Another consideration was that it would be difficult to ensure the efficient application of modern communication tech-

niques if one were to simply enhance the old NTSC standard. The approach that was eventually selected involved separating the functions of the conventional and the HDTV transmissions while requiring that HDTV programs be concurrently transmitted in conventional format [83].

2.3.1.3 Coverage area policy and planning factors

The Advisory Committee on Advanced Television Systems (ACATS) issued in 1991 a series of recommendations relative to the HDTV service requirements. The most important of these requirements were:

- The HDTV service area should be comparable to the current NTSC grade B service area.
- The interference to an existing NTSC service by an HDTV signal should be no worse than the current interference into an NTSC signal by another NTSC signal.
- In order to meet simulcast channel allocation goals, co-channel transmitters may have to be separated by as little as 100 miles.

In Appendix A.1, we give some details regarding the determination of the NTSC service contours. In the absence of similar results for digital transmission, efforts have been made to try to use existing data on NTSC coverage to predict coverage of digital HDTV systems. However, it is felt that great care must be employed in interpreting or applying such predictions to HDTV broadcasting, since there are significant differences between NTSC transmission and digital HDTV transmission: because NTSC signals have most of their energy concentrated around the visual carrier while HDTV signals have a much more uniform power spectral density, the performance variability as a function of location or time should be smaller in the case of HDTV; as well, much more sophisticated signal processing techniques are used at the receiver to mitigate certain types of impairments (such as co-channel interference and multipath). It therefore becomes important to examine the statistics of each type of impairment individually. Other factors, such as terrain and atmospheric conditions, may well cause the true coverage to vary considerably from the predictions.

2.3.2 Interference mechanisms

Receivers tuned to a UHF channel may suffer interference arising from a number of sources including: co-channel interference; adjacent channels; images of the sound and picture carriers; beats with the local oscillator and with the intermediate frequencies; and intermodulation between station carriers. The mechanisms producing these interfering signals may be linear (image interference signals), or nonlinear (intermodulation, IF beats). The net result is that

interference at a given carrier frequency may be caused by signals with the same carrier frequency or by channels located above and below it by 1, 2, 3, 4, 5, 7, 8, 14, and 15 channel numbers, as shown in Table A.3 of Appendix A.3.

2.3.2.1 Co-channel interference

As can be inferred from Table A.3, co-channel interference from neighboring NTSC stations is of particular importance. The mandated minimum spatial separation between co-channel NTSC stations is 155 miles in the UHF band. In order to accommodate a larger number of stations, it is estimated that this separation will have to be reduced to less than 100 miles. Clearly, the co-channel interference problem can only be made worse by the introduction of additional transmitters, both for the new HDTV service and for the existing NTSC service, since it is not possible to increase the power of one transmitter without affecting a neighboring transmitter's service areas. This source of impairment is more difficult to overcome than most other types of interference. For instance, noise is generated mostly in the receiver front-end and can be reduced by, among other things, better low-noise amplifiers and the appropriate design of the tuner. The other types of interference shown in Table A.3 can also often be overcome by more elaborate tuner designs. But since the channel selection tuning mechanisms used in television receivers to provide channel selection are based upon signal frequency, even the best tuner may not reject an undesired co-channel signal. As a consequence, it is generally agreed that the HDTV service will be co-channel interference limited, rather than noise limited.

2.3.2.2 Adjacent channel interference

Adjacent channel interference usually results from nonlinear effects that take place in the tuner of the television receiver. Adjacent channel interference may also be due the presence of a nearby high-power transmitter operating on a frequency band adjacent to the desired band. In such a case, because of nonlinear effects in the transmitter, this transmitter may produce power at frequencies outside its assigned band. This phenomenon, known as spectral regrowth, may be partially avoided by the use of a pre-equalizer filter and pre-compensation in the transmitter.

2.3.2.3 Taboo channels

In the past, only a few of the possible channels have been allocated in any one location because of the interference constraints mentioned above and other considerations. The rest are unusable channels and have come to be known as "taboo channels".

The lack of radio frequency spectrum will now force the FCC to allow these "taboo channels" to be used for HDTV transmission. Given this fact, it is important to realize that many of the sources of interference can be reduced by improving the design of the tuner, with the notable exception of co-channel interference. In particular, modern double conversion tuners greatly reduce the sources of interference. Such tuners will be required for HDTV receivers, principally to mitigate the effect of strong NTSC signals located at these taboo frequencies. On the other hand, because of the relatively low HDTV transmission power, interference caused from HDTV into NTSC by the mechanisms outlined previously should not be too severe and should not require specially designed NTSC receivers.

2.3.3 Medium and receiver limitations

2.3.3.1 Noise

On a radio link such as broadcast HDTV, noise enters the receiver both through the antenna and from internal sources in the receiver. At the radio frequencies of concern to us, both sources of noise are modeled very well as white and Gaussian. White noise is completely characterized by its spectral density $N_0 = kT_n/2$, where k is Boltzmann's constant ($k = 1.38 \cdot 10^{-23}$W/K/Hz) and T_n is the temperature in degrees Kelvin. In radio communications, it is common to use the noise temperature, expressed in degrees Kelvin, to characterize the noise. The noise incident on the antenna depends on the effective noise temperature in the direction the antenna is pointed. The noise introduced internal to the receiver depends on the design and sophistication of the receiver. It is customary to refer all noise sources to the input to the receiver and define an equivalent noise temperature at that point. Depending on the design, noise generated inside the receiver may or may not be dominant. For typical NTSC tuner designs using reasonably cheap low-noise amplifiers, the main source of noise is the tuner. For super-cooled maser amplifiers, such as are used for deep-space communications, the background noise is the main limitation to system performance.

2.3.3.2 Multipath

Multipath propagation occurs when there are multiple propagation paths between the transmitter and the receiver. It is a common phenomenon at VHF and UHF. Multipath may be caused by reflections from objects in the environment, or under exceptional circumstances by layer inversions in the atmosphere. A straightforward multipath condition occurs when one or several alternate paths to the receiver are created by reflections from fixed obstacles such as mountains or tall buildings. A more complicated multipath condition occurs when

the environment is dynamic, which may include moving reflectors, transmitters or receivers. Airplanes, automobile traffic and even swaying trees and buildings are all considered moving reflectors or scatterers.

Multipath has radically different effects on analog and digital transmission systems. In analog systems, such as NTSC, multipath will manifest itself as multiple images, as a result of the simple relationship between the video signal and the channel waveform. These multiple images are so common in analog systems that they have received the name of "ghosts". In addition to multiple images, changes in color, hue and saturation may result if the color burst of a close-in (short delay) reflection falls on the color burst of the main signal. One common recognizable result of ghosting is the presence of a hazy greyish vertical bar - the horizontal blanking interval of the delayed signal - being received at the wrong time and displayed on top of a television image. If the multipath is dynamic, the effects can be very disruptive, albeit usually temporary. One such example is the so-called "airplane flutter" effect.

In a digital system, multipath propagation results in intersymbol interference, which may be dynamic, and which causes frequency-dependent attenuation across the signal bandwidth. Equalization is required to mitigate the effect of multipath propagation. Multipath fading or frequency-selective attenuation has received a lot of attention in digital radio communications. There, the principal cause of multipath fading is the existence of anomalous propagation conditions often related to unusual temperature and humidity profiles; the transmission medium has a layered structure, which, under specific conditions, allows multiple paths to reach the receiver. Such conditions are rare, but are important in the case of digital radio, where an extremely high link reliability is critical. Multipath fading due to anomalous atmospheric conditions is not expected to be a major concern for digital terrestrial television broadcasting.

There are, however, other causes of multipath fading which are of much greater concern in the case of HDTV transmission. Just as for analog transmission, reflections from obstacles, fixed and moving, are expected to be the main cause of multipath. These effects are all the more severe as the antennas used to receive television signals are not nearly as directional as those typically used on digital radio microwave links. Unfortunately, there appear to have been very few experimental studies and very little precise characterization of the effect of multipath fading on broadband systems such as digital television. One recent study [54], however, was conducted to measure the multipath environment in situations that correspond closely to over-the-air HDTV channels, in both the VHF and UHF bands. In particular, the delay spread and the strength of the multipath were measured under a variety of conditions, in the vicinity of Denver and San Francisco. It appears from this study that multipath strengths are stronger at UHF than VHF by an average of 2 to 4 dB, while the delay spread, anywhere between 1 and 14 μs, is highly variable, with no obvious dependence on identifiable environmental factors.

In another digital transmission experiment conducted in Glenview, Illinois [29], it is reported that reception at the grade B distance (48 miles) was in general stable, with little fading for the terrain involved, with a 30 ft Yagi type antenna. It is also mentioned that reception beyond the grade B contour was subject to substantial and rapid temporal fading. According to the authors, an adequately elevated antenna would substantially decrease the temporal fading and should provide satisfactory reception. In particular, they report satisfactory reception with a 190 ft antenna at a distance of 70 miles from the transmitter.

2.3.4 Implications for the HDTV service

As can be inferred from the previous sections, the advanced television systems currently being developed for terrestrial broadcast applications must be capable of operating in a very challenging environment. The transmitted signal is both bandwidth and power limited, and the channel is characterized by multipath and interference from other stations. In addition, HDTV is required to have minimal impact on current NTSC coverage areas and signal quality.

Since the overall radio spectrum allocated to over-the-air television broadcasting is to remain unchanged, HDTV must resort to using channels that had previously been designated as unusable because of interference considerations (the so-called taboo channels) and must be capable of operating at significantly reduced co-channel spacings, with powers 10-15 dB below current NTSC transmitters. This low-power requirement, coupled with the necessity for reduced co-channel spacings, means that interference from NTSC will be particularly strong in some locations.

In the next section we give an overview of the major building blocks that are used for channel coding purposes in current digital HDTV systems. Channel coding is examined more thoroughly in Chapter 4.

2.4 Transmission systems for HDTV

2.4.1 Major functions

HDTV transmission systems must be capable of delivering a high-rate digital stream with high reliability, even under severe channel conditions. In this section we describe only the general features of such systems, which now exist in the form of prototypes, without providing theoretical justifications. The theoretical justifications are given in subsequent chapters. In particular, Chapter 4 develops the concepts necessary to analyze and characterize the HDTV

broadcast channel and shows how these concepts can be used to optimize transmission under various criteria.

A high-level system description of the functions performed by a transmission system is shown in Figure 2-3. A fundamental function of the transmission system is to encode the data

Figure 2-3: A high-level view of a transmission system.

so that it can be sent reliably through the channel. This function is known as error-control coding. By means of an error-control code (or transmission code), a noisy channel is made to act like a deterministic and reliable channel. The task of recovering the source data from the encoded data is parallel to the task of compacting data in source coding. However, encoding with an error-control code is generally very easy, while decoding is often complex and costly, which is the converse of the source coding situation.

A second function of the transmission system is to provide a mapping between the digital domain in which error-control codes typically operate and the analog, continuous-time domain of the physical transmission medium. This function is implemented in the modulator/demodulator blocks. A task of the modulator is to transform the digital data stream into a waveform representation of the data that can be accepted by the channel. The waveform design problem, often called pulse shaping, must take into consideration the characteristics of the channel. Because the channel is subject to various forms of noise, distortion, and interference, the received waveform differs from the transmitted waveform. The demodulator must convert the received waveform into a stream of discrete channel symbols based on a best estimate of the transmitted symbol or sequence of symbols. In addition, the demodulator must resolve synchronization, timing, and carrier acquisition issues in order to provide useful information at its output. Although these issues will not be examined in depth in this thesis, they are very important in practice and must be resolved satisfactorily before the benefits of channel coding can be reaped.

2.4.2 High-level block diagram

A complete, albeit schematic, view of a typical HDTV transmission system is shown in Figure 2-4. The multiplexed data, which comprises digital video and audio information, together with auxiliary and control data, is first converted into two digital waveforms by block and trellis

encoding and digital filtering. The digital streams are then transformed into analog waveforms, quadrature modulated at an IF frequency typically close to 44 MHz, and further filtered with a SAW filter to remove out-of-band components before being translated to the assigned frequency in the VHF or UHF band and amplified by a high-power amplifier (HPA). The receiver uses a double-conversion tuner to recover the analog waveform at a center frequency of 43.5 MHz. The waveform is then filtered with a SAW filter at IF, demodulated, converted to a digital stream and processed by trellis and Reed-Solomon decoders.

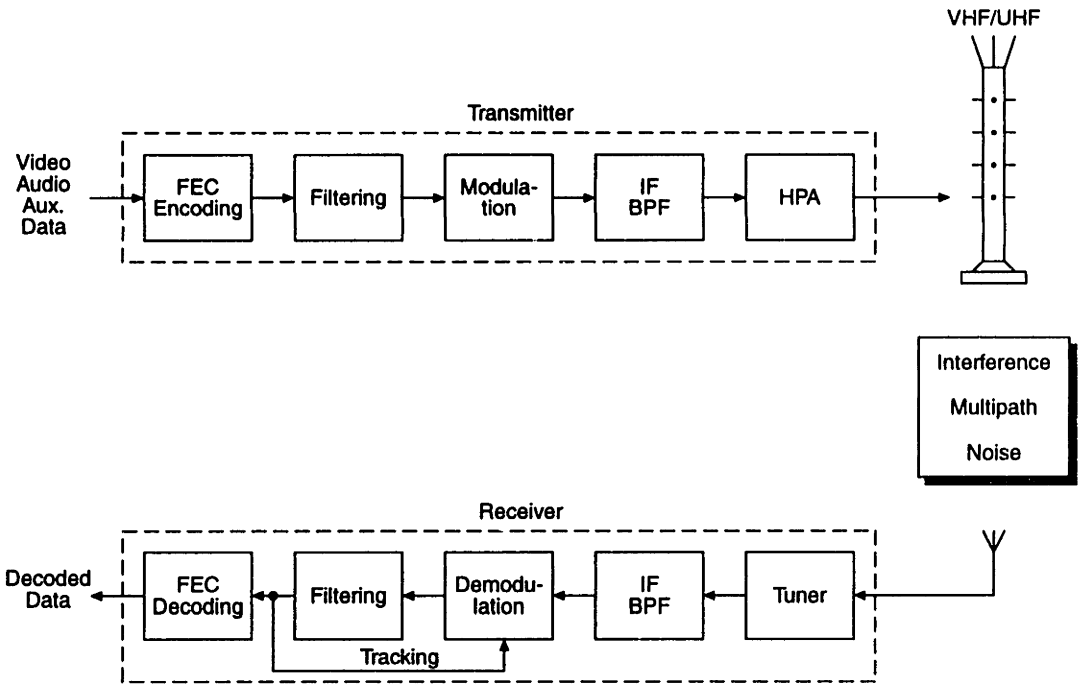

Figure 2-4: Block diagram of a generic HDTV transmission system.

In contrast to source coding, much of the complexity of the transmission system lies in the design of the receiver. In addition to demodulation and error-correction, the receiver must be able to generate a local reference signal synchronized in both phase and frequency to the carrier used in the modulation process at the transmitter. Another function of the receiver is to extract symbol timing so that the demodulated signal can be sampled in synchronism with the transmitter clock.

Since the available bandwidth is limited, it is also necessary to shape the impulse response

of the signal so that little power is emitted outside the assigned band. In many cases, the channel introduces distortions such as dispersion and fading. There are a variety of ways of compensating for these effects. Some may be transmitter-based, while others are receiver-based. Adaptive equalization is one such technique which is often implemented at the receiver end. The next subsections outline some of these issues in somewhat more detail.

2.4.3 Error control

An error-control code, or transmission code, is designed for one of two purposes: error detection or error correction. Error detection can be used to increase reliability. Error correction carries error detection one step further by using the redundancy to correct errors.

There are two broad classes of techniques for introducing redundancy into a signal, both of which can be used in combination. The first method is to increase the symbol rate by inserting extra symbols in the data stream, thereby expanding the bandwidth of the transmitted signal. The second method is to increase the number of symbols in the alphabet. Increasing the size of the alphabet is usually the better approach on bandlimited media such as broadcast HDTV, since increasing the symbol rate also increases the bandwidth and the amount of noise that enters the receiver. Both techniques are used in combination in a number of HDTV systems.

There are two main techniques for decoding the data: "hard-decision" decoding and "soft-decision" decoding. Hard-decision decoding consists of making a decision on the transmitted symbol that best matches the received symbol and then mapping the sequence of decoded symbols to the corresponding sequence of information bits. In contrast, soft-decision decoding makes direct decisions on the sequence of information bits. Soft-decision decoding is capable of providing better performance at the expense of implementation complexity, since it makes use of information that the slicer would otherwise throw away. Both of these decoding techniques are used in current HDTV prototypes.

Channel codes fall into two broad classes: block codes and convolutional (trellis) codes. Both hard and soft decoding are used for block and convolutional codes, although soft-decision decoding for block codes tends to be more costly than for convolutional codes. Block codes, in the form of Reed-Solomon codes, are used alone, or in combination with convolutional codes, in all current HDTV systems. Block codes are used to provide burst-error protection as well as coding gains, although in a concatenated coding scheme, most of the coding gain is typically achieved by the inner trellis code, and burst-error protection is provided by the outer code. This aspect is explored in more detail in Chapter 4.

2.4.4 Modulation and pulse shaping

2.4.4.1 Modulation

Modulation is the means by which a stream of symbols from a discrete alphabet is converted to a stream of waveforms, which are in some way matched to the characteristics of the transmission channel. Among the wide variety of modulation schemes used in digital communications, multilevel modulation schemes such as QAM (quadrature amplitude modulation) and VSB (vestigial sideband modulation) are especially interesting as they combine high spectral efficiency and power efficiency.

In traditional point-to-point communications, the data rate corresponding to the reliable transmission of symbols across the channel is fixed and chosen to best use the capacity of the channel at a nominal channel signal-to-noise ratio. In some cases, however, the transmitter must communicate with a multiplicity of receivers, each operating with a different signal-to-noise ratio. Such is the case for the broadcast channel, where receivers may be placed anywhere inside the so-called coverage area of the transmitter. In order to exploit more efficiently the resulting variable capacity of the broadcast channel, multiple- or variable-rate systems have been proposed. One such system using time-division multiplexing with 2 different constellations has been implemented [97]. Some work has been carried out to try and apply multiresolution modulation to the broadcast channel as well. In a multiresolution transmission scheme, signal constellations such as QAM are embedded in such a way that different data streams can be recovered at different signal-to-noise ratios. The embedding might take place in the phase-amplitude domain or more generally in the signal space domain. However, to the best of our knowledge, there are no existing systems using a truly multiresolution approach to transmission.

In the previous discussion, it was implicitly assumed that error-control and modulation are distinct and largely independent functions. The seminal work of Ungerboeck [86, 87] has shown, however, that it is often possible to improve on the performance of the transmission by combining coding and modulation. The result is known as coded modulation. Coded modulation is at the junction of communication theory and information theory and is presently a very active area of research. While there are well-established results pertaining to the Gaussian channel model, much work remains to be done in the application of coded modulation to other, less ideal channels. This includes the bandlimited, intersymbol interference or frequency-selective channel, and the fading channels (both frequency-selective and non-frequency-selective) characteristic of transmission to mobile receivers. An important theme in this thesis is the combination of coded modulation with practical methods to combat specific impairments such as multipath and co-channel interference.

2.4.4.2 Pulse shaping

The combined effects of the transmitter and receiver filters and the propagation medium determine the overall pulse shape associated with the modulation process. The purpose of pulse shaping is to ensure zero intersymbol interference for the ideal channel while limiting the length of the impulse response. Pulse shaping is typically performed at both the transmitter and receiver. Zero intersymbol interference is achieved by choosing an overall pulse shape with a maximum value at some instant t_0 and zero values at multiples of the signaling interval T, i.e. at instants $t = kT + t_0$. Any pulse with this property is called a Nyquist pulse. There are a wide variety of possible Nyquist pulses, but perhaps the most popular is the so-called raised-cosine pulse

$$p(t) = \frac{\sin(\pi t/T)}{\pi T/T} \frac{\cos(\pi \alpha t/T)}{1 - (2\alpha t/T)^2} \tag{2.1}$$

where $0 \leq \alpha \leq 1$ is the roll-off factor. This pulse has its maximum at $t = 0$ and is zero at all $t = kT$. Its Fourier transform, $P(f)$ is T for all $|f| < (1 - \alpha)/2T$ and is zero for all $|f| > (1 + \alpha)/2T$. The shape of the impulse response and the corresponding Fourier transform are shown in figure 2-5.

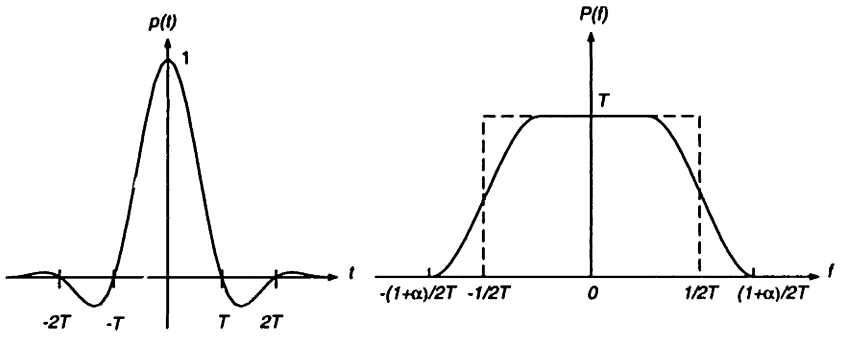

Figure 2-5: Raised cosine pulse $p(t)$ with $\alpha = 0.5$. $P(f)$ is the Fourier transform of $p(t)$.

The raised-cosine pulse is strictly bandlimited and spans a bandwidth of $(1 + \alpha)/T$. Among all possible Nyquist pulses, the smallest RF bandwidth that can be achieved is $1/T$ which is often referred to as the Nyquist bandwidth. This minimum bandwidth is achieved for $\alpha = 0$. A raised-cosine pulse with $\alpha > 0$ exceeds this minimum bandwidth by α/T, which is called the excess bandwidth. The choice of the pulse shaping parameters, e.g. roll-off factor or excess bandwidth, involves many considerations and represents a tradeoff between bandwidth efficiency and peak power.

Another important consideration is how to apportion the shaping of $P(f)$ between the transmitter and receiver. The popular (and theoretically optimal, in AWGN) approach is to provide the same amount of shaping at the transmitter and receiver. For raised-cosine filtering,

this gives rise to square-root raised cosine filters with frequency response $\sqrt{P(f)}$. This even division of the spectral shaping yields the best detection performance for a given transmitter power and a white Gaussian noise channel, as well as for adjacent channel interference. An alternative approach would consist of choosing a receive filter chosen to equalize the average of a class of channel characteristics [76].

The implementation of Nyquist filtering is often done in discrete time with finite impulse response (FIR) filters. It is not possible to implement a raised-cosine filter exactly with an FIR filter, since the impulse response of the raised-cosine filter has infinite support. Typically, an approximation of the desired response is implemented in discrete time at baseband, and further pulse shaping is performed at IF (intermediate frequency). One advantage is that it is possible to better attenuate the sidelobes that result from the digital filtering.

2.4.5 Equalization

A typical HDTV transmission channel is rarely ideal. Signal distortions occur due to many factors, including multipath propagation, fading, co-channel and adjacent channel interference, nonlinear amplification or even improper filtering. Linear distortions may be compensated in several ways: by applying some form of filtering to the received signal (which is known as "equalizing" the signal), by estimating the distortion and canceling it as part of the decoding process, or by coding the signal at the transmitter so that it is relatively immune to channel distortions (transmitter-based techniques). These aspects are treated in more detail in Chapter 6. This section is meant to provide a general overview of the equalization process.

The function of a receiver-based equalizer can best be understood by considering the overall channel response $h(t)$, which includes the filtering in the modulation and demodulation processes. Equalizers are commonly designed to make this overall response satisfy Nyquist's first criterion - having regular zero-crossings spaced at multiples of the symbol interval T - so that at the receiver, the transmitted data symbols can be detected without any mutual interference. This condition is equivalent to saying that the "folded" spectrum (the channel response after sampling at the symbol-rate), defined as

$$H'(f) = \frac{1}{T}\sum_{n} H(f - n/T), \tag{2.2}$$

should be constant over the interval $|f| \leq 1/2T$. Figure 2-6 shows the folded spectrum of a channel response that satisfies Nyquist's first criterion. This strategy, known as zero-forcing equalization, ignores the effect of the channel noise. In Section 2.4.5.4, we explain how to design more robust equalizers.

Equalization may be implemented either in the IF stage or at baseband. As is explained in

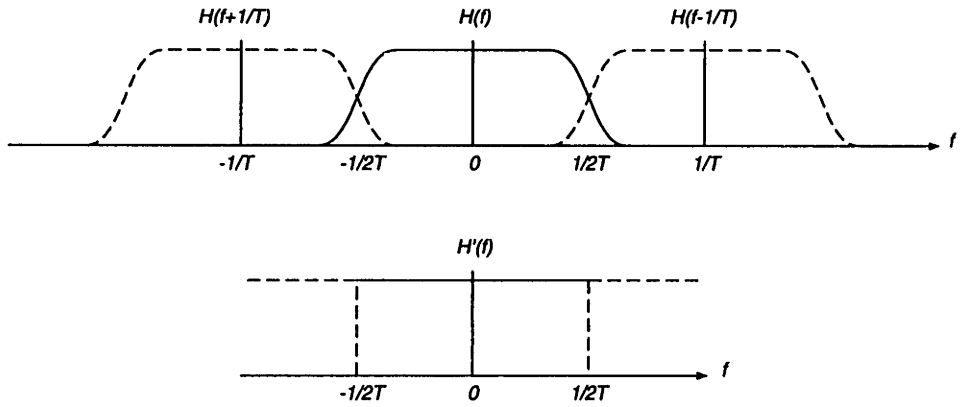

Figure 2-6: Folded spectrum $H'(f)$ of a channel response satisfying Nyquist's first criterion.

Section 2.4.6, IF implementation has advantages with respect to carrier recovery, but baseband equalizers are sometimes preferred for technological reasons (easier digital implementation) and additionally provide compensation for asymmetrical modem imperfections.

2.4.5.1 Linear equalizers

In QAM systems, two separate data streams are transmitted orthogonally on a single carrier. Ideally, each data stream appears at its own baseband detector in the receiver without interference from the other stream and without pulse distortion. In general, however, this is not the case, and both in-phase distortion and quadrature distortions occur, thereby requiring equalizers with complex coefficients and complex arithmetic (complex add and multiply operations). A complex multiplication requires 4 real multiplications and 2 real additions. It is important to note that PAM and QAM are equally hardware-efficient. Figure 2-7 shows the realization

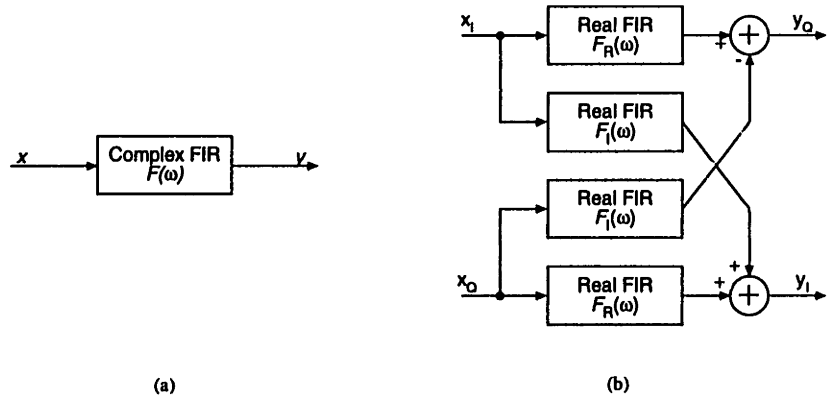

Figure 2-7: Baseband linear equalizer for QAM (a) complex implementation (b) real implementation.

of a baseband linear equalizer with real filters. Each filter $F_i(\omega)$ is implemented as a finite impulse response (transversal) filter. The filters $F_R(\omega)$ help to combat the interference in the in-phase and quadrature components, while the filters $F_I(\omega)$ are meant to compensate for the cross-interference between the two channels.

The ability of a linear equalizer to reduce intersymbol interference is determined by the number of delay-line taps and the position of the reference tap. For HDTV applications, several hundred taps are common. The center tap is chosen so as to provide protection against both minimum and non-minimum phase multipath. Linear equalizers of this type are able to compensate for some amplitude and all phase (group-delay) distortion. However, the performance of linear equalizers is poor on channels with deep nulls, because, in attempting to obtain an overall flat folded spectrum, the linear equalizer effectively enhances the receiver noise at the nulls and other distortions such as co-channel and adjacent channel interference.

So far we have only mentioned linear equalization using FIR filters. Another possibility would be to use IIR (or linear feedback) filters. However, these have not, in practice, been used due to a lack of guaranteed stability, a lack of a quadratic performance surface, and minor performance gain over transversal equalizers. A more useful equalizer is a nonlinear feedback equalizer.

2.4.5.2 Decision-feedback equalizers

This nonlinear equalizer technique is based on direct cancellation of the intersymbol interference from previously detected symbols. Figure 2-8 shows the structure of such an equalizer.

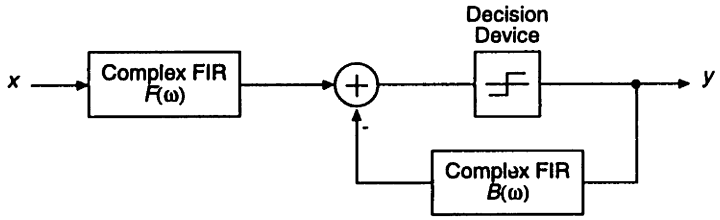

Figure 2-8: Decision-feedback equalizer.

The forward part is similar to the linear equalizer discussed earlier. However, decisions made on the equalized signal are fed back via a second transversal filter.

The feedforward section of the equalizer attempts to compensate for precursor intersymbol interference. Postcursor interference, including any associated with the operation of the feedforward section, is cancelled in the feedback section, and since this later cancellation is noise-free, effective equalization is possible even for fades that produce an infinite in-band null.

Note that the necessity to feed back decisions without delay implies that decision-feedback equalizers must be realized at baseband.

Given the advantages of decision-feedback equalization, a natural question is the following: given the same overall number of coefficients, how do decision-feedback and linear equalizers compare? There is no definitive answer to this question. The combination of a feedforward section and a feedback section gives good performance in the presence of minimum-phase multipath, but with non-minimum-phase multipath, if precursor intersymbol interference dominates, the performance is similar to the linear equalizer. Thus assigning the taps to the feedforward section may yield better performance even though DFE is in theory able to compensate for amplitude distortion without as much noise enhancement as the linear equalizer!

2.4.5.3 Optimization criterion

Linear and decision-feedback equalizers may be designed using different criteria. Two such criteria are the so-called zero-forcing criterion (ZF) and the mean-square error criterion (MSE).

Under the ZF criterion, the error sequence at the input of the decision device is constrained to be free of ISI. A linear equalizer designed according to a ZF criterion (LE-ZF) effectively whitens the channel spectrum, without regard to noise enhancement. A decision-feedback equalizer designed according to a ZF criterion avoids the noise enhancement that occurs in a linear equalizer due to the cancellation of the postcursor ISI.

Under the MSE criterion, the error sequence at the input of the decision device is allowed to contain both ISI and noise and the objective is instead to minimize the variance of the error. By relaxing the no-ISI constraint and tolerating a small amount of ISI, it is possible to decrease the variance of the overall error. In general, the smaller error results in improved receiver performance.

A more detailed discussion of the different optimization criteria is contained in Chapter 6.

2.4.5.4 Adaptation

In practice, the performance of an equalizer depends on the criterion used to adapt the equalizer characteristics to those of the time-varying channel. For HDTV applications, the time variations of the channel typically occur at a slow rate compared to the signaling rate, so that they can be tracked by relatively simple adaptation algorithms.

Historically, the first criterion used to adapt the equalizer coefficients was the ZF criterion. The adaptation is carried out by cross-correlating the error sequence with the *desired* sequence.

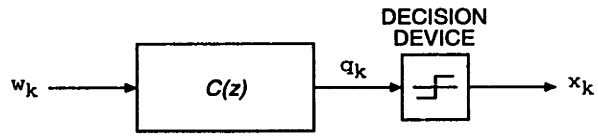

Figure 2-9: Discrete-time linear equalizer.

In general, it is not possible to eliminate ISI completely with a finite-length filter. When the equalizer coefficients are optimally adjusted, the error sequence is (partially) orthogonal to the data sequence, implying the absence of ISI within the window of the equalizer. Specifically, with the notations of Figure 2-9, let us consider the case of a linear equalizer with N coefficients defined by the vector

$$\mathbf{c}^t = [c_{-L}, \cdots, c_0, \cdots, c_L] \tag{2.3}$$

where $\mathbf{c}^t$ denotes the transpose of vector $\mathbf{c}$, $L = (N-1)/2$. Let us also define the vector of decisions

$$\mathbf{x}_k^t = [x_{k+L}, \cdots, x_k, \cdots, x_{k-L}] \tag{2.4}$$

At the $(j+1)$-th iteration of the adaptation algorithm, the filter coefficients are given by

$$\mathbf{c}^{j+1} = \mathbf{c}^j - \Delta e_k \mathbf{x}_k^* \tag{2.5}$$

where $\mathbf{c}^j$ is the vector of coefficients at step j, Δ is a small adaptation constant or step size, $e_k = q_k - x_k$ and $\mathbf{x}_k^*$ denotes the complex conjugate of $\mathbf{x}_k$. Simplifications of the algorithm are possible, for instance by using the sign of the error e_k and/or the vector of signs $\mathrm{sgn}(\mathbf{x}_k)$. In general, these simplified versions result in slower convergence.

Better performance can be achieved if the equalizer is adjusted to minimize the mean-squared error at the equalizer output, defined as the sum of powers of the uncancelled inter-symbol interference and noise. This forms the basis for the "stochastic gradient" algorithm, also known as the least-mean-squares (LMS) algorithm. Since the mean-squared error is a quadratic function of the tap gains, convergence is always assured, independent of the level of noise or interference. At the $(j+1)$-th iteration of the adaptation algorithm, the filter coefficients are given by

$$\mathbf{c}^{j+1} = \mathbf{c}^j - \Delta e_k \mathbf{w}_k^* \tag{2.6}$$

where

$$\mathbf{w}_k^t = [w_{k+L}, \cdots, w_k, \cdots, w_{k-L}] \tag{2.7}$$

is the vector of past and future inputs to the equalizer.

2.4.6 Synchronization

Before symbol detection can take place, two essential functions must be performed by the receiver in order to demodulate the received signal coherently: synchronization of the demodulating carrier (carrier recovery) and symbol timing (timing recovery). For correct performance, the locally generated reference waveforms must be accurately phase-locked to those produced in the transmitter. It is often desirable, in a bandwidth- and power-limited transmission system, that both recovery circuits extract their references from the received signal rather than from a separate pilot tone, as otherwise a portion of the limited transmitter power and/or bandwidth would have to be allocated to the transmission of the pilot tone. However, in some extreme conditions of co-channel interference or severe multipath, a distinct pilot tone may be required. In the case of data-directed carrier and timing recovery, the recovery circuits should be robust to the distortions introduced by the channel, including multipath distortion and co-channel interference. If synchronization is lost, then, when conditions improve, reacquisition should be as rapid as possible over the full range of frequency uncertainty in the incoming signals.

2.4.6.1 Carrier recovery

The frequency uncertainty of the carrier is determined by the stability of the microwave local oscillators used for IF/RF up- and down-conversion, and is typically more than an order of magnitude larger than the symbol timing loop bandwidth (In the case of the CCDC DigiCipher, the symbol timing loop bandwidth is approximately 100 Hz, while it is 5 kHz for the carrier loop).

The carrier recovery process should be sufficiently accurate that the phase error θ is low in both its static value and its fluctuations (phase jitter). The accuracy of the carrier recovery is crucial for high-level coded modulation schemes. As the complexity of high-level modulation schemes increases, so does their sensitivity to phase jitter, and the carrier recover circuit must provide correspondingly tighter control.

One method of carrier recovery is to put the IF signal through a nonlinearity, chosen so as to produce a spectral line at the carrier frequency, or some multiple thereof, and to extract the line component with a phase-locked loop (PLL). Alternatively, the carrier line component may be generated by using the detected data stream to remodulate the IF signal. A third approach, the decision-directed method, is especially suitable for QAM constellations with a large number of points. This third method is expanded below.

The A/D converter outputs, $\hat{I}$ and $\hat{Q}$, are digital streams representing the transmitted data

sequences. Because of additive noise, intersymbol interference (ISI) and other distortions, the digital outputs will lie not at M discrete points in the $I - Q$ plane but, rather, in small regions near these points. By measuring the difference between the received point and the M discrete points, an error signal can be formed, which can be low-pass filtered and applied to a VCO to control the carrier frequency and phase. Thus the carrier recovery process acts like a phase-locked loop. By appropriately choosing the circuit parameters, the desired acquisition and tracking of the received carrier can be achieved. To further aid in the acquisition process, it is possible to add a periodic signal to the VCO in order to effectively sweep a relatively large frequency range, until the carrier is acquired.

In the design of the carrier acquisition circuit, it is important to consider the effect of channel distortions. While it is possible to optimize the loop parameters for operation under normal acquisition conditions (ideal Gaussian channel), any signal distortions introduced by co-channel interference, multipath propagation, or other distortions will increase the loop noise spectral density and reduce the phase detector gain. In general, this implies that the signals used for carrier recovery should be derived from the output of the adaptive channel equalizer. This presents no problem with IF equalizers, but, with baseband implementations, the carrier recovery loop will include the time-varying equalizer, causing considerable complications, particularly in the case of fast-varying multipath conditions. Because of the long delay associated with a baseband equalizer, the loop gain of the carrier recovery has to be reduced to ensure stability, thereby impairing the ability to track rapidly-varying carrier phase. In the case of broadcast HDTV, long delays are difficult to avoid since a receiver must be capable of operating under widely varying multipath conditions.

Another important practical difficulty arises with decision-directed carrier recovery loops when trellis coding is used. Unlike a slicer, a trellis decoder does not make immediate decisions. Decisions must be postponed for several tens of symbol intervals. The delay can undermine the stability of the PLL. To overcome this difficulty, a slicer is added to the receiver and the slicer decisions are used to compute the phase error. The slicer decisions are not as reliable as the decisions made by the trellis decoder, but at least they are made promptly.

Finally, care also needs to be taken to minimize any interaction between the equalizer adaptation algorithm and the control of the carrier-recovery loop.

A block diagram of a combined carrier recovery and equalization system is shown in Figure 2-10. Typically, in such a scheme, carrier recovery and equalization are coordinated jointly. The baseband signal is first equalized, and then the equalizer output is de-rotated by the output of the decision directed PLL. The equalizer starts with blind equalization since at the beginning decision-directed coefficient update is not possible if there are channel distortions. After the blind equalizer converges, the equalizer is switched to a decision-directed mode. The error sig-

nals for the blind and decision-directed coefficient update are formed differently. In the blind equalization case, the error signal corresponds to that of the constant modulus algorithm and is given by

$$e_k = |x_k|^2 - E[|x_k|^2] \tag{2.8}$$

In the decision-directed mode, the equalizer is adapted using any of a number of available methods (e.g. the LMS algorithm) and the error signal is the difference between the desired signal and the equalizer output.

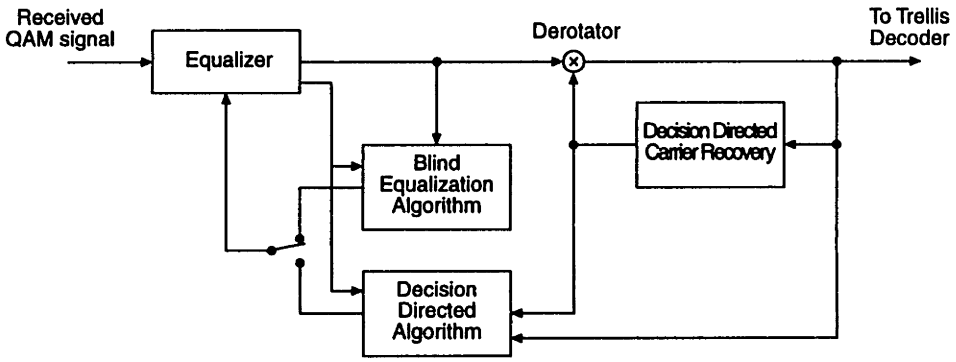

Figure 2-10: Joint carrier recovery and equalization.

2.4.6.2 Timing recovery

Timing recovery is somewhat less critical, in terms of performance sensitivity, than carrier recovery, but is important nonetheless. Under normal conditions, uncertainty in the frequency of the timing reference can be kept rather small, typically of the order of one part in 10^6. A popular approach is to square the outputs of the low-pass filters and extract from their sum the spectral line component at frequency $1/T$. A simplified diagram is shown in Figure 2-11. This line component could be generated instead via a square-law envelope detection of the IF signal. It is also possible to apply decision-directed methods to timing recovery.

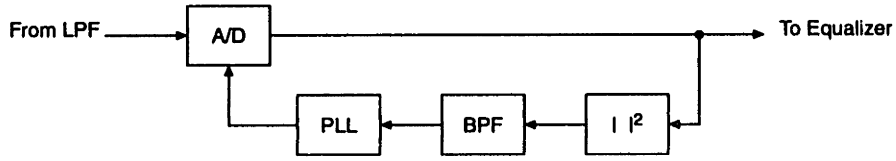

Figure 2-11: Simplified timing recovery loop.

It is important to note, however, that timing phase errors can have a deleterious effect on

equalizers with tap spacing equal to the signaling interval T (sometimes called synchronous equalizers) [76]. Transversal equalizers have transfer functions that are periodic in the frequency domain, and in synchronous equalizers the period is equal to the Nyquist bandwidth (the reciprocal of the symbol period). Since roll-off factors of 15% are typical for transmission with high-bandwidth efficiency, synchronous equalizers cannot make independent corrections in both the Nyquist bandwidth and the excess bandwidth, so that exact equalization is generally impossible. To see how the residual distortion is influenced by shifts in the symbol timing phase, note that, because of the sampled detection process, the equalizer effectively operates on the folded channel spectrum, whose shape depends on the phase of the sampling clock [63]. An improper sampling instant may lead to a folded spectrum with deep troughs or even nulls, and this considerably limits the performance obtainable from a synchronous equalizer.

Fractionally-spaced equalizers are able to overcome this difficulty. For example, consider a system designed with a raised-cosine spectral roll-off, in which case the signal bandwidth never exceeds twice the Nyquist bandwidth. An equalizer with tap spacings equal to $T/2$ synthesizes a transfer function with a period equal to twice the Nyquist bandwidth, and is insensitive to changes in the sampling instant. Indeed, FSEs can perform much or all of the receiver filtering.

2.4.7 High-power amplification

Current planning factors call for average transmitter effective radiated powers (ERP) of 24 dBk (decibel referred to 1 kW) for 32QAM and 20.4 dBk for 16QAM. It is easy to compute the peak-to-average ratios for the 16QAM and 32 QAM constellations. These are equal to 2.55 dB and 2.30 dB respectively. However, the peak-to-average ratios of the analog waveform are larger than these values because of filtering. Simulations of 16QAM and 32QAM filtered by a square-root raised cosine filter with excess bandwidth $\alpha = 0.1$ yield peak-to-average ratios of 7.25 dB and 6.55 dB respectively. IF filtering may further increase the peak-to-average ratios. Such peak-to-average ratios are problematic because they bring the peak powers of digital HDTV within the same range as NTSC peak powers. However, digital transmission of high-rate QAM signals places very stringent requirements on linearity at each stage of processing. Figure 2-12 shows a typical transfer characteristic of a klystron high power amplifier such as is used for NTSC UHF transmission [5].

The nonlinear amplitude and phase characteristics of these amplifiers cause intermodulation products and out-of-band spectral regrowth. The impact of even relatively small amplitude and phase distortions (on the order of 10% AM/AM conversion and a few degrees AM/PM conversion) can be quite severe when signaling with multiphase/amplitude waveforms. This effect is expected to be aggravated by the use of trellis-coded modulation. To mitigate the effect that

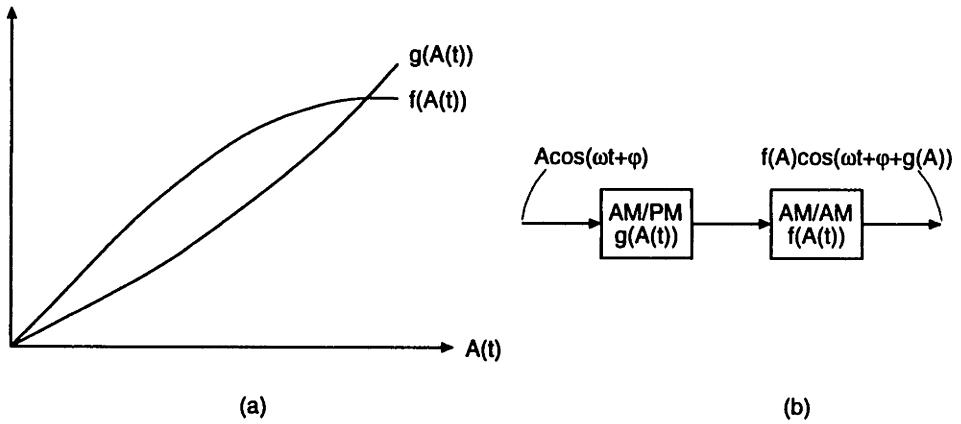

Figure 2-12: (a) Typical amplitude and phase transfer functions of an envelope nonlinearity. (b) Model for AM/AM and AM/PM envelope nonlinearity.

such a nonlinearity might have on the performance of the transmission system, it is possible to apply some form of pre-compensation (if the nonlinearity is memoryless, one can predistort the signal by using the inverse functions $f^{-1}(A)$ and $g^{-1}(A)$). It is still too early to predict precisely the impact such nonlinearities will have on the efficiency of the transmission, nor is it the purpose of this thesis to study these impairments. However, while investigating other aspects of the transmission system, it is desirable to keep them in mind.

2.5 Conclusion

In this chapter, we have attempted to provide an overview of the requirements and characteristics of HDTV for terrestrial broadcast applications. The video requirements were briefly outlined. The requirements for over-the-air broadcasting were then discussed. While some of the requirements may be subject to change, we chose to describe the elements that appear to be common to most transmission systems. These include coding, modulation, filtering and synchronization.

In many ways, the techniques proposed so far for HDTV represent a combination of the techniques used in digital telephony and those used for satellite transmissions. There are, however, a number of important differences between the television broadcast channel and these better studied channels. The next chapter discusses in greater depth the HDTV broadcast channel. In particular, the characteristics of multipath (or frequency selective channels) and fading channels will be explored in more detail. Co-channel interference, an impairment specific to HDTV, will also be discussed.

3

Modeling channel distortion

3.1 Introduction

Like most other real-world communication channels, HDTV systems designed to communicate information over the terrestrial broadcast channel face a variety of impairments. In the previous chapter, it was seen that some of these impairments are due to regulatory constraints while others are due to transmission medium and system limitations. The most important impairments, however, prove to be multipath propagation (both static and dynamic), co-channel interference from neighboring television transmitters (both NTSC and HDTV), channel and receiver noise, and fading. One of the challenging aspects of designing a transmission system for such a channel is that these impairments are a priori unknown and may vary from receiver to receiver.

In this chapter, we establish mathematical models for the HDTV broadcast channel in order to provide a basis for the design of reliable transmission schemes for digital high-definition television broadcasting. In particular, we review the characteristics of multipath (or frequency-selective) channels and fading channels. A clear distinction between these two types of channels is useful in analyzing the performance of multicarrier modulation schemes in the last chapter of this thesis.

3.2 Bandwidth constraint

In contrast to channels such as the voiceband telephone channel, there are no significant physical restrictions on the bandwidth of radio frequency channels. However, in order to enable multiple communication links to share the same medium without mutual interference,

regulatory bodies have traditionally chosen to partition the radio frequency spectrum into non-overlapping frequency bands. This is known as frequency division multiplexing (FDM). While FDM may not be optimum for certain types of channels, it is by far the most common scheme in use for the transmission of analog information. Both commercial radio and television transmissions are based on FDM. Digital television too will use FDM, as it is required to operate within the existing VHF and UHF bands, in coexistence with analog television.

In practice, FDM is implemented by assigning a predefined and unique frequency band to each communication link. Interference between adjacent channels (Adjacent Channel Interference, or ACI) is kept to a minimum by placing strict limitations on the amount of out-of-band energy that each user can produce. Typically, the body in charge of regulating the use of the radio spectrum (the FCC in the United States) publishes a set of emission masks which specify the overall shape and tolerance of the transmitted signal spectrum. In order to achieve the desired spectral shaping, the transmitter must be equipped with bandpass filters with very sharp cutoffs and very high stopband attenuations (typically of the order of 40 dB or higher at the band edge). Similar bandpass filters are also required at the receiver in order to eliminate all but the desired signal. A complicating factor is the nonlinear characteristic exhibited by certain types of high-power amplifiers (HPA) in the transmitter. These nonlinearities create out-of-band energy, a process known as spectral regrowth. In order to limit the amount of out-of-band emissions to acceptable levels, it is common to perform some filtering after amplification by the HPA.

Thus, even though there are no physical bandwidth limitations from a modeling standpoint, one can think of the transmitter bandpass filter as being part of the channel (in the absence of nonlinearities) since the effect is the same as if the channel itself had a frequency response corresponding to the transmit filter. It is in this sense that the channel is bandlimited.

3.3 Multipath impairments

On many communication channels, energy spreads and disperses in time. For radio channels such as UHF and VHF television channels, time dispersion is caused primarily by the existence of multiple paths between transmitter and receiver: this process is known as multipath propagation. For instance, there may be a line-of-sight path, and in addition several paths resulting from reflections off buildings or other obstacles such as hills and mountains. It is worth noting that free-space propagation in itself does not introduce appreciable dispersion. However, antennas have gains that depend on frequency, so that the free-space channel, including transmitting and receiving antennas, exhibits a slowly-varying dependence of attenuation on frequency. At UHF, the relative variation of the frequency response is of the order of a small

fraction of a dB across the 6 MHz bandwidth, and is therefore normally neglected.

In the case where the received signal is composed of a small number of distinct paths with little temporal variability, the channel may be modeled as a linear time-invariant filter with impulse response

$$h(t) = \sum_k \alpha_k \delta(t - \tau_k) \tag{3.1}$$

where each path is characterized by a time delay τ_k and an attenuation α_k. This simple model is illustrated in Figure 3-1.

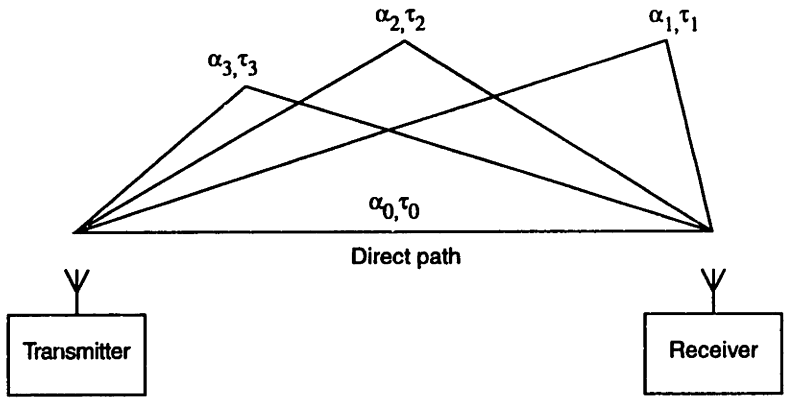

Figure 3-1: Discrete multipath model.

Under normal circumstances the strongest signal, corresponding to the direct path, reaches the receiver first, and weaker indirect signals (sometimes called echoes) follow. This type of multipath propagation causes each received symbol to be corrupted by postcursor intersymbol interference (ISI). It is also possible, under special conditions, that there is no direct path between transmitter and receiver. The strongest signal may then be preceded by several leading echoes, causing precursor ISI to corrupt each received symbol. Methods for combatting these impairments are examined in Chapters 6 and 7.

Clearly, the corresponding frequency response is given by

$$H(\omega) = \sum_k \alpha_k \exp(-j\omega\tau_k) \tag{3.2}$$

This frequency response can be expressed in magnitude-phase form by

$$H(\omega) = |H(\omega)| \exp(j\Phi(\omega)) \tag{3.3}$$

Conventionally, the channel is characterized by a dB attenuation $A(\omega)$ and a delay distortion (or group delay) $D(\omega)$, where

$$A(\omega) = -20 \log |H(\omega)| \tag{3.4}$$

$$D(\omega) = -\frac{\partial \Phi(\omega)}{\partial \omega} \tag{3.5}$$

When the maximum time delay difference $\Delta\tau$ between the paths is small compared to the inverse of the signal bandwidth W ($|W\Delta\tau| \ll \pi$), the effect of the multipath is a signal attenuation and group delay that are nearly constant across the bandwidth. This case corresponds to a narrowband model. When the delay spread is greater than the inverse of the signal bandwidth ($|W\Delta\tau| \gg \pi$), the attenuation and group delay will vary across the bandwidth of the signal. Such a channel is said to be frequency selective. It is interesting to note that the phase of the k-th path changes by 2π whenever τ_k changes by $1/f_c$, where f_c is the carrier frequency. Typically, f_c is a large value, and as a consequence, the phase varies very rapidly even for small changes in the transmitter/receiver geometry. For example, at 600 MHz, a phase change of π corresponds to displacing the antenna by a half wavelength, or 0.25 m. The attenuation α_k, on the other hand, will vary very little over such a small distance. Therefore, while the channel frequency response will vary substantially, and in a seemingly random fashion, for relatively small changes in the position of the receiver with respect to the transmitter, the power output of the channel as a function of time delay will remain almost the same.

A more complex model results if there are a large number of scatterers in the neighborhood of the receiver. For example, a complex multipath structure may result from the presence of dense vegetation in a wooded residential area, or from the presence of many reflective surfaces (buildings) in an urban environment. In such cases, it is more appropriate to view the received signal as consisting of a continuum of multipath components. Because the multipath structure is highly complex, an exact description of the channel characteristics would be impossible or unwieldy. Therefore, the channel behavior is often described in statistical terms, as though the underlying phenomena were random. A possible statistical description would be through a random impulse response function $h(t)$, relating the channel input $x(t)$ to the channel output $y(t)$ through

$$y(t) = \int_{-\infty}^{\infty} x(t-\tau)h(\tau)\,d\tau \tag{3.6}$$

In this model, $h(\tau)$ represents the response of the channel at time t due to an impulse at time $t-\tau$. $h(t)$ is a random function which depends on the location of the receiver. An antenna at a different location in the same area will receive a signal with similar statistical characteristics, but will not have the same impulse response function $h(t)$. A statistical description of the channel characteristics can be helpful in determining an average receiver performance.

In general, multipath has adverse effects on the performance of the receiver. From a practical point of view, therefore, it is desirable to ensure that there is a line-of-sight path between the transmitter and receiver. In such cases, highly directional antennas can provide effective protection against multipath when the direction of arrival of the multipath is sufficiently different from the direction of the LOS signal. When this is not the case, equalization must be performed inside the receiver. The subject of equalization is treated in depth in Chapters 6 and 7.

3.4 Fading impairments

So far, the models for multipath have been static channels. However, even when the transmitter and receiver are at fixed locations with respect to one another, multipath propagation is a time-varying phenomenon, due to many possible factors including atmospheric phenomena and transmitter tower sway. Other sources of temporal variations of the channel characteristics include reflections from airplanes, automobile traffic, or even swaying trees in the neighborhood of the receiver.

Let us consider again the case where the received signal is formed by a number of distinct paths. As shown in [75], the channel may be modeled as

$$h(\tau, t) = \sum_k \alpha_k(t)\delta(\tau - \tau_k(t)) \tag{3.7}$$

In some cases, it is more appropriate to view the received signal as consisting of a continuum of multipath components. Then the received signal $y(t)$ is expressed as

$$y(t) = \int_{-\infty}^{\infty} \alpha(\tau, t)x(t - \tau)\, d\tau \tag{3.8}$$

Because of the time-varying nature of the multipath, the delays are random variables which cause the different paths to combine with random phases. Because the carrier frequency is large, the respective phases of the different paths vary randomly so that the paths combine in an unpredictable, time-dependent fashion. When the number of paths is large, the central limit theorem can be applied and the time-variant impulse response becomes a complex-valued Gaussian random variable.

The properties of such a random time-varying channel are best described statistically, via a number of correlation and power spectral density functions. One possible characterization is via the coherence bandwidth and coherence time functions.

3.4.1 Coherence bandwidth

The coherence bandwidth of a channel is the maximum width of the band in which the statistical properties of the transmission coefficients of two sinusoids are strongly correlated. Coherence bandwidth can be defined as that frequency separation Δf for which the magnitude of the normalized complex coefficients first drops below a certain value (typically taken to be 0.5). Thus, two sinusoids with frequency separation greater than Δf will be affected differently by the channel. The coherence bandwidth function is directly related to the time-delay spread of the channel, mentioned earlier. An estimate of the coherence bandwidth can be obtained by

taking the inverse of the time-delay spread, that is

$$\Delta f \approx \frac{1}{T_m} \tag{3.9}$$

where T_m is the time-delay spread arising from multipath propagation [75].

When the coherence bandwidth is small compared to the bandwidth of the transmitted signal, the fading is said to be frequency-selective. This is frequently the case in HDTV broadcasting: for a typical value of $T_m = 10\mu s$, the coherence bandwidth is of the order of 100 kHz, which is many times smaller than the transmission bandwidth of 6 MHz.

3.4.2 Coherence time

The coherence time of a channel is used to characterize the time variations of the channel. The time variations in the channel are evidenced as a Doppler broadening and, in addition, as a Doppler shift of a spectral line. A measure of the coherence time of the channel is the inverse of the Doppler spread of the channel, that is

$$\Delta T_c \approx \frac{1}{B_d} \tag{3.10}$$

where B_d is the Doppler spread of the channel. A slowly changing channel has a large coherence time, or equivalently a small Doppler spread. In general, this is believed to be the case for HDTV, since time variations take place on the scale of several thousands of symbols.

3.4.3 Receiver performance

In general, receiver performance degrades with smaller coherence bandwidths and shorter coherence times. An effective countermeasure is to use time and frequency diversity to establish a reliable communication channel between transmitter and receiver. However, these diversity techniques reduce the data rate that can be transmitted through the channel. The degree to which the data rate must be reduced in order to achieve reliable communications depends on the extent to which a multipath channel is fading. The severity of the fading process is typically much larger when the receiving unit is mobile than when it is fixed. In the case of high-data-rate transmissions to fixed receivers, as is the case for the planned HDTV service, the channel variations are typically slow compared to the signaling interval. In many cases, it is possible to assume that the channel characteristics do not change over the period of usage. These aspects will be considered in detail in Chapter 8, when examining the performance of multicarrier modulation.

3.5 Interference impairments

3.5.1 NTSC co-channel interference

With the overall radio spectrum allocated to over-the-air television broadcasting remaining unchanged, HDTV must resort to using channels that had previously been designated as unusable because of interference considerations (the so-called taboo channels). The requirement of coexistence with NTSC transmissions limits the power available for HDTV broadcasting; however, it is generally agreed that, in order to be commercially viable, a new terrestrial broadcasting service will need to provide coverage comparable to the NTSC grade B service areas. These assumptions are based on the notion that the infrastructure of the new service will be similar to the existing one, with a relatively small number of transmitter stations providing service to fairly large areas.

The low-power requirement, coupled with the necessity for reduced co-channel spacings, means that interference from NTSC will be particularly strong in some locations. Figure 3-2 summarizes some of the essential parameters of the problem.

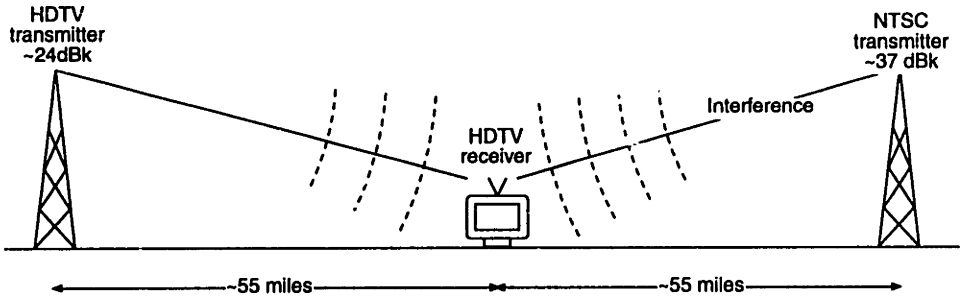

Figure 3-2: NTSC co-channel interference from spatially adjacent transmitter.

Current planning factors indicate that the transmission channel will be interference-limited rather than noise-limited for a sizable proportion of the coverage area. In order to make efficient use of the limited power and bandwidth resources, it is important to design transmission schemes that specifically address the co-channel interference problem. This topic will be covered in detail in Chapter 6. In this section, we describe the main characteristics of an NTSC signal and then develop several models which will be used in subsequent chapters to evaluate receiver techniques designed to combat NTSC co-channel interference.

3.5.2 NTSC signal format

An NTSC composite video signal is made up of several components: a video signal derived from the picture information by scanning a raster in an interlaced fashion; synchronizing pulses to help the receiver maintain proper line and field synchronization; and, blanking pulses to make the retrace lines invisible during the retrace intervals. A short segment of a composite video signal corresponding to two NTSC scan lines is shown in Figure 3-3, where, for simplicity, the short burst of the color subcarrier on the back porch of the blanking pulses has been omitted. Following the sequence of line scans is a vertical blanking interval representing 5 to 8 percent of the duration of a field. A special sequence of vertical synchronization pulses is transmitted during this interval to synchronize the receiver's vertical sweep.

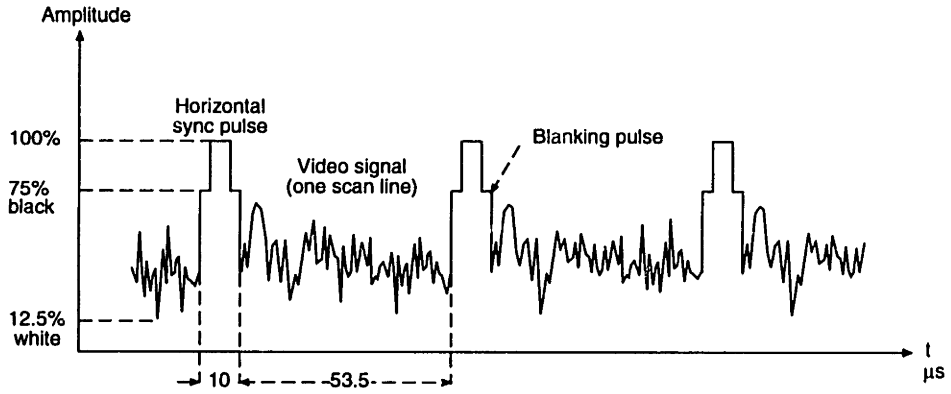

Figure 3-3: NTSC composite video signal.

The sequence of blanking and synchronization pulses is defined very precisely in the NTSC standard and is easily detectable by specialized circuitry. We will therefore assume that the interference caused by the synchronization information can be removed by specialized means without prejudice to the received signal, and we will, instead, focus our attention on the random part of the composite signal, namely the video and audio signals. In the absence of specialized circuitry to remove the synchronization pulses, we will see that the receiver can still be made to function correctly by relying on the burst-error correction capability of block codes and by interleaving the signal sequence appropriately.

For color television, the video signal consists of three components: a luminance signal $x_Y(t)$ and two chrominance components $x_I(t)$ and $x_Q(t)$. These components are typically obtained by a linear combination of a set of primary color signals such as red, green and blue, as produced by a color television camera. An important consideration in the choice of the YIQ signal components is the fact that the luminance signal can be used directly by monochrome television receivers without further processing. Another consideration relates to

the bandwidth and power of the different components. On average the chrominance signals $x_I(t)$ and $x_Q(t)$ are much smaller than the luminance signal $x_Y(t)$ and occupy a much smaller effective bandwidth. Thus, $x_I(t)$ and $x_Q(t)$ can be bandlimited without seriously affecting the perceived quality of the reproduced color picture. Typically, $x_I(t)$ is bandlimited to 1.5 MHz, and $x_Q(t)$ is bandlimited to 0.6 MHz.

The audio information represents a very small portion of the total information carried by the television signal since the unmodulated signal bandwidth is approximately 10 kHz. The power of the aural carrier is typically 7 to 13 dB below that of the visual carrier.

Let us now consider how the luminance, chrominance and audio information are transmitted within a 6 MHz band. An idealized view of the NTSC spectrum, as transmitted, is shown in Figure 3-4.

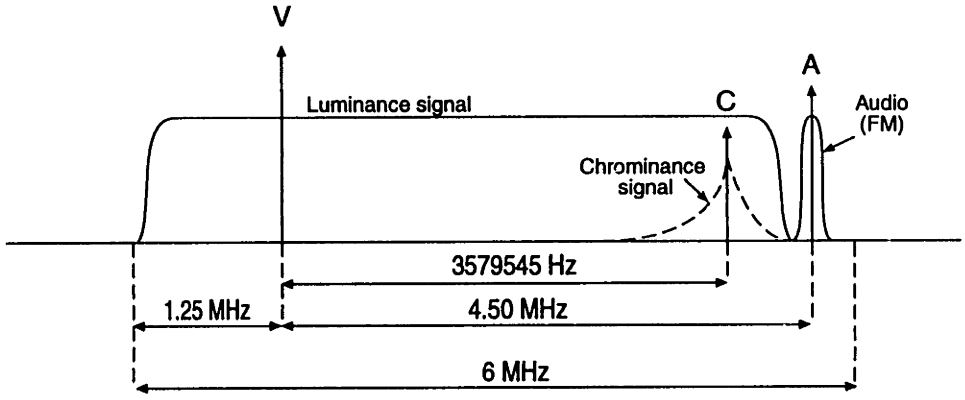

Figure 3-4: Idealized spectrum of transmitted NTSC signal.

In order to conserve bandwidth, the luminance signal is transmitted using vestigial sideband modulation (VSB). The transmitted signal has a number of characteristics. The upper sideband of the video signal is transmitted without attenuation up to 4 MHz. Signal components above 4 MHz are attenuated so that the video signal does not interfere with the lower sideband of the sound carrier located 4.5 MHz away from the video carrier. The lower sideband of the picture carrier is transmitted without attenuation over the range 0 to .75 MHz. It is important to note that the modulated video signal, as transmitted, is not shaped like a VSB signal. Precise VSB shaping is performed at the receiver before demodulation. This implies that the interference signal as seen by an HDTV receiver is mostly an AM signal with a small VSB component corresponding to the high spatial frequencies of the picture. Thus, the luminance component can be written as

$$s_Y(t) = A[1 + x_Y(t)]\cos\omega_V t + Ay_Y(t)\sin\omega_V t \tag{3.11}$$

where $x_Y(t)$ is the luminance waveform, ω_V is the NTSC carrier frequency and $y_Y(t)$ is a term

arising from the VSB modulation ($y_Y(t)$ is equal to zero for double-sideband AM and to the Hilbert transform of $x_Y(t)$ for pure single-sideband modulation). Since $|y_Y(t)| \ll 1$, we will approximate the luminance component by

$$s_Y(t) = A[1 + x_Y(t)] \cos \omega_V t \tag{3.12}$$

Further bandwidth savings are achieved in the NTSC system by exploiting the spectral properties of signals obtained by raster-scanning two-dimensional images. Specifically, successive scan lines of a television picture are on average highly correlated. This holds true for both the luminance and the chrominance signals. As a result, for most pictures, there is very little spectral energy between the line-rate harmonics, making it possible to interleave the chrominance and luminance spectra within the same frequency band. Spectrum interleaving is accomplished by offsetting the chrominance subcarrier by exactly $227.5 f_H$ (approximately 3.58 MHz) with respect to the luminance carrier, where f_H is the NTSC line rate ($\approx$ 15.734 kHz). The two chrominance signals are used to modulate two quadrature components of the color subcarrier, thus defining a double-sideband suppressed-carrier signal centered around the color subcarrier. However, this implies that the modulated version of $x_I(t)$ extends above the allocated total channel bandwidth, and when the composite signal is bandlimited to 4.2 MHz, $x_I(t)$ loses part of its upper sideband.

In summary, we can describe the video signal by the following relation

$$\begin{aligned} s(t) &= A[1 + x_Y(t)] \cos \omega_V t \\ &\quad + x_Q(t) \sin \omega_C t \\ &\quad + x_I(t) \cos \omega_C t + \hat{x}_I(t) \sin \omega_C t \end{aligned} \tag{3.13}$$

where ω_V and ω_C are the frequencies of the video and color carriers respectively, and where $\hat{x}_I(t)$ is a term resulting from the partial removal of the upper sideband of $x_I(t)$.

As an aside, there is an additional advantage to choosing a frequency offset that is an odd multiple of one-half the line frequency. When a color signal is applied to a monochrome display, the relatively high-frequency variations produced by the chrominance signal reverse in phase from line to line. This produces flickering in small areas that average out in time and space. Thus, under normal viewing conditions, the chrominance signal produces very little disturbance on a monochrome display.

Finally, the audio signal is transmitted by frequency modulation on a separate carrier located 4.5 MHz above the visual carrier, with a frequency deviation of 25 kHz, which, assuming an audio bandwidth of 10 kHz, amounts to an FM bandwidth of 70 kHz. Thus, there is no spectral overlap between the audio signal and the video signal.

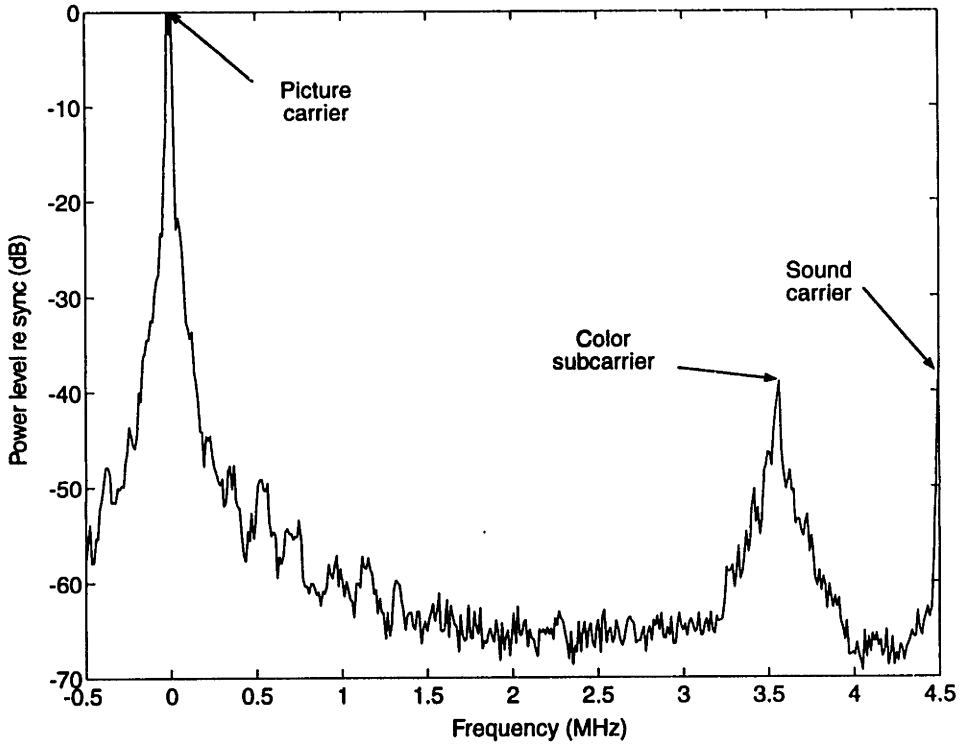

Figure 3-5: Amplitude spectrum of a typical NTSC program video signal averaged over a one-hour period.

3.5.3 Luminance signal models

So far, we have examined how the video signal is formatted for transmission. We have seen that the luminance signal is bandlimited to 4.2 MHz before transmission and transmitted using a form of VSB modulation. If the actual spectrum had the shape indicated on Figure 3-4, there would be very little scope for reducing the impact of co-channel interference. We will show in Chapter 6 that the ability to reject co-channel NTSC interference is directly related to the predictability of the interference, which, in turn, is related to the spectral flatness of the interference. Let us here examine the power spectral density of an actual signal. Figure 3-5 displays a representative example of the power spectrum of an NTSC signal averaged over a one hour period.

Several observations can be made based on this graph:

- Most of the signal power is concentrated around the video carrier frequency and therefore, from an interference standpoint, the luminance portion of the NTSC signal is the most important contributor to NTSC co-channel interference impairments.
- The power spectral density decreases rapidly away from the video carrier frequency.

Thus, the NTSC signal is mostly lowpass.

- A substantial amount of power is used by the video carrier itself.

Several more observations can be made by examining the details of the spectrum around the video carrier frequency or at baseband, before modulation. A schematic view of the luminance power spectrum at baseband is shown in Figure 3-6. This figure illustrates that the NTSC

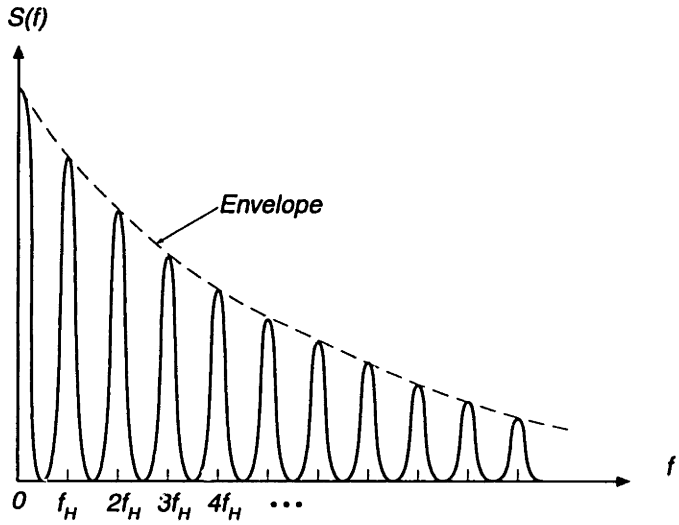

Figure 3-6: Spectrum of a raster-scanned video signal.

luminance spectrum exhibits strong periodicities at the line-scan rate f_H = 15.75 kHz and its harmonics. The peaks in Figure 3-6 are due to the vertical sampling inherent in raster-scanning and to the high correlation between successive scan lines. In addition:

- The bandwidth of the spectral envelope is determined mainly by the horizontal spatial frequencies.
- The width of the harmonic peaks is determined mainly by the vertical spatial frequencies.

Most pictures are highly correlated, both along the vertical dimension and along the horizontal dimension. For such pictures, there is very little spectral energy between the line-rate harmonics, and the envelope of the spectrum tends to have a relatively narrow bandwidth.

Figure 3-7 shows the detail of the power spectral density function for a simulated luminance signal with vertical and horizontal normalized correlations equal to 0.9. From this graph, it is clear that the energy is concentrated near DC in a few narrow peaks separated by the line scan rate.

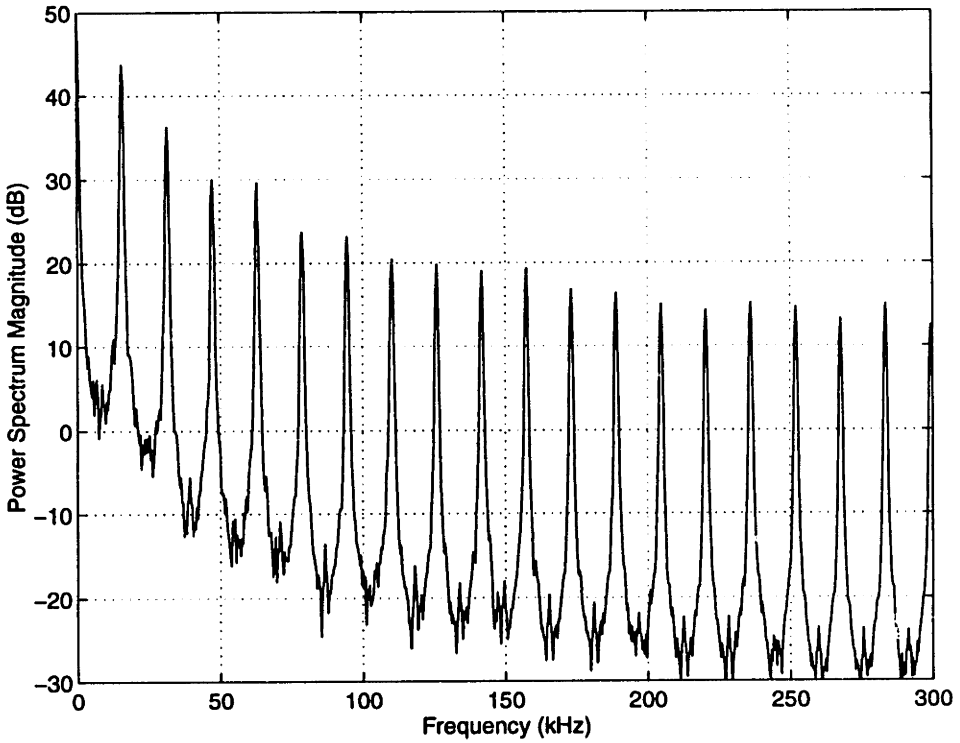

Figure 3-7: Spectrum of luminance signal near DC (simulation).

In order to develop intuitive understanding and derive some analytical results, we will find it useful to develop simple models to describe the spectrum of the luminance signal. Although the actual implementation of interference reduction techniques are typically adaptive and do not assume a specific model, models provide useful guidelines for evaluating different equalization and interference reduction techniques.

One particularly simple way of modeling the statistical properties of an image is by means of a two-dimensional Markov process. We are interested in predicting samples of this process using a prediction model. Here, we shall confine our discussion to all-pole linear prediction models, as they lend themselves to easy analysis and are very useful in practice. We also assume that the signal is sampled, in order to work with discrete-time signals.

3.5.3.1 Random field model

Let us assume that the image data is produced by a stationary Markov model with a separable autocorrelation function of the form

$$R_{xx}(x_h, x_v) = \sigma_x^2 \exp(-\alpha|x_h| - \beta|x_v|) \tag{3.14}$$

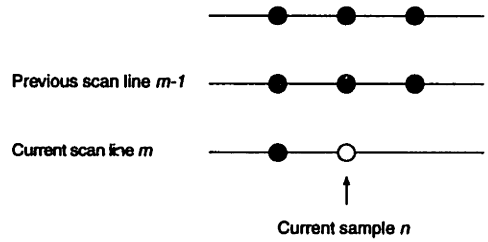

Figure 3-8: Two-dimensional prediction.

where x_h and x_v are the spatial shifts in horizontal and vertical image directions and α and β describe respective amounts of correlation. Let us use a spatially discretized description, with

$$\rho_h = e^{-\alpha}; \qquad \rho_v = e^{-\beta} \tag{3.15}$$

Using integer-valued variables k_h and k_v,

$$R_{xx}(k_h, k_v) = \sigma_x^2 \rho_h^{|k_h|} \rho_v^{|k_v|} \tag{3.16}$$

We will assume in the remainder that $\rho_h = \rho_v = \rho$.

In the next paragraphs, we examine the effect of modeling the two-dimensional random field with simple prediction models and estimate the loss that results from a mismatch between the source model and the prediction model.

3.5.3.2 First-order prediction

One of the simplest methods of predicting the current sample is by using the neighboring sample on the current line or the sample located above the current sample. This is first-order prediction. Let the prediction be denoted by $\hat{x}(n) = h_1 x(n-1)$. The prediction error is

$$z(n) = x(n) - h_1 x(n-1) \tag{3.17}$$

and the variance of the error is

$$\sigma_z^2 = (1 + h_1^2 - 2\rho h_1)\sigma_x^2 \tag{3.18}$$

where σ_x^2 is the variance of the signal. The minimum prediction error is achieved for $h_1 = \rho$, and is equal to $\sigma_z^2 = (1 - \rho^2)\sigma_x^2$.

Consider the case of mismatched predictor where $h_1 = 1$. The prediction error is then equal to $\sigma^2 = 2(1 - \rho)\sigma_x^2$, implying a loss of $2(1 - \rho)/(1 - \rho^2)$. For $\rho = 0.95$, this represents a loss of 0.1 dB.

3.5.3.3 Second-order prediction

A better prediction may involve using two previous samples, for example $\hat{x}(m,n) = h_1 x(m,n-1) + h_2 x(m-1,n)$. This assumes a source model of the form

$$x(m,n) = h_1 x(m,n-1) + h_2 x(m-1,n) + z(m,n) \tag{3.19}$$

The optimum values of the taps are

$$h_1 = h_2 = \rho/(1+\rho^2) \tag{3.20}$$

and the prediction error is $\sigma_x^2(1-\rho^2)/(1+\rho^2)$. For $\rho = 0.95$, the error is 2.8 dB smaller than with the optimal first-order predictor.

3.5.3.4 Third-order prediction

Consider a prediction of the form $\hat{x}(m,n) = h_1 x(m,n-1) + h_2 x(m-1,n) + h_3 x(m-1,n-1)$, i.e. a model of

$$x(m,n) = h_1 x(m,n-1) + h_2 x(m-1,n) + h_3 x(m-1,n-1) + z(m,n) \tag{3.21}$$

The optimal tap setting is $h_1 = h_2 = \rho, \quad h_3 = -\rho^2$. The variance is then equal to $\sigma_z^2 = \sigma_x^2(1-\rho^2)^2$. For $\rho = 0.95$, the error is 10.1 dB smaller than with the optimal first-order predictor.

An approximation to this predictor is $h_1 = h_2 = 1, \quad h_3 = -1$. The prediction can be written in two ways to provide more insight

$$\hat{x}(m,n) = x(m,n-1) + (x(m-1,n) - x(m-1,n-1)) \tag{3.22}$$

$$= x(m-1,n) + (x(m,n-1) - x(m-1,n-1)) \tag{3.23}$$

In other words, the prediction is $x(m,n-1)$ plus estimate of horizontal slope, or $x(m-1,n)$ plus estimate of vertical slope.

3.5.3.5 Raster-scanned signal

The luminance signal is obtained by raster-scanning a two-dimensional image of width N. The map $(m,n) \mapsto mN+n$ defines the raster-scanning operation. Eq. (3.21) with optimal tap settings then becomes

$$x(n) = \rho x(n-1) + \rho x(n-N) - \rho^2 x(n-N-1) + z(n) \tag{3.24}$$

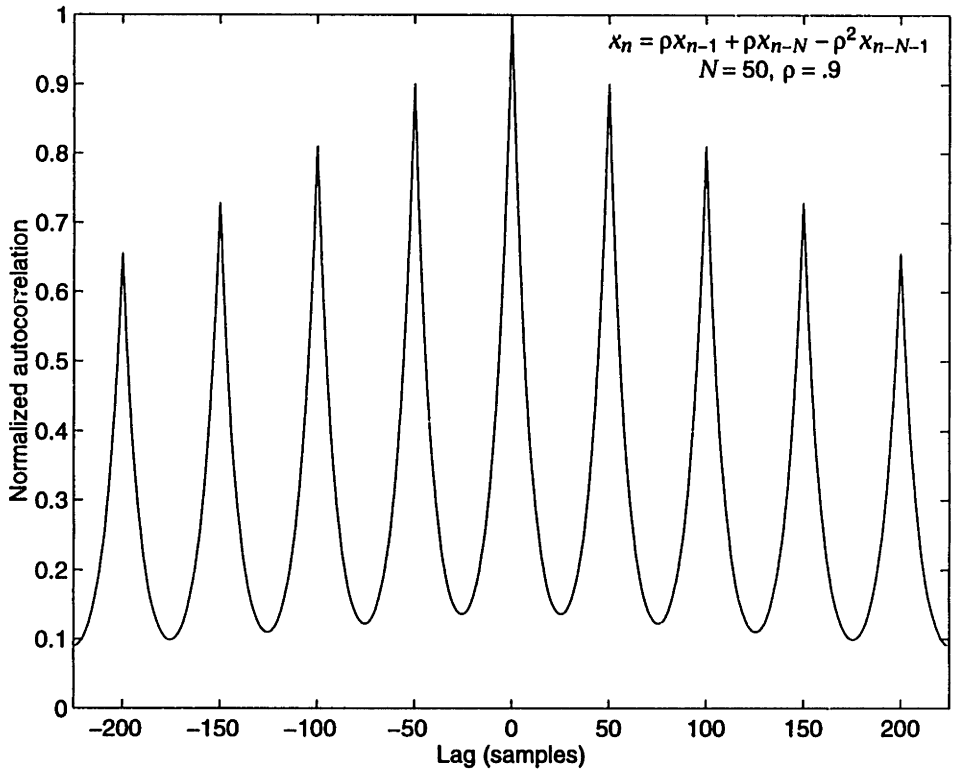

Figure 3-9: Normalized autocorrelation function for an interference model of the form $x(n) = \rho x(n-1)+\rho x(n-N)-\rho^2 x(n-N-1)+z(n)$, with $N = 50$ and $\rho = .9$.

This signal model exhibits some of the characteristics of the interference signal that we will be trying to reduce in Chapter 6. The normalized autocorrelation function for $\rho = 0.9$ and $N = 50$ is shown in Figure 3-9. We shall use this model in the simulations of Chapter 6. Strong correlations exist between samples separated by a multiple of the line length, as is the case in a real-world NTSC signal.

3.6 Conclusion

In this chapter, we have outlined the channel impairments that are believed to be the most important for HDTV broadcasting. These include multipath impairments, fading impairments and interference from neighboring co-channel NTSC transmitters. We have proposed a mathematical model for the NTSC interference that exhibits some of the observed characteristics of an NTSC signal, from the point of view of the impact on an HDTV signal. This model will later be used to assess the performance of difference equalization and interference rejection schemes.

4

Channel coding for the HDTV Gaussian channel

4.1 Introduction

In this chapter, we begin by introducing several fundamental concepts of channel coding, providing a sound theoretical basis for later chapters. To this end, we introduce the classical channel coding concepts of channel capacity and channel signal-to-noise ratio (SNR) and the newer concept of normalized signal-to-noise ratio [42] as they apply to the ideal bandlimited Gaussian channel. These concepts are helpful in understanding the fundamental limits of communication over channels such as the bandlimited multipath channel.

Next, we consider the specific case of the digital broadcast channel in order to identify specific characteristics. A distinguishing feature of the digital broadcast channel is the absence of a reverse channel. Transmission schemes that require the active cooperation of the transmitter in order to achieve a reliable transfer of information are therefore excluded. This includes many schemes used on telephone channels where the channel is initially probed and the transmitter characteristics are set up accordingly. For the digital broadcast channel, the inability to tailor the transmit spectrum, power, and data rate to each individual receiver means that many receivers will operate far below the channel capacity limit.

Other features specific to HDTV broadcast transmission can however be exploited. For instance, there is little reason not to use techniques such as concatenated coding on the digital television channel, since low delay is not as critical as for other channels. Block coding, even though it imposes a fixed decoding delay, is also universally used in digital television broadcasting. Heavy use of interleaving is also possible, and is very beneficial.

Currently proposed digital HDTV systems use a simple trellis code with a low coding gain, or even no trellis code at all. In this chapter, we examine the rationale for these choices. We investigate the tradeoffs involved in choosing an efficient error-control coding scheme.

We make use of the general concepts introduced at the beginning of this chapter to evaluate different coding schemes whenever possible. Where the applicability of these concepts is questionable, a simulation approach is used. We compute the detailed weight distribution of several trellis codes to quantify the effect of non-minimum-distance error events on performance at low signal-to-noise ratios, and show why some of the concatenated coding schemes currently proposed are able to achieve good performance at the error rates at which they were designed to operate.

4.2 Channel capacity and normalized SNR

4.2.1 The bandlimited Gaussian channel

A basic but quite general channel model is the so-called bandlimited Gaussian channel. Figure 4-1 shows its general structure.

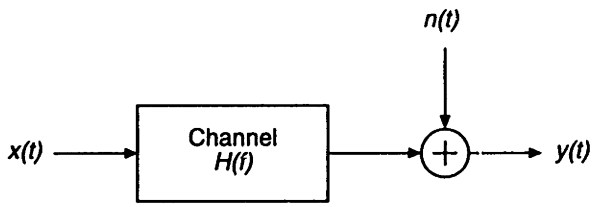

Figure 4-1: The bandlimited Gaussian channel model.

In this model, the channel output is given by

$$y(t) = x(t) * h(t) + n(t)$$

where $*$ denotes convolution, $h(t)$ is the impulse response of the channel and $n(t)$ is additive Gaussian noise. The input signal $x(t)$ is assumed to be a random process which must satisfy bandwidth and power constraints

$$\int_W S_{xx}(f)df \leq P$$

where W and P are the bandwidth and power constraints respectively, and $S_{xx}(f)$ is the power spectral density of the input process. The noise process $n(t)$ is characterized by its power spectral density $S_{nn}(f)$. A quantity which will subsequently be important is the channel signal-

to-noise function $\mathrm{SNR}_c(f)$, defined as

$$\mathrm{SNR}_c(f) = \frac{|H(f)|^2}{S_{nn}(f)} \tag{4.1}$$

The limitations of this model are clear. This model is adequate for linear time-invariant (LTI) channels where the noise is additive and independent of the input. It does not apply to nonlinear, time-varying channels, or to channels degraded by non-Gaussian noise or interference. Still, it is a very useful model for many practical channels, and in particular for the HDTV channel between a transmitter and a single receiver.

4.2.2 Channel capacity

Information theory provides a particularly simple characterization of the bandlimited Gaussian channel. Indeed, a cornerstone result is that a channel such as that of Figure 4-1 is characterized by a single parameter, the channel capacity $\tilde{C}$. The significance of this parameter for coding is that there exist coding schemes for any data rate $\tilde{R} < \tilde{C}$ (in bits per second) that achieve arbitrarily low error probabilities Pr(E), and, conversely, that there exists no scheme with rate $\tilde{R} > \tilde{C}$ that can achieve a low error probability Pr(E).

The channel capacity is obtained by maximizing the mutual information $I(X;Y)$ between channel input X and output Y, over all input distributions. For the bandlimited Gaussian channel, this maximum is attained for a Gaussian input $x(t)$, and the mutual information (in bits per second) is given by:

$$I(X;Y) = \int \log_2(1 + S_{xx}(f)\,\mathrm{SNR}_c(f))df \tag{4.2}$$

Maximization of $I(X;Y)$ subject to the power constraint $\int S_{xx}(f)df < P$ yields the channel capacity $\tilde{C}$. As described in [47, 42], the solution to this problem is obtained by means of a Lagrange multiplier technique and is known in information theory as the water-pouring theorem. The theorem states that the input power spectrum should be chosen as

$$S_{xx}^{\mathrm{opt}}(f) = \begin{cases} K - 1/\mathrm{SNR}_c(f), & f \in W; \\ 0, & \text{otherwise} \end{cases} \tag{4.3}$$

where W is the frequency band for which $K \geq 1/\mathrm{SNR}_c(f)$ and the parameter K is determined by 'water pouring' so that $\int_W S_{xx}^{\mathrm{opt}}(f)df = P$, as illustrated in Figure 4-2.

The channel capacity is then

$$\tilde{C} = \int_W \log_2(1 + S_{xx}^{\mathrm{opt}}(f)\,\mathrm{SNR}_c(f))df \tag{4.4}$$

$$= \int_W \log_2(K\ \mathrm{SNR}_c(f))df \tag{4.5}$$

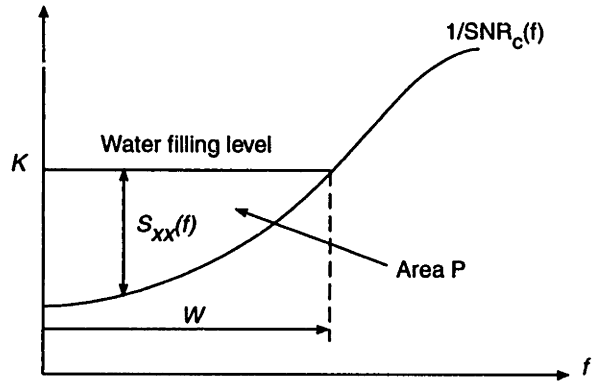

Figure 4-2: Determination of the capacity-achieving spectrum $S_{xx}(f)$ by water pouring.

and represents the upper bound on the achievable data rate R. The power allocation formula (Eq. (4.3)) provides some insight into how to optimize a transmission system for a non-ideal AWGN channel characterized by a frequency response $H(f)$. Eq. (4.3) says that the input signal to the Gaussian channel should be chosen with a spectrum which is large at frequencies where $\text{SNR}_c(f)$ is large.

For a channel with ideal (flat) frequency response $|H(f)| = 1$ over a single continuous band W of width $|W|$, and zero elsewhere, the capacity reduces to the well-known result

$$\bar{C} = \int_W \log_2(1 + \text{SNR}) df = |W| \log_2(1 + \text{SNR}) \tag{4.6}$$

where $\text{SNR} = S_{xx}\,\text{SNR}_c = (P/W)/S_{nn}$ is the usual definition of the signal-to-noise ratio at the receiver.

The capacity of the discrete-time Gaussian channel is similar. If $|W|$ is finite, then we know we can convert the continuous-time channel without loss of information to a discrete-time complex channel with symbol interval $T = 1/|W|$, by generating the input $x(t)$ as a filtered sequence $\sum x_k p(t - kT)$ of complex symbols x_k, where the impulse response $p(t)$ has power proportional to $S_{xx}^{\text{opt}}(f)$ over W, and by similarly sampling the output $y(t)$ every T seconds. The process is shown in Figure 4-3.

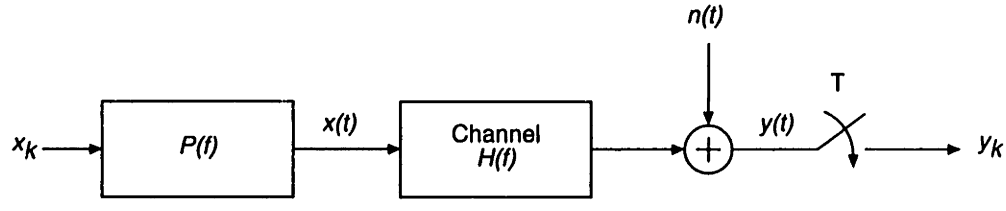

Figure 4-3: The discrete-time bandlimited Gaussian channel model.

For the ideal discrete-time channel, it is customary to define the capacity in bits per two-dimensional symbol as

$$C = \tilde{C}/|W| = \log_2(1 + \text{SNR}) \tag{4.7}$$

where SNR is the ratio of the average energy per symbol $E[|x_k|^2]$ to the noise spectral density N_0.

4.2.3 Normalized signal-to-noise ratio

By analogy with the ideal AWGN channel, we shall define a channel signal-to-noise ratio SNR(C) for the general Gaussian channel as

$$\text{SNR}(C) = 2^C - 1 \tag{4.8}$$

so that the capacity formula takes the same functional form as in the ideal case, i.e.

$$C = \log_2(1 + \text{SNR}(C)) \tag{4.9}$$

in bits per two-dimensional symbol.

It is shown in [22] that the channel signal-to-noise ratio defined in Eq. (4.8) corresponds to the maximum signal-to-noise ratio achievable by an unbiased MMSE decision-feedback equalizer when the power is allocated as in Eq. (4.3). This result is quite striking, as it says that the capacity of any arbitrary bandlimited Gaussian channel is determined by a single parameter, $\text{SNR}_{\text{MMSE-DFE,U}}$ independent of any other channel characteristic.

Thus the general Gaussian channel is simply characterized by two parameters, the capacity achieving bandwidth W (in Hz) and the capacity C (in bits per complex symbol). The channel capacity C represents the upper bound on the data rate R (in bits per complex symbol) that any communication system can achieve with an arbitrarily low probability of error $\Pr(E)$. In other words, for the probability of error to be small, we must have

$$R < C \tag{4.10}$$

Such a characterization allows us to regard a general channel with a given W and SNR(C) as being more or less equivalent to an ideal channel with the same parameters.

Intuitively, the "goodness" of a practical coding scheme is measured by the gap between the actual rate R and the ultimate limit C. In practice, however, the performance is typically expressed in terms of the signal-to-noise ratio required to achieve a given probability of error (e.g. $\Pr(E) = 10^{-6}$) and, since the channel capacity depends on the signal-to-noise ratio, it is difficult to compare different transmission schemes. For example, uncoded 16-QAM requires

about 7 dB more than uncoded 4-QAM to achieve the same probability of error at high SNR, but the channel capacity at this higher SNR is likewise higher. With this in mind, it is convenient to normalize the channel signal-to-noise ratio $\text{SNR}(C) = 2^C - 1$ by the quantity $2^R - 1$. Forney calls the ratio of these two quantities the *normalized signal-to-noise ratio* SNR_{norm} [42].

$$\text{SNR}_{\text{norm}} = \frac{\text{SNR}(C)}{2^R - 1} \tag{4.11}$$

With this definition of the normalized signal-to-noise ratio, the converse of the channel capacity theorem says that in order for the probability to be small, we must have $\text{SNR}_{\text{norm}} > 1$. While this may appear to be a simple exercise in normalization, the following discussion shows that SNR_{norm} has a more fundamental meaning.

For high SNR, the normalized signal-to-noise ratio becomes

$$\text{SNR}_{\text{norm}} \simeq \text{SNR}(C)/2^R \tag{4.12}$$

Therefore, at high SNRs, SNR_{norm} gives an accurate estimate of the difference between the capacity C and the actual rate R (called rate gap):

$$\log_2(\text{SNR}_{\text{norm}}) \simeq C - R \tag{4.13}$$

or equivalently,

$$\text{SNR}_{\text{norm}}(\text{dB}) \simeq 3(C - R) \tag{4.14}$$

At low SNRs, SNR_{norm} approximates the ratio C/R and is proportional to the signal-to-noise ratio per bit of information E_b/N_0, since

$$\text{SNR}_{\text{norm}} \simeq \text{SNR}(C)/(R \ln 2) = E_b/N_0 \log_2 e. \tag{4.15}$$

The parameter E_b/N_0 has traditionally been used to compare different transmission schemes, usually at low SNRs.

In addition, it is easy to show that the symbol error probability for large QAM constellations (requiring high values of the SNR) is well approximated by

$$\Pr(E) \simeq 4 \cdot Q[(3 \cdot \text{SNR}_{\text{norm}})^{1/2}] \tag{4.16}$$

where $Q[x]$ is the Gaussian probability of error function, $Q[x] = \int_y^\infty p(y)dy$, where $p(y)$ is a Gaussian distribution with mean 0 and standard deviation 1. Thus, there is a universal performance curve $\Pr(E)$ versus SNR_{norm} for all uncoded QAM schemes at high SNR's [42]. This curve is shown in Figure 4-4.

From Eq. (4.14), the rate gap $C - R$ is therefore approximately 2 bits per complex symbol if the desired rate is $\Pr(\text{E}) \simeq 10^{-3}$ and 3 bits per complex symbol if $\Pr(\text{E}) \simeq 2 \cdot 10^{-6}$ in the high-SNR domain. Equivalently, there is an SNR gap of about 9 dB for error rates of the order of 10^{-6} between uncoded QAM modulation and the ultimate limit, the channel capacity.

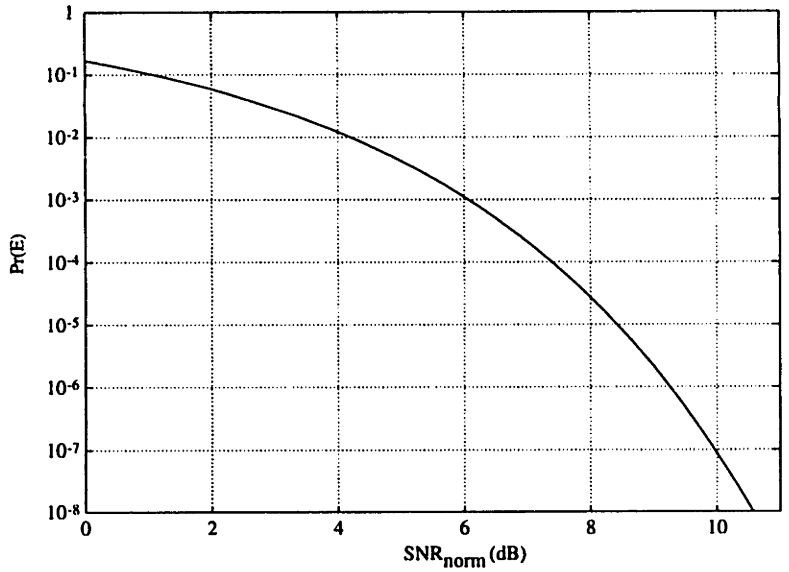

Figure 4-4: Probability of error vs. normalized SNR for high-rate QAM.

4.3 Combined modulation and coding

From an information-theoretic standpoint, the problem of achieving capacity can be stated as a problem of packing spheres in a higher dimensional Euclidean space. In fact, the early work of Shannon [84] on proving the existence of an upper bound on the rate at which data can be transmitted through a channel relied on geometric arguments, which said that in order to approach capacity, disjoint small spheres must be packed into a large sphere in such a way that the volume that is not within any of the small spheres becomes a vanishingly small fraction of the total volume. In this signal-space picture, the center of a small sphere is a codeword, the squared radius of the small sphere is proportional to the noise power, and the squared radius of the large sphere is proportional to the signal power.

Until recently, it was assumed that the sphere-packing proof of the coding theorem was merely a non-constructive proof which did not give any indication as to how to build practical codes capable of approaching capacity. It is now understood that the construction of dense sphere packings - e.g., the construction of lattice-based sphere packings such as the 24-dimensional superdense Leech lattice or the family of 2^n-dimensional Barnes-Wall lattices - can lead to very efficient codes. Such codes combine modulation and coding, since each point of the lattice belongs to the signal space, while the specification of the lattice is based on an algebraic code.

Prior to that realization, much of the coding literature dealt with the design of binary codes over GF(2). It turns out that this was the proper approach for low-SNR channels where the

binary code sequences are mapped to signal sequences bit by bit, using a simple mapping from (0,1) to a two-point (-d/2,d/2) PAM constellation. Error protection is achieved by introducing redundancy in the data stream. The redundancy introduced by the binary code results in a increase of the symbol rate and therefore of the signal bandwidth, but on a power-limited channel, this in itself is not a problem. The increased bandwidth, however, results in a noise increase which has to be more than compensated for by the coding scheme in order to make coding worthwhile. The problem of designing codes for the low-SNR case is well understood, and there exist both sophisticated algebraic techniques to construct good binary codes and efficient implementations of reasonable computational complexity to decode them.

Historically, the concept of coded modulation was not introduced in the framework of lattice-based code constructions but rather in the trellis codes of Ungerboeck, who was interested in finding efficient transmission techniques for the bandlimited Gaussian channel. Ungerboeck's work was the key development that opened the field of coded modulation and triggered interest in the design of new signal-space codes.

In developing the concept of coded modulation, Ungerboeck made the following important observations. Consider a memoryless discrete-time channel with discrete input random process $\{X_k\}$, input alphabet Ω_x and continuous output random process $\{Y_k\}$. The mutual information $I(X;Y)$ can be written in terms of the channel transition probability $f_{Y|X}(y|x)$ and the probability distribution of the input $p_X(x)$

$$I(X;Y) = \sum_{x\in\Omega_x} p_X(x) \int_{\Omega_y} f_{Y|X}(y|x) \log_2 \frac{f_{Y|X}(y|x)}{\sum_{x\in\Omega_x} p_X(x) f_{Y|X}(y|x)}\, dy \tag{4.17}$$

Assume further that we are only interested in codes with uniform input distributions and that the additive noise is Gaussian with variance $2\sigma^2$. The mutual information can then be numerically evaluated by Monte Carlo integration. Figure 4-5 shows the capacity of several discrete-input continuous-output memoryless Gaussian channels, namely the 4PSK, 8QAM, 16QAM and 32QAM channels, together with the channel capacity limit for the discrete-time AWGN channel with no constraints on the input.

Let us assume that for a particular AWGN channel, an acceptable probability of error is achievable without coding at some SNR using a constellation of size M. Using coding we can reduce the SNR at the same probability of error, or reduce the error probability at the same SNR, but the improvement is limited by the channel capacity. The key observation made by Ungerboeck is that most of this theoretical reduction can be achieved by using a constellation of size $2M$ plus a coding algorithm. For example, from Figure 4-5, we see that in order to transmit 4 bits per signaling interval using an uncoded two-dimensional constellation such as 16QAM, the SNR must be 20.9 dB for a probability of error of 10^{-6}. If we double the size of the constellation and use 32QAM instead, error-free transmission of 4 bits per signaling interval is

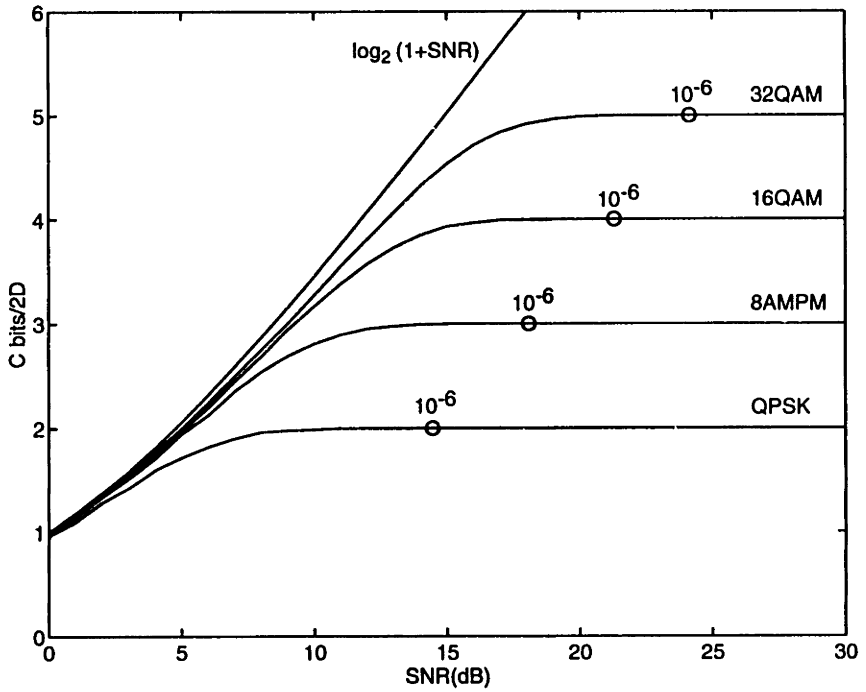

Figure 4-5: Channel capacity of bandlimited Gaussian channels for discrete-valued equiprobable inputs and continuous-valued outputs (Monte Carlo calculation).

theoretically possible (assuming unlimited encoding and decoding complexity) at 13 dB. Using larger constellations can only improve the coding gain by less than 1 dB. Since there is no increase in bandwidth with coded modulation, there is no more noise than with the uncoded system, unlike with binary coding. However, there is a power penalty associated with using larger constellations which has to be more than offset by coding so that there is coding gain.

4.3.1 Trellis-coded modulation

In a classic paper [86], Ungerboeck proposed a series of simple coding schemes capable of achieving coding gains of the order of 3 to 6 dB using a technique called "mapping by set partitioning". The essential new concept introduced by Ungerboeck was to allow an expansion of the two-dimensional signal set from a size of M to a size of $2M$ to provide redundancy for coding and to design coding and signal-mapping functions jointly, so as to minimize the "free distance" (minimum Euclidean distance) between coded signal sequences [87]. This allowed the construction of modulation codes whose free distance significantly exceeded the minimum distance between uncoded modulation signals, at the same information rate, bandwidth and signal power. Initially, the codes used to provide the necessary redundancy were convolutional codes. The technique of combining convolutional coding and modulation is known as trellis-

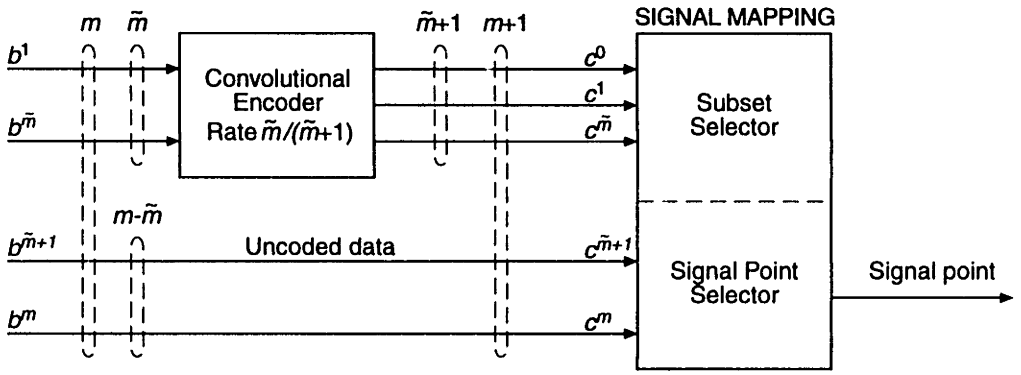

Figure 4-6: Block diagram of an Ungerboeck encoder/modulator for trellis-coded modulation.

coded modulation (TCM) since these schemes can be described by a state-transition diagram similar to the trellis diagrams of binary convolutional codes. For TCM, however, the trellis branches are labeled with signal points rather than binary symbols.

The general structure of an Ungerboeck encoder/modulator is shown in Figure 4-6. At each signaling interval, m binary digits are simultaneously presented to the encoder. The first $\tilde{m}$ bits are input to the convolutional encoder which in turn generates $\tilde{m}+1$ output bits denoted $c^0, c^1, \cdots, c^{\tilde{m}}$. These bits select a subset of the constellation, while the remaining uncoded bits, denoted $c^{\tilde{m}+1}, \cdots, c^m$, are used to select the signal within the subset.

Figure 4-7 shows a possible partitioning of a 32QAM constellation into subsets of progressively increasing intra-subset distances. The subsets labeled A_0 through A_7 are selected by 3 coded bits c^0, c^1, c^2 produced, for example, by a rate 2/3 convolutional code ($\tilde{m} = 2$). Each subset contains 4 points, which are selected by 2 uncoded bits c^3, c^4 ($m - \tilde{m} = 2$). With respect to the initial constellation, the intrasubset distance has been increased by a factor $2\sqrt{2}$. Since 4 information bits are conveyed through the channel during each signaling interval, the spectral efficiency of the code is 4 bits/s/Hz. Thus, the 32QAM TCM scheme achieves the same spectral efficiency as uncoded 16QAM. However, provided the convolutional code and the mapping of bits to signal points are chosen properly, the performance of 32QAM TCM will be superior to its uncoded 16QAM counterpart.

Let us consider a simple example, that of an 8-state convolutional encoder. The convolutional encoder is shown in Figure 4-8(a). The corresponding 8-state trellis is shown in Figure 4-8(b). On the left of the state transition diagram are shown the subset labels corresponding to each of the 32 branches (state transitions). Let us now estimate the performance gain of 32QAM TCM over uncoded 16QAM. The squared Euclidean distance between points within a subset (intra-subset distance) is equal to $d_3^2 = 8d_0^2$ by construction. The minimum squared distance between different signal sequences is easily found by inspection of the trellis

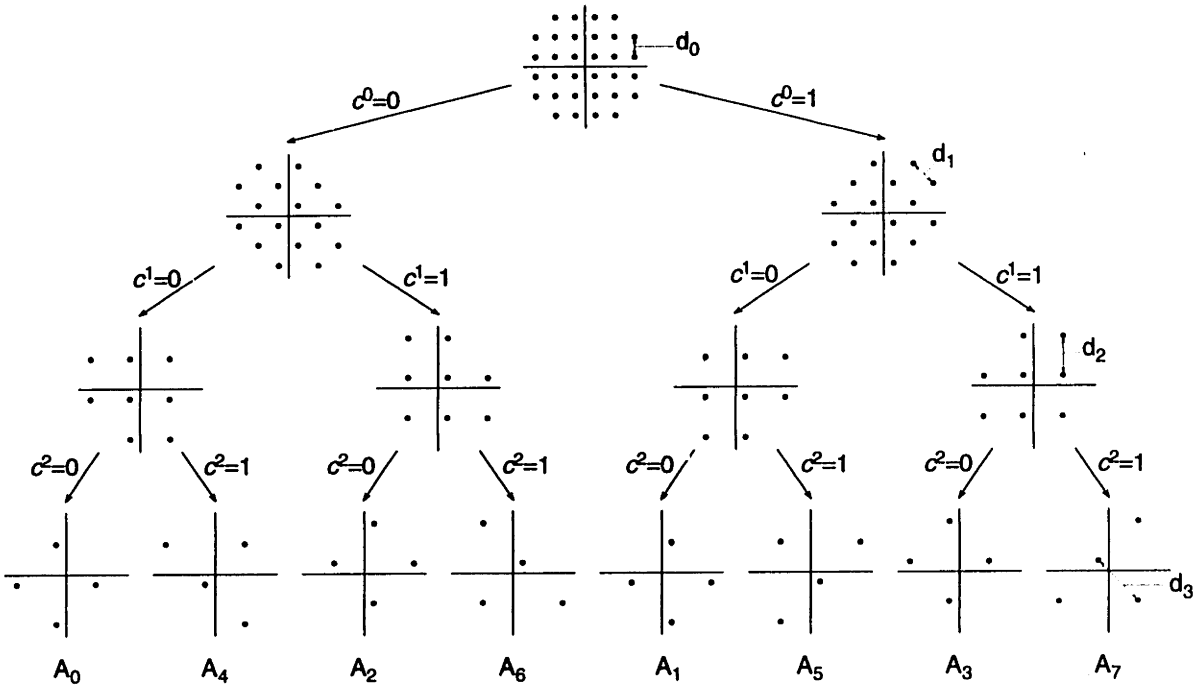

Figure 4-7: Set partitioning of a 32QAM constellation.

in Figure 4-8. One minimum distance error event is the path that diverges from state 0 at time t, passes through state 3 at time $t+1$, through state 6 at time $t+2$ and remerges with the all-zero-state path at time $t+3$. The minimum squared distances along each of the branches are d_1^2, d_0^2 and d_1^2. Thus, the minimum distance along the path is equal to $2d_1^2 + d_0^2$ or $5d_0^2$. Since this distance is smaller than the intra-subset distance, the majority of the error events will be at distance $5d_0^2$ from the correct path. Thus, the minimum distance of the trellis code is 5 times larger than in the uncoded scheme. However, the 32QAM constellation requires twice as much power as the 16QAM constellation, since the average power for the 32QAM constellation is $20d_0^2$ while that of the 16QAM constellation is $10d_0^2$. Thus the asymptotic coding gain of 32QAM TCM over 16QAM is equal to

$$\gamma = 10\log_{10}\left(\frac{5d_0^2}{20d_0^2} \Big/ \frac{d_0^2}{10d_0^2}\right) = 3.98\,\text{dB} \tag{4.18}$$

We also note that the asymptotic coding gain of this 8-state trellis code is greater than the 64-state trellis code proposed in the DigiCipher and Channel-Compatible DigiCipher systems [48, 66]. In these systems, the asymptotic coding gain of the trellis code was 3.01 dB, which would seem to suggest that the overall performance could easily be improved by close to 1 dB by using a more powerful trellis code. We will see, however, that on a channel such as the broadcast television channel, where the delay requirements are not as stringent as on some of

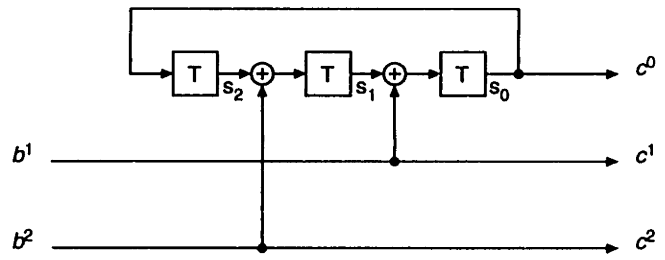

(a) Convolutional encoder for the 2-dimensional 8-state 32QAM code.

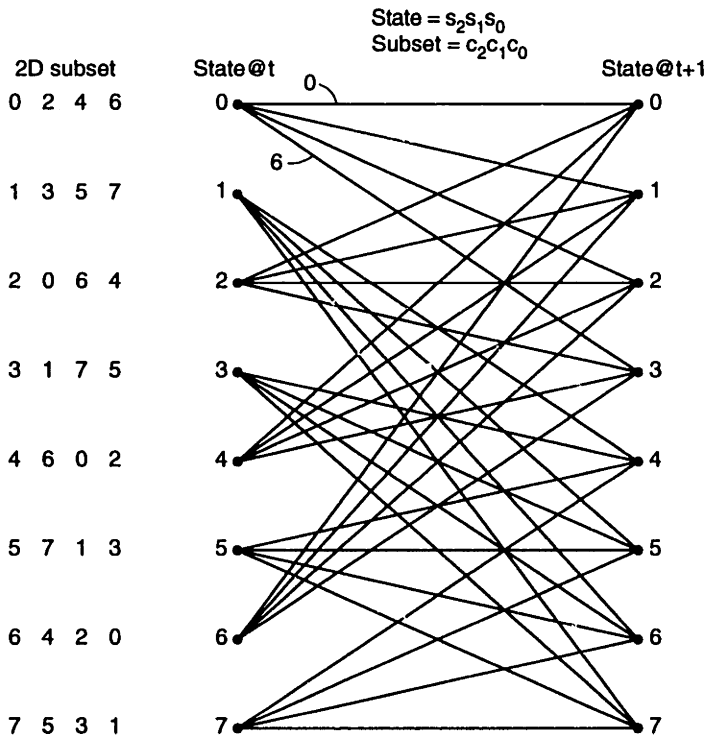

(b) Trellis diagram for the convolutional code shown in (a).

Figure 4-8: Convolutional encoder for the 8-state 32QAM trellis code and corresponding trellis diagram.

the classical two-way channels, it is advantageous to use trellis coding in combination with an algebraic block code (e.g. a Reed-Solomon code), in a concatenated arrangement. Under these conditions, we will show that the asymptotic coding gain is a poor predictor of the performance of the overall system; the error performance at relatively high error rates, which depends not just on the minimum-distance error events but rather on a spectrum of error events, is a more important determinant of the overall performance.

Before examining the use of concatenated coding, we now present briefly the wider framework in which trellis codes are situated: signal-space codes. Because this approach is more general than the construction technique used by Ungerboeck, one is able to better separate the different aspects which contribute to the overall coding gain. We provide formal definitions of the asymptotic coding gain, the effective coding gain and the error coefficient. For an introduction to coset codes and a comprehensive treatment of a variety of lattice and trellis codes, the interested reader is referred to the papers by Forney in [40, 41].

4.3.2 Signal-space codes

There are several ways in which Ungerboeck trellis codes can be generalized. Instead of using two-dimensional constellations for S, one can use a multidimensional constellation. As well, the signal constellation may be viewed as a finite subset of a multidimensional array. The array may be a lattice or a lattice translate Λ which may be partitioned using a sublattice Λ' of Λ. Instead of using a linear convolutional code to label the subset sequences, one may use a block code or a convolutional code, which may be linear or nonlinear. These extensions are included in the following definition of a signal space code.

A signal space code $\mathbb{C}$ may be constructed from the following three elements: 1) a signal set S that is a discrete subset of a signal space W, 2) a labeling $f : S \rightarrow A$ of S by a label alphabet A and, 3) a label code C that is a subset of a label sequence space A^I. If the label code is a block code, then the signal space code is an array in a higher-dimensional space. If it is a convolutional code, then the signal space code is a trellis code, an infinite-dimensional array in sequence space [40, 42].

Figure 4-9 illustrates an encoder for a signal space code $\mathbb{C}$ constructed in this way. An encoder for the label code C generates a label code sequence $\mathbf{c} \in \mathrm{C}$. The label map $m : A \rightarrow m(A)$ independently maps each component c_k of the label code sequence $\mathbf{c}$ into the corresponding subset $m(c_k)$ of S. This determines a sequence $m(\mathbf{c})$ of subsets of S. In order to determine a specific signal space code sequence $\mathbf{s}$, uncoded bits select a specific signal point $s_k \in m(c_k)$ from each selected subset $m(c_k)$ of S. It is important to note that the signal points need not be two-dimensional. This description of signal space codes allows for the selection of

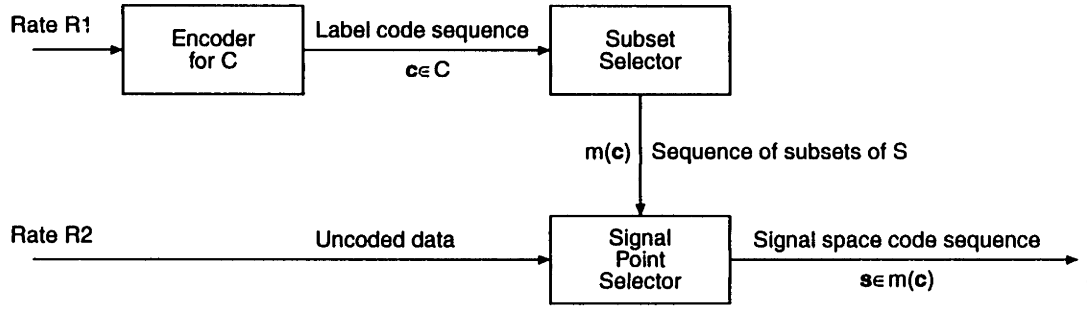

Figure 4-9: Encoder for a signal space code $\mathbb{C}$.

multidimensional signal points.

The code distance properties, and thus the fundamental coding gain, are essentially determined by the choice of the label code C, the labeling f, and the distance properties of S, but are largely independent of the exact shape of S. The overall performance of the signal space code, however, depends on the shape of S, the distance properties of S and the distance properties of the label code C. What, then, are the respective contributions of the different elements of the code? The language of coset codes that was introduced by Calderbank and Sloane [15] and Forney [40] has provided clear answers to this question.

Let us consider a signal set that consists of points taken from a lattice Λ and that are contained in some bounding region $\mathbb{R}$. The subset selection is based on the partition of the lattice Λ by a sublattice Λ' into a set of cosets of Λ' identified by their coset representatives.

There are three sources of performance gain in a coset code. The first stems from the properties of the lattice Λ itself. By choosing a lattice with better distance properties than the two-dimensional rectangular lattice, it is possible to achieve a coding gain, which we denote by γ_Λ. This coding gain is given by

$$\gamma_\Lambda = \frac{d^2_{\min}(\Lambda)}{V^{2/N}(\Lambda)} \tag{4.19}$$

where N is the dimension of the lattice Λ, $d_{\min}$ is the minimum Euclidean distance between points in the lattice and $V(\Lambda)$ is the fundamental volume of the lattice, i.e. the volume of N-dimensional space associated with each lattice point [40].

The second source of performance gain comes from the label code C. Since the code C only allows certain sequences of cosets to be sent to the signal point selector, it can be used to ensure a certain minimum distance between coset sequences, at the expense of introducing redundancy in the coset sequences. Let $d^2_{\min}(C)$ be the minimum distance between any two sequences of cosets allowed by the code C. It is then possible to show that the coding gain due

to C is given by

$$\gamma_C = \frac{d^2_{\min}(C)}{d^2_{\min}(\Lambda)2^{\rho(C)}} \tag{4.20}$$

where $\rho(C)$ is the normalized redundancy (in bits/2D) of the code C, defined as

$$\rho(C) = \frac{2}{N}r(C) \tag{4.21}$$

where $r(C)$ is the number of redundant bits generated by the code per N dimensions. The combined coding gain due to the lattice and the code $\gamma_C = \gamma_C\gamma_\Lambda$ is called the asymptotic coding gain (sometimes also called the nominal coding gain).

The last source of performance gain comes from the shape of the bounding region $\mathbb{R}$. By choosing a boundary shape that requires a smaller energy than a two-dimensional square region, it is possible to achieve a shaping gain, which we denote by γ_R. It is possible to show that the shaping gain is equal to

$$\gamma_R = \frac{N \cdot V^{2/N}(\mathbb{R})}{12 \cdot P(\mathbb{R})} \tag{4.22}$$

where $V(\mathbb{R})$ is the volume of the bounding region and $P(\mathbb{R})$ is the average energy of a uniform, continuous distribution of points in $\mathbb{R}$ (continuous approximation for high-rate codes, see [40, 42]).

Thus, the performance gain of the coset code compared to an uncoded rectangular lattice with a rectangular shaping region is given by

$$\gamma = \gamma_\Lambda \cdot \gamma_C \cdot \gamma_R \tag{4.23}$$

and the overall probability of error is approximately given by

$$\Pr(E) = K(\mathbb{C}) \cdot Q\left[(3 \cdot \gamma_\Lambda \cdot \gamma_C \cdot \gamma_R \cdot \mathrm{SNR}_{\mathrm{norm}})^{1/2}\right] \tag{4.24}$$

where $K(\mathbb{C})$ is the error coefficient (average number of nearest neighbor signal sequences at the minimum distance).

Multidimensional lattices offer the prospect of increased coding gains but in general, lattices with large coding gains also have a large number of nearest neighbors. This must be so, since the coding gain increases without limit as the number of dimensions goes to infinity, but we know from the analysis of QAM modulation that the gap is only 9 dB at an error rate of 10^{-6}. Thus, it would appear that a measure of the real coding gain at a given error rate would be more meaningful than the coding gain γ. By analogy with Eq. (4.16), we define the effective coding gain $\gamma_{c,\mathrm{eff}}$ as the coding gain that would be obtained if the number of nearest neighbors was 4, as in the case of 2-dimensional QAM, that is $\gamma_{c,\mathrm{eff}}$ satisfies the equation

$$4 \cdot Q[(3 \cdot \gamma_{c,\mathrm{eff}} \cdot \gamma_R \cdot \mathrm{SNR}_{\mathrm{norm}})^{1/2}] = \frac{2}{N}K(\mathbb{C}) \cdot Q\left[(3 \cdot \gamma_C \cdot \gamma_R \cdot \mathrm{SNR}_{\mathrm{norm}})^{1/2}\right] \tag{4.25}$$

where the factor $2/N$ on the right hand side is used to normalize the error coefficient to two dimensions.

These results have the advantage that they make it possible to compare different signal space codes with different dimensions and different label codes C whereas the previous definition of the coding gain, which compared a given code with an uncoded modulation scheme with the same bandwidth and same spectral efficiency was more restrictive.

4.3.2.1 An example and practical considerations

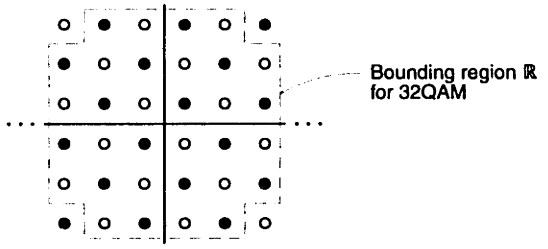

Figure 4-10: Lattice $\Lambda = \mathbb{Z}^2 + (1/2, 1/2)$ (black and white dots) and sublattices $R\Lambda$ (black dots) and $R\Lambda + [1, 0]$ (white dots). Also shown is the boundary for 32QAM.

Returning to the Ungerboeck 32QAM 8-state trellis code, we can see that the trellis code is based on the 8-way partition $\mathbb{Z}^2/2R\mathbb{Z}^2$.The set partitioning operation may be viewed as a chain partition $\Lambda/R\Lambda/2\Lambda/2R\Lambda$, where Λ is the two-dimensional integer lattice $\mathbb{Z}^2$ and R is the two-dimensional "rotation operator" (see [15, 40, 42]).

$$R = \begin{bmatrix} 1 & 1 \\ 1 & -1 \end{bmatrix} \tag{4.26}$$

Note that this operator includes, in addition to a rotation by $\pi/4$, a scaling by $\sqrt{2}$ and an interchange of the two coordinates. The first partition of the lattice is shown in Figure 4-10.

The lattice coding gain γ_Λ is equal to 1 (since Λ is rectangular) and the coding gain γ_C is equal to 5/2 (since the normalized redundancy is equal to 1 and the minimum distance $d^2_{\min}(C)$ is equal to 5). The non-rectangular shape of the boundary region provides a small amount of shaping gain ($\approx$ 0.14 dB). The average number of nearest neighbors for this 8-state convolutional code and lattice is found to be $K(\mathbb{C}) = 16$ (assuming infinite data rate). Forney [42] uses the rule of thumb that every doubling of K over the QAM coefficient $K = 4$ costs about 0.2 dB at an error rate of 10^{-6} [40]. With this rule, the effective coding gain of the 8-state code is 3.96 – 0.4 = 3.56 dB.

It is not clear, however, how accurate this approximation is for signal sets of intermediate size. Constellation sizes between 16 and 64 have been considered for HDTV transmission.

As well, trellis codes are often used as inner codes in concatenation with block codes, which implies that the error probability at the operating point of the trellis code is much larger than 10^{-6}. The number of nearest neighbors given above assumed a constellation with an infinite number of points. If one wants to take boundary effects into account, it is best to enlist the help of a computer to find the number of codewords at the minimum distance. The determination of the number of nearest neighbors is complicated by the fact that the trellis code is not linear in the sense that the sum of two codewords is not in general a codeword. Thus a brute-force approach would require that all pairs of codewords be examined. Fortunately, it is possible to simplify the search somewhat by using certain regularity properties of the trellis code. Using a bidirectional stack algorithm similar to [78], we found the average number of nearest neighbors to be equal to 6.7158 for 32QAM, which is substantially different from the asymptotic number of nearest neighbors of 16.

It is also important to note that the validity of Eq. (4.24) is limited to low error rates ($P_b \lesssim 10^{-6}$). In our case, we are more interested in intermediate error rates in the range 10^{-2} to 10^{-4}. Therefore, it is of interest to perform computer simulations to estimate the real coding gain accurately. As well, rather than rely solely on computer simulations, it would also be interesting to provide closer analytical approximations to the real error rate. To this effect, one can use the first dominant terms of the union bound. However, even the union bound is not very tight when the error coefficients are large or the signal-to-noise is small. In the next subsection, we provide computer simulations for a set of trellis codes and show the usefulness of the normalized signal-to-noise ratio. We then follow these results by a determination of the detailed weight distribution of selected trellis codes, and compare the approximation obtained by using the first terms of the union bound with the Monte Carlo simulation results.

4.3.3 Performance of selected trellis codes

In this section, we consider two approaches to the evaluation of the performance of trellis codes. The first approach is to evaluate the performance by Monte Carlo averaging. The second involves the estimation of the detailed weight structure of the code and use of performance bounds. In general, simulations require long run times and are most useful for short constraint length codes and small signal-to-noise ratios[1]. Furthermore, they do not yield direct insight into the properties of the codes but rather display the aggregate effect of several factors. Performance bounds can be an interesting alternative to Monte Carlo simulations, but need

[1]Each point (SNR, P_b) on a performance curve is obtained by generating a data sequence long enough for 100 errors to occur. We give a justification for this rule in Appendix C. Thus, at an error rate of 10^{-6}, 10^8 points are required to define the point (SNR, 10^{-6}).

to be relatively tight in order to be useful in real-world applications. Both approaches are considered here.

4.3.3.1 Performance evaluation by Monte Carlo simulation

Figure 4-11 shows the performance of 6 different 2-dimensional trellis codes obtained by Monte Carlo simulation. These codes were first published by Ungerboeck [86, 87] and can also be found in [40]. The codes shown here are based on the 8-way partition of $2\mathbb{Z}^2 + (1,1)$, using the set partitioning principles introduced by Ungerboeck. As is evidenced by this graph, for a given number of states, each additional bit of information per complex symbol requires an additional 3 dB of power. At $P_b = 10^{-6}$, the real coding gain achieved by going from 8 states to 64 states is of the order of 1 dB. At intermediate P_b, the coding gain is greatly reduced (less than 0.5 dB). At high P_b, the performance of the 64-state trellis codes is marginally worse than that of the corresponding 8-state codes. This is likely caused by the larger number of error events at distances greater than the minimum distance. For high error rates, these terms must be taken into account, whereas they can be neglected at low error rates. This aspect is investigated in the next subsection.

One characteristic of these two-dimensional trellis codes is that they require a minimum of 1 bit of redundancy per complex symbol. One way to improve on the performance of these codes is to reduce the redundancy by coding signal points in a higher dimensional space. Wei has argued that among the family of low-complexity trellis codes, those based on multidimensional rectangular constellations have several advantages over 2-dimensional trellis codes of comparable complexity [90]. A first advantage is the generally smaller error coefficients and larger coding gains. A second advantage is the reduced size of the constituent 2D constellations. A third advantage is that it is easier to design codes with additional features such as rotational invariance and tolerance to phase ambiguities when using multidimensional constellations. Wei shows that some multidimensional trellis codes offer a better tradeoff between complexity and Gaussian noise performance. A particularly good code is the 16-state 4-dimensional trellis code proposed by Wei in [90]. Its spectral efficiency is 4 bits/2D, and it is therefore comparable in terms of data rate to the 2-dimensional 32QAM schemes considered so far for use in HDTV broadcasting. Figure 4-12 shows the performance of this 16-state 4-dimensional trellis code.

In order to compare these different trellis codes, one can use the normalized SNR. Figure 4-13 shows the performance of the 8-state 2D codes together with the 4D Wei code on a common normalized signal-to-noise scale. For clarity, we have not included the 64-state codes. From this graph, one can see that all the 8-state codes have approximately the same performance, in accordance with analytical predictions. The 4D code appears to be slightly better at low error

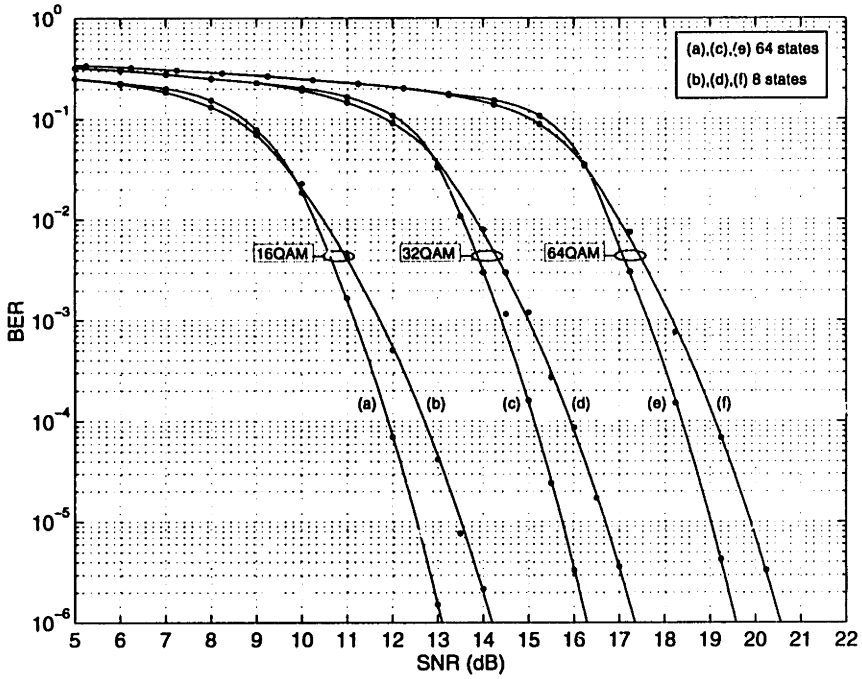

Figure 4-11: Performance of 8 and 64-state 2-dimensional Ungerboeck trellis codes for 16, 32 and 64 QAM, obtained by Monte Carlo simulation. The spectral efficiencies are equal to 3, 4 and 5 bits/s/Hz.

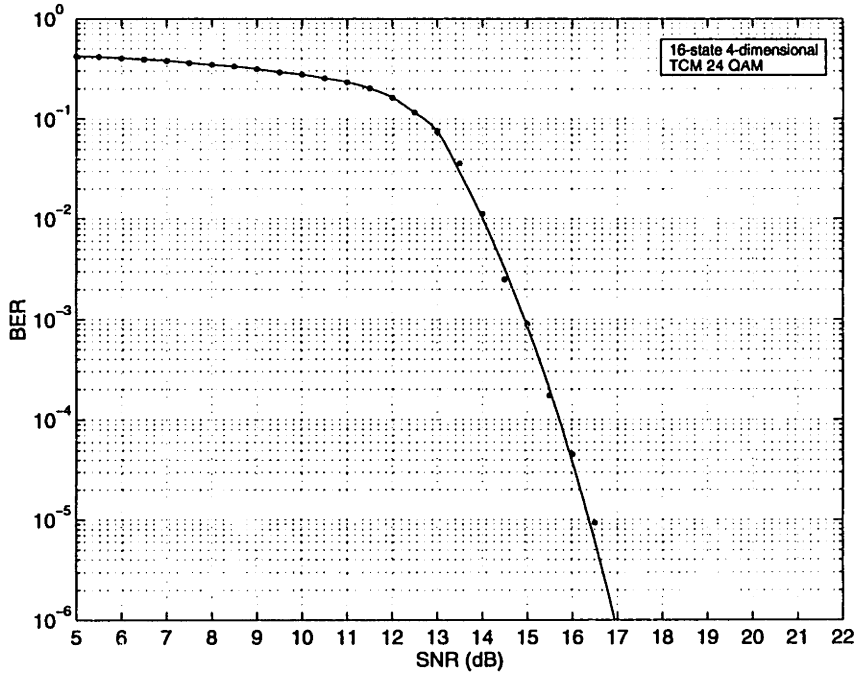

Figure 4-12: Performance of 16-state 4-dimensional Wei trellis code with spectral efficiency of 4 bits/s/Hz, obtained by Monte Carlo simulation. The 4-dimensional constellation of 2^9 points is constructed as a subset of the concatenation of 2 constituent 2D constellations with 24 points.

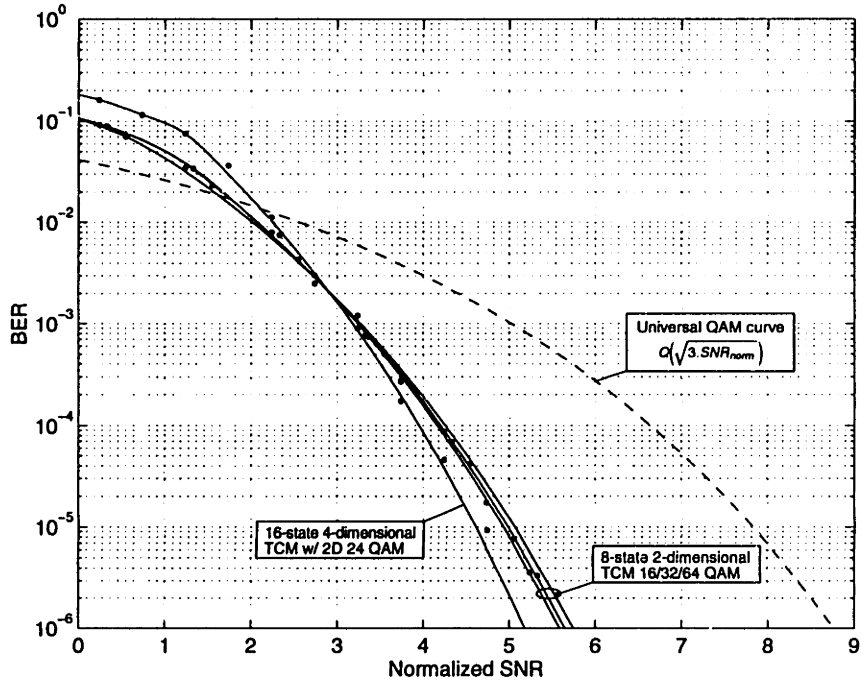

Figure 4-13: Comparison of the Wei 16-state 4-dimensional code with the Ungerboeck 8-state 2-dimensional codes, on a normalized signal-to-noise scale.

rates and somewhat worse at intermediate to high error rates. This may be due in part to to the decoding procedure, which, for this simulation, did not ensure after Viterbi decoding that the decoded 4D points were valid constellation points (see [90]).

4.3.3.2 Analytic performance bounds

In section 4.3.2, an estimate of the error performance was provided by Eq. (4.24) for high signal-to-noise ratios. At mid to low signal-to-noise ratios, this estimate is loose. A better performance bound is provided by the union bound on the first error-event probability [89].

As previously, we denote by $\mathbb{C}$ the set of all possible signal space sequences. Let $\mathbf{s} \in \mathbb{C}$ be a transmitted sequence and $\hat{\mathbf{s}} \in \mathbb{C}$ be the decoded sequence. Let us define the distance between $\mathbf{s}$ and $\hat{\mathbf{s}}$ as

$$d(\mathbf{s}, \hat{\mathbf{s}}) = \sum_k d(s_k, \hat{s_k}) \tag{4.27}$$

where $d(.,.)$ is a metric that has this additive property. As was seen earlier, for an AWGN channel, the squared *Euclidean* distance $d(\mathbf{s}, \hat{\mathbf{s}})$ between two signal space sequences $\mathbf{s}$ and $\hat{\mathbf{s}}$ determines the likelihood of receiving $\hat{\mathbf{s}}$ given that $\mathbf{s}$ was sent. A decoder based on maximum likelihood sequence detection will search the code space $\mathbb{C}$ for the sequence $\hat{\mathbf{s}}$ nearest in the Euclidean distance sense to the received sequence $\mathbf{y}$.

Given two signal space sequences $\mathbf{s}$ and $\hat{\mathbf{s}}$, we define a first error event in the following way: Let T be the trellis associated with the trellis code, with each branch labeled by a signal point selector or a channel signal point. A first error event of length L is said to occur when the paths in the trellis T corresponding to the two signal space sequences $\mathbf{s}$ and $\hat{\mathbf{s}}$ are identical for all times up to a certain time k, diverge at time k, remain distinct for L branches and eventually remerge at time $k + L$. The probability of choosing the path corresponding to $(\hat{s}_k, \hat{s}_{k+1}, \ldots, \hat{s}_{k+L-1})$ when $(s_k, s_{k+1}, \ldots, s_{k+L-1})$ was sent is called the pairwise error probability [7], and is denoted by $P(\mathbf{s}_L \rightarrow \hat{\mathbf{s}}_L)$. Thus,

$$P(\mathbf{s}_L \rightarrow \hat{\mathbf{s}}_L) = \Pr\{d(\mathbf{y}_L, \hat{\mathbf{s}}_L) < d(\mathbf{y}_L, \mathbf{s}_L)\} \tag{4.28}$$

A useful performance measure is the probability that at time k, the decoded path diverges from the correct path. We call this error probability the first error event probability. We assume here that this probability does not depend on the time instant k. Given the definition of an error event, the first error event probability Pr(E) is the union over all error events of all lengths L and all transmitted sequences of the pairwise probability of error. An upper bound on the first error event probability is provided by the so-called union bound [89], which in this case can be written

$$\Pr(\mathrm{E}) \leq \sum_{L, \mathbf{s}_L, \hat{\mathbf{s}}_L} P(\mathbf{s}_L) P(\mathbf{s}_L \rightarrow \hat{\mathbf{s}}_L) \tag{4.29}$$

where the sum is over all correct and incorrect paths and all error event lengths $L = 1, 2, \ldots$. Therefore, the first error event probability is the average of the pairwise error probability over all signal space sequences (correct and incorrect). For the AWGN channel, $P(\mathbf{s}_L \rightarrow \hat{\mathbf{s}}_L)$ depends on the squared Euclidean distance between the correct and incorrect paths and not on the actual length of the error event. Indeed, if d is the Euclidean distance corresponding to an error event of length L, the pairwise error probability can be written

$$P(\mathbf{s}_L \rightarrow \hat{\mathbf{s}}_L) = Q\left(\frac{d}{2\sigma}\right) \tag{4.30}$$

Therefore, grouping all the contributions with the same Euclidean distance and ordering the summation by increasing distances, we obtain

$$\Pr(E) \leq \sum_{d=d_{\text{free}}}^{\infty} A_d Q\left(\frac{d}{2\sigma}\right) \tag{4.31}$$

where d_{free} is the minimum free distance of the code and A_d represents the *average* number of signal space sequences at distance d from a correct sequence, where the average is taken over all signal space sequences.

The bit error probability is the average number of bit errors per information bit. A bound on the bit error probability can be obtained in a similar fashion

$$P_b \leq \frac{1}{k} \sum_{d=d_{\text{free}}}^{\infty} B_d Q\left(\frac{d}{2\sigma}\right) \tag{4.32}$$

where k is the number of information bits per two dimensional symbol and B_d is the average number of information bits on all paths at distance d from the correct path, where the average is again taken over all signal space sequences.

In general, the first few terms of the weight distribution are sufficient to provide a reasonably accurate estimate of the first error event probability and of the bit error rate. In the case of linear codes, A_d can be determined by calculating the number of codewords at distance d from the all-zero codeword. In particular, the weight distribution of linear convolutional codes can be determined by a simple computer search procedure based on the Viterbi algorithm.

For general trellis codes, however, the determination of A_d and B_d is difficult because it involves examining all possible error events from all possible correct paths. In particular, for an N-state code, the calculation of the weight distribution of the code requires the determination of the transfer function of an N^2-state trellis diagram. This makes the determination of an upper bound unmanageable for any practical code. For a restricted class of codes, however, Zehavi and Wolf showed that it is possible to compute the weight distribution of the code from the error state diagram [96]. Such trellis codes must satisfy strong symmetry conditions which we refer to here as ZW symmetry.

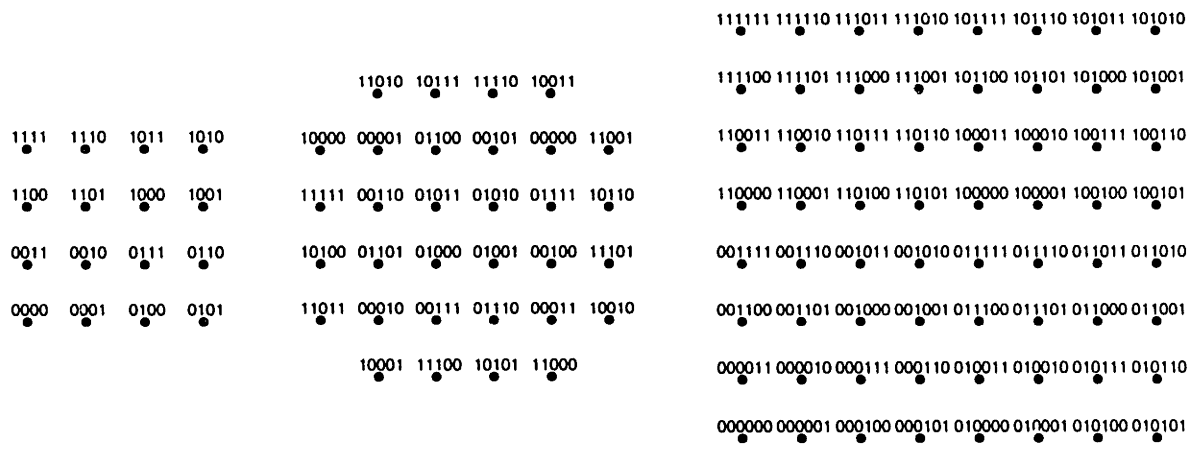

Figure 4-14: Constellation mappings used in the simulations

Briefly, the ZW symmetry condition says the following: consider the time-zero subset $A_0 = m(C_0)$ formed by the signal points that can be generated when the encoder is in state zero, where C_0 is the subgroup of signal selectors, and m is the mapping function, together with the label translates $A_i = m(C_i)$ of A_0, where C_i is a coset of C_0. If, for each selector e and all selectors $a \in C_i$ the set of all squared Euclidean distances $d(m(a), m(a \oplus e))$ is the same for all subsets (identical weight profile), then the distance properties of the trellis code can be determined from the trellis diagram for the error sequence. In [7], Biglieri *et al.* state sufficient conditions for using the N-state error diagram to determine the distance profile. A sufficient condition for the ZW symmetry condition to hold is that there exists an isometry between the time-zero subset A_0 and A_i.

Here, in order to compute the weight distribution of a number of trellis codes, we choose signal mappings such that the ZW symmetry condition is verified. We consider trellis codes based on the rectangular lattice $2\mathbb{Z}^2 + (1,1)$. The signal set maps are shown in Figure 4-14. These were chosen so as to satisfy Zehavi-Wolf (ZW) symmetry conditions as well as obey the usual Ungerboeck set partitioning rules. Figure 4-15 shows the detailed mapping of a 32QAM constellation which has the required symmetry properties. The two subsets A_0 and A_1 are the first level of the partition tree. The map $m(\mathbf{c}) \rightarrow m(\mathbf{c} \oplus 00011)$ is an isometry that maps every point in A_0 to a point in A_1 by a rotation of 90^o.

The calculation of the weight distribution was carried out, not by the transfer function technique suggested in [96], but by using a bidirectional stack search procedure. The results of a number of calculations for a set of relevant codes are shown in Tables 4.1, 4.2, 4.3, 4.4 and 4.5. A number of interesting observations can be made: The 4-state codes based on QAM constellations have a low multiplicity coefficient, which reflects the fact that the

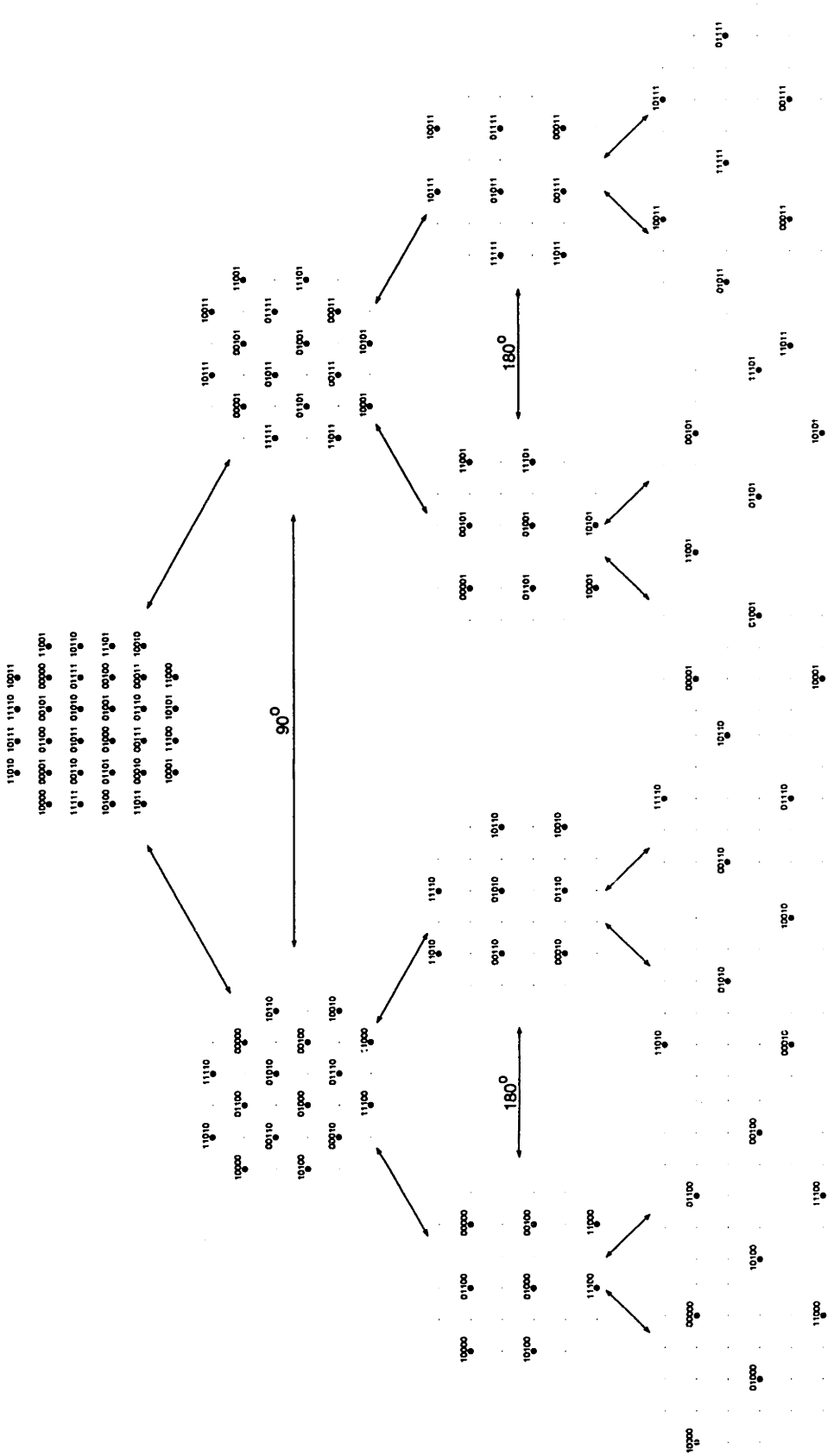

Figure4-15: Detail of the 32QAM constellation mapping.

shortest error events are one branch long and correspond to "parallel transitions" in the trellis diagram (multiple transitions corresponding to identical initial and final states). Thus, for such codes, the impact of the error coefficient on the performance is very small (the asymptotic coding gain is very close to 3.01 dB). As the number of states increases, the multiplicity coefficient corresponding to d_{free} generally also increases. The multiplicity also increases with the size of the constellation. Another interesting observation is that the progression of code distances is constant, which appears to be a characteristic of lattice-based codes. The multiplicity coefficient is also seen to increase rapidly with increasing squared Euclidean distance.

In Table 4.3, we show the weight distribution of a set of trellis codes that were proposed for HDTV transmission by Heegard *et al.* in [50]. For these codes, the underlying convolutional code was the standard rate 1/2 constraint length 7 NASA code with generator polynomials 133_8 and 171_8. The weight distribution is markedly different from Ungerboeck-type trellis codes. These codes are based on only a 4-way partition of $2\mathbb{Z}^2 + (1,1)$ and therefore only achieve a coding gain of 3 dB. However, because of the very large Hamming distance of the convolutional code, there are only 2 non-zero coefficients below 40, and these are remarkably small. For instance, for 16QAM, the first multiplicity coefficient corresponding to a squared free distance of 16 is only 2. The next one at distance 32, again corresponding to a 1 branch long error event, is 5. Thus, one can expect the error performance to remain relatively good, even at low SNR.

Table 4.4 shows the weight distribution of a 1-dimensional code corresponding to an 8PAM signal set. This code is identical to one recently proposed for the standard for terrestrial broadcasting of HDTV. The free distance of the code is slightly larger compared to 2D trellises with the same number of states, when normalized by a factor of 2. The multiplicity coefficients are characteristically low, as should be expected for one-dimensional constellations of small size. Both of these features make such codes attractive for use in concatenated schemes, as we shall see. However, two drawbacks must be stated. Firstly, the constellation expansion ratio is also twice as large, thereby reducing the effective free distance by a factor of two. Thus, the free distance divided by 2 is an equivalent measure of code performance. Secondly, the peak-to-average ratio of this one-dimensional code is slightly higher than that of 2-dimensional codes of equivalent rate, when two-dimensional shaping is used.

Finally, Table 4.5 shows the weight distribution of several Ungerboeck trellis codes with large free distance for which the multiplicity coefficient is very small. In order to achieve a small multiplicity coefficient, the number of states must be increased until the minimum distance error events correspond to parallel transitions, which, in this case, is achieved for 512 states. Accordingly, the complexity is also substantially increased.

Signal Set	States	Rate	d^2	A_d	B_d
16QAM	4	1/2	16	2.000	3.000
			20	7.594	29.531
			24	22.781	126.562
			28	68.344	448.031
			32	210.031	1562.125
			36	653.062	5465.815
16QAM	8	2/3	20	3.938	16.562
			24	13.891	67.469
			28	46.742	279.555
			32	155.762	1084.172
			36	514.807	4101.951
16QAM	16	2/3	24	9.156	53.781
			28	27.211	146.461
			32	79.238	594.922
			36	321.978	2572.553
16QAM	64	2/3	28	8.172	44.406
			32	27.727	186.688
			36	74.647	619.463
32QAM	4	1/2	16	2.500	4.750
			20	13.432	86.205
			24	43.653	387.620
			28	141.872	1538.051
			32	469.083	5929.346
			36	1584.276	22804.203
32QAM	8	2/3	20	6.693	46.225
			24	25.264	206.062
			28	92.310	924.027
			32	337.944	3983.887
			36	1223.353	16693.767
32QAM	16	2/3	24	19.109	164.310
			28	47.376	436.521
			32	191.476	2312.253
			36	760.222	10120.535
32QAM	64	2/3	28	15.855	149.819
			32	62.354	706.191
			36	194.797	2648.059

Table 4.1: Weight distribution of several two-dimensional trellis codes based on 4- and 8-way partitions of the rectangular lattice $2\mathbb{Z}^2 + (1,1)$.

Signal Set	States	Rate	d^2	A_d	B_d
64QAM	4	1/2	16	3.000	6.000
			20	16.413	85.080
			24	57.446	420.878
			28	201.060	1745.941
			32	714.961	7105.829
			36	2586.087	28950.219
64QAM	8	2/3	20	8.230	48.039
			24	33.410	224.276
			28	130.565	1054.021
			32	509.486	4782.351
			36	1969.693	21137.383
64QAM	16	2/3	24	24.765	183.732
			28	68.144	505.385
			32	282.016	2782.353
			36	1218.698	12964.027
64QAM	64	2/3	28	22.503	172.473
			32	90.980	843.937
			36	301.475	3351.857

Table 4.2: Weight distribution of several two-dimensional trellis codes based on 4- and 8-way partitions of the rectangular lattice $2\mathbb{Z}^2 + (1,1)$ (cont'd).

Signal Set	States	Rate	d^2	A_d	B_d
16QAM	64	1/2	16	2.000	2.000
prac			32	5.000	10.000
			40	634.315	7342.681
32QAM	64	1/2	16	2.500	4.000
prac			32	8.000	23.250
			40	1756.376	25152.614
64QAM	64	1/2	16	3.000	6.000
prac			32	11.250	40.500
			40	2963.283	47527.987

Table 4.3: Weight distribution of "practical" trellis code for 16/32/64 QAM based on a 4-way partition of the rectangular lattice $2\mathbb{Z}^2 + (1,1)$. The underlying convolutional code is the standard rate 1/2 constraint length 7 NASA convolutional code.

Signal Set	States	Rate	$d^2/2$	A_d	B_d
8PAM	4	1/2	18	1.000	2.000
			20	1.250	3.000
			22	1.750	5.000
			24	2.562	8.375

Table 4.4: Weight distribution of 1-dimensional trellis code for 8 PAM based on a 4-way partition of the lattice $2\mathbb{Z}+1$ and Ungerboeck's 4-state rate 1/2 code.

Signal Set	States	Rate	d^2	A_d	B_d
16QAM	512	2/3	32	1.000	1.000
			36	12.492	93.945
			40	41.115	377.652
32QAM	512	2/3	32	1.750	2.500
			36	25.145	350.681
			40	112.169	1726.112
64QAM	512	2/3	32	2.250	4.000
			36	42.099	439.207
			40	186.248	2313.621

Table 4.5: Weight distribution of 2-dimensional trellis code based on 8-way partition of the rectangular lattice $2\mathbb{Z}^2 + (1,1)$ with low multiplicity.

As was stated earlier, the first several terms in the union bound can be used to obtain a closer estimate of the real error performance and bit error rate at moderate to low signal-to-noise ratios. This aspect is now investigated for several trellis codes. Figure 4-16 shows the performance of 4-state, 16-state and 64-state codes using 16/32/64 QAM signal sets. A comparison with Figure 4-11 shows that the upper bound is tight at high SNR. However, the union bound does not show the cross-over effect displayed in Figure 4-11.

Figure 4-17 further shows the accuracy of the union bound for the 8-state 32QAM scheme of Figure 4-13. Here we show the effect of incorporating a varying number of terms in the approximation. As can be seen from the figure, the lower estimate based on the average number of nearest neighbors at the minimum distance yields a good approximation for high SNR but tends to be quite loose at moderate SNR. The error performance based on the inclusion of the first 5 terms in Eq.(4.32) provides an estimate which is much tighter at moderate SNR but is still quite loose at low SNR. This should not be surprising, as the union bound includes terms corresponding to codewords whose Voronoi regions do not share any faces with the reference codeword. A tighter bound would be obtained by considering only the local distance profile of the code rather than the global distance profile.

Figure 4-18 show similar results for the 64-state 32QAM scheme. The approximation appears to be tighter even at low signal-to-noise ratios. This may be due to the fact that fewer non-local distances are included in the approximation. Both of these figures show the important role played by non-minimum distance error events at moderate SNR's. This must be taken into account when evaluating the performance of concatenated coding schemes. From these simulations, it can also be inferred that tight performance estimates can be obtained from the first few terms of the weight distribution and thus can provide a useful alternative to Monte Carlo simulations at moderate SNR.

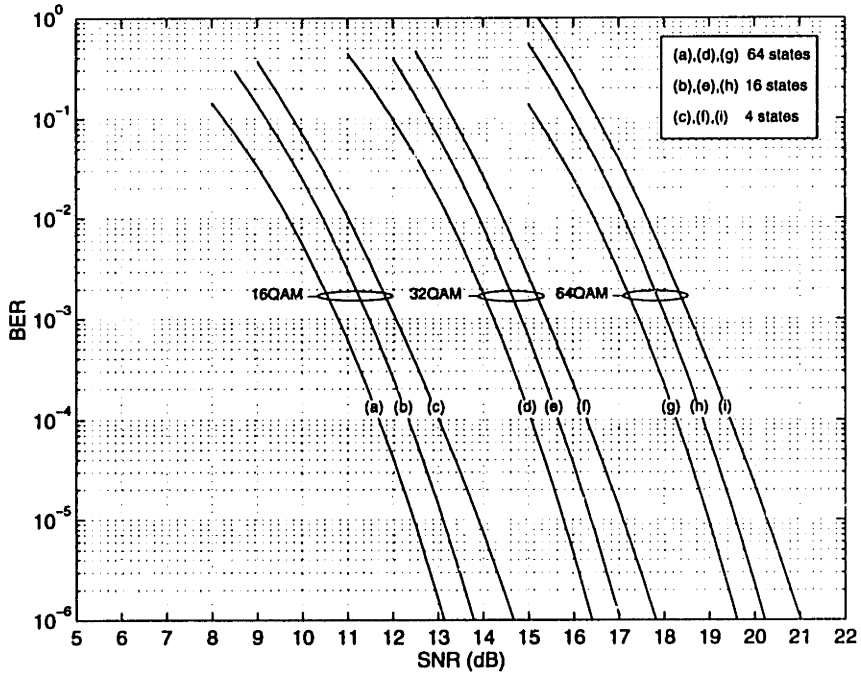

Figure 4-16: Code performance based on the union bound.

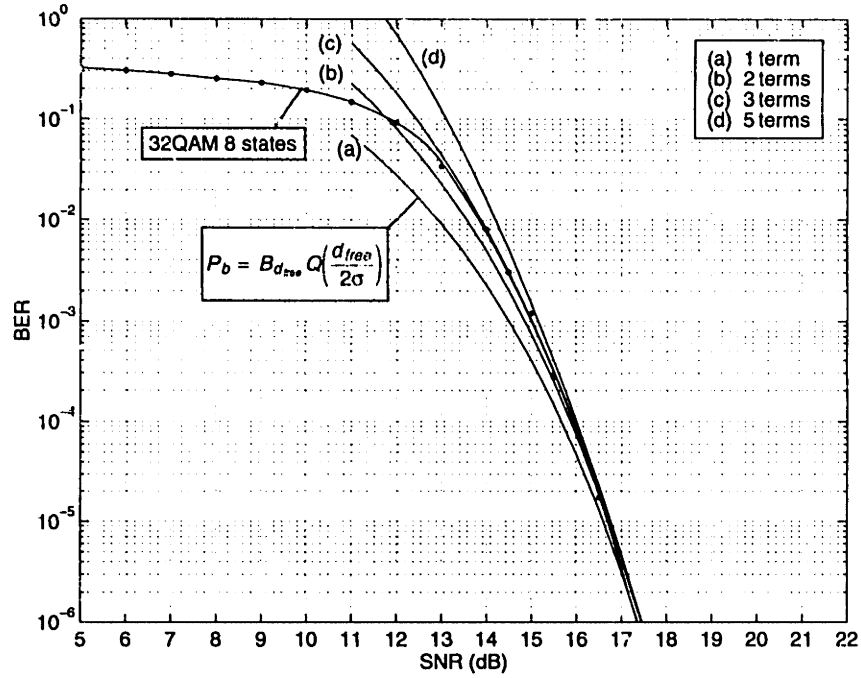

Figure 4-17: Influence of the number of terms in the union bound estimate Eq. (4.32) for an 8-state 32QAM Ungerboeck trellis code. Also shown is the performance as determined by Monte Carlo simulations (see Figure 4-11).

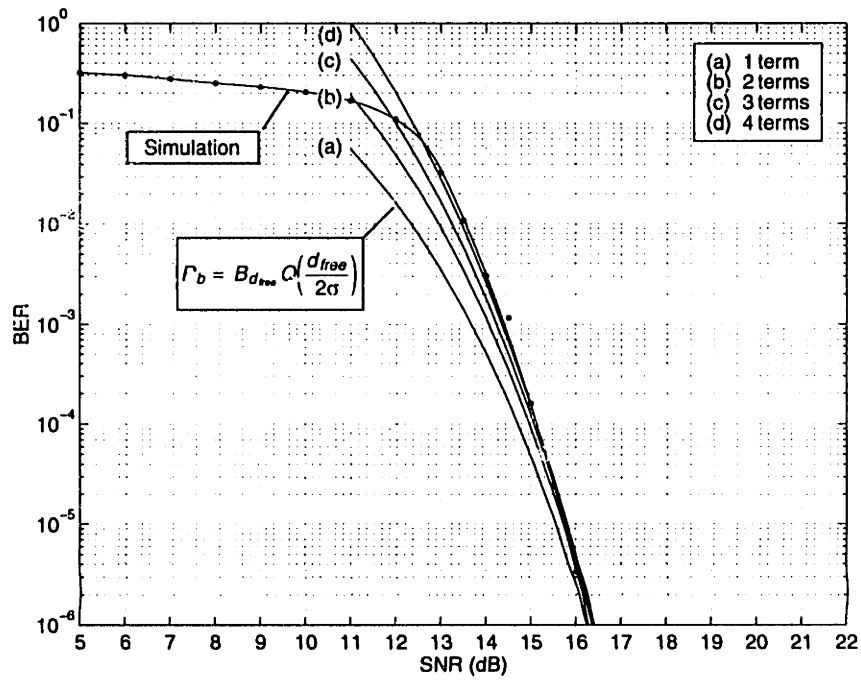

Figure 4-18: Influence of the number of terms in the union bound estimate Eq. (4.32) for a 64-state 32QAM Ungerboeck trellis code. Also shown is the performance as determined by Monte Carlo simulations (see Figure 4-11).

4.4 Concatenated coded modulation

Achieving high coding gains in a single stage with a trellis code requires a large degree of complexity. Forney suggests the following rule of thumb: "it takes two states to get 1.5 dB, four states to get 3 dB, 16 states to get 4.5 dB, perhaps 64 states to get 5.25 dB, and 256 states to get 6 dB, as long as we require a reasonably small error coefficient" [40]. As can be seen, complexity increases rapidly to a point of diminishing returns past approximately 5 dB.

Rather than attempt to achieve the desired performance in a single stage, it is often advantageous to implement the channel coding in multiple stages. This is the idea behind the technique known as concatenated coding [38]. In a two-stage concatenated coding scheme, the channel coder consists of two codes, an "inner code", which is adapted to the physical channel characteristics, and an "outer" code, which is adapted to the outer channel (sometimes called superchannel) composed of the physical channel and the inner code. The inner code is usually designed to correct most of the channel errors. The outer code, usually a high-rate code, is used to reduce the error rate to the desired level. The primary reason for using a concatenated code is to achieve a low error rate or a large error correction capability with an overall complexity which is less than that which would be required by a single coding operation. Optimal decoding of the concatenated code would require that the decoder operate on the joint state space of the inner and outer codes, but joint decoding is normally too complex to implement. Furthermore, it is not clear that there would be any advantage in using a concatenated code, as compared to a single-stage code of equivalent constraint length or block length, since its complexity would be comparable to that of a single-stage code. Thus, the usual approach is to process the data through the inner decoder first, and through the outer decoder second, possibly with side information from the inner decoder.

One of the most popular concatenated coding schemes in use today in satellite communications (cf. CCSDS - Consultative Committee for Space Data Systems - recommendation for channel coding [23]) and elsewhere utilizes a convolutional code of relatively low rate ($R = k/n = 1/2$) as the inner code and a Reed-Solomon (RS) code as the outer code. Such a scheme, because of the ensuing bandwidth expansion, cannot be used in terrestrial HDTV applications. A natural extension of this idea to a bandlimited channel consists of using a bandwidth-efficient inner code such as a trellis code with a conventional RS outer code. With properly chosen inner and outer codes, this scheme has the potential for offering several advantages: small bandwidth expansion; reasonable complexity; and large coding gain.

Figure 4-19 shows a two-stage concatenated coding scheme using a Reed-Solomon block code as the outer code and a trellis code as the inner code. The encoding process goes as follows: the binary information sequence is divided into blocks of K symbols comprising b

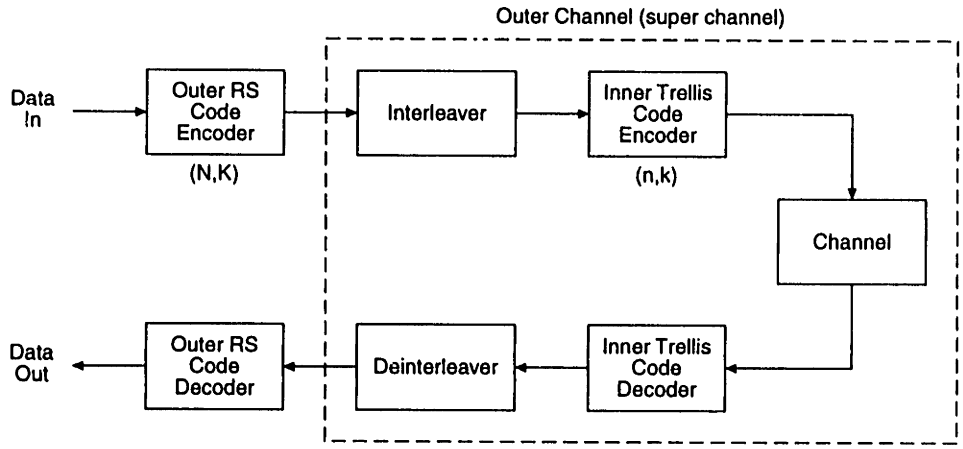

Figure 4-19: Concatenated coding using an inner trellis code and outer Reed-Solomon code.

bits each (for a total of Kb bits per block) and is applied to the input of a RS encoder operating over $GF(2^b)$. The RS encoder appends a set of $N-K$ parity check symbols to the input to form an N-symbol codeword which is symbol-interleaved and then serially encoded by the trellis encoder. Decoding is accomplished in the reverse order. The inner trellis code and outer RS code play complementary roles: the inner trellis code is capable of correcting random errors efficiently and puts out a data stream which contains rare error events which extend over several symbols. The outer code can correct these error bursts very efficiently, provided that they are shorter than the error-correction capability of the outer code. One perspective is to say that the inner code acts to match the characteristics of the physical channel with that of the outer code. The equivalent channel formed by the inner code's input/output is sometimes called the "superchannel" [45] or outer channel.

The role of the symbol interleaver is simply to spread out the error bursts when they occur so that the deinterleaved symbol stream contains a more or less constant density of erroneous symbols. A simple block-based implementation of such an interleaver consists of reading in the output from the RS encoder into a matrix row-wise and reading out the data column-wise. Thus if the matrix has m rows, the delay through the interleaver is mN symbols. By increasing the size of the matrix, one can interleave symbols over a wider span.

Such a scheme appears to be particularly well adapted to the television broadcast situation. Because of the broadcast nature of terrestrial HDTV, delays due to block processing and interleaving are much less critical than in two-way communication schemes. Because of the high data rate required for the transmission of video information for HDTV applications, even with a long block length and deep interleaving, delays are small in comparison to the acquisition times required for constructing a complete frame of video information. A further motivation for using block coding as the outer code is the fact that the information to be transmitted is

typically packetized at a higher level and therefore is naturally amenable to block processing. Finally, in situations where there is strong co-channel interference from NTSC signals, the inner decoder is likely to produce error bursts corresponding to the strong edges in the horizontal and vertical synchronization pulses occuring at a rate of 15.75 kHz and 60 Hz. An outer code with burst error correction capability is thus highly desirable. Since delay is not a major concern in HDTV terrestrial broadcasting, the interleaving depth is assumed to be chosen large enough so that errors at the output of the deinterleaver can be considered independent. RS codes provide both coding gain and burst protection, and are therefore, as stated above, particularly well suited to the television broadcast situation.

4.4.0.3 Error performance analysis

We consider a concatenated coding scheme formed by an outer RS code (N, K) over $GF(2^b)$ and an inner trellis code with QAM constellation and rate R_1 bits/complex symbol. The inner code is decoded using the Viterbi algorithm. The outputs of the Viterbi decoder are grouped into b-bit symbols. We assume that interleaving is sufficiently deep so that symbol errors are independent within each block. The error performance has been derived in Appendix B. For an (N, K) RS code, the error correcting capability t is such that $N - K = 2t$. The block error rate is approximated by

$$P_{\text{block}} \leq \sum_{i=t+1}^{n} \binom{n}{i} P_{\text{in}}^{i} (1 - P_{\text{in}})^{n-i} \tag{4.33}$$

where P_{in} is the symbol error probability at the input of the RS decoder.

The bit error rate performance is also derived in Appendix B. The relationship between the decoded bit error rate and the input symbol error rate, based on Eq. (B.9), is shown in Figure 4-20 for a Reed-Solomon code with 8-bit symbols, parameterized by the error-correcting capability of the code t. It is clear from this graph that the output bit error rate decreases very rapidly as a function of the input symbol error rate, and that the slope is steeper as the amount of redundancy increases. However, increasing the error correction capability of the block code also results in a rate decrease. Therefore, a tradeoff exists between signaling efficiency and error correction capability.

In this application, the block error rate is the natural figure of merit, since each block typically corresponds to a unit such as an HDTV video line. When an uncorrectable error within a block occurs, some action is taken regardless of the number of bit errors that occured. This typically involves repeating the corresponding line from the previous frame or replacing the line corresponding to the erroneous block by the average of neighboring lines.

Clearly, the performance and complexity of the RS decoder depends on the symbol size b.

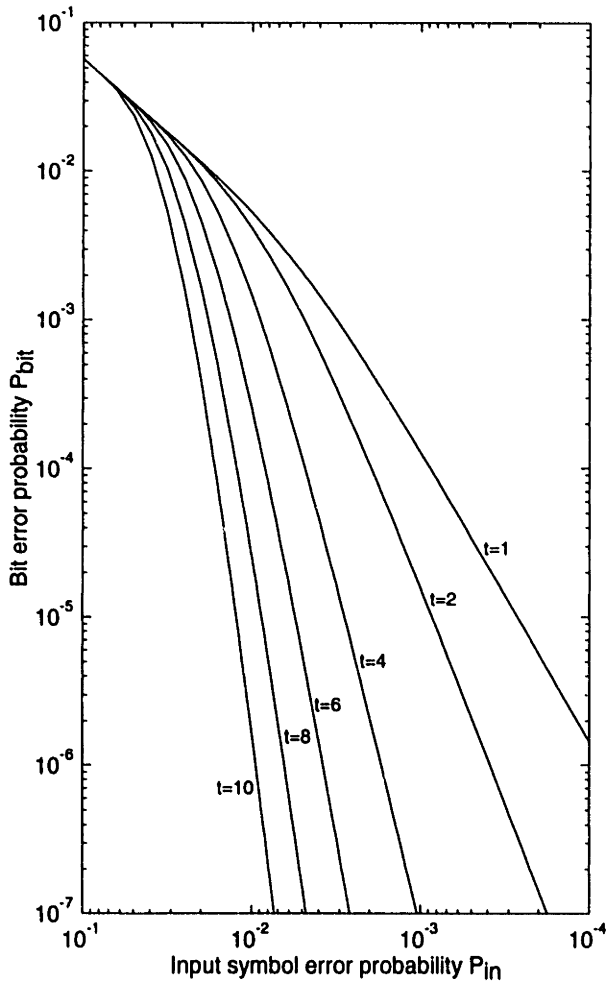

Figure 4-20: P_{bit} versus P_{in} for t-error-correcting RS code $(256, 256 - 2t)$ over GF(2^8).

In general, only relatively small values of b are of interest, since the complexity of decoders operating over larger fields render such codes impractical to implement. Here, we consider in the examples only $b = 8$ (which implies $N \leq 256$), in part because commercial hardware for such codes operating over $GF(2^8)$ is readily available, and the performance improvements that can be achieved with larger b's do not appear to justify the additional expense.

An important issue concerns the optimization of such a concatenated scheme. We now, through simulation, consider the influence of block length on the overall performance. The rate of the concatenated code is given by

$$R = \frac{K}{N} R_1 \text{bits/complex symbol} \tag{4.34}$$

where R_1 is the rate of the inner trellis code.

4.4.0.4 Simulation results

The simulation results presented in this section are semi-analytic in that they rely on Eq. (4.33) for the determination of the block error rate but use Monte Carlo simulations for the determination of the input symbol error rate. In Appendix B, we provide several approximations to convert between bit and symbol error rates. However, simulations show that these approximations tend to be quite loose at the error rates of interest and yet, a precise determination is critical to the accurate determination of the RS output error rate. Therefore, we have chosen here to estimate the symbol error rate from Monte Carlo simulations. Simulations entirely based on the Monte Carlo method were also carried out to verify the accuracy of the semi-analytic approach used here. These showed that the semi-analytic approach was accurate, if sometimes a bit pessimistic (actual error rate measurements tend to be slightly lower than predicted by Eq. (4.33)).

Influence of the block length In order to judge the performance of the coding scheme, we can examine the block error rate as a function of the normalized signal-to-noise ratio. Simulation results are shown in Figure 4-21. Shown on the figure are the different block error rate performance curves for varying input block sizes K and a fixed output block size $N = 208$. The block length N is chosen equal to that selected in the proposed standard for HDTV broadcast. Other choices could have been made, including the perhaps more appropriate maximum block size $N = 256$. The trellis code used for this example is a 4-state 32QAM Ungerboeck-type code. The block error rates are plotted against the normalized SNR, in order to make the results independent of the data rate. It is clear from this figure that the optimal performance occurs near $K = 188$. The corresponding data rate is then 3.62 bits/s/Hz. An alternative view is shown in Figure 4-22 where the normalized SNR is plotted against the overall

data rate at a block error probability of 10^{-5}. The normalized SNR is shown to be minimized in the vicinity of 3.62 bits/s/Hz.

Influence of the number of trellis code states Figure 4-23 shows the effect of the number of states of the inner trellis code on the overall performance. From this, is can be seen that, at fixed RS block length, the performance of the concatenated code increases with the number of states, but that the increase is relatively small (approximately 0.5 dB when increasing the number of states from 4 to 64, i.e. a complexity factor increase of 8). A similar conclusion can be drawn from Figure 4-25, where again the coding gain increase is less than .5 dB at a block error rate of 10^{-4}. Thus, it would appear that little is gained by increasing the complexity of the trellis code.

A closer look, however, shows that the higher complexity trellis codes can decrease the requirements on the error correction capability of the outer code. Figure 4-26 shows the normalized SNR as a function of information rate for three different trellis codes. It is clear from this graph that increasing the complexity of the inner code allows the information rate to be increased, approximately from 3.6 bits/2D symbol to 3.75 bits/2D symbol, for an inner code with 64 states. The real coding gain is also improved (now more than 0.7 dB at a block error rate of 10^{-5}). While the coding gain increase may not seem worthwhile, the ability to transmit a higher data rate is much more important. At a signaling rate, this increase is equivalent to more than 0.8 Mb/s.

For comparison, the performance of the 4-state one-dimensional 8PAM trellis code proposed recently as a possible standard for HDTV terrestrial broadcasting is also shown in Figure 4-27. The performance is comparable to that of the 16-state 2-dimensional code shown in Figure 4-25. This is most likely due to the unusually low multiplicity coefficients of the first terms of the weight distribution of the code. Figure 4-28 shows that the normalized SNR has a broad minimum centered at $K = 188$ and $R = 3.62$ bits/s/Hz. This performance does not appear to be as good as that achieved by the more powerful two-dimensional trellis codes shown in Figures 4-25 and 4-26. The reason for this is that the performance of the 8PAM trellis code is slightly better that the equivalent 2-dimensional schemes at low SNR because of the small error coefficients of the weight distribution. This advantage disappears as the redundancy of the outer code is decreased and the inner code is designed to operate at a lower output error rate.

Thus, to summarize, we have shown that the choice of a powerful inner trellis code is important to optimize jointly coding gain and data rate. A good strategy appears to be to choose a powerful inner code of reasonable complexity, but with as little a multiplicity coefficient as possible, and to minimize the redundancy of the outer code so as to achieve high information rate and high reliability. A more complete study would require examining the influence

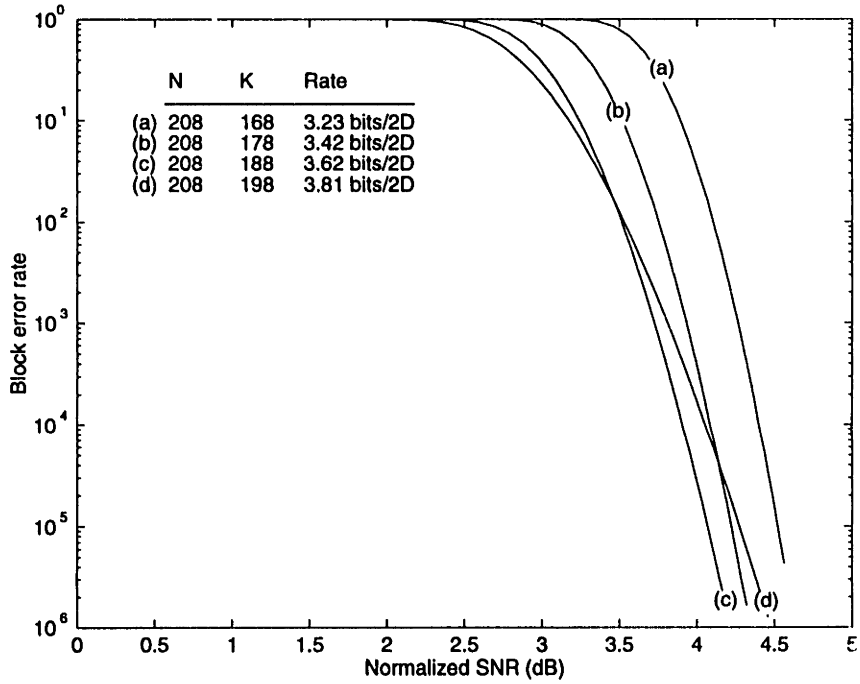

Figure 4-21: Performance of the concatenated code scheme based on inner 4-state 32QAM trellis code and RS outer code for different data length values.

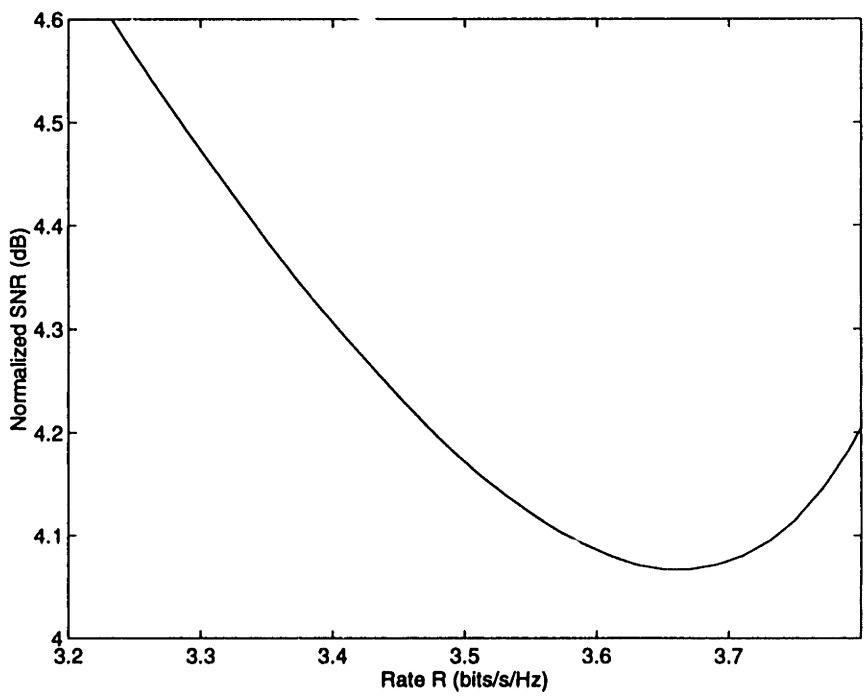

Figure 4-22: Normalized signal-to-noise ratio as a function of code rate for concatenated scheme with RS $(208, K)$ outer code (K even) and 4-state 32QAM trellis code at a block error rate of 10^{-5}.

of constellation size, inner and outer code redundancies on error performance and decoder complexity.

4.4.0.5 Analysis based on the union bound

The block error rate is given by

$$P_{\text{block}} \leq \sum_{i=t+1}^{n} \binom{n}{i} P_{\text{in}}^{i} (1 - P_{\text{in}})^{n-i} \tag{4.35}$$

The symbol error rate can be estimated from the union bound

$$P_{\text{in}} \cong \sum_{d=d_{\text{free}}}^{\infty} K_d Q\left(\frac{d}{2\sigma}\right) \tag{4.36}$$

where, in a manner analogous to the error coefficient in Eq.(4.32), K_d represents the average number of symbol errors on all paths at Euclidean distance d from the correct code sequences. Thus,

$$P_{\text{block}} \leq \sum_{i=t+1}^{n} \binom{n}{i} \left(\sum_{d=d_{\text{free}}}^{\infty} K_d Q\left(\frac{d}{2\sigma}\right) \right)^{i} \left(1 - \sum_{d=d_{\text{free}}}^{\infty} K_d Q\left(\frac{d}{2\sigma}\right) \right)^{n-i} \tag{4.37}$$

Let us simplify by retaining only the first term in the first summation, since this quickly becomes the dominant term at moderate error rates

$$P_{\text{block}} \cong \binom{n}{t+1} \left(\sum_{d=d_{\text{free}}}^{\infty} K_d Q\left(\frac{d}{2\sigma}\right) \right)^{t+1} \left(1 - \sum_{d=d_{\text{free}}}^{\infty} K_d Q\left(\frac{d}{2\sigma}\right) \right)^{n-t-1} \tag{4.38}$$

As a first approximation, we can choose to examine the performance at high SNR, in which case, the first term of the weight distribution accurately reflects the performance of the trellis code. Therefore Eq.(4.38) becomes

$$P_{\text{block}} \approx \binom{n}{t+1} K_d^{t+1} Q\left(\frac{d}{2\sigma}\right)^{t+1} \tag{4.39}$$

Using the approximation $Q(x) \leq \frac{1}{2}\exp(-x^2/2)$ for $x \gg 1$, Eq.(4.39) becomes

$$P_{\text{block}} \approx \binom{n}{t+1} \frac{K_d^{t+1}}{2^{t+1}} \exp\left(-\frac{d^2(t+1)^2}{8\sigma^2}\right) \tag{4.40}$$

Therefore, with respect to the trellis code alone, the free distance is multiplied by $(t+1)$ but the error coefficient is also multiplied by a factor K equal to

$$\binom{n}{t+1} \frac{K_d^{t}}{2^{t+1}} \tag{4.41}$$

The growth of the error coefficient limits the coding gain that can be achieved by increasing the error correction capability of the code t. This is the effect observed in Figure 4-26, where the normalized SNR increases when t is increased past its optimal setting.

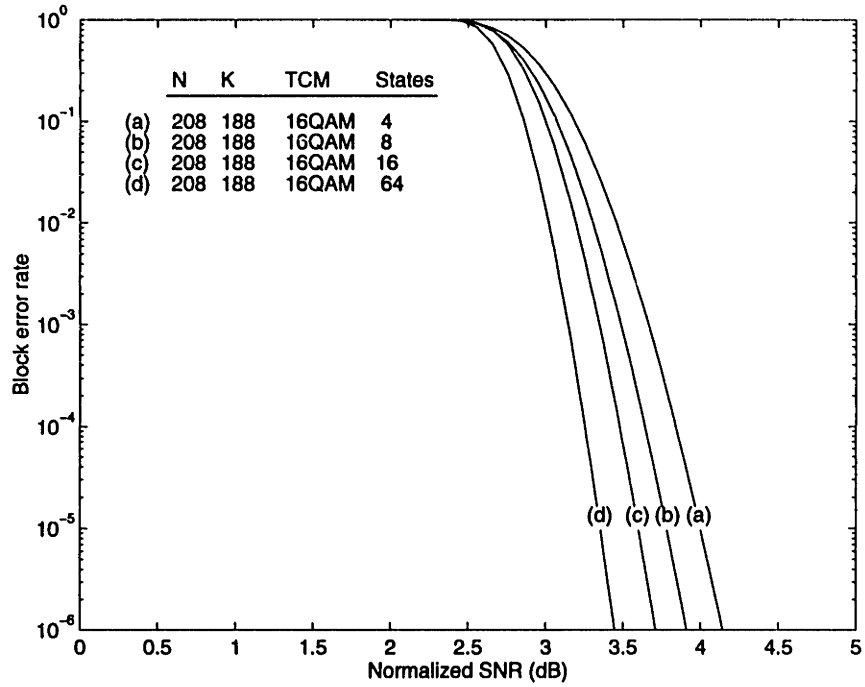

Figure 4-23: Concatenated code performance as a function of the number of states of a 16QAM Ungerboeck inner trellis code.

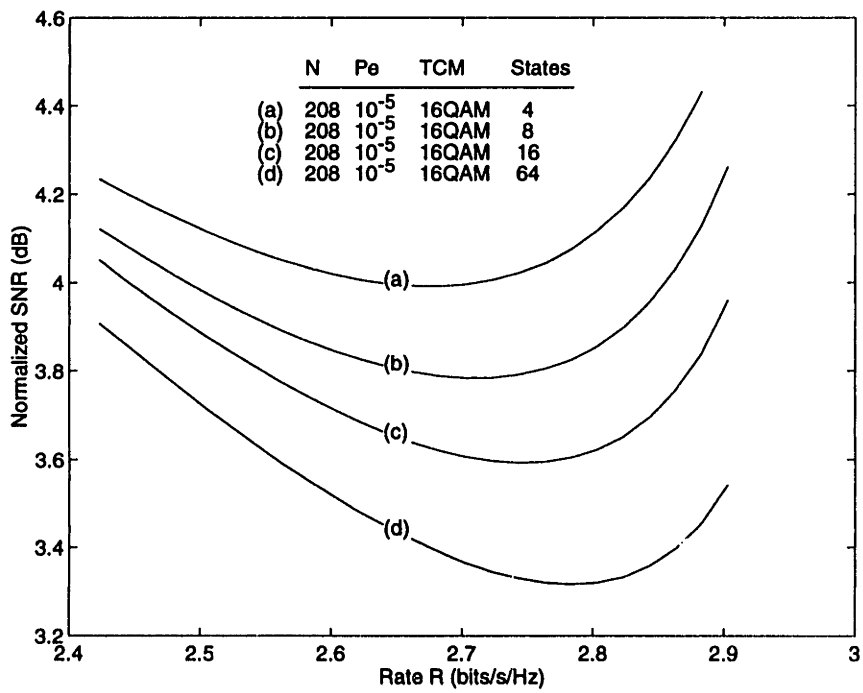

Figure 4-24: Normalized signal-to-noise ratio as a function of code rate for concatenated scheme with RS $(208, K)$ outer code (K even) and 4, 8, 16 and 64 state 16QAM trellis code at a block error rate of 10^{-5}.

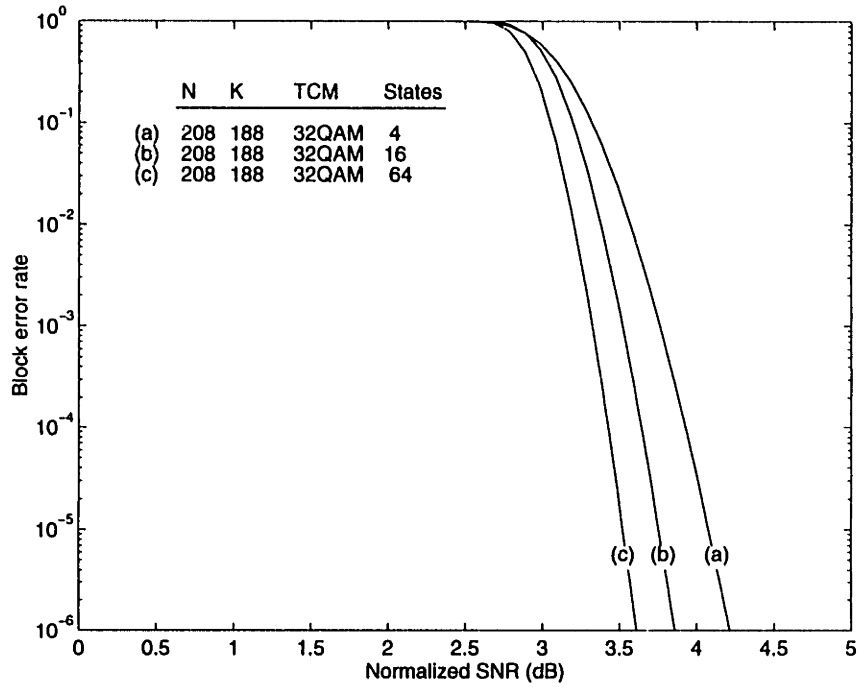

Figure 4-25: Concatenated code performance as a function of the number of states of a 32QAM Ungerboeck inner trellis code.

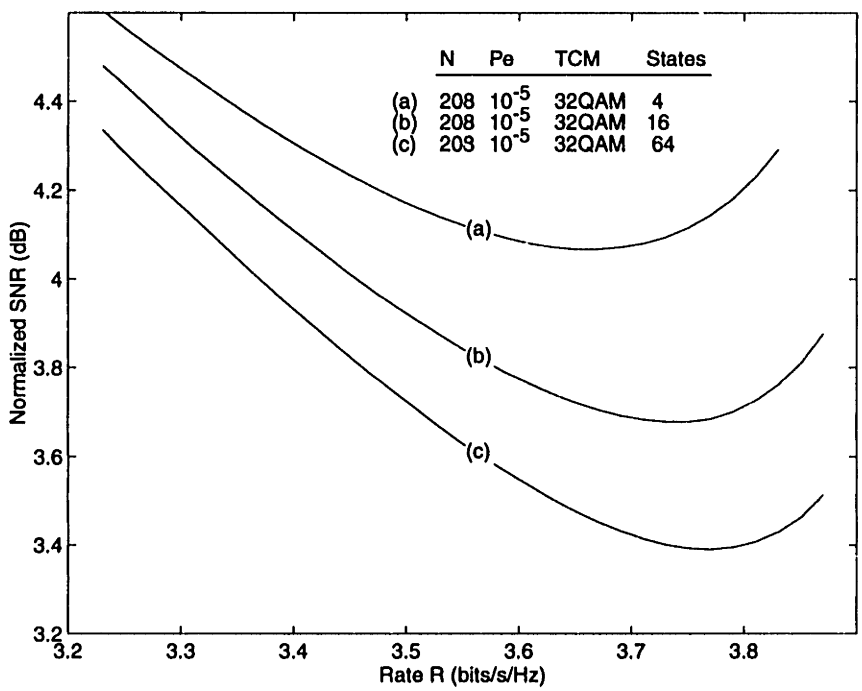

Figure 4-26: Normalized signal-to-noise ratio as a function of code rate for concatenated scheme with RS $(208, K)$ outer code (K even) and 4, 16 and 64 state 32QAM trellis code at a block error rate of 10^{-5}.

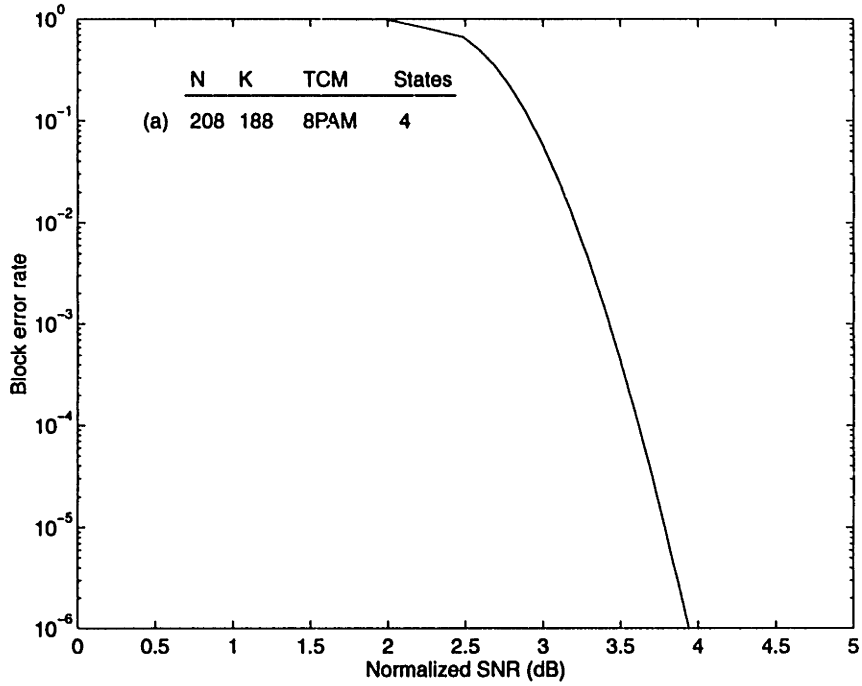

Figure 4-27: Concatenated code performance as a function of the number of states of a 1-dimensional 4-state 8PAM Ungerboeck inner trellis code.

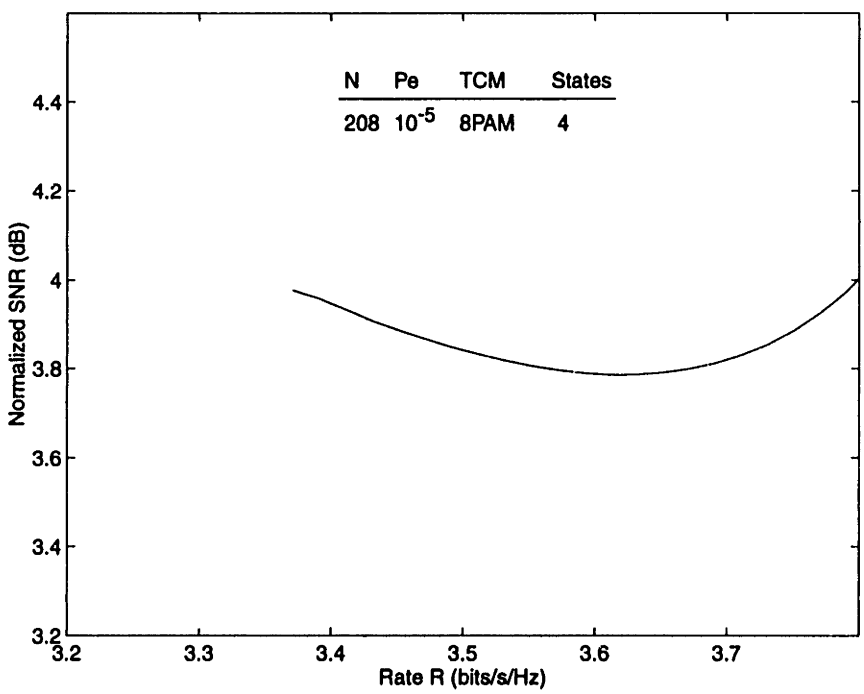

Figure 4-28: Normalized signal-to-noise ratio as a function of code rate for concatenated scheme with RS $(208, K)$ outer code (K even) and a 4-state 8PAM trellis code at a block error rate of 10^{-5}.

4.5 Conclusion

In this chapter, after introducing the concepts of channel capacity and normalized signal-to-noise ratio, we have investigated the performance of several bandwidth-efficient coded modulation schemes. The weight distribution of a number of interesting codes for HDTV were computed, and the influence of various parameters (number of states, path multiplicity, dimensionality) was discussed. In order to achieve a better complexity/performance tradeoff, and in an effort to exploit the additional properties of the HDTV channel, we have evaluated the performance of concatenated coding schemes combining various trellis codes and Reed-Solomon codes. We have shown that the performance of such concatenated codes can be improved by choosing sufficiently powerful inner codes and adjusting the error correction capability of the outer code accordingly. By contrast, in the current HDTV standard proposal, a relatively powerful outer code is used in combination with a very simple inner code which delivers a high output error rate. Our result suggests that the performance of the concatenated scheme can be improved by ensuring that the inner code operates at a lower output error rate and by correspondingly decreasing the redundancy of the outer code, at the cost of an increase in decoder complexity.

5

Multi-rate channel coding for the HDTV broadcast channel

5.1 Introduction

A number of characteristics distinguish the television broadcast channel from better-studied channels such as the two-way point-to-point telephone channel. An obvious difference is that there are many receivers for each transmitter, and thus, since signal strength is a function of distance, receivers located far away from the transmitter must operate at a degraded signal-to-noise ratio (see Figure 5-1).

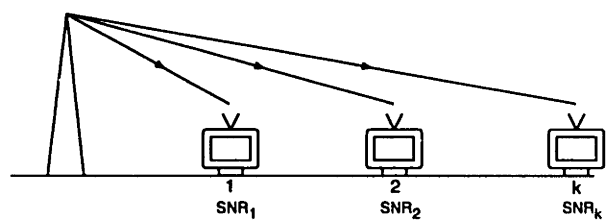

Figure 5-1: Television broadcast channel.

The approach generally adopted so far in practice has been to design the transmission system for the worst-case receiver conditions. This obviously seems to be a rather inefficient use of channel resources, since many receivers operate at unnecessarily low error rates. For these receivers, the SNR gap to capacity is very large. How can this be improved? A natural idea, and one which has received considerable attention [1, 26, 77, 88, 91, 97], is to transmit a signal with different "resolutions". This seems all the more appropriate as the information being

transmitted over the channel is not necessarily of uniform importance. Video information, for example, can be partitioned, at some (hopefully small) source coding cost, into several data streams with varying degrees of importance. Therefore, transmission schemes that provide different levels of error protection for the different data streams would appear to be of interest.

Since channel capacity is a function of the receiver signal-to-noise ratio, it is clear that the channel capacity of receivers far away from the transmitter will be smaller than that of receivers close to the transmitter. Figure A-1 in Appendix A.1 shows that the difference in field strength between receivers within a 10 mile radius from the transmitter and receivers located near the NTSC grade B service contour may be as large as 40 dB[1]. The implication is that receivers closest to the transmitter should be able to support a far greater data rate than receivers located near the boundary of the service area (using the rule that each additional bit/2D-symbol requires an additional 3 dB, the inner-city channel could potentially support 13 additional bits/2D-symbol!). Transmission schemes designed solely to meet constraints at the fringes of the coverage area are unable to take advantage of the increased capacity of receivers located near the transmitter.

An obvious solution to this problem is to distribute the power spatially, by using multiple low-power transmitters. Unfortunately, such a scheme is not being considered at the present time because it is thought to be too expensive to broadcasters and would require a drastic rethinking of spectrum allocation issues. Furthermore, from a technical standpoint, receivers would have to cope with strong co-channel signals from neighboring cells, and it is not clear that immunity to strong echoes can be achieved without resorting to steerable directional antennas or using some form of spatial diversity reception.

With this in mind, it may be advantageous to seek a partial solution, by attempting to deliver different amounts of data to different receivers. In effect, this is what is done unintentionally with analog television broadcast, where different grades of service have been defined (Grade B, Grade A and City Grade, see Appendix A.1). Such an arrangement is evidently also possible with a digital system by transmitting different data streams with different levels of protection, so that receivers with high signal-to-noise ratios can receive more information than receivers with low signal-to-noise ratios.

Transmission of different information streams to different receivers implies a certain degree of dependence between source and channel coding, when the different data streams are semantically related. A case in point is the transmission of video information.

Video information is in principle very amenable to processing at different rates. There is a

[1]Figure A-1 shows the expected value of the field strength for an NTSC signal, but it is reasonable to assume that the rate of attenuation of a digital HDTV signal would not be very different.

considerable body of literature on the topic of multirate, multiresolution, and multiscale image and video coding. Some of the better developed techniques include pyramid coding schemes based on wavelet, subband and transform decompositions. Intrinsically, these schemes provide a means of coding video information at different rates and of viewing the information at different scales and resolutions.

In general, however, in order to provide satisfactory results at several scales simultaneously, a price must be paid. Video coding schemes that provide multiple resolutions require higher overall data rates than their single resolution counterparts. Thus, in designing such a system, one has to weight the loss of coding efficiency against the increase of flexibility provided by a multirate source coder. A complicating factor is that the relationship between picture quality and data rate is not a fixed one. It is highly dependent on picture content. There is no guarantee that a system designed to deliver fixed subsets of the data with different degrees of reliability can achieve the target picture quality or resolution at all levels simultaneously.

In this chapter, we restrict our attention to the channel coding problem, leaving the joint source/channel coding problem to future research. Issues involved in using the broadcast channel efficiently are examined. At the outset, it should be noted that the problem of designing codes for the general broadcast channel remains largely an unsolved problem. The solutions that have been found so far, which we outline in the next sections, are only partially satisfactory and are in many ways ad-hoc.

In a first part of the chapter, we examine some of the fundamental limits on the transmission of information over broadcast channels. This topic has received some attention in the field of information theory [24, 6, 31]. In particular, Cover [24] has studied the problem of optimizing the transmission of a broadcast channel from an information-theoretic point of view and concluded that, for a certain class of broadcast channels, the so-called degraded broadcast channels [24, 31], high joint rates of transmission are best achieved by superposing high-rate and low-rate information rather than by using time or frequency multiplexing.

In a second part, we examine some practical schemes that may be used to transmit multiple information streams to different receivers and analyze the advantages and disadvantages of the proposed methods. One such practical scheme is a three-level scheme based on a multiresolution 64QAM constellation. Performance results are presented which show that a range of rates and signal-to-noise ratios can be achieved in a simple manner.

5.2 The memoryless Gaussian broadcast channel

Let us consider the simple discrete-time Gaussian broadcast model consisting of one transmitter and two receivers shown in Figure 5-2. The generalization to N receivers is straight-

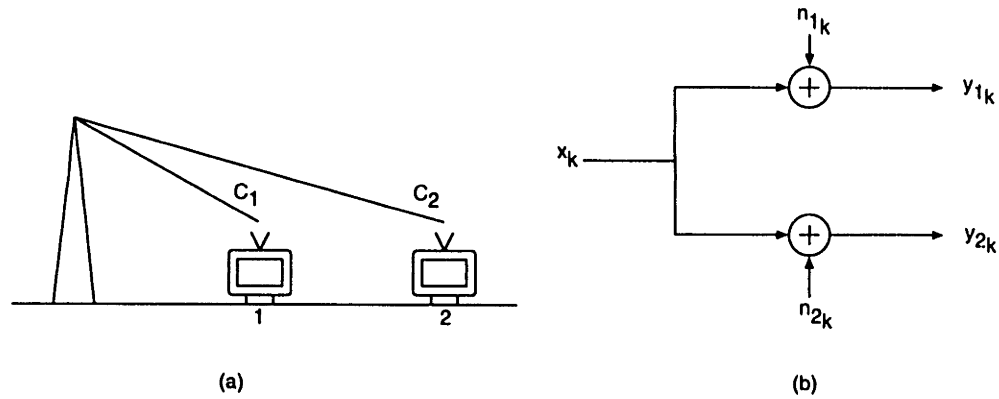

Figure 5-2: (a) Broadcast channel with one transmitter and two receivers. (b) Discrete-time Gaussian broadcast model.

forward. The basic problem is to find the set of *simultaneously* achievable rates R_1 and R_2 to each of the receivers. The class of channels considered is the class of degraded broadcast channels. A broadcast channel is said to be degraded if the probability transition function factors:$p(y_2, y_1|x) = p(y_1|x)p(y_2|y_1)$. A more rigorous definition can be found in [25]. This is a reasonable model for the television broadcast channel, where the signal is more attenuated further from the transmitter.

Let $\{n_{1k}\}$ and $\{n_{2k}\}$ be sequences of independent identically distributed (i.i.d.) complex Gaussian random variables (RV) with zero mean and respective variances N_1 and N_2. We can assume with no loss of generality that $N_1 < N_2$. At time index k, x_k is sent and $y_{1k} = x_k + n_{1k}$ and $y_{2k} = x_k + n_{2k}$ are received. Let there be a power constraint on the transmitter power $E[|x_k|^2] = S$. From Eq. (4.9), the transmission channels to the receivers have respective channel capacities C_1 and C_2 , in bits/2D-symbol, given by

$$C_1 = \log_2\left(1 + \frac{S}{N_1}\right) \quad \text{and} \quad C_2 = \log_2\left(1 + \frac{S}{N_2}\right) \tag{5.1}$$

5.2.1 Maximin approach

The first approach is to send information at the maximum rate compatible with channel 2. The maximum achievable rate is therefore $\min(C_1, C_2)$ for both channels, i.e. $R_1 = R_2 = C_2$. Cover calls this the maximin approach [24]. Note that this applies to channels other than the Gaussian channel.

The techniques that can be used to approach this rate are the same as in the point-to-point communication problem. Signal space codes, for example, would allow us to approach C_2 to within a few dB, with reasonable complexity. This is the approach used in the current generation of HDTV transmission systems. If $C_1 \gg C_2$, it may be argued that this is an inefficient use of the channel resources.

5.2.2 Multiplexing approach

Another approach consists in sending information at rate C_1 for a fraction λ_1 of the time (or frequency) and at rate C_2 for a fraction λ_2 of the time with $\lambda_1 + \lambda_2 = 1$. The information rates to the two receivers are then

$$R_1 = \lambda_1 C_1 + \lambda_2 C_2 = \lambda_1 \log_2\left(1 + \frac{S}{N_1}\right) + \lambda_2 \log_2\left(1 + \frac{S}{N_2}\right) \tag{5.2}$$

$$R_2 = \lambda_2 C_2 = \lambda_2 \log_2\left(1 + \frac{S}{N_2}\right) \tag{5.3}$$

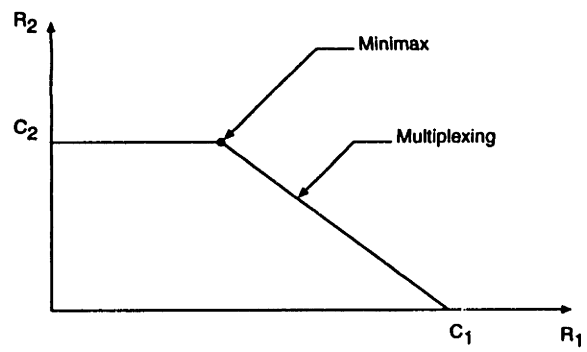

Figure 5-3: Achievable rates using the minimax and multiplexing methods for the broadcast channel (after [24]).

Both the maximin and multiplexing approaches are shown in Figure 5-3 for two receivers. In the multiplexing approach, a rate decrease for channel 2 is traded for a rate increase for channel 1 in the ratio $C_2/(C_2 - C_1)$.

In practice, the multiplexing approach may be implemented by sending a high-rate constellation or code for a fraction λ_1 of the time and a low-rate constellation or code for the remainder. A dual-rate system of this type was proposed for a first version of one of the HDTV prototypes [97], but the approach was later abandoned. It is clear that this scheme is suboptimal since, when the high rate code is decoded correctly, the low rate code is decoded with an unnecessarily low probability of error. From a theoretical standpoint, the suboptimality is seen from the fact that it is possible to find schemes that yield a larger increase of the rate in channel 1 for the same rate decrease in channel 2.

5.2.3 Superposition approach

Let us see how we can improve on the performance of the multiplex scheme. Let us assume that $x_k = x_{1k} + x_{2k}$, where $\{x_{1k}\}$ and $\{x_{2k}\}$ are sequences of i.i.d. Gaussian RVs with 0 mean and variance αS and $(1-\alpha)S$ respectively.

Receiver 2 considers both x_{1k} and n_{2k} as noise, and therefore, messages may be sent to receiver 2 at rates less than

$$R_2 = \log_2\left(1 + \frac{(1-\alpha)S}{\alpha S + N_2}\right) \tag{5.4}$$

Since $N_1 < N_2$, receiver 1 can also correctly determine the transmitted sequence x_2 with arbitrarily low probability of error. Upon decoding of x_2, given y_1, receiver 1 then subtracts x_2 from y_1 , yielding $y_1 - x_2 = x_1 + n_1$. At this stage channel 1 may be considered to be a Gaussian channel with input power constraint αS and additive zero mean Gaussian noise with variance N_1. The capacity of this channel is $R_1 = \log_2(1 + \alpha S/N_1)$ bits per complex symbol. This informal argument shows that

$$R_1 = \log_2\left(1 + \frac{(1-\alpha)S}{\alpha S + N_2}\right) + \log_2\left(1 + \frac{\alpha S}{N_1}\right) \tag{5.5}$$

$$R_2 = \log_2\left(1 + \frac{(1-\alpha)S}{\alpha S + N_2}\right) \tag{5.6}$$

may be simultaneously achieved, for any $0 \leq \alpha \leq 1$. These rate pairs, shown in Figure 5-4, dominate the multiplexing rates.

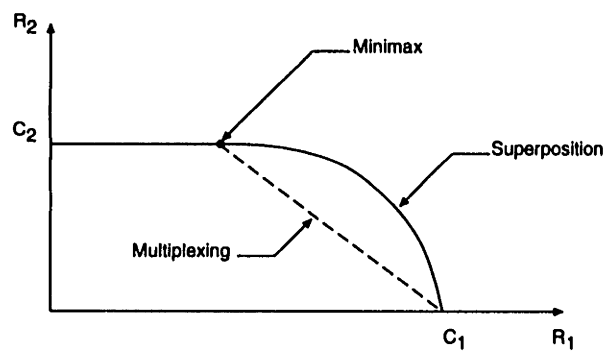

Figure 5-4: Achievable rates using the minimax, multiplexing and superposition approaches for the Gaussian broadcast channel (after [24]).

This shows that, at least in principle, a better way to communicate information simultaneously to the two receivers is by superposing information intended for receiver 1 onto the information intended for receiver 2. This concept has an interesting graphical interpretation shown in Figure 5-5. The important information, destined to be correctly received by the low-SNR receiver, is shown as black dots in the set of possible codewords. Surrounding these dots

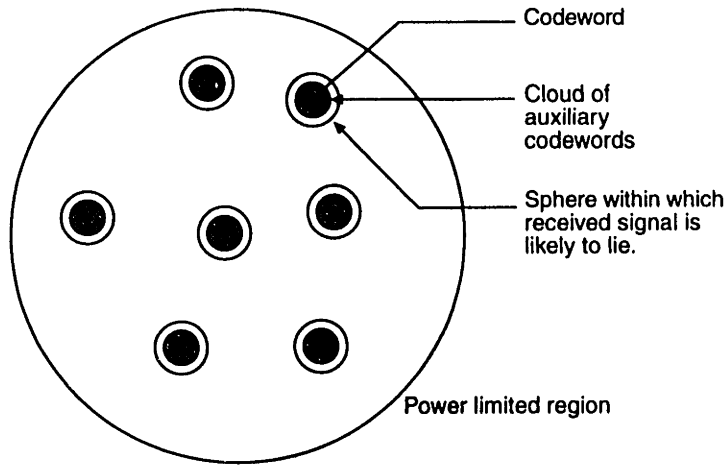

Figure 5-5: Superposition coding in the two-receiver case.

are clouds of auxiliary codewords which are destined to be correctly decoded by the high-SNR receiver. The combination of the codewords for receiver 1 and 2 is additionally degraded by noise, which defines a sphere where the received signal is likely to lie. The radius of this sphere is proportional to the standard deviation of the noise at the receiver under consideration.

We should note that these results do not take into account the important issue of decoding complexity, and therefore may not be reflected in actual coding schemes. However, they may be used as guidelines for designing practical coding schemes.

5.3 Simple embedded constellations

The superposition coding approach suggests that an efficient way of transmitting information may be via "embedded" coding. Different forms of embedded coding have been previously proposed. A simple method is achieved by defining embedded constellations in a 2-dimensional complex signal space. One such constellation using a 4QAM constellation embedded in an analog QAM constellation is described by Schreiber in [82] for the purpose of transmitting both analog and digital information. Uz *et al.* [88, 77] have described several signal constellations that implement what they call multiresolution modulation. The emphasis of their work is on joint source/channel coding. Recently, Wei [91] has also proposed a series of coding schemes for 2-resolution transmission systems that achieve good performance/complexity tradeoffs. Several of these schemes rely on embedded constellations. Two possible non-uniform constellations[2]

[2]Constellations such as shown in Figure 5-6(b) are in general not geometrically uniform in the sense defined by Forney but possess nevertheless a high degree of symmetry. (a) is a finite subconstellation of a geometrically uniform array; (b) is not.

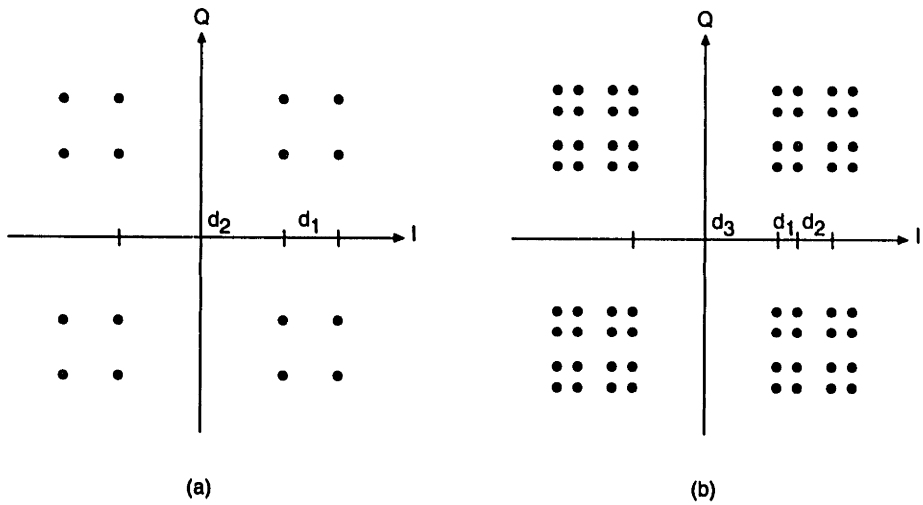

Figure 5-6: (a) Non-uniformly spaced 16QAM constellation with embedded 4QAM. (b) Non-uniformly spaced 64QAM constellation with embedded 16QAM and 4QAM.

are shown in Figure 5-6. Such embedded constellations are characterized by the property that points are clustered together at different scales. Conversely, these constellations may be regarded as having been obtained by recursively splitting an initial set of constellation points at a base level into progressively more points at the next higher level. Without coding, the constellation in Figure 5-6(a) can convey 4 bits/2D-symbol at high SNRs and close to 2 bits/2D-symbols at intermediate SNRs.

The question we seek to answer here is, how much is lost by choosing a non-uniform constellation rather than a uniform constellation of the same rate? This question can be answered by computing the mutual information between channel input and output. Let us restrict our attention to codes with uniform input distributions. Assuming a Gaussian channel, we can write the output of the channel as

$$y = x + w \tag{5.7}$$

where x is a symbol drawn from a finite alphabet of size M and w is a sample from a complex white Gaussian noise process with zero mean and variance $2\sigma^2$. The general expression for a memoryless channel with discrete-valued inputs and continuous-valued outputs was given in Eq. (4.17), which we adapt here to the case where the input symbols are equiprobable

$$I(X;Y) = \frac{1}{M}\sum_{i=1}^{M}\int_{\Omega_y} f_{Y|X}(y|x_i)\log_2\left(\frac{f_{Y|X}(y|x_i)}{\sum_{j=1}^{M}\frac{1}{M}f_{Y|X}(y|x_j)}\right)dy \tag{5.8}$$

$$= \log_2(M) - \frac{1}{M}\sum_{i=1}^{M} E\left[\log_2\left(\sum_{j=1}^{M}\exp\left(\frac{-|x_i + w - x_j|^2 + |w|^2}{2\sigma^2}\right)\right)\right] \tag{5.9}$$

where, in Eq. (5.9), the integration over the complex variable y has been replaced by the expec-

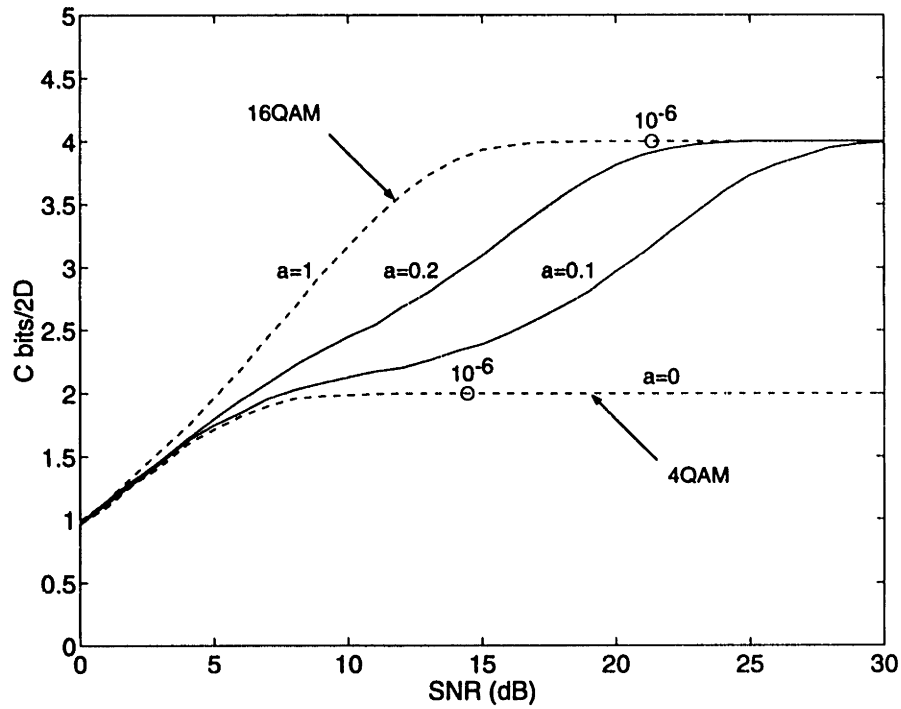

Figure 5-7: Information conveyed by non-uniform constellation over bandlimited AWGN channel, as a function of SNR.

tation operator over the normally distributed noise variable. We have evaluated this expression by Monte Carlo simulation, using a Gaussian random number generator to generate samples of w. The result displaying the information conveyed by the non-uniform constellation as a function of SNR is shown in Figure 5-7 for the constellation of Figure 5-6(a). The curves are parameterized with $a = d_1/d_2$. Also shown on the figure are the information rates corresponding to the constituent uniform constellations, 16QAM and 4QAM.

It is clear from this figure that embedded constellations are intrinsically inefficient as compared to constellations with uniformly distributed points. For instance, to transmit 4 bits per signaling interval using a uniform 16QAM constellation, the required SNR is 20.9 dB for an error of 10^{-6}. The non-uniform 16QAM constellation with $a = 0.1$ has an information rate of approximately 3.15 bits per signaling interval at SNR=20.9 dB. Moreover, a complex coding scheme would be required to achieve that rate.

One advantage of such an embedded constellation is that simple decoding schemes can be used when the receiver is operating near one of two SNR values.

Let us now return to the theoretical results concerning the code multiplexing approach. An interesting fact, which does not appear to have been studied in the literature, is that graphs similar to the ones presented in Sec. 5.2.3 can be obtained for the uncoded modulation case. We

choose to restrict our attention to the case of embedded QAM schemes. Let us assume that the constellation is formed of subconstellations with minimum intra-subconstellation distance d_1 and inter-subconstellation distance d_2. Let the rate corresponding to each subconstellation be R_1' and the rate corresponding to the centroids of the subconstellations be R_2. As an example, Figure 5-6(a) shows an embedded constellation with $R_1' = 2$ and $R_2 = 2$.

The average energy of the constellation is easily calculated to be, in the case where R_1' and R_2 are even

$$S_x = \frac{2^{R_1'} - 1}{6} d_1^2 + \frac{2^{R_2} - 1}{6} \left[d_2 + (2^{R_1'/2} - 1) d_1 \right]^2 \tag{5.10}$$

In this equation, the first term corresponds to the average energy of the subconstellation. It is derived using the fact that the average energy of an integer-spaced M-point PAM constellation is $(M^2 - 1)/12$. The second term corresponds to the centroid constellation.

For the case where R_1' is odd, the average power becomes

$$S_x = \frac{2^{R_1'+1} - 1}{12} d_1^2 + \frac{2^{R_2} - 1}{6} \left[d_2 + (2^{(R_1'+1)/2} - 1) \frac{d_1}{\sqrt{2}} \right]^2 \tag{5.11}$$

Receivers 1 and 2 are characterized by signal-to-noise ratios $\mathrm{SNR}_1 = S_x/2\sigma_1^2$ and $\mathrm{SNR}_2 = S_x/2\sigma_2^2$ respectively. Let us now assume that the threshold error rate for correct detection is 10^{-6}. In both cases, the probability of error is of the form [42]

$$\mathrm{Pr}_1 \approx K_1 \cdot Q\left(\frac{d_1}{2\sigma_1}\right) \qquad \text{and} \qquad \mathrm{Pr}_2 \approx K_2 \cdot Q\left(\frac{d_2}{2\sigma_2}\right) \tag{5.12}$$

where K_1 and K_2 are close to 4 for QAM (edge effects may reduce the multiplicity coefficients for small constellations).

Let a be the number such that

$$K \cdot Q\left(\frac{a}{2}\right) = 10^{-6} \tag{5.13}$$

where, for simplicity, K is taken equal to 4.

Let

$$\alpha = \sqrt{\frac{\mathrm{SNR}_1}{\mathrm{SNR}_2}} = \frac{\sigma_2}{\sigma_1} \tag{5.14}$$

Then, Eq. (5.10) yields the following relation between R_1' and R_2

$$R_2 = \log_2 \left(6 \cdot \frac{\frac{2 \cdot \mathrm{SNR}_1}{a^2} - \frac{2^{R_1'} - 1}{6}}{(\alpha + (2^{R_1'/2} - 1))^2} + 1 \right) \tag{5.15}$$

A similar expression can be obtained from Eq. (5.11) for the case where R_1' is assumed to be odd. Note that it is also possible to use what Forney [42] calls the continuous approximation for R_1' when the signal-to-noise difference between the two receivers is large enough. Likewise, when SNR_2 is large enough, the continuous approximation can be used for R_2.

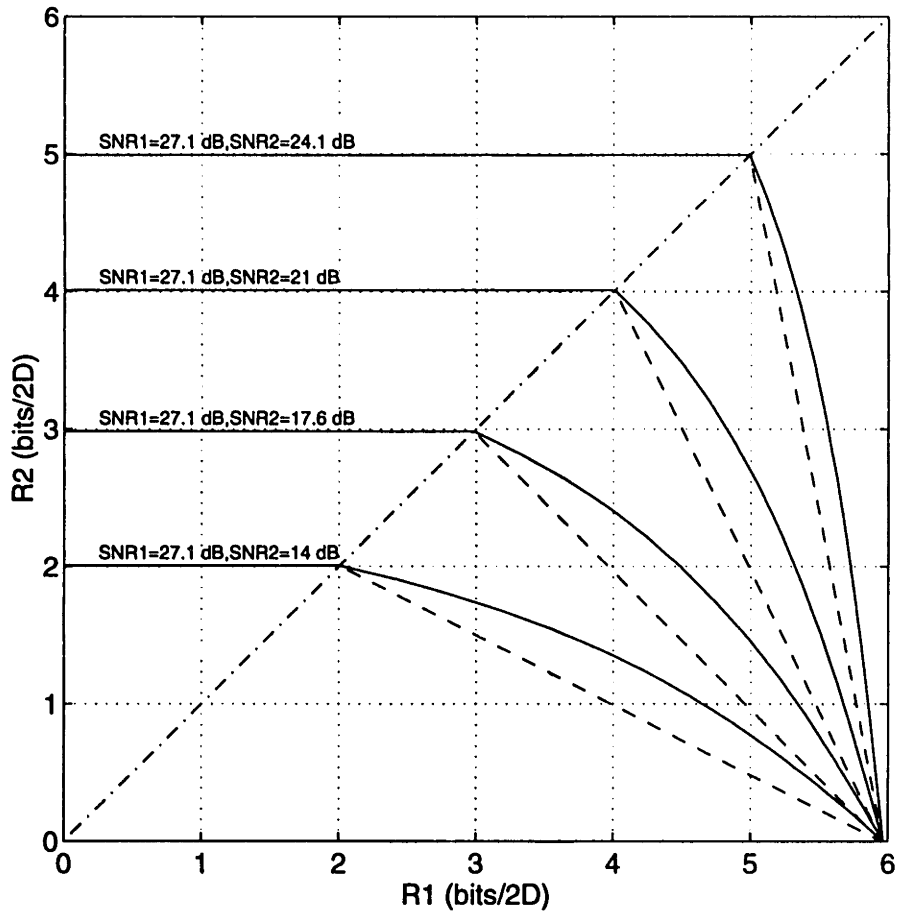

Figure 5-8: Achievable transmission rates for two-resolution system using uncoded modulation.

Let $R_1 = R_1' + R_2$ denote the total rate than can be delivered to receiver 1. Figure 5-8 is a graph of the jointly achievable rates (R_1, R_2) for the two receivers using superposition (solid lines) and multiplexing (dotted lines), without coding. Although the expression of the average constellation energy was obtained assuming the rate of the subconstellation was integer and even, we have chosen to present the results with R_1 and R_2 taken as real numbers. Very similar curves are obtained when starting from Eq. (5.11). These curves show that, even for uncoded modulation, there is a clear advantage to using superposition rather than multiplexing of information. They also show, however, the rather severe penalty that is incurred in order to provide simultaneous information to two receivers. It appears that the advantage of superposition over multiplexing is the most important when the difference of SNR between the two receivers is small. When the difference is large, a relatively small decrease of the basic rate R_2 can result in a substantial increase of the higher rate R_1. For instance, with $\text{SNR}_1 = 27.1$ dB and $R_2 = 14$ dB, a decrease of R_2 by 0.6 bits/2D results in an increase of 2 bits/2D for R_1. With $\text{SNR}_2 = 21$ dB, a decrease of the basic rate by 1 bit/2D increases R_1 by only 0.8 bit/2D. The advantage of

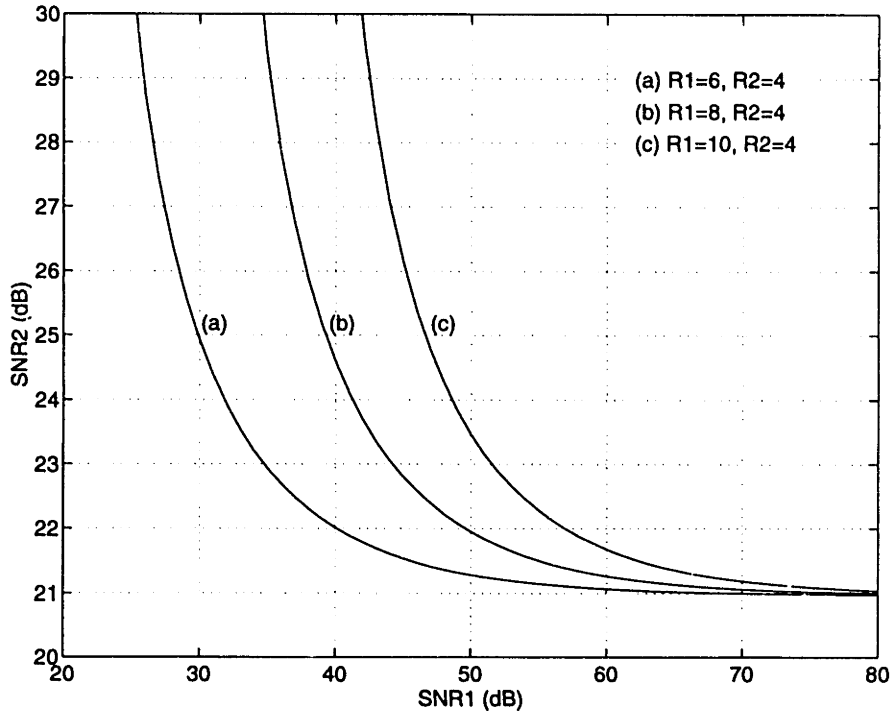

Figure 5-9: Required signal-to-noise ratios for two-resolution system using superposition with uncoded modulation.

superposition over multiplexing also increases as a function of SNR_1. These tradeoffs are shown in another fashion in Figure 5-9. Here, each curve shows the possible combinations of signal-to-noise ratios at the two receivers in order to achieve a rate pair (R_1, R_2). As SNR_1 increases, SNR_2 converges to the single resolution signal-to-noise ratio, as expected. For the example shown, this limit is approximately 21 dB. The power penalty incurred by receiver 2 in order to support an increased rate to receiver 1 is thus the difference between the operating value and the asymptotic value. For example, in order to convey an additional 4 bits/2D to receiver 1, the SNR penalty to receiver 2 is 4 dB if $SNR_1 = 40$ dB. The power penalty decreases as SNR_1 increases.

Based on these curves, it would appear that the main benefit of superposition for broadcasting would be for the case when one wants to add a low-power signal to the basic signal. The low-power signal would be received correctly within a small coverage area, but the penalty to the basic signal would then be small. This may be an interesting strategy, bearing in mind that the majority of the population is located within a small distance from the city centers where the transmitters are typically located.

We now show how, using a practical constellation example, unequal error protection can be achieved with embedded constellations.

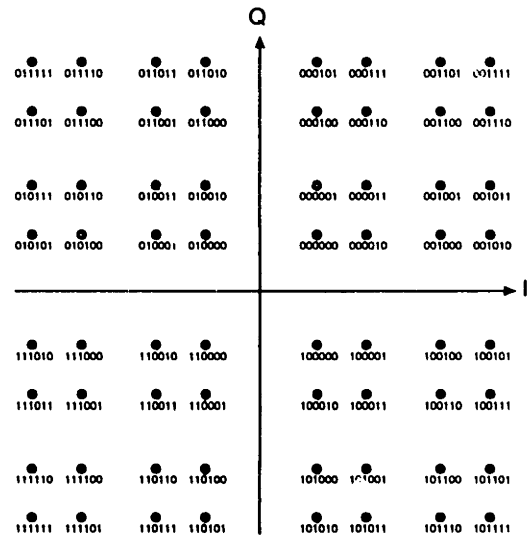

Figure 5-10: Labeling for unequal 64QAM constellation.

Let us consider the 64QAM constellation of Figure 5-6(b). We can label the points in a hierarchical fashion, so that points belonging to the same "cluster" of points at a given level have the same bit pattern for some of the bits. An example of labeling with 90° phase invariance (provided differential encoding is performed on the two leftmost bits) is shown in Figure 5-10. Each point is labeled with a bit pattern shown below the constellation point. The unequal 64QAM constellation is formed of three levels. The first level is the original constellation. At the second level, the constellation is partitioned into 4 subsets (the 16 points in each quadrant). The bits corresponding to this first partition are the 2 leftmost bits in the labeling. The resulting subsets are further partitioned into subsets of 4 points each. The bits corresponding to the second partition are the 2 middle bits. Finally the 2 rightmost bits specify the point within the 4 point subset. Let us now examine the bit error rate for the 3 different groups of bits. It is easy to see that the bit error rates are approximately given by

$$P_{b1} \simeq Q\left(\frac{d_1}{2\sigma}\right)(1 - 2P_{b2}) + P_{b2} \tag{5.16}$$

$$P_{b2} \simeq \frac{1}{2}\left[Q\left(\frac{d_2}{2\sigma}\right) + Q\left(\frac{d_2+2d_1}{2\sigma}\right)\right](1 - 2P_{b3}) + P_{b3} \tag{5.17}$$

$$P_{b3} \simeq \frac{1}{4}\left[Q\left(\frac{d_3}{2\sigma}\right) + Q\left(\frac{d_3+2d_1}{2\sigma}\right) + Q\left(\frac{d_3+2d_2+2d_1}{2\sigma}\right) + Q\left(\frac{d_3+2d_2+4d_1}{2\sigma}\right)\right] \tag{5.18}$$

where d_1, d_2 and d_3 are the distances shown in Figure 5-6(b) and σ^2 is the noise variance per dimension. The uniform constellation corresponds to $d_1 = d_2 = d_3$. In general (i.e. in all cases except $d_1 \ll d_2 \ll d_3$), these equations reduce to

$$P_{b1} \simeq Q\left(\frac{d_1}{2\sigma}\right) \tag{5.19}$$

$$P_{b2} \simeq \frac{1}{2} Q\left(\frac{d_2}{2\sigma}\right) \tag{5.20}$$

$$P_{b3} \simeq \frac{1}{4} Q\left(\frac{d_3}{2\sigma}\right) \tag{5.21}$$

It is interesting to note the reduction of the error coefficient for P_{b2} and P_{b3}, as compared to the corresponding error rates for 4QAM with equivalent distances d_2 and d_3 respectively. This is due to the fact that d_2 and d_3 specify the minimum distance between subsets at level 2 and 3, but most points in the subsets are at distances greater than d_2 and d_3 respectively.

Simulation results are shown in Figure 5-11 for $d_2/d_1 = d_3/d_2 = 1.5$ and Figure 5-12 for $d_2/d_1 = d_3/d_2 = 3$. Also shown in Figure 5-11 are the bit error rate curves corresponding to 64QAM and 16QAM. As can be seen, there is very close agreement between error rates obtained via Monte Carlo averaging and the previous approximations. By varying the relative ratios between d_1, d_2 and d_3, it is possible to arbitrarily specify the gap between the different error rate curves.

These results show that, for $d_2/d_1 = d_3/d_2 = 1.5$, the performance gap between the least protected bits and 64QAM is about 3 dB while the most protected bits offer an added protection of 4.6 dB at a bit error rate of 10^{-5}. In order to provide increased protection for a fraction of the bits, the protection on the remainder is substantially decreased.

For $d_2/d_1 = d_3/d_2 = 3$, the difference between different levels is close to 10 dB at a bit error rate of 10^{-5} and the most robust data stream has a threshold SNR lower than 16QAM by approximately 4 dB. Not surprisingly, the performance of the least protected data stream has a threshold SNR higher than 64QAM by approximately 10 dB.

5.4 Unequal error protection coding

The methods examined thus far to achieve different levels of error protection have been based on distributing the constellation points unevenly either in two-dimensional Euclidean space (multiresolution constellations) or in time (time-multiplexing of constellations with different spectral efficiencies). It seems legitimate, however, to try to apply more sophisticated forms of coding to the broadcast channel to make better use of the channel resources.

Since conservation of bandwidth and power remains a prime objective in the unequal error protection schemes considered here, it is natural to consider schemes that include some form of coded modulation. Coded modulation by itself is capable of achieving 3 to 6 dB of coding gain over the AWGN channel. However, it is thought that, in order to provide coverage areas with a meaningful difference in area served, the difference in threshold SNR between the different information streams should be on the order of 10 dB or more. This may be inferred

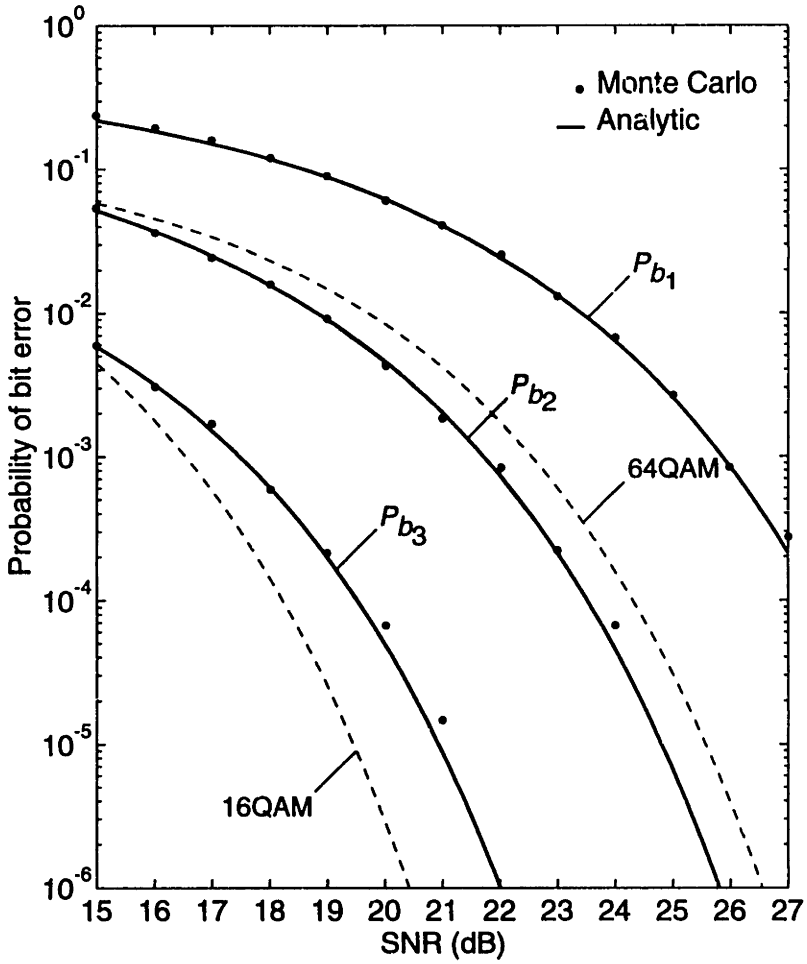

Figure 5-11: Performance of non-uniform 64QAM constellation, with $d_2/d_1 = d_3/d_2 = 3/2$.

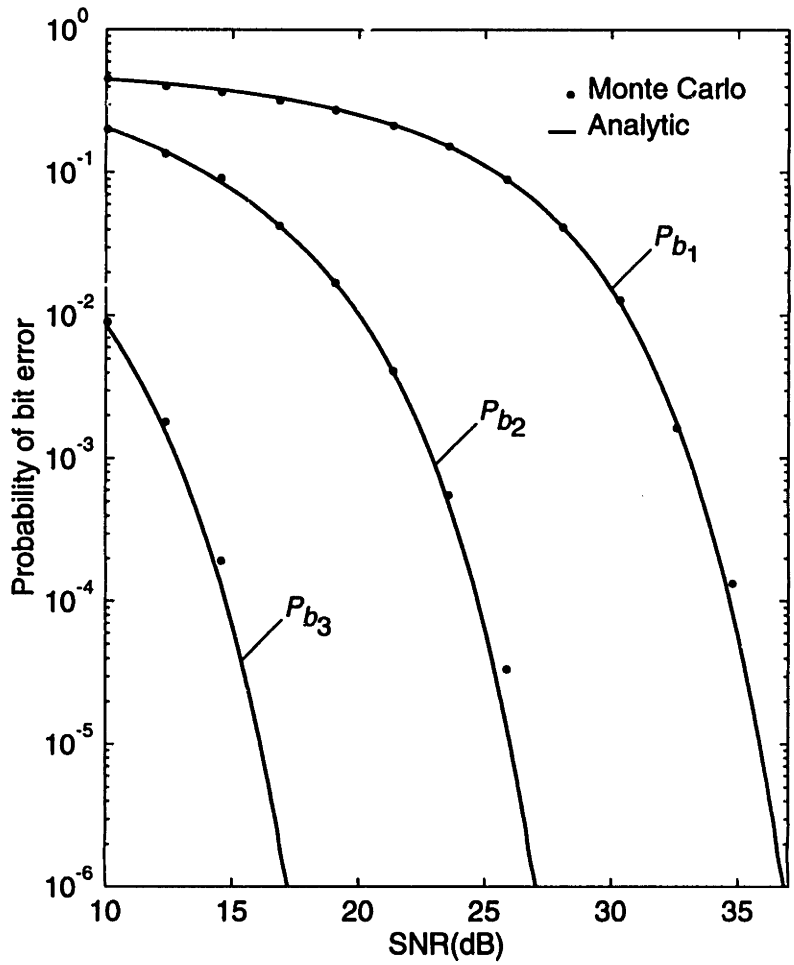

Figure 5-12: Performance of non-uniform 64QAM constellation, with $d_2/d_1 = d_3/d_2 = 3$.

from Figure A-1 of Appendix A.1, where the field strength is shown to decrease by almost 10dB for every additional 10 miles from the transmitter, once the range is greater than 20 miles.

Therefore it seems that an approach that would rely solely on the coding gains achievable by coded modulation will not be able to provide the desired range of threshold signal-to-noise ratios between the different data streams. Several attempts at implementing unequal error protection through coding alone have been made, but these have generally not been successful in the context of HDTV [37]. Accordingly, the right approach appears to be one which combines in some form the general information theoretic arguments presented in the previous section with the principles of coded modulation developed for the Gaussian channel.

Various schemes for achieving unequal error protection by combining some form of coding with uniform or non-uniform constellations have been described in the literature [26, 14, 77, 91]. These schemes can be in general divided into two families: Schemes that use the time-multiplexing concept and schemes that use the multiresolution concept.

5.4.1 Coded modulation with time-multiplexing

The combination of trellis coding and time-multiplexing of different constellations has been proposed by a variety of authors [14, 91], apparently as a generalization of the two-rate scheme originally proposed by Zenith [97]. The general idea is very straightforward and consists of time-multiplexing several trellis codes, each optimized to convey a nominal number of bits. The structure of a time-multiplexed encoder is shown in Figure 5-13. By varying the fractions of time that each trellis code is used, various data rates for each data stream can be achieved. As stated before, such a scheme is very flexible but it may be somewhat inefficient compared to schemes employing unequal constellations. In general, the switching between codes is fixed.

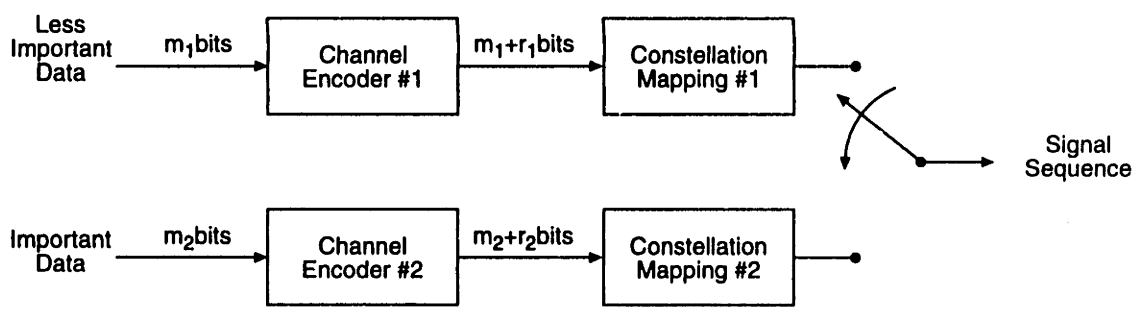

Figure 5-13: Encoder for trellis-coded time-multiplexing.

Calderbank has considered a variant where a code selects the different constellations in a given ratio [14]. In order to facilitate decoding and achieve the desired difference in SNR threshold

between the two data streams, the constellations corresponding to the two data streams are chosen to occupy disjoint concentric regions. It is not clear that this technique achieves better results that the simpler technique described above.

5.4.2 Coded modulation with unequal constellations

The combination of trellis coding and unequal constellations has also been proposed by a number of authors [26, 14, 77, 91]. Because the broadcast channel is of the degraded type, this would appear to be the better solution, for the reasons pointed out by Cover. However, one has to be careful in reaching such a conclusion in practice, because the two techniques should also be compared on the basis of complexity.

Among the various proposals for coded modulation with unequal constellations, several stand out. Wei has proposed several schemes with two levels of protection based on the combination of trellis coded modulation and unequal constellations. Figure 5-14 shows the structure of the encoder for his schemes. An interesting aspect of Wei's work is that the constellations considered have the same type of multiresolution properties as described previously, but are somewhat less "regular". This is because the design of the constellation, the constellation mapping and the choice of the encoders are carried out jointly, to reduce power requirements. In order to reduce bandwidth requirements, the constellations used in Wei's schemes have expansion ratios greater than one, which is to be expected for a coded modulation scheme for which bandwidth conservation is a concern.

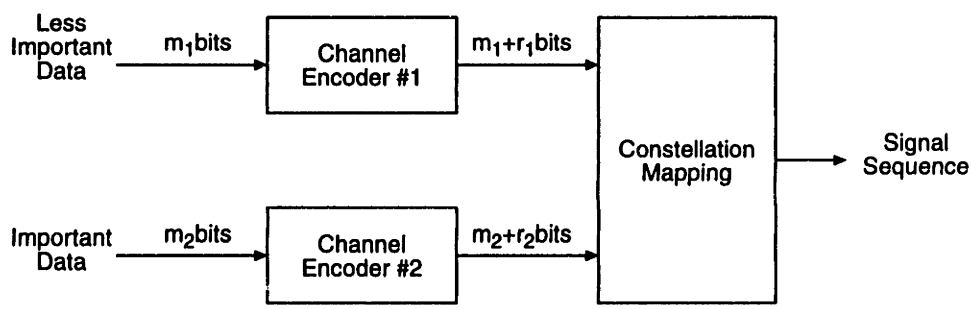

Figure 5-14: Encoder for coded modulation with unequal error protection and non-uniform constellations (Wei [91]).

Calderbank has also proposed a variety of schemes based both on multilevel codes and unequal constellations. These schemes may be viewed as an adaptation of the multilevel coding concepts described in earlier work on multilevel codes and multistage decoding [11] but there are substantial differences. Indeed, the principles used for the construction of multilevel codes

for the broadcast channel are quite different from those used to construct multilevel codes for the Gaussian channel.

In the Gaussian channel case, a multilevel code is constructed from a signal set S that admits a uniform n-level partition $S = S_0/S_1/\ldots/S_n$ and from a series of codes $C_1,\ldots,C_n$ controlling each partitioning stage [11]. The uniform property makes it possible to use a single code at level j to label the subsets resulting from the partition S_{j-1}/S_j. The partition chain $S = S_0/S_1/\ldots/S_n$ is chosen so that the minimum intrasubset squared distances $d_0/d_1/\ldots/d_n$ increase as rapidly as possible, and the codes $C_1,\ldots,C_n$ are chosen such that, at each level j, the product of the Hamming distance $d_H(C_j)$ of each code C_j by the Euclidean squared distance d_{j-1} is almost the same at all partition levels. Generally, the partitioning is such that signal sets at all levels belong to a lattice or a lattice translate. Decoding of such multilevel codes is normally carried out, for complexity reasons, by a suboptimal multistage procedure (C_1 is first decoded, then C_2, etc.). The code performance is then governed by the weakest product $d_H(C_j)d_{j-1}$. In addition, a side effect of this staged decoding is to increase the path multiplicity and therefore reduce the effective coding gain that would be achievable with a true ML decoding algorithm. In practice, this code construction technique, although elegant, has not been much used as there has not been any evidence that multilevel codes could achieve a better performance/complexity tradeoff than single level codes.

For the broadcast channel case, the uniform property needs to be retained, but the actual partitioning should be different. The rationale for this is that it would be difficult to achieve a large enough difference between the coding gains of the different data streams by partitioning a lattice into sublattices, for any reasonable complexity, and as we have seen with suboptimal decoding, the error performance is governed by the smallest product $d_H(C_j)d_{j-1}$. In the broadcast channel case, the partitioning is carried out using the multiresolution concepts outlined previously. Each partitioning stage splits a set of signal points into subsets belonging to different regions. Thus each code divides the constellation into clusters of progressively smaller spatial extents. A benefit of using this type of partitioning is that the path multiplicity is reduced as compared to the Gaussian channel case, when decoding with a suboptimal multistage decoder. The reason for this is similar to what happens with uncoded unequal constellations. Only those signal points that are on the boundary of a decision region contribute to the path multiplicity. With the same notations as above, the performance for data stream j is governed by the product $d_H(C_j)d_{j-1}$. A multistage decoding procedure will deliver data streams with different levels of protection.

We stated in the previous paragraph that unequal error protection based on partitioning of a single constellation should in general use a multiresolution constellation rather than a lattice-based constellation to achieve a sufficient difference in error protection levels. This, however,

is not a necessary condition. A large threshold difference between two levels of protection can also, under certain conditions, be achieved with a lattice-based constellation, but it appears that that coding is then relatively inefficient. To demonstrate this, we consider the following concrete example.

Consider the 8-state 32QAM trellis-coded modulation scheme described in Section 4.3.1. In this scheme, 2 bits are encoded by a convolutional code into 3 bits which select one of 8 possible subsets, while the remaining 2 bits select a specific point within the selected subset. The normal decoding procedure consists of two stages: first, the distance between the received point and the nearest point in each subset is computed (subset decoding), and second, ML decoding is applied to the trellis labeled with the subset distances. Now consider the simplified decoding procedure: first, the nearest point in the constellation is selected, and the two bits corresponding to the selected signal point within the selected subset are put out. Second, the subset distances are computed and the Viterbi decoding operation is carried out as was done previously. This decoding procedure defines two data streams with unequal error rates. The data stream corresponding to the uncoded bits (1/2 of the total data rate) has the error performance of uncoded 32QAM, while the data stream corresponding to the coded bits has an error performance 3.98 dB better than 16QAM. Therefore the performance difference between the two data streams is close to 7 dB. The scheme can be generalized in a straightforward manner. However, it is hardly an optimal scheme, since, for the same complexity, one could actually achieve a lower error rate on the uncoded bits because the intra-subset distance is $8d_0^2$ as compared to $5d_0^2$ for the coded bits.

5.4.3 A practical coding scheme for a 3-resolution system

All the schemes considered by Wei and Calderbank have two levels. In principle, the extension to more levels is straightforward. However, in order to achieve a high overall code rate, each of the constituent codes must be high-rate codes, which in practice restricts the choice of codes. In this section, we examine how the performance of the unequal 64QAM constellation investigated in the previous section can be improved by using high-rate codes.

One possibility is to use punctured convolutional codes, possibly concatenated with RS codes, in order to achieve a high overall rate. Punctured codes were proposed by Yasuda *et al.* as a practical method to implement high-code rates from a basic rate 1/2 convolutional code [95]. Such convolutional codes seem to be well suited to coding the 3 levels of the partition tree of a 64QAM constellation, since at each level, the partition is 4-way, and if one only considers the nearest neighbors, each resolution is formed of 4 subsets. Furthermore, punctured codes can be decoded with a single Viterbi decoder, irrespective of the code rate,

which may be multiplexed to handle the three data streams simultaneously.

Figure 5-15 shows the structure of the encoder for such a scheme.

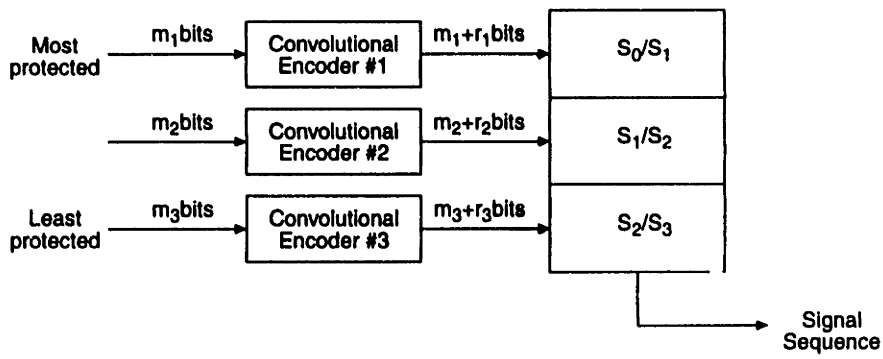

Figure 5-15: Encoder for multilevel coding with non-uniform constellations.

We have listed in Table 5.1 the minimum Hamming distance d_H, and the weight B_d of the minimum distance error events, as tabulated by Yasuda [95]. The choice of the punctured codes is very flexible, and can be tailored to the specific data rates and performance requirements. For instance, if the same rate 8/9 code is used for all levels of the partition, and the constellation of Figure 5-10 is used, the SNR threshold for all the curves shown on Figure 5-12 will be decreased by 4.7 dB and the overall code rate will be 8/9. Instead, one can seek to improve the performance of the intermediate data stream while maintaining the overall data rate by penalizing either of the other data streams. One advantage of this strategy is that the receiver only requires one decoder, irrespective of the rate used to encode each level. This may make the use of such a code attractive in situations where the data rate of one of the streams needs to be adjusted. Figure 5-16 shows the performance of the multilevel code for various code rates.

5.5 Conclusion

In this chapter, we showed that transmission schemes capable of taking advantage of the variable capacity of the broadcast channel may be an attractive alternative to single rate schemes. It should be said, however, that although video information is in principle very amenable to processing at different rates, video coding schemes that provide multiple resolutions generally require higher overall data rates than their single resolution counterparts. The natural partitioning of data for efficient video coding does not necessarily match the natural partitioning for channel coding. Furthermore, the relationship between picture quality and data rate is not

Code Rate	States	d_H	B_d
1/2	64	10	36
2/3	64	6	3
3/4	64	5	42
4/5	64	4	12
5/6	64	4	92
6/7	64	3	5
7/8	64	3	9
8/9	64	3	13

Table 5.1: Minimum distance and weight of punctured codes derived from the standard rate 1/2 constraint length 7 NASA convolutional code with generators 133_8 and 171_8 (from [95]).

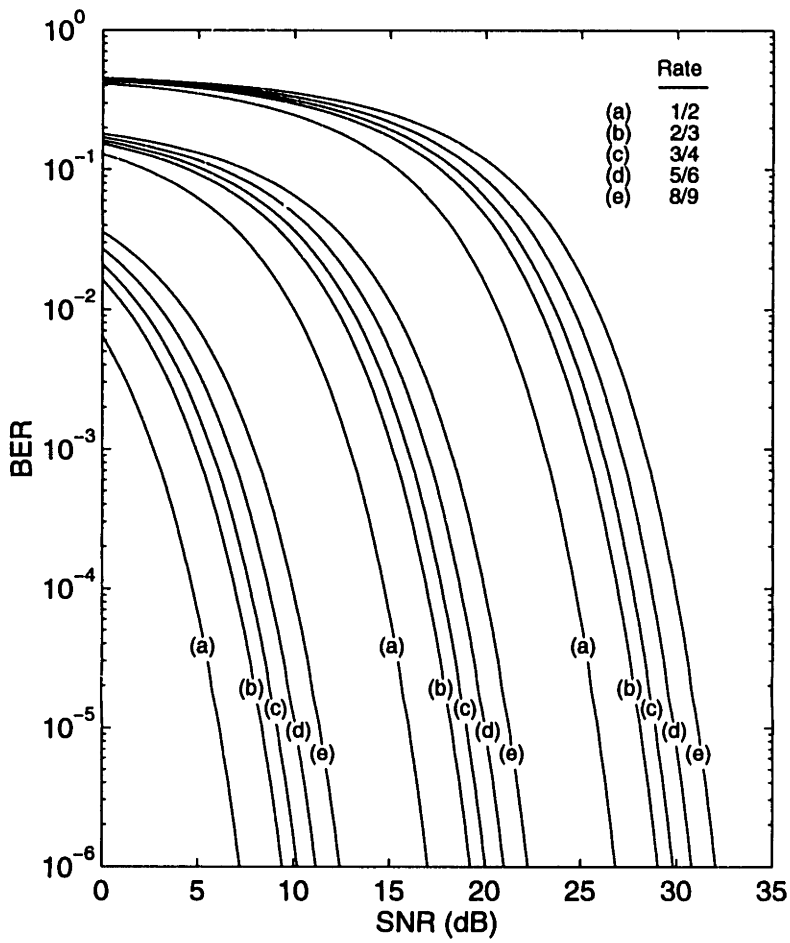

Figure 5-16: Performance of coded non-uniform 64QAM constellation, with $d_2/d_1 = d_3/d_2 = 3$ and punctured convolutional codes of rate (n-1)/n.

a fixed one, but rather, is highly picture dependent. Thus, there is no guarantee that a system designed to deliver fixed subsets of the data with different degrees of reliability can achieve the target picture quality or resolution at all levels simultaneously. The problem of jointly optimizing the source coding and channel coding systems is a fruitful area for future research. Here, we have instead restricted our attention to the channel coding problem, keeping in mind that a price must be paid for the added flexibility the proposed schemes provide.

In the first part of the chapter, we considered the case of uncoded modulation and derived practical curves that bear a strong resemblance to the information-theoretic curves showing the jointly achievable transmission rates for a two-receiver configuration. These results seem to suggest that the main benefit of superposition for broadcasting purposes may be for the case when one wants to add a low-power high-rate signal to the basic signal. The high-rate signal would be received correctly within a small coverage area (e.g. city-wide coverage), but the penalty to the basic signal would then be small. We also examined various ways in which coding could be integrated into a multiresolution system to achieve higher coding efficiency. Finally, we proposed a practical multilevel coded scheme capable of achieving a variety of rates and performances, at about the same complexity as single-resolution schemes.

6

Equalization and interference rejection with uncoded modulation

6.1 Introduction

A typical HDTV transmission channel is rarely ideal. Signal distortions caused by multipath propagation and improper filtering are common. Under some conditions, co-channel interference from distant NTSC transmitters can be the main performance limiting factor. Additional sources of performance degradation include adjacent channel interference, and time-dependent phenomena such as fading. Nonlinear effects in the transmitter and receiver may also lead to further limitations. For instance, transmitter high power amplifiers often have nonlinear amplitude and phase transfer characteristics when operated near saturation, causing nonlinear signal distortions.

For PAM, linear amplitude and phase distortions cause each transmitted symbol to extend beyond the interval used to represent that symbol and as a consequence, successive symbols interfere with one another. This phenomenon is known as intersymbol interference. There are a number of classic techniques that can be used to compensate for linear channel distortions and reduce the amount of intersymbol interference. These are referred to as channel equalization techniques. In general, channel equalization involves applying some form of filtering to the received signal in order to restore some properties of the transmitted signal. Since the received signal is also degraded by noise, the effect of filtering on the noise component of the received signal also has to be taken into account. Linear filtering of the received signal to reduce intersymbol interference generally results in enhancing the noise. There is therefore a tradeoff between accurately canceling the interference and minimizing the noise. In this chapter, we will review several criteria for designing the equalizer. The simplest is the so-called zero-

forcing (ZF) criterion which aims to cancel the intersymbol interference completely. Another is the mean-square error (MSE) criterion, which seeks to minimize the sum of the noise and intersymbol interference. The MSE criterion is often considered to be the better criterion of the two because it is more directly related to a quantity that is in practice very important: the probability of error.

In the case of terrestrial broadcast HDTV, a major source of degradation is co-channel interference from NTSC transmitters. For the reasons developed in Chapter 2, the signal received by some HDTV receivers will be corrupted by strong NTSC co-channel interference. One distinguishing feature of this interference signal is that the distribution of power across the receiver bandwidth is strongly non-uniform. Provided the interference can be assumed to be stationary and Gaussian (usually a somewhat pessimistic assumption), the problem of detecting the signal in the presence of co-channel interference can be formulated as an equalization problem, where the noise source is non-white. Fortunately, this problem can be shown to be equivalent to the white noise case, at least theoretically, provided the channel response is appropriately modified.

In this chapter, we develop the classical concepts of linear and decision-feedback equalization and apply these concepts to the problem of NTSC interference rejection. We propose a new method of combatting co-channel interference from NTSC based on a decision-feedback structure. We examine and evaluate three other methods previously proposed to reduce co-channel interference rejection and compare their performance to that of the new scheme. We introduce several reduced-complexity receiver structures that take advantage of the known characteristics of the interference and compare their performance to the unconstrained linear and decision-feedback equalizers. We show that reduced-complexity receiver structures are indeed very effective at reducing co-channel interference and have the added important advantage of reducing the risk of error propagation when decision-feedback is used.

We assume in this chapter that no coded modulation is used as part of the transmission scheme. Therefore, decisions are performed on a symbol-by-symbol basis. In general, however, it is desirable to combine coded modulation and equalization. This topic is discussed in detail in Chapter 7.

6.1.1 Notations and definitions

The following notations and definitions will be used in the remainder of this chapter:

Arithmetic and geometric means Given a non-negative real valued function $f(x)$, the arithmetic mean of $f(x)$ over X is denoted

$$\langle f \rangle_A = \frac{1}{|X|} \int_X f(x)\, dx \tag{6.1}$$

where $|X|$ is the size or measure of the set X.

The geometric mean of $f(x)$ over X is denoted

$$\langle f \rangle_G = \exp\left\{ \frac{1}{|X|} \int_X \log f(x)\, dx \right\} \tag{6.2}$$

It is well known that

$$\langle f \rangle_G \leq \langle f \rangle_A \tag{6.3}$$

with equality if and only if $f(x)$ is constant over X.

Z-transform and discrete-time Fourier transform In the following, $H(z)$ denotes the Z-transform of the discrete-time sequence h_k, defined as $H(z) = \sum_{k=-\infty}^{+\infty} h_k z^{-k}$. The following relations can easily be shown: $h_{-k} \longleftrightarrow H(1/z)$, $h_k^* \longleftrightarrow H^*(z^*)$, $h_{-k}^* \longleftrightarrow H^*(1/z^*)$. The (discrete-time) Fourier transform of h_k is defined as $H(e^{j\theta}) = H(z)|_{z=e^{j\theta}}, -\pi \leq \theta \leq \pi$. It exists if h_k is absolutely summable.

Power spectrum of a discrete-time random process Let $\{x_k\}$ be a wide-sense stationary (WSS) discrete-time random process. The autocorrelation sequence of the random process $\{x_k\}$ is defined as $R_x(k) = E[x_{n+k} x_k^*]$. Let $S_x(z)$ be the Z-transform of the autocorrelation sequence $R_x(k)$.

The power spectral density (PSD) or power spectrum of $\{x_k\}$ is obtained by evaluating $S_x(z)$ on the unit circle. Equivalently, the PSD is the Fourier transform of the autocorrelation sequence, i.e.

$$S_x(e^{j\theta}) = \sum_{k=-\infty}^{+\infty} R_x(k) e^{-jk\theta}, \qquad -\pi \leq \theta \leq \pi \tag{6.4}$$

The power spectrum is real since the autocorrelation is conjugate symmetric. It is also non-negative for all values of θ. In the sequel, we will also refer to $S_x(z)$ as the power spectrum.

Folded spectrum Let $h(t)$ denote the impulse response of a continuous-time channel. We define the sampled autocorrelation function by

$$\rho_h(k) = \int_{-\infty}^{+\infty} h(t) h^*(t - kT)\, dt \tag{6.5}$$

Since $\rho_h(k)$ is a sampled version of a function with Fourier transform $|H(\omega)|^2$, its discrete-time Fourier transform $S_h(e^{j\omega T})$ is given by

$$S_h(e^{j\omega T}) = \sum_{k=-\infty}^{+\infty} \rho_h(k) e^{-j\omega kT} = \frac{1}{T} \sum_{k=-\infty}^{+\infty} \left| H\left(\omega + k\frac{2\pi}{T}\right) \right|^2 \tag{6.6}$$

We call $S_h(e^{j\omega T})$ the folded spectrum of $h(t)$. The energy σ_h^2 of the pulse $h(t)$ is equal to $\rho_h(0)$.

Canonical channel A channel $H(z)$ with impulse response h_k which is causal ($h_k = 0$ for $k < 0$), monic ($h_0 = 1$) and minimum-phase (all poles inside the unit circle, all zeros inside or on the unit circle) will be called canonical [22]. Correspondingly, we define an anti-canonical impulse response as one which is anti-causal, monic, and maximum-phase (zeros on or outside the unit circle, poles outside the unit circle). Note that for a canonical channel, $\|H\|^2 = \sum_k |h_k|^2 \geq 1$ with equality if and only if the channel is ideal, i.e., $H(z) = 1$.

Spectral factorization Let $S_x(z)$ be the power spectrum of a random process $\{x_k\}$ such that both $S_x(e^{j\theta})$ and $\log(S_x(e^{j\theta}))$ are integrable on the interval $(-\pi, \pi)$. It then follows from spectral factorization theory that

$$S_x(z) = S_0 \cdot G(z) \cdot G^*(1/z^*) \tag{6.7}$$

where S_0 is a positive constant equal to the geometric mean of $S_x(z)$ and where $G(z)$ is a canonical response. $S_x(z)$ is said to be factorizable. Note that the variance of x_k (or average symbol energy) is equal to $S_0\|G\|^2$.

Parseval's theorem Returning to the continuous-time channel $h(t)$, let us assume that the power spectrum of the sampled autocorrelation function is factorizable

$$S_h(z) = A_h^2 G_h(z) G_h^*(1/z^*) \tag{6.8}$$

then the energy of the pulse $h(t)$ is given by the useful relation

$$\sigma_h^2 = \int_{-\infty}^{+\infty} |h(t)|^2 \, dt = A_h^2 \sum_{k \leq 0} |g_{h,k}|^2 = A_h^2 \|G_h\|^2 \tag{6.9}$$

6.2 General performance bounds

6.2.1 System model

Let us consider a system model of the type shown in Figure 6-1. This model is used to describe the baseband equivalent of a real passband HDTV channel.

The channel is characterized by a complex impulse response $c(t)$ with Fourier transform $C(f)$ and additive complex Gaussian noise $n(t)$ with double-sided spectral density $N_0 S_n(f)$. It is assumed that there is a power constraint on the channel input.

The input waveform is $\sum_k x_k p(t - kT)$, where the data sequence x_k is a sequence of independent identically distributed complex random variables x_k, with mean zero and variance (or

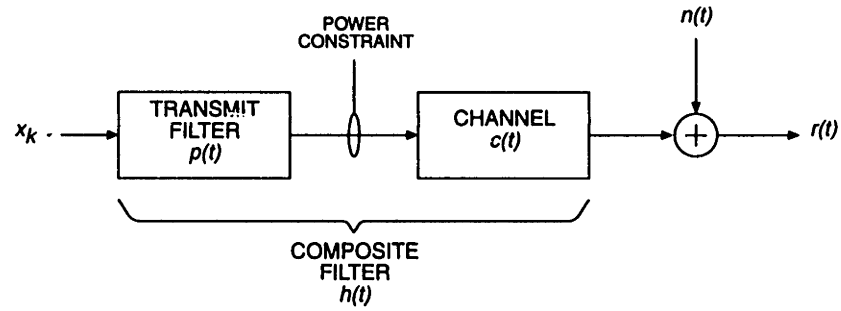

Figure 6-1: System model.

average symbol energy) $S_x = E[|x_k|^2]$. The symbol interval is T seconds. The transmit filter is characterized by a complex response $p(t)$ with Fourier transform $P(f)$. The composite response of the transmit filter and channel will be denoted $H(f) = P(f)C(f)$ with inverse Fourier transform $h(t)$.

6.2.2 Matched filter (MF) front end

White noise channel model Let us first assume that the complex Gaussian noise is white, i.e. $S_n(f) = 1$. It is well known that, without loss of generality, the receiver may always consist of a matched filter characterized by a complex response $h^*(-t)$ with Fourier transform $H^*(f)$, a symbol rate sampler, whose output is a sequence y_k of complex output symbols, and further discrete-time processing. The sequence y_k forms a set of sufficient statistics for the received signal detection [39]. By this, we mean that the matched filter output is information-lossless. This result is quite remarkable, when we consider that symbol-rate sampling at the matched filter output is generally at less than the Nyquist rate, so aliasing of both noise and signal is inherent in this sampling. This aliasing will not compromise the performance of the receiver as long as the filter before the sampling is a matched filter. The front end for the receiver is shown in Figure 6-2.

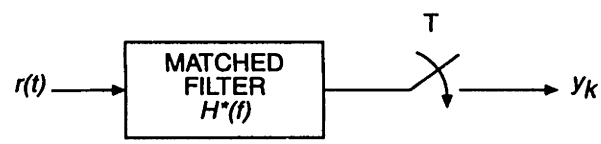

Figure 6-2: Front end for channel $h(t)$ and white noise with spectral density N_0, consisting of matched filter and symbol-rate sampler.

Non-white noise channel model When the noise is non-white with spectral density $N_0 S_n(f)$, the received signal may be first whitened with a filter $1/\sqrt{S_n(f)}$. The corresponding front end consisting of the matched filter with transform $H^*(f)$ normalized by $S_n(f)$ and symbol rate

sampler again generates a set of sufficient statistics.

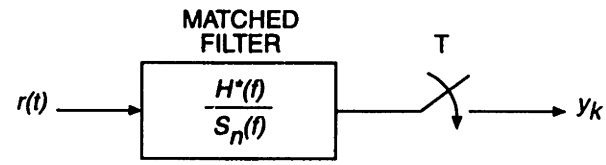

Figure 6-3: Front end for channel $h(t)$ and nonwhite noise with spectral density $N_0 S_n(f)$.

Discrete-time model The noise samples at the sampler output are not white, but rather have the power spectrum $N_0 S_{h,n}(e^{j\omega T})$, where

$$S_{h,n}(e^{j\omega T}) = \frac{1}{T}\sum_{k=-\infty}^{\infty} \frac{|H(f+k/T)|^2}{S_n(f+k/T)}, \qquad \omega = 2\pi f \tag{6.10}$$

The discrete-time model for the channel and receiver front end consisting of a sampled matched filter is shown in figure 6-4. The impulse response of the equivalent discrete-time channel is two-sided conjugate symmetric.

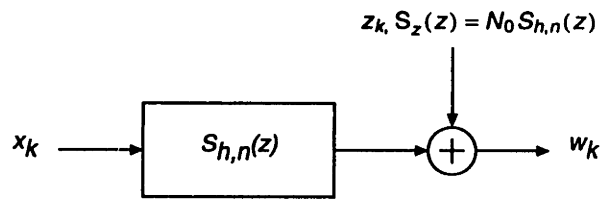

Figure 6-4: Discrete-time model for channel with impulse response $h(t)$, noise with PSD $N_0 S_n(f)$ and receiver front end consisting of a MF and symbol-rate sampler.

Whitened Matched Filter (WMF) Let us further assume that the spectrum $S_{h,n}(z)$ is factorizable, i.e.,

$$S_{h,n}(z) = A_{h,n}^2 G_{h,n}(z) G_{h,n}^*(1/z^*) \tag{6.11}$$

where $A_{h,n}^2$ is equal to the geometric mean of $S_{h,n}(z)$, and $G_{h,n}(z)$ is a canonical response. We can then apply the maximum-phase whitening filter $1/A_{h,n}^2 G_{h,n}^*(1/z^*)$ to the output of the matched filter, yielding an output noise process that is white Gaussian with variance $N_0/A_{h,n}^2$.

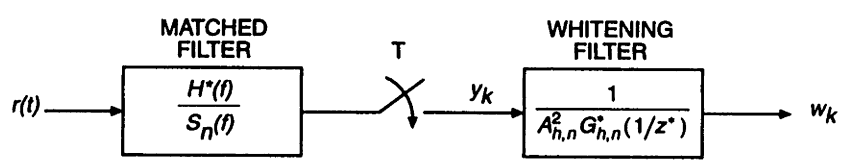

Figure 6-5: Whitened matched filter for channel with impulse response $h(t)$ and nonwhite noise with PSD $N_0 S_n(f)$.

The resulting discrete-time model from input symbols to WMF outputs is shown in figure 6-6. The effect of the whitening filter on the signal has been to eliminate the non-causal and

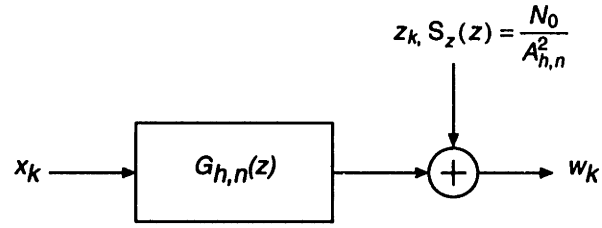

Figure 6-6: Discrete-time model for channel with impulse response $h(t)$, noise with PSD $N_0 S_n(f)$ and receiver front end consisting of a whitened matched filter and symbol-rate sampler.

non-minimum-phase portion of the ISI. For this reason, it is sometimes called a precursor equalizer. Stated another way, the whitening filter has made the equivalent discrete-time channel response causal and minimum-phase.

For the case where the noise is white, $S_n(f) = 1$, and thus the noise at the output of the whitening filter has variance N_0/A_h^2, where A_h^2 is a positive constant equal to the geometric mean of $S_h(z)$.

At this point, it is worth noting that the whitened matched filter does not exist for all non-rational folded spectra. In addition, a whitened matched filter may be difficult to implement in practice. The problem comes from the whitening filter $1/G_h^*(1/z^*)$ which is anti-causal (and maximum-phase). When the folded spectrum contains zeros, the whitening filter becomes an IIR filter. Since it is also anti-causal, it can only be approximated, e.g. by an FIR filter and delay.

6.2.3 Performance bounds: the MFB and the MLSE

Figure of Merit In general, we are interested in minimizing the probability of error. It can be shown that when a minimum distance receiver is used for the equivalent discrete-time channel of figure 6-6, the error probability is approximately

$$P_e = K\,Q\left(\frac{1}{2}\sqrt{\gamma}\right), \quad \gamma = d_{\min}^2/\sigma^2 \tag{6.12}$$

where $d_{\min}$ is the minimum Euclidean distance between pairs of known signals, $K \geq 1$ is the error coefficient, equal to the average number of signals at the minimum distance $d_{\min}$, and $\sigma^2 = N_0/2A_h^2$ is the variance of the real or imaginary parts of the additive noise. γ will be called the figure of merit.

More generally, for a suboptimal receiver, the error is still given by Eq. (6.12) but the uncertainty or error on the quantity $d_{\min}$ may include terms other than Gaussian noise. It is

therefore natural to define $2\sigma^2$ as the *variance of the error* we make in estimating $d_{\min}$. As will be seen shortly, in a zero-forcing equalizer, $2\sigma^2$ reduces to the variance of a complex Gaussian noise process, but in the case of equalizers based on a mean-square error criterion, $2\sigma^2$ also includes contributions from intersymbol interference terms. Even though the error is no longer Gaussian, we will still use the figure of merit $\gamma = d_{\min}^2/\sigma^2$ as a measure of the performance of the receiver.

The WMF leads to two upper bounds on the performance in the presence of ISI.

Matched Filter Bound (MFB) The first bound is the matched filter bound, which presumes that a single data symbol has been transmitted. No receiver can have a lower error probability than an optimum receiver for a single pulse. For an isolated pulse x_0 at time 0, the output of the channel is

$$w_k = x_0 g_{h,k} + z_k \tag{6.13}$$

The ML detector is a matched filter with transfer function $G_h^*(1/z^*)$ followed by a sampler at time $t = 0$ and a slicer. The minimum distance for the set of known signals is

$$d_{\min}^2 = \min \sum_{k=0}^{\infty} |x_0^{(1)} g_{h,k} - x_0^{(2)} g_{h,k}|^2 = x_{\min}^2 \sum_{k=0}^{\infty} |g_{h,k}|^2 \tag{6.14}$$

where $x_0^{(1)}$ and $x_0^{(2)}$ are two different symbols, the minimization is over all pairs such that $x_0^{(1)} \neq x_0^{(2)}$, and $x_{\min}$ is the minimum distance within the data-symbol alphabet. Therefore

$$d_{\min}^2 = \frac{x_{\min}^2 \sigma_h^2}{A_h^2} \tag{6.15}$$

where $\sigma_h^2 = A_h^2 \sum_{k=0}^{\infty} |g_{h,k}|^2$ is the energy of the pulse $h(t)$. Since the noise variance is $2\sigma^2 = N_0/A_h^2$, the figure of merit for the matched filter bound is given by

$$\gamma_{\text{MF}} = \frac{d_{\min}^2}{\sigma^2} = x_{\min}^2 \cdot \frac{\sigma_h^2}{N_0/2} \tag{6.16}$$

Another performance measure closely related to the figure of merit is the signal-to-noise ratio. Since the variance of the signal component is $S_x \|G_h\|^2$ and the noise variance is N_0/A_h^2, the SNR for the MFB is

$$\text{SNR}_{\text{MF}} = \frac{S_x \sigma_h^2}{N_0} \tag{6.17}$$

In the presence of ISI, the receiver will not, in general, achieve the matched filter bound, because the matched filter does not take into account the ISI. However, γ_{MF} provides a very useful benchmark, since the difference between the figure of merit of the actual receiver and γ_{MF} is a measure of the severity of the ISI, as well as the effectiveness of the methods to counter the effects of ISI.

Bound based on MLSE Another upper bound on the figure of merit is γ_{MLSE}, the figure of merit for a detector based on maximum likelihood sequence estimation (MLSE). In order to derive this figure of merit, let us consider how maximum likelihood sequence detection is implemented. Figure 6-7 shows an MLSE detector applied to the output of the WMF.

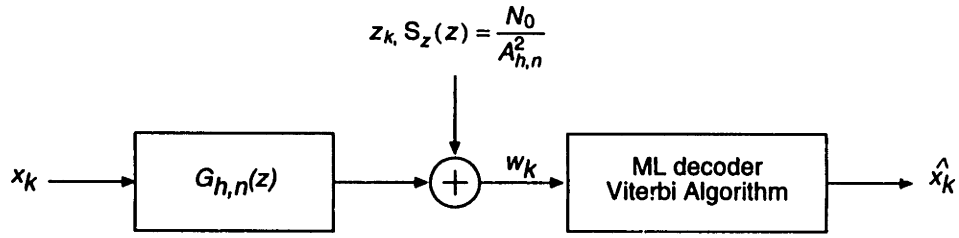

Figure 6-7: MLSE applied to the output of the WMF.

We restrict our attention to the case where a finite sequence of symbols is transmitted. Since K can be made as large as desired, this is not a serious restriction. However, because the length of the data symbols is finite, the set of possible sequences at the channel output, although possibly very large, remains finite. The noise at the output of the WMF is white and Gaussian, and thus, the detection problem reduces to choosing the sequence of K data symbols that minimizes the Euclidean distance

$$\min_{x_k, 1 \le k \le K} \sum_{m=1}^{\infty} |w_m - \sum_{k=1}^{K} x_k g_{h,m-k}|^2 \tag{6.18}$$

The figure of merit for a detector based on MLSE is

$$\gamma_{\text{MLSE}} = \frac{d_{\min}^2}{N_0/2A_h^2} = \frac{d_{\min}^2 A_h^2}{N_0/2} \tag{6.19}$$

where the minimum distance is given by

$$d_{\min}^2 = \min_{\substack{\epsilon_k, 1 \le k \le K \\ \epsilon_1 \neq 0}} \sum_{m=1}^{\infty} |\sum_{k=1}^{K} \epsilon_k g_{h,m-k}|^2 \tag{6.20}$$

where $\{\epsilon_k, 1 \le k \le K\}$ is a non-zero sequence of error symbols, $\epsilon_k = x_k^{(1)} - x_k^{(2)}$. The minimization is over all sequences of $x_k^{(1)}$ and $x_k^{(2)}$ that are not equal.

It is easy to show that $d_{\min}^2 \le x_{\min}^2 \sum_{k=0}^{\infty} |g_{h,k}|^2$ and therefore that

$$\gamma_{\text{MLSE}} \le \gamma_{\text{MFB}} \tag{6.21}$$

The significance of the MLSE upper bound resides in the fact that it represents the best performance that can be achieved by any receiver based on equalization or any other technique for countering ISI. Furthermore, the difference between γ_{MF} and γ_{MLSE} is a measure of the severity of the ISI, and is not indicative of any shortcomings in the design of the receiver.

In practice, MLSE can be efficiently implemented using the Viterbi algorithm. However, even with the Viterbi algorithm, the decoding complexity grows exponentially with the channel memory length. Except for short channel impulse responses, MLSE is difficult to implement. We will now examine a series of techniques, from simple to more complex, which can be used to combat intersymbol interference, or as encountered on television channels, co-channel interference. The first set of techniques, which we first examine in the context of uncoded modulation, are conventional: these are, in order, linear equalization with a zero-forcing criterion; linear equalization with a minimum-mean-square error criteria; decision-feedback equalization with a zero-forcing criterion; and, decision-feedback equalization with a minimum-mean-square criterion. Following this we examine how these schemes can be implemented in the context of HDTV. We then examine additional techniques to improve the performance further, without a substantial increase in complexity.

6.3 Linear equalization: ZF and MSE

One of the simplest methods for reducing or eliminating intersymbol interference is to apply an appropriately designed linear filter to the received signal before making a decision as to which signal was sent. Making use of the results from Section 6.2.2, we apply the linear filter to the output of the canonical channel impulse response, since we have shown that the WMF can be used to transform the continuous-time channel into a discrete-time canonical channel (assuming that the spectrum $S_{h,n}(z)$ is factorizable). The general form of a discrete-time channel with a linear equalizer $C(z)$ is shown in figure 6-8.

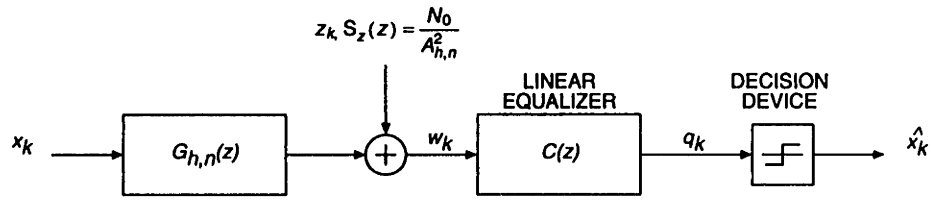

Figure 6-8: Discrete-time channel with linear equalizer $C(z)$.

The linear equalizer may be designed using different criteria. Two such criteria are the so-called zero-forcing criterion (ZF) and the mean-square error criterion (MSE). These are developed in the next subsections.

6.3.1 Zero-forcing linear equalizer

The simplest type of receiver equalizer is the zero-forcing equalizer (LE-ZF). By effectively whitening the channel spectrum, this equalizer eliminates ISI altogether, without regard to noise enhancement. This can easily be done by choosing the receive filter to satisfy the Nyquist criterion at the slicer input. Since the matched filter and symbol-rate sampler is the optimal front end for any receiver, the zero-forcing equalizer can be placed at the output of the sampled matched filter. In order to satisfy the Nyquist criterion, the filter must be a discrete-time symbol-rate filter with frequency response $G_h^{-1}(z)$. The term "zero-forcing" refers to the fact that the ISI is constrained to be entirely absent at the input of the slicer. Since $G_h(z)$ is canonical, the equalizer $G_h^{-1}(z)$ has all its poles inside or on the unit circle; hence it is a causal filter, although it is not necessarily minimum-phase or stable, because of the possibility of poles on the unit circle.

Combining the equalizer $G_h^{-1}(z)$ with the WMF discrete-time model of figure 6-6 yields the model shown in figure 6-9.

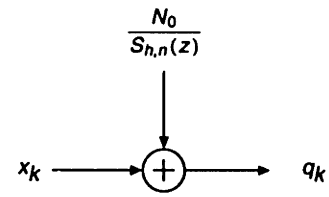

Figure 6-9: Equivalent discrete-time linear equalizer with zero-forcing criterion.

From figure 6-9, the figure of merit $\gamma_{\text{LE-ZF}}$ is readily shown to be

$$\gamma_{\text{LE-ZF}} = \frac{x_{\min}^2}{N_0/2} \frac{1}{\langle 1/S_{h,n} \rangle_A} \tag{6.22}$$

where $S_{h,n}$ stands for $S_{h,n}(e^{j\omega T})$ and the arithmetic mean is taken over the interval $[-\pi/T, \pi/T]$.

The noise enhancement factor $1/\langle 1/S_{h,n} \rangle_A$ is greater or equal to 1 with equality if and only if the channel is ideal. If the channel is reasonably constant over the interval $[-\pi/T, \pi/T]$, the noise enhancement will not be very serious. If the channel has a near null, the noise enhancement will be large. If it has an actual null, the equalizer structure is not even defined since the channel response is not invertible. Such a situation is encountered in HDTV broadcasting when the received signal consists of a direct signal and a strong delayed signal (such as produced by a specular reflection on an obstacle) or when the received signal includes a strong co-channel NTSC component (this may be the case, for example, when there is an NTSC transmitter close-by). In the latter case, noise enhancement occurs because the *equivalent* channel has a near null, which the equalizer tries to compensate for.

We have thus far assumed that the receiver front end consisted of a WMF, resulting in an equivalent discrete-time channel with a causal minimum-phase filter $G_{h,n}(z)$. In this case, the equalizer was the causal filter $G_{h,n}^{-1}(z)$. The WMF front end should be viewed as a conceptual structure rather than as an actual filter. This is because in practice, a WMF may be difficult to implement. For example, in the case of a broadcast channel, the channel response will depend on the location of the receiver and may be time-dependent. This implies that the receiver must be capable of adapting to the characteristics of the channel. Typically, adaptive filters are easier to implement in discrete-time than in continuous-time. Therefore, it is useful to develop equalizer structures that do not assume a WMF front end but instead assume a simple symbol-rate sampler. Fortunately, this does not present any difficulties in the case of linear equalization.

Let the response of the discrete-time channel be $H(z)$ and let us assume that the channel output is corrupted by discrete-time Gaussian noise with power spectral density $S_z(z)$. $H(z)$ can be thought of consisting of the concatenation of a zero-phase section $H_{\text{zero}}(z)$, a canonical section $H_{\text{min}}(z)$ and an anti-canonical section $H_{\text{max}}(z)$, i.e. $H(z) = H_0 H_{\text{min}}(z) H_{\text{max}}(z) H_{\text{zero}}(z)$, where H_0 is a constant. The zero-forcing linear equalizer for this channel is simply $C(z) = 1/H(z)$ (cf. Figure 6-10). Clearly, in order for $C(z)$ to be stable, we must have $H_{\text{zero}}(z) = 1$. The minimum-phase term is not a problem since the inverse is also causal minimum-phase. However, the anti-causal part has an inverse which is also anti-causal maximum-phase, and therefore is impractical to implement.

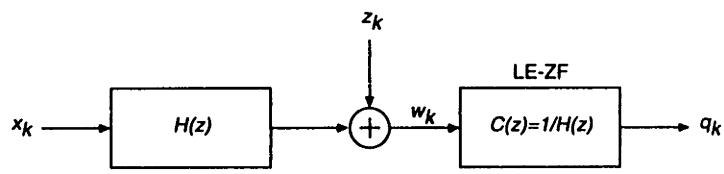

Figure 6-10: Linear equalizer with zero-forcing criterion for discrete-time channel $H(z)$.

The variance of the error is equal to

$$2\sigma^2 = \left\langle S_z/|H|^2 \right\rangle_A \tag{6.23}$$

and therefore the figure of merit is equal to

$$\gamma_{\text{LE-ZF}} = \frac{2x_{\text{min}}^2}{\langle S_z/|H|^2 \rangle_A} \tag{6.24}$$

6.3.2 Mean-square error linear equalizer

Instead of requiring that there be no intersymbol interference at the input of the decision device, one can instead seek to minimize the mean-square error at the decision point. Let e_k denote the difference between the slicer input and the current data symbol. Assuming the slicer (or decision device) does not make errors, e_k is the difference between the slicer input and the slicer output. The basic idea with MSE equalization is that, by relaxing the no-ISI constraint and tolerating a small amount of ISI, it is in general possible to decrease the variance of the overall error.

In order to find the optimum equalizer, we can proceed in at least two ways. One way is to use the well-known fact that: in order to minimize the error power, the error sequence e_k must be orthogonal to the input sequence w_k to the equalizer, i.e. $E[e_k w_l] = 0$ for all k, l. A second way is to express the spectrum of the error as a function of the frequency response of the equalizer, $C(z)$, and to choose $C(z)$ to minimize the power of the error at each frequency.

For brevity, we will omit the arguments of the Z-transforms in the derivations. For instance, G should be taken to mean $G(z)$, G^* to mean $G^*(1/z^*)$ and S_x to mean $S_x(z)$. The orthogonality condition between e_k and w_k can be written compactly

$$E[EW^*] = 0 \tag{6.25}$$

where $E = X(GC - 1) + ZC$ and $W = XG + Z$, and G is the frequency response of the equivalent discrete-time channel. Replacing E and W, the condition becomes

$$E[(X(GC - 1) + ZC)(X^*G^* + Z^*)] = 0 \tag{6.26}$$

Using the fact that the input sequence x_k and the noise sequence z_k are uncorrelated, we can easily reduce the condition to

$$C(S_x GG^* + S_z) - S_x G^* = 0 \tag{6.27}$$

Another way of obtaining the result is to express the power spectral density of the error signal as a function of the signal and noise inputs

$$S_e = S_x(GC - 1)(G^*C^* - 1) + S_z CC^* \tag{6.28}$$

In order to minimize the mean-square error, which is the arithmetic mean of $S_e(z)$ evaluated on the unit circle, we minimize $S_e(z)$ at each frequency. By completing the square or taking the derivative with respect to C (since C is not constrained in complexity, C can be chosen independently at each frequency), we obtain

$$C(S_x GG^* + S_z) - S_x G^* = 0 \tag{6.29}$$

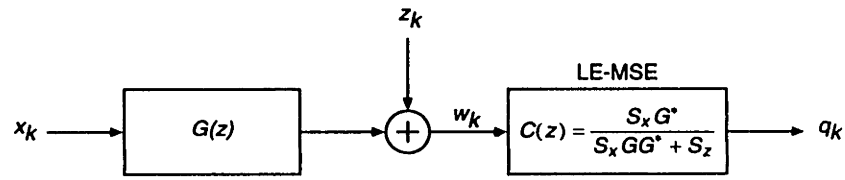

Figure 6-11: Linear equalizer with MSE criterion for discrete-time channel $G(z)$.

which agrees with the previous result. Thus, the optimum equalizer is

$$C = \frac{S_x G^*}{S_x GG^* + S_z} = \frac{G^*}{GG^* + S_z/S_x} \tag{6.30}$$

Using the fact that $S_w = S_x GG^* + S_z$, the MSE becomes

$$2\sigma^2 = \left\langle \frac{S_z}{GG^* + S_z/S_x} \right\rangle_A = \left\langle \frac{S_x S_z}{S_w} \right\rangle_A \tag{6.31}$$

and the figure of merit is given by

$$\gamma_{\text{LE-MSE}} = \frac{2\chi^2_{\min}}{\langle S_z/(|G|^2 + S_z/S_x)\rangle_A} \tag{6.32}$$

Clearly, we have

$$\gamma_{\text{LE-ZF}} \leq \gamma_{\text{LE-MSE}} \tag{6.33}$$

It is important to note that nowhere have we used the fact that G was the canonical channel response. The results stand for any G representing the discrete-time equivalent response of a channel whose output is sampled at the symbol rate. The linear equalizer based on an MSE criterion is shown in Figure 6-11.

Several observations are in order. In the general case, when the receiver front end is simply a sampler rather than a continuous-time matched filter followed by a sampler, the equalizer is seen to consist of two parts. The first part, G^*, is a discrete-time filter matched to the discrete-time equivalent response of the channel. The second part, $S_x/(S_x GG^* + S_z)$ minimizes the error at its output. In contrast with the zero-forcing equalizer, the LE-MSE remains defined even when the channel response has zeros on or outside the unit circle. As can be seen from the figure of merit, the term N_0/S_x serves to mitigate the effect of nulls located on the unit circle, keeping the error term finite (as long as $N_0 > 0$).

However, the performance of the LE-MSE may still be poor when the channel has a near null or in the presence of strong co-channel interference.

In the case where the receiver front end is a WMF, the MSE is given by

$$2\sigma^2 = N_0 \langle 1/(S_{h,n} + N_0/S_x)\rangle_A, \tag{6.34}$$

yielding a figure of merit

$$\gamma_{\text{LE-MSE}} = \frac{x_{\min}^2}{N_0/2} \frac{1}{\langle 1/(S_{h,n} + N_0/S_x) \rangle_A} \tag{6.35}$$

Therefore

$$\gamma_{\text{LE-ZF}} \leq \gamma_{\text{LE-MSE}} \tag{6.36}$$

with $\gamma_{\text{LE-ZF}}$ approaching $\gamma_{\text{LE-MSE}}$ as the channel SNR increases.

6.4 Decision-feedback equalization: ZF and MSE

The previous analysis has shown that linear equalization may not provide satisfactory performance when the channel response or the noise spectrum exhibit strong variations across the Nyquist bandwidth. It is also clear that linear equalization is suboptimal, since the error sequence at the input of the decision device is correlated. If we assume that the decisions are correct, it should be possible to reduce the correlation of the noise or error sequence through the use of a prediction filter. This is the basic idea behind the decision-feedback equalizer (DFE).

6.4.1 DFE-ZF

The structure of the DFE based on a zero-forcing criterion is shown in figure 6-12 in the case of a receiver front end consisting of a WMF. In this case, the structure of the DFE is particularly

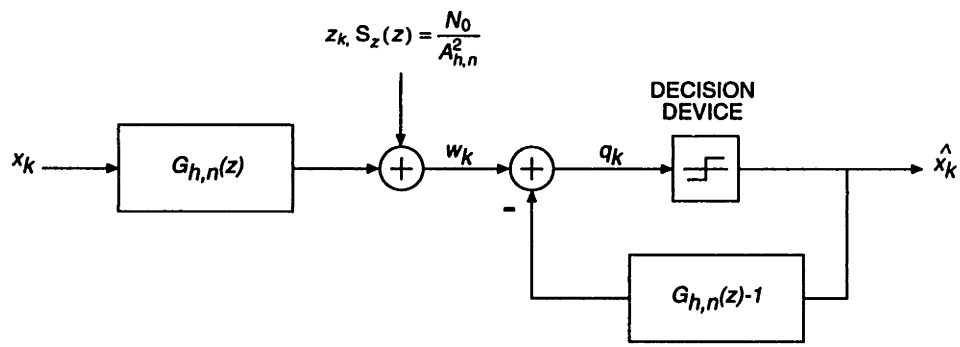

Figure 6-12: Discrete-time channel with zero-forcing decision-feedback equalization.

simple because the output of the WMF is monic and causal. Therefore the residual ISI g_k at the decision point contains only postcursor terms, $k > 0$. If we assume that the decision device does not make errors when estimating x_k, $\hat{x}_k = x_k$, we can cancel the tail of the impulse response $\sum_j g_j x_{k-j}$ by subtraction. Thus the intersymbol interference is completely removed,

and the noise is white with variance N_0/A_h^2. The resulting figure of merit is

$$\gamma_{\text{DFE-ZF}} = \frac{x_{\min}^2}{N_0/2A_h^2} = \frac{x_{\min}^2}{N_0/2} \frac{1}{\langle 1/S_{h,n} \rangle_G} \tag{6.37}$$

This shows that $\gamma_{\text{DFE-ZF}}$ and $\gamma_{\text{LE-ZF}}$ are simply related by the ratio of the geometric mean to the arithmetic mean of the folded spectrum. Therefore,

$$\gamma_{\text{LE-ZF}} \leq \gamma_{\text{DFE-ZF}} \tag{6.38}$$

with equality only when there is no ISI.

It is also interesting to note the relationship between DFE-ZF and LE-ZF. For LE-ZF, the equalizer $C(z) = 1/G_h(z)$ is placed before the decision device. This filter may be equivalently implemented as a feedback filter $G_h(z) - 1$, whose output is subtracted from the input w_k. As mentioned earlier, since $G_h(z)$ is canonical, $G_h(z) - 1$ is causal, and is stable if $G_h(z)$ does not have any zeros on the unit circle. If we now insert the decision device inside the feedback loop, we obtain the DFE-ZF. Placing the decision device inside the feedback loop has several advantages. The noise enhancement that occurred in the linear equalizer due to the cancellation of the postcursor ISI has been suppressed. As well, the DFE-ZF remains stable even when the channel response has nulls (i.e. $G_h(z)$ has zeros on the unit circle). From this point of view, the insertion of the decision device inside the feedback loop has a stabilizing effect (if we assume that the decision device is putting out correct decisions).

Generalization So far we have assumed that the receiver front end consisted of a WMF and we have derived the structure of the decision-feedback equalizer that achieves zero intersymbol interference at the input of the decision device. We have found that the noise at the input of the decision device was white. Let us now relax the requirement that the receiver front end be a WMF followed by a symbol-rate sampler. Instead, we will assume that the channel output is directly sampled at the symbol rate. Let us determine the structure of the DFE under these assumptions.

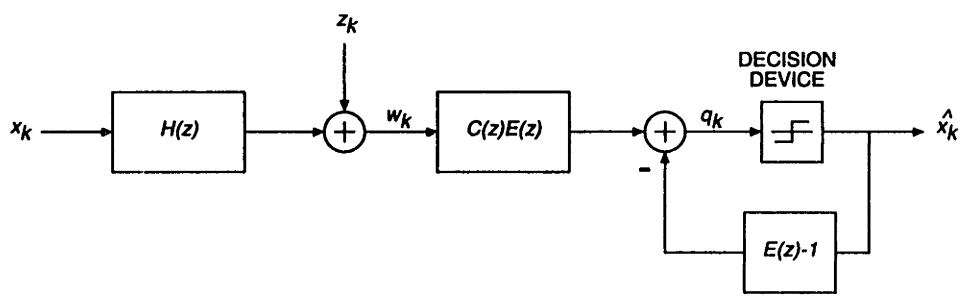

Figure 6-13: Decision-feedback equalizer for discrete-time channel $H(z)$.

Figure 6-13 shows the structure of the DFE. The first part of the receiver is identical to the linear equalizer of Figure 6-10 and consists of a linear equalizer $C(z)$. Following the equalizer $C(z)$ is a prediction filter $E(z)$ which is used to whiten the noise and minimize the noise variance. Any intersymbol interference introduced by the linear prediction filter can be removed by the feedback filter $E(z) - 1$, since the feedback loop implements the equivalent of $1/E(z)$ with the symbol sequence as input (assuming the decision device does not make any errors). Clearly, $E(z)$ must be causal and monic for the feedback loop to be causal. The optimal prediction filter is easily determined from linear prediction theory. Let us assume that the spectrum of the error signal at the output of the equalizer $C(z)$ is $S_E(z)$. Minimum phase factorization of $S_e(z)$ allows us to write

$$S_E(z) = A_E^2 G_e G_e^* \tag{6.39}$$

where G_e is a canonical filter and $A_E^2 = \langle S_E \rangle_G$ is the prediction error at the output of the optimal prediction filter. The optimal prediction filter is the monic minimum-phase filter $E(z) = 1/G_e(z)$. For a zero-forcing equalizer, $C(z) = 1/H(z)$ and therefore the spectrum of the error signal is given by

$$S_E(z) = \frac{S_z}{HH^*} = \frac{A_z^2 G_z G_z^*}{|H_0|^2 H_{\min} H_{\max} H_{\min}^* H_{\max}^*} \tag{6.40}$$

Thus, the optimal prediction filter is given by

$$E = \frac{H_{\min} H_{\max}^*}{G_z} \tag{6.41}$$

yielding a prediction error of

$$2\sigma^2 = \left\langle S_z/|H|^2 \right\rangle_G = A_z^2/|H_0|^2 \tag{6.42}$$

The feedforward filter, or precursor equalizer, is given by

$$CE = \frac{1}{H_0} \frac{H_{\max}^*}{H_{\max}} \frac{1}{G_z} \tag{6.43}$$

It consists of an allpass filter $H_{\max}^*/H_{\max}$ followed by a noise whitening filter $1/G_z$. Since the allpass filter does not modify the spectrum of the noise, it is not surprising that the whitening filter is simply given by the inverse of G_z. We also notice that, for the zero-forcing DFE, the response of the channel and precursor equalizer is equal to E and therefore is canonical, i.e. there will be only postcursor ISI at the output of the precursor equalizer. All the postcursor ISI is eliminated by the feedback filter without noise enhancement.

6.4.2 DFE-MSE

It is possible to improve on the performance of the DFE-ZF by relaxing the requirement that all ISI be absent from the input to the decision device. Instead, in the same fashion as for the

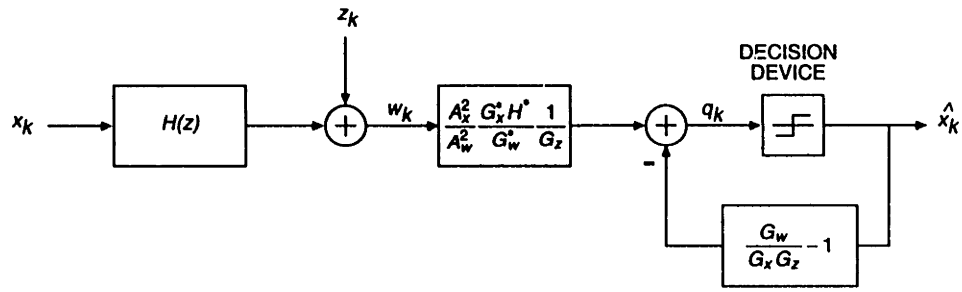

Figure 6-14: Decision-Feedback equalizer with MSE criterion for discrete-time channel $H(z)$.

LE-MSE, one can seek to minimize the variance of the error at the input of the decision device. The same reasoning as for the DFE-ZF can be used to determine the optimal prediction filter that minimizes the error at its output. The equalizer filter C is chosen to minimize the variance of the error. The solution is thus the same as for the LE-MSE. We have seen that the spectrum of the error at the output of the LE-MSE was given by

$$S_E(z) = \frac{S_x S_z}{S_w} = \frac{S_x S_z}{S_x HH^* + S_z} \tag{6.44}$$

Using a minimum-phase spectral factorization of $S_w = A_w^2 G_w G_w^*$, the optimal prediction filter becomes

$$E = \frac{G_w}{G_x G_z} \tag{6.45}$$

resulting in a prediction error of

$$2\sigma^2 = \left\langle \frac{S_x S_z}{S_w} \right\rangle_G = \left\langle \frac{S_z}{|H|^2 + S_z/S_x} \right\rangle_G \tag{6.46}$$

Using the expression of C from Eq. (6.30), we find that the feedforward filter is given by

$$CE = \frac{A_x^2}{A_w^2} \frac{G_x^* H^*}{G_w^*} \frac{1}{G_z} \tag{6.47}$$

In contrast with the DFE-ZF, the precursor equalizer does not whiten the noise and the noise is no longer Gaussian. Figure 6-14 summarizes the choices of the feedforward and feedback filters.

By comparing Eqs. 6.42 and 6.46, we find that

$$\gamma_{\text{DFE-ZF}} \leq \gamma_{\text{DFE-MSE}} \tag{6.48}$$

One of the possible drawbacks of using DFE is the problem of error propagation. We examine in the next subsection a method of avoiding the error propagation problem.

6.4.3 Tomlinson-Harashima precoding

The idea of Tomlinson-Harashima (TH) precoding is to move the cancellation of the postcursor ISI to the transmitter, where the past transmitter symbols are known without the possibility of errors [85, 67]. However, this means that the postcursor ISI impulse response $G_h(z)$ must be known at the transmitter. In practice, in most situations, this impulse response must be measured at the receiver using adaptive filter techniques and passed back to the transmitter in order to use transmitter precoding. This limits the usefulness of the technique in the case of HDTV broadcast transmission. However, we will examine forms of TH precoding which are useful to combat co-channel interference.

The basis of transmitter precoding is the observation that the channel model through the WMF, $G_h(z)$, and LE equalizer $G_h^{-1}(z)$, can be reversed without compromising the requirement that the Nyquist criterion be satisfied at the slicer input. Therefore the linear equalizer can be placed at the transmitter. There are several advantages to this: first, since the receiver is now the WMF followed directly by the slicer, the noise at the slicer input is that of the WMF, that is, it is the same as for the DFE. Thus, even though the receiver uses linear equalization, it does not suffer the noise enhancement of linear equalization because the linear equalization is done prior to the channel, where the noise is introduced. Second, there is no longer a danger of error propagation, and as a consequence, TH precoding may actually achieve slightly better performance than DFE-ZF.

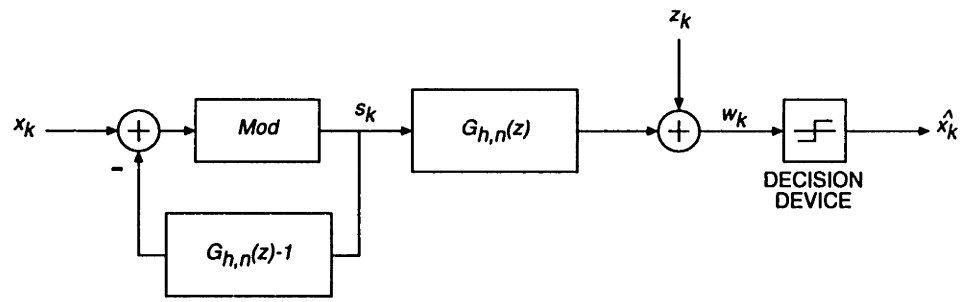

Figure 6-15: Discrete-time channel with equalization implemented at the transmitter with Tomlinson-Harashima precoding.

Simply doing the equalization at the transmitter is not practical, however, because it increases the peak and average ratios of the transmitter signal. If the impulse response of $G_h^{-1}(z)$ is $f_{h,k}$, then the peak transmitted sample is increased by a factor of $\sum_{k=0}^{\infty} |f_{h,k}| > 1$. Likewise, if the data symbols are independent and identically distributed, then the average power of the transmitted symbols is increased by a factor $\sum_{k=0}^{\infty} |f_{h,k}|^2$.

In order to avoid the increase in power, further processing is required. This processing is signal dependent. A particularly simple case is the case of PAM signaling. Let us assume that

the signal set consists of M points evenly spaced on the real axis, e.g., $\{\pm 1, \pm 3, \cdots, \pm(M-1)\}$. The transmitted signal s_k is formed by first subtracting the tail $\sum_{j>0} f_{h,j} s_{k-j}$, (which is the operation equivalent to decision-feedback at the receiver) and then reducing the resulting signal to the interval $(-M, M]$ via a modulo $2M$ operation. An equivalent view of the processing is the following: consider the feedback loop without the modulo reduction; we may generate the same signal q_k as that out of the feedback loop with the modulo reduction by adding to the input x_k a sequence of multiples of 2M, $\{i_k \cdot 2M\}$ chosen so that the transmitter signal q_k falls in the range $(-M, M]$. Thus, in the absence of noise, the received signal w_k is the modified data $x_k + i_k \cdot 2M$, which may be detected on a symbol-by-symbol basis. Figure 6-15 illustrates the precoding technique. Figure 6-16 shows how, in the case of M-PAM, the precoding operation may be viewed as a linear filtering by $1/G_{h,n}$ of a modified sequence $x_k + i_k \cdot 2M$.

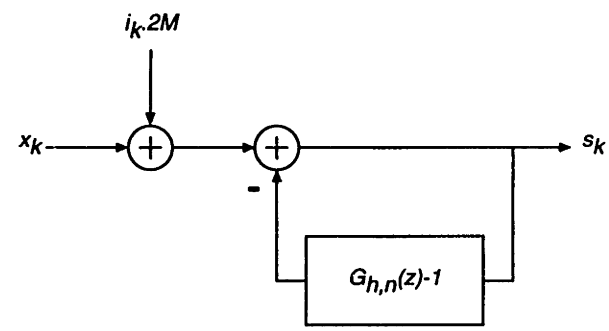

Figure 6-16: Equivalent transmitter precoder for M-PAM signaling.

The decision device for TH precoding differs slightly from the one used for DFE. With DFE, the signal points at the input of the decision device belong to the original signal set. With TH precoding, they extend beyond that range. Therefore, the decision device must first determine the nearest odd integer to the received point and then reduce the result to bring it in the range $(-M, M)$. Consider for example an 8-PAM signal set $\{\pm 1, \pm 3, \pm 5, \pm 7\}$ and a channel $G_{h,k}(z) = 1 - z^{-1}$. The receiver signal set is then $\{\pm 1, \pm 3, \cdots, \pm 15\}$. Figure 6-17 shows the different signal sets for an 8-PAM signal set. The extension to QAM modulation with independent I and Q channels is straightforward. For a general channel, the transmitted symbol s_k is pseudo-randomly distributed over the continuous interval $(-M, M]$, unless the filter coefficients are integers. Thus, there is a small power penalty associated with TH precoding compared to DFE. This penalty is small, however, and decreases with the size of the constellation. For an M point constellation, the penalty is approximately $M^2/M^2 - 1$.

When the filter coefficients are integers (such a channel is sometimes called a partial-response (PR) channel), it is possible, by a small modification of the precoding process, to ensure that the transmitted constellation is unchanged after passing through the precoder. Let us consider the 8-PAM constellation with odd-integer points as defined above and a chan-

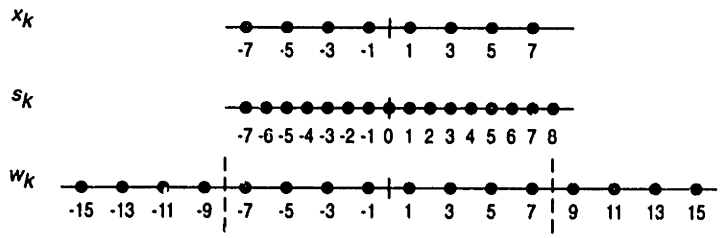

Figure 6-17: TH precoding signal sets for 8-PAM modulation and channel $G_{h,n}(z) = 1 - z^{-1}$.

nel $G_{h,k}(z) = 1 - z^{-1}$. A modified constellation can be obtained by translating the original constellation so that one of the symbols in the modified constellation is at the origin. Let V (V=1 in this case) be the translation. The modulo operation now consists of reducing the symbol $t_k + u_k$ modulo $2M$ to bring it in the interval $(-M + V, M + V]$. The resulting symbol is then translated back by -V. Figure 6-18 illustrates the process of an 8-PAM constellation and a channel of the form $G_{h,n}(z) = 1 - z^{-K}$.

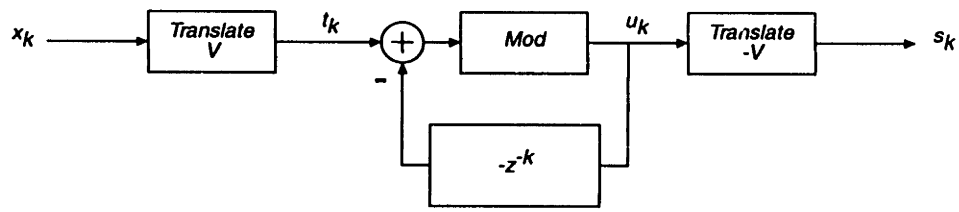

Figure 6-18: Modified TH precoding for 8-PAM modulation and channel $G_{h,n}(z) = 1 - z^{-K}$.

The signal set corresponding to the received sequence, after passing through the channel $G_{h,k}(z) = 1 - z^{-1}$, is shifted and expanded. Figure 6-19 shows the different signal constellations corresponding to a transmitted 8-PAM constellation. The advantage here is that the transmitted constellation is unchanged. However, the receiver must still operate on an expanded constellation.

TH precoding for uncoded modulation has not been widely used in practice. One drawback is the requirement that the transmitter have knowledge of the channel impulse response. Another drawback is the small increase in transmitter power incurred by using TH precoding as opposed to DFE. In addition, although error propagation in DFE can occur, it is not, in practice, an important source of degradation. Thus, DFE is generally preferred to TH precoding in the case of uncoded modulation. The real interest of TH precoding comes when coded modulation is used in combination with equalization, as we shall see subsequently.

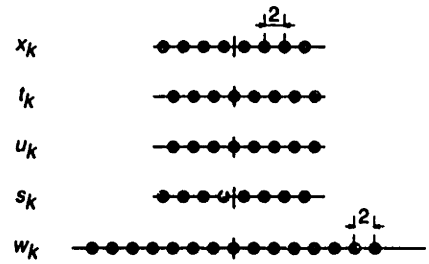

Figure 6-19: Modified TH precoding signal sets for 8-PAM modulation and channel $G_{h,n}(z) = 1 - z^{-1}$.

6.5 Application to the NTSC co-channel interference problem

We now examine how these equalization schemes can be applied to the problem of interference reduction. In this section we assume an ideal channel, the only impairment being co-channel interference. We also restrict our attention to uncoded systems. Subsequent sections will examine how interference reduction and channel equalization can be combined, and how channel coding and channel equalization can be combined. But first, let us consider the methods that have been proposed to date to combat NTSC co-channel interference.

6.5.1 Previous NTSC interference reduction methods

There are essentially three methods that have been proposed for reducing NTSC co-channel interference.

6.5.1.1 Frequency division multiplexing method

The first idea consists of shaping the transmit spectrum so as to avoid the frequencies likely to contain high power interfering signals. In one implementation [1], the transmitted signal consisted of two frequency multiplexed QAM signals occupying disjoint frequency bands. No signal energy is present around the NTSC video carrier frequency and the audio subcarrier.

There are several problems with such a scheme:

- It sacrifices a certain amount of channel capacity in exchange for interference immunity. For the majority of receivers, NTSC interference will not be a problem. Therefore, it appears this scheme is unnecessarily wasteful of bandwidth.
- It is transmitter dependent and therefore has a built-in inefficiency, since it is not possible

to recover the unused portions of the spectrum once all NTSC stations are eventually taken off the air.

- The implementation of such a scheme tends to be more difficult than a single carrier scheme. In the proposed scheme, carrier and timing recovery relied on only one of the signals, and thus used only a fraction of the power available in the total signal. Phase jitter on the second carrier may not be correctly determined from the phase of the first carrier.

6.5.1.2 Precoding/comb filtering method

A second method, which is functionally equivalent to the TH precoding technique described in Section 6.4.3, is proposed in [97, 30]. It consists of a digital precoder at the transmitter and either a comb filter or a "post-coder" at the receiver. A block diagram is shown in Fig. 6-20. The precoder is inserted between the encoder (in this case a Reed-Solomon encoder) and the

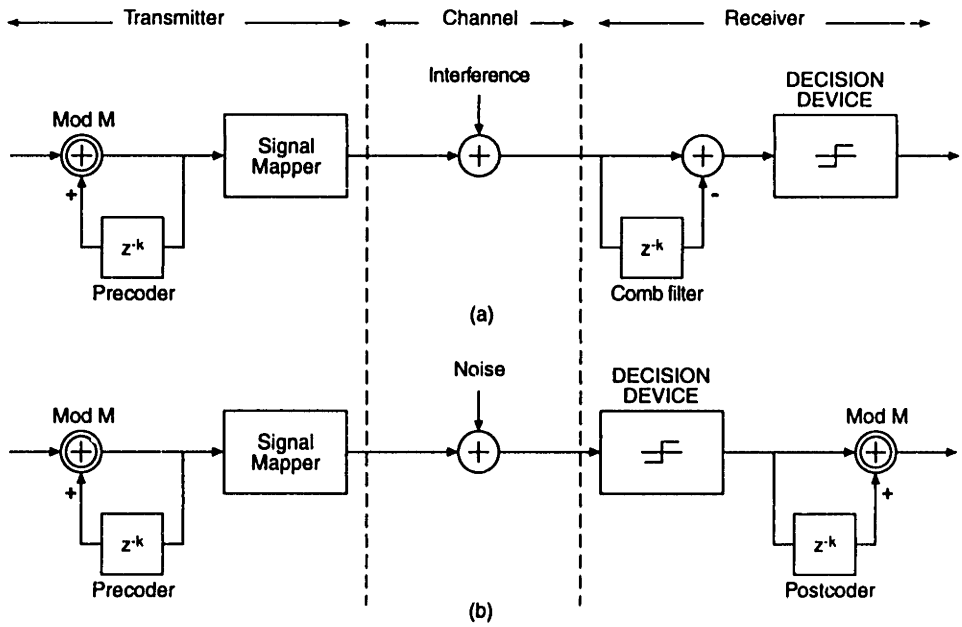

Figure 6-20: (a) Precoding and comb filtering. (b) Precoding and postcoding

modulator and operates in the digital domain. The input to the precoder is an M-level data stream. It is precoded with a modulo-M adder and a k-symbol delay element. The receiver implements a comb filtering operation. By choosing the delay element appropriately, spectral nulls can be positioned close to the locations of the NTSC video, color and audio carrier frequencies, thereby eliminating the steady-state portion of the interference. In [97, 30], this delay is chosen equal to 12 samples of a single-sideband signal. The main reason given for

choosing a 12-symbol delay is the fact that the filter coefficient is then equal to 1. A modified slicer maps the (2M-1)-level signal out of the comb filter into an M-level signal. In the absence of noise, the signal is thus correctly recovered.

This method has the following drawbacks:

- The interposition of the comb filter at the receiver causes an SNR reduction of 3 dB.
- Hard-decision decoding is required for postcoding (the slicer is placed before the postcoder). This method is therefore not compatible with ML soft decision decoding.
- Such an algorithm cannot easily be made adaptive.
- There is no way of smoothly trading off noise performance for interference performance.
- Only the steady state portion of the interference is removed.

In subsequent sections, we refer to this scheme as the precoding/comb filtering scheme.

6.5.1.3 NTSC recursive cancellation method

A third method, recently proposed in [81], mitigates NTSC interference by subtracting from the received signal the output from a set of parallel narrowband recursive filters centered at the harmonic frequencies of the NTSC line rate. The principle is illustrated in Figure 6-21.

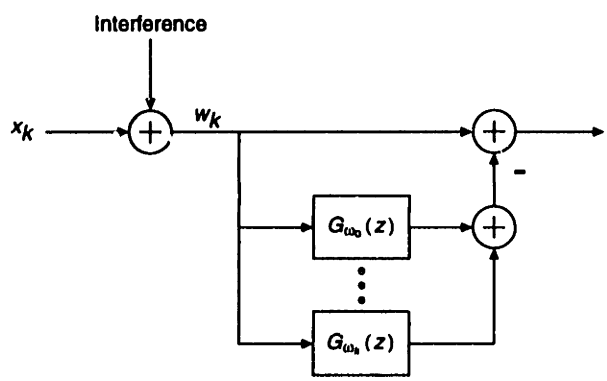

Figure 6-21: Interference rejection with bank of narrowband filters.

Here, the filters denoted $G_{\omega_k}(z)$ are bandpass filters with center frequency ω_k. The combined output of these filters is subtracted from the received signal, in order to reduce the amount of interference. The proposed IIR filters are of the form

$$G_{\omega_k}(z) = G_k \cdot \frac{\mu_k(1 - \cos\omega_k z^{-1})}{1 - 2(1-\mu_k)\cos\omega_k z^{-1} + (1-2\mu_k)z^{-2}} \tag{6.49}$$

where μ_k is a coefficient controlling the filter bandwidth at $\omega = \omega_k$, and G_k is a gain coefficient controlling the depth of the notch in the response of the equivalent filter $H(z) = 1 - \sum_k G_{\omega_k}(z)$.

In [81], the only parameter that is adaptively adjusted is the frequency ω_0 corresponding to the video carrier frequency. The center frequencies of the other filters are assumed to have a fixed relationship with respect to the video carrier frequency. The gains and bandwidths are fixed because of the difficulty of adapting them based on the characteristics of the interference. An approximate scheme is described in [81] for determining the video carrier frequency of the interferer. Additionally, a simple scheme based on the ratio of powers at frequencies ω_k and $\omega_{\text{ref}} = 4.2$ MHz is proposed for detecting the presence of an interference signal at frequency ω_k. Depending of whether this ratio is above or below a nominal threshold, the filter centered at frequency ω_k is switched in or out.

Among the advantages of using such a scheme are the facts that the scheme is receiver-based and modulation-format independent. Among the disadvantages is the fact that it does not attempt to weight interference rejection against intersymbol interference creation, and may, in some circumstances, actually distort the signal more than reject the interference when the interference peaks are not distributed according to the assumptions. The reported results show an improvement of approximately 3 dB as compared to the performance in the absence of a filter at an SNR of 20 dB.

In subsequent sections, we refer to this scheme as the recursive NTSC cancellation scheme.

6.5.2 New receiver structures

Figure 6-22 shows the different receiver structures that can be used to reduce the NTSC co-channel interference. Since we assume that the channel is ideal, the LE-ZF would apply the sampled output from the channel directly to the decision device. Thus the receiver performance would simply depend on the signal-to-interference ratio (SIR) in the traditional way.

Figure 6-22(a) shows the optimal MSE linear equalizer for a signal with a flat spectral density S_x degraded by interference with spectral density $S_z(z)$. At low SIR, the frequency response of the equalizer is essentially the inverse of the power spectrum of the interference. The equalizer is non-causal but can be approximated with a sufficient delay. The error at the input of the decision device is neither white nor Gaussian, but is minimized in a mean-square sense. As the SIR increases, the filter frequency response becomes flat, as expected.

Figure 6-22(b) shows the performance of the zero-forcing decision-feedback equalizer. The forward filter $F(z) = 1/G_z(z)$ is a causal filter which acts as an interference whitener and predictor, since $1/G_z(z)$ is the optimal predictor for an interference signal with spectral density

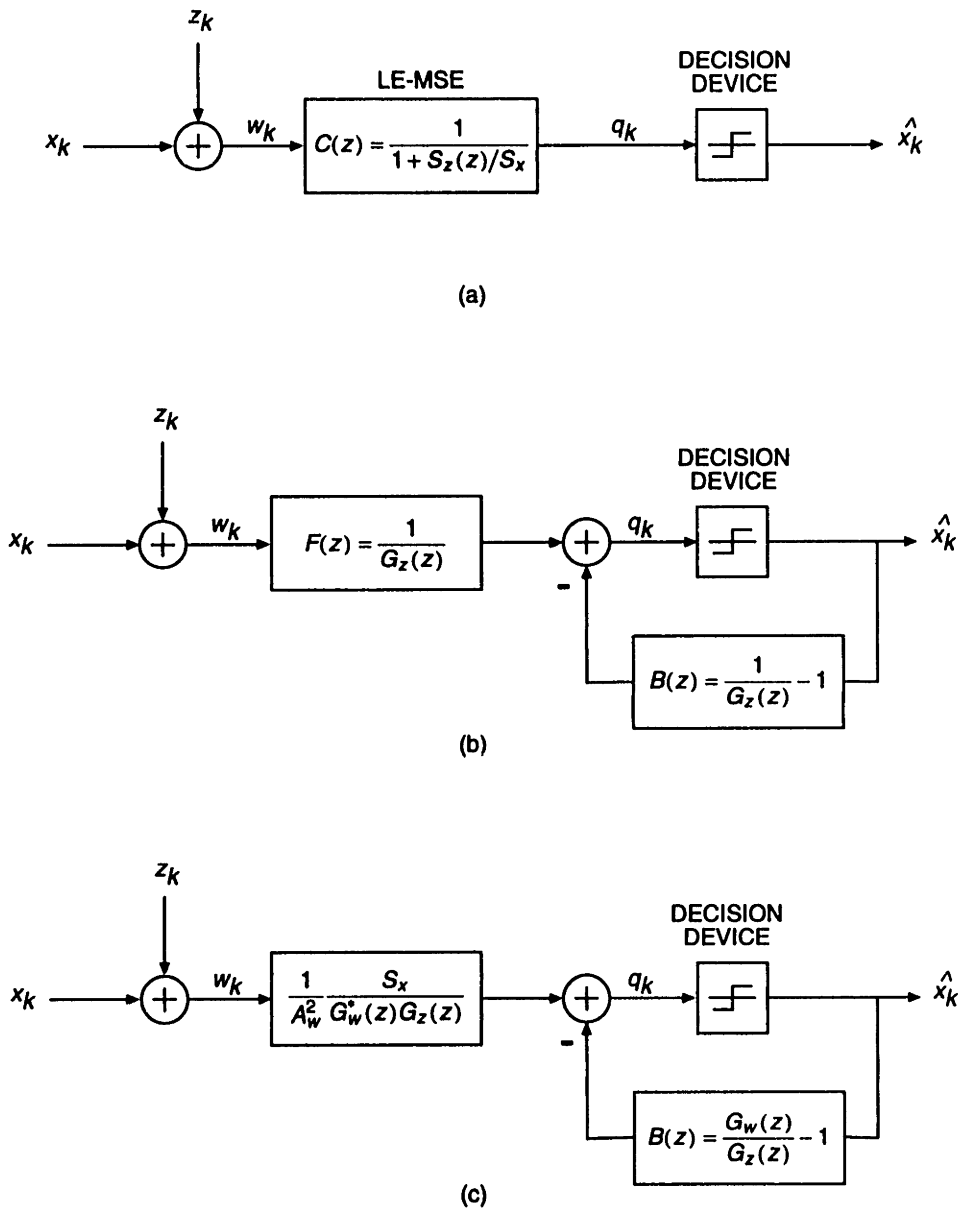

Figure 6-22: Interference rejection based on (a) LE-MSE (b) DFE-ZF (c) DFE-MSE.

$A_z^2 G_z(z) G_z^*(1/z^*)$. As a result of the filtering, ISI is present in the output of the forward equalizer. However, because the forward equalizer is causal, this ISI is of postcursor type only and can be canceled with the aid of a decision-feedback section. This is the task of the feedback filter $B(z) = 1/G_z(z) - 1$, which cancels the postcursor ISI terms without noise enhancement.

Figure 6-22(c) shows a further refinement of the decision-feedback equalizer. In this scheme, the forward filter and feedback filter attempt, in concert, to minimize the mean-square error at the input of the decision device. The forward filter contains a term $1/G_w^*(z)$ which is anticausal. At large SIR, this term is close to 1. Therefore, at high SIR, the forward filter is close to $1/G_z(z)$ and the feedback filter to $1/G_z(z) - 1$, thus yielding the zero-forcing decision-feedback equalizer solution. At small SIR, the extent of the forward filter increases to include a larger number of precursor samples. At the same time, the feedback filter is able to remove the postcursor ISI and inverse filter the causal portion of the interference spectrum. The term $1/G_w^*(z)$ represents the contribution from precursor samples. Precursor ISI introduced by this term cannot be canceled by the decision-feedback filter, and therefore contributes to the error. However, using appropriately weighted precursor samples also results in a reduction of the interference, and overall, the MSE is reduced compared to the DFE-ZF.

6.5.3 Performance evaluation

In order to assess the effectiveness of the different schemes, we can either simulate the communication system degraded by varying degrees of real or simulated co-channel interference, or we can assume models for the co-channel interference and derive the performance of the schemes under the assumed model. The first approach has the advantage of being "closer" to the real-world situation. However, it provides an answer which is the result of many combined interactions. One problem is that the characteristics of the interference can only be estimated. Another problem is that implementation losses (e.g. error propagation degradations in the feedback filter) may render comparisons difficult. The modeling approach, on the other hand, makes it easy to show the influence of different parameters, but may provide results which are not representative of a real system. With both the advantages and disadvantages in mind, we have chosen to explore the two approaches.

We justified in Chapter 3 why an autoregressive process may be a reasonable model for the NTSC interference. The simplest, albeit trivial, such model is the first-order autoregressive model. A somewhat better model is a third-order autoregressive model using previous pixels on the current and previous scan lines. We now examine how these models can be applied to the interference rejection problem.

Since we seek to investigate the interference problem in the absence of multipath distor-

tions, we can assume that the channel frequency response is ideal ($H(z) = 1$). Figure 6-23 shows the discrete-time channel model corresponding to a signal corrupted by NTSC interference. The interference is described by an innovation process $\{n_k\}$ and a filter $1/A(z)$ where $A(z)$ is a monic causal polynomial.

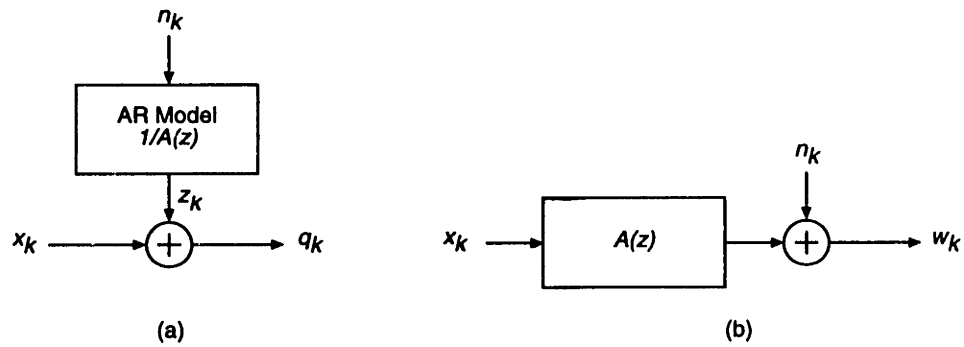

Figure 6-23: (a) Discrete-time NTSC interference model. (b) Equivalent white noise channel model.

In order to find the equalizer for the discrete-time interference model of Figure 6-23(a), we first solve the problem of finding the equalizer for the corresponding white noise channel of Figure 6-23(b). It is easy to show that the LE-MSE $C(z)$ for the first case is related to the LE-MSE $C_1(z)$ of the white noise channel through $C(z) = C_1(z)A(z)$. Similarly, the feedforward filter $F(z)$ and feedback filter $B(z)$ of Figure 6-22(c) are related to their corresponding white noise counterparts through $F(z) = F_1(z)A(z)$ and $B(z) = B_1(z)$. This is a consequence of the fact that $A(z)$ is assumed monic and causal.

6.5.3.1 First-order interference model

We first assume that the interference is described by a simple first-order prediction model of the form

$$z_k = \rho_1 z_{k-1} + n_k \tag{6.50}$$

where $\rho_1 = \rho e^{-j\Phi}$ is the value of the normalized autocorrelation coefficient for a unit time lag, as defined in Eq. (3.16). A typical value for a low-detail image would be $\rho = 0.97$ and $\rho = 0.90$ for a high-detail image [55]. The innovation n_k is a zero-mean complex white Gaussian noise process with variance $2\sigma_n^2$, where

$$\sigma_n^2 = (1 - \rho^2)\sigma_z^2 \tag{6.51}$$

and $2\sigma_z^2$ is the variance of the interference, or equivalently, the integral of the PSD $S_z(z)$ over the interval of definition. This (simplistic) first-order prediction model describes the overall shape of the PSD of the interference, which is mostly dependent on the correlation between samples on a same scan line.

Let us denote by γ_0 the figure of merit of an ideal channel corrupted by AWGN with variance $2\sigma_z^2$

$$\gamma_0 = \frac{x_{\min}^2}{\sigma_z^2} \tag{6.52}$$

Baseline: the matched filter bound Since the performance of any receiver is upper bounded by that of the matched filter, we shall use the MFB as the benchmark against which we will compare all other schemes. Referring to Figure 6-23(b), we can write

$$\gamma_{\text{MF}} = \frac{d_{\min}^2}{\sigma_n^2} = \frac{x_{\min}^2 \sigma_A^2}{(1-\rho^2)\sigma_z^2} \tag{6.53}$$

where $\sigma_A^2 = 1 + \rho^2$ is the energy of the received pulse for the equivalent channel. Thus, the MFB can be written

$$\gamma_{\text{MF}} = \frac{1+\rho^2}{1-\rho^2}\gamma_0 \tag{6.54}$$

MLSE The figure of merit of MLSE is given by

$$\gamma_{\text{MF}} = \frac{d_{\min}^2}{\sigma_n^2} \tag{6.55}$$

The minimum distance $d_{\min}$ can be found by inspection or computed by applying the Viterbi algorithm to the ML trellis corresponding to the channel $A(z)$. For the case where $A(z) = 1 - \rho_1 z^{-1}$, it is easy to show that $d_{\min}^2 = x_{\min}^2(1+\rho^2)$. Thus, in this special case, the figure of merit of MLSE is the same as the matched filter bound.

$$\gamma_{\text{MLSE}} = \gamma_{\text{MF}} = \frac{1+\rho^2}{1-\rho^2}\gamma_0 \tag{6.56}$$

It is worth noting that for $\rho_1 = 1$ and $\rho_1 = -1$, there is an infinite number of error events at the minimum distance, leading to a quasi-catastrophic behavior of the ML decoder. Therefore, the performance of the MLSE will not match the MFB even though the minimum distance is the same as that of the MFB.

LE-ZF Referring to Figure 6-23(a), it is easy to see that the figure of merit of the zero-forcing linear equalizer is equal to γ_0

$$\gamma_{\text{LE-ZF}} = \gamma_0 = \frac{1-\rho^2}{1+\rho^2}\gamma_{\text{MF}} \tag{6.57}$$

and is therefore substantially worse than the performance of MLSE.

LE-MSE The figure of merit is dependent on the SNR and is given by

$$\gamma_{\text{LE-MSE}} = \frac{x_{\min}^2}{\sigma_n^2}\left\langle \frac{1}{AA^* + \sigma_n^2/\sigma_x^2} \right\rangle_A^{-1} \tag{6.58}$$

$$= \gamma_0 \sqrt{\left(1 + \frac{\sigma_n^2}{(1-\rho)^2\sigma_x^2}\right)\left(1 + \frac{\sigma_n^2}{(1+\rho)^2\sigma_x^2}\right)} \tag{6.59}$$

$$= \gamma_{\text{LE-ZF}} \sqrt{\left(1 + \frac{\sigma_n^2}{(1-\rho)^2\sigma_x^2}\right)\left(1 + \frac{\sigma_n^2}{(1+\rho)^2\sigma_x^2}\right)} \tag{6.60}$$

As expected, the figure of merit of LE-MSE converges to that of LE-ZF for large SNR.

DFE-ZF Since $A(z)$ is causal, the figure of merit of the DFE-ZF is simply given by

$$\gamma_{\text{DFE-ZF}} = \frac{x^2_{\min}}{\sigma_n^2} = \frac{x^2_{\min}}{\sigma_z^2(1-\rho^2)} = \frac{\gamma_0}{1-\rho^2} = \frac{\gamma_{\text{MF}}}{1+\rho^2} \tag{6.61}$$

which shows that for $0.9 \leq \rho < 1$, the figure of merit of DFE-ZF is within 3 dB of γ_{MLSE}, a much better result than $\gamma_{\text{LE-MSE}}$.

DFE-MSE The variance of the error is given by Eq. (6.46). Therefore, the figure of merit of the DFE-MSE is given by

$$\gamma_{\text{DFE-MSE}} = \frac{x^2_{\min}}{\sigma^2} = \frac{x^2_{\min}}{\left\langle \frac{\sigma_n^2}{AA^* + \frac{\sigma_n^2}{\sigma_x^2}} \right\rangle_G} = \gamma_{\text{DFE-ZF}} \left\langle \frac{1}{AA^* + \frac{\sigma_n^2}{\sigma_x^2}} \right\rangle_G^{-1} \tag{6.62}$$

Simulation results We now examine, by simulation, the performance of each of these equalization schemes for an interference signal assumed to be specified by Eq. (6.50). We have seen that this problem is equivalent to a white noise channel with response $H(z) = A(z)$.

Figure 6-24 shows the symbol error rate of 16QAM over a channel of the form $H(z) = 1 - 0.5z^{-1}$. All the error rate curves are plotted against the signal-to-interference ratio. With the notations of Figure 6-23(a), the signal-to-interference ratio is given by SIR $= \sigma_x^2/\sigma_z^2$. It is also possible to define an equivalent signal-to-noise ratio at the output of the equivalent channel model by SNR $= \sigma_x^2\langle AA^*\rangle_A/\sigma_n^2$, which, in this case, is equal to SNR $= \sigma_x^2(1+\rho^2)/\sigma_n^2$. Thus, SIR $= (1-\rho^2)/(1+\rho^2)$ SNR. For $\rho = 0.5$, the signal-to-interference ratio is lower than the signal-to-noise ratio by 2.2 dB, implying that the interference power can be 2.2 dB higher than white noise, with the same effect on the probability of error.

Several observations can be made regarding Figure 6-24: firstly, for this channel, the optimization criterion (ZF or MSE) has almost no influence on the error performance, both for linear and decision-feedback equalization; secondly, linear equalization is inferior to decision-feedback equalization by approximately 1.25 dB; in addition, the SNR gap between DFE and the matched filter bound is approximately 1 dB. These simulation results confirm the analytical results since the ratio $\gamma_{\text{LE-MSE}}/\gamma_{\text{LE-ZF}} = 0.12$ dB at SNR = 20 dB, the ratio $\gamma_{\text{DFE-MSE}}/\gamma_{\text{DFE-ZF}} = 0.07$ dB, and the ratio $\gamma_{\text{DFE-ZF}}/\gamma_{\text{LE-ZF}} = 1.25$ dB.

Figure 6-25 shows the symbol error rate of 16QAM over a channel of the form $H(z) = 1 - 0.9z^{-1}$. Here, we see that the difference between linear and decision-feedback equalization is considerable. This result is in agreement with the analysis, since $\gamma_{\text{DFE-ZF}}/\gamma_{\text{LE-ZF}} = 20$ dB at SNR = 20 dB. The difference between LE-ZF and LE-MSE is about 2 dB. From the previous analysis, the predicted difference is $\gamma_{\text{LE-MSE}}/\gamma_{\text{LE-ZF}} = 2.25$ dB and the ratio $\gamma_{\text{DFE-MSE}}/\gamma_{\text{DFE-ZF}} =$

0.30 dB both at SNR = 20 dB. These values are confirmed by the simulation results. The difference between the signal-to-interference ratio SIR and the signal-tc-noise ratio is 9.8 dB. Thus, the interference power can be 9.8 dB higher than the corresponding white noise power for the same probability of error.

Analysis It is instructive to examine the evolution of the tap settings for both the LE-MSE and the DFE-MSE for this simple model. Figure 6-26 shows how the equalizer taps change as a function of the signal-to-interference ratio and the corresponding frequency response. At high SIR, the equalizer is essentially a zero-forcing equalizer and the frequency response is flat. As the amount of interference increases, the equalizer taps are adjusted to exploit the correlation of the current sample with previous and subsequent samples. This is achieved by subtracting weighted values of the neighboring samples from the current sample. The equalizer is clearly non-causal, but can be closely approximated with a sufficient delay. As the SIR becomes very low, the estimate becomes biased. This is especially obvious at SIR = -10 dB, where the tap value for the current sample is close to 0.5. This can also be inferred from Figure 6-22(a). The equalizer is of the form $C(z) = 1/(1 + S_z(z)/S_x)$. Since, in general, $S_z(z)$ has a non-zero zero-order coefficient, $C(z)$ will not be monic. This means that, while the LE-MSE minimizes the mean-square error at the equalizer output, it does not minimize the probability of error. This is due to the fact that the error sequence is not Gaussian, so that there is no equivalence between minimizing the MSE and minimizing the symbol error probability. In fact, the performance can be slightly improved by unbiasing the output of the equalizer by multiplying it by $1/c_0 = 1 + \langle S_z \rangle_A / S_x$.

Figure 6-27 shows how the taps of the DFE feedforward and feedback coefficients are adjusted as a function of SIR. For large SIR, the feedforward filter approaches the DFE-ZF, with a feedforward filter acting as a noise predictor with frequency response $F(z) = 1/G_z(z) = 1 - \rho z^{-1}$, and the feedback filter canceling the (causal) ISI introduced by the noise predictor. As the SIR decreases, the feedforward filter extends to include more precursor samples but it is also clear that the DFE becomes biased, since the reference weight value is different from unity. Therefore, a signal dependent component will be present in the error signal at the input of the decision device. It is clear that, while this solution minimizes the MSE, the error probability will not in general be minimized by this choice of the tap weights. It is possible to remove this bias by scaling the feedforward and feedback filter coefficients. However, the difference between the biased and unbiased DFE is quite small for this channel configuration.

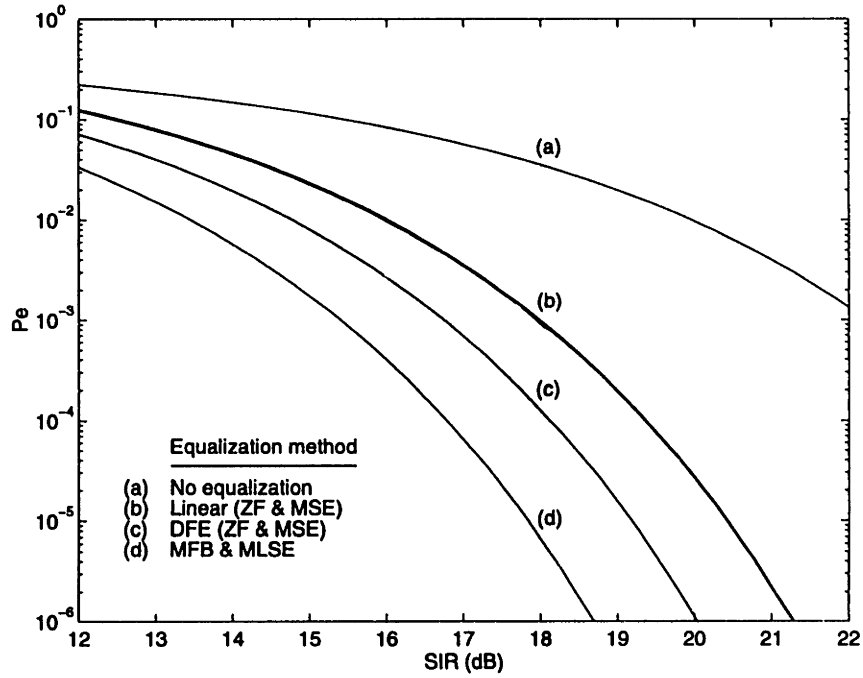

Figure 6-24: Performance of 16QAM with linear and decision-feedback equalization for an equivalent white noise channel of the form $H(z) = 1 - 0.5z^{-1}$.

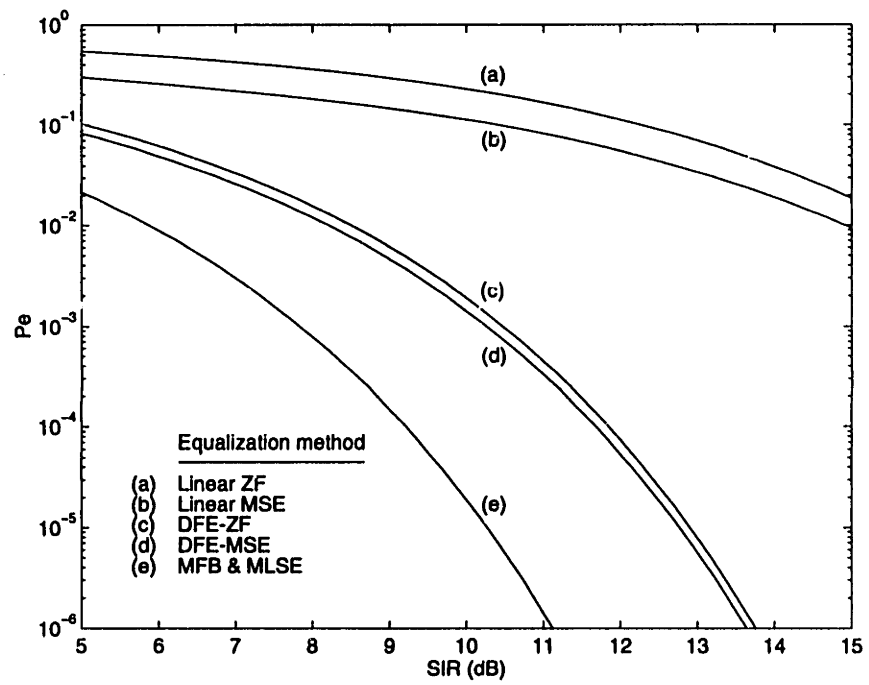

Figure 6-25: Performance of 16QAM with linear and decision-feedback equalization for an equivalent white noise channel of the form $H(z) = 1 - 0.9z^{-1}$.

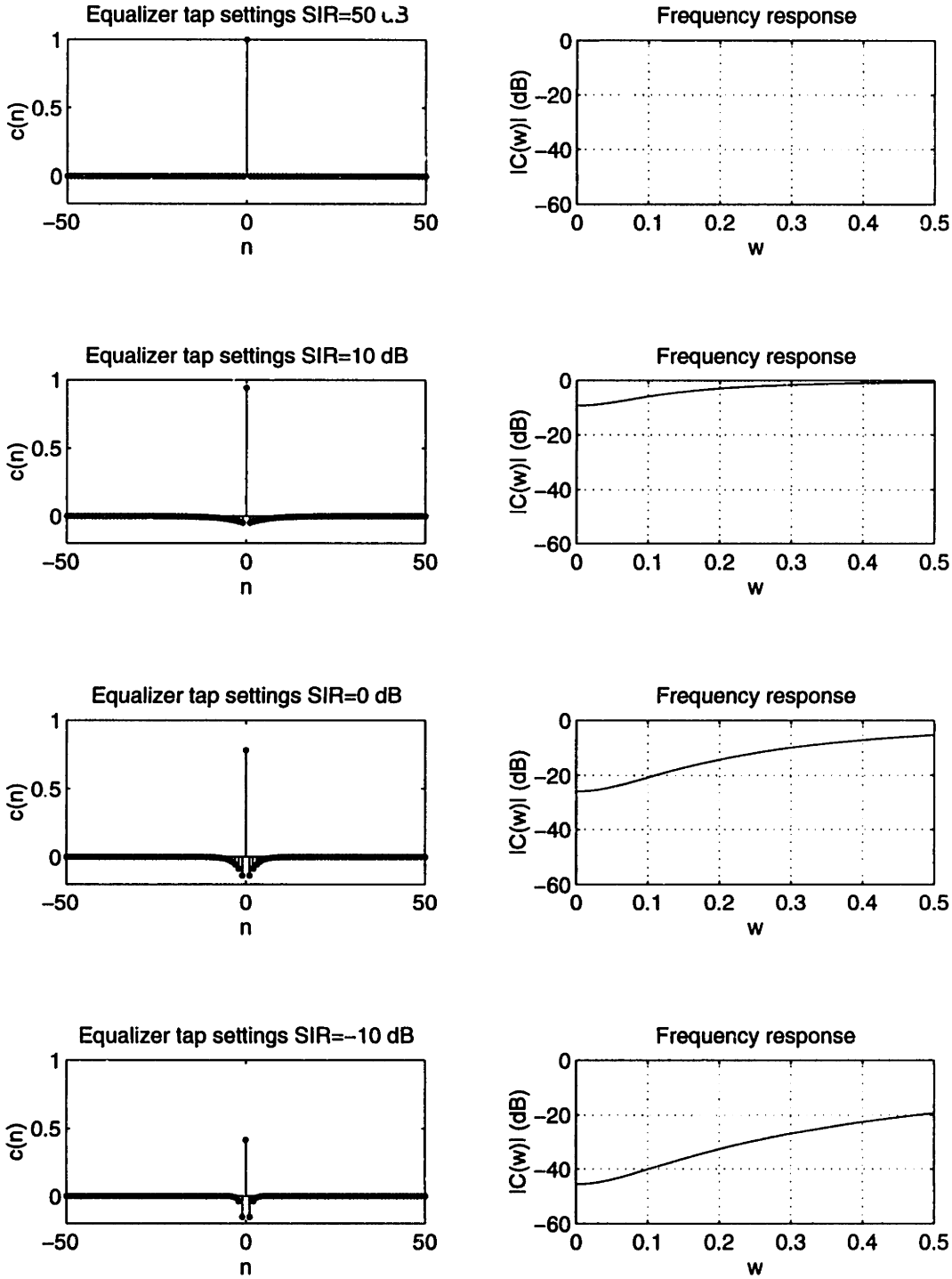

Figure 6-26: Evolution of the equalizer tap settings for the LE-MSE as a function of SIR for a first-order autoregressive interference model with $\rho = 0.9$.

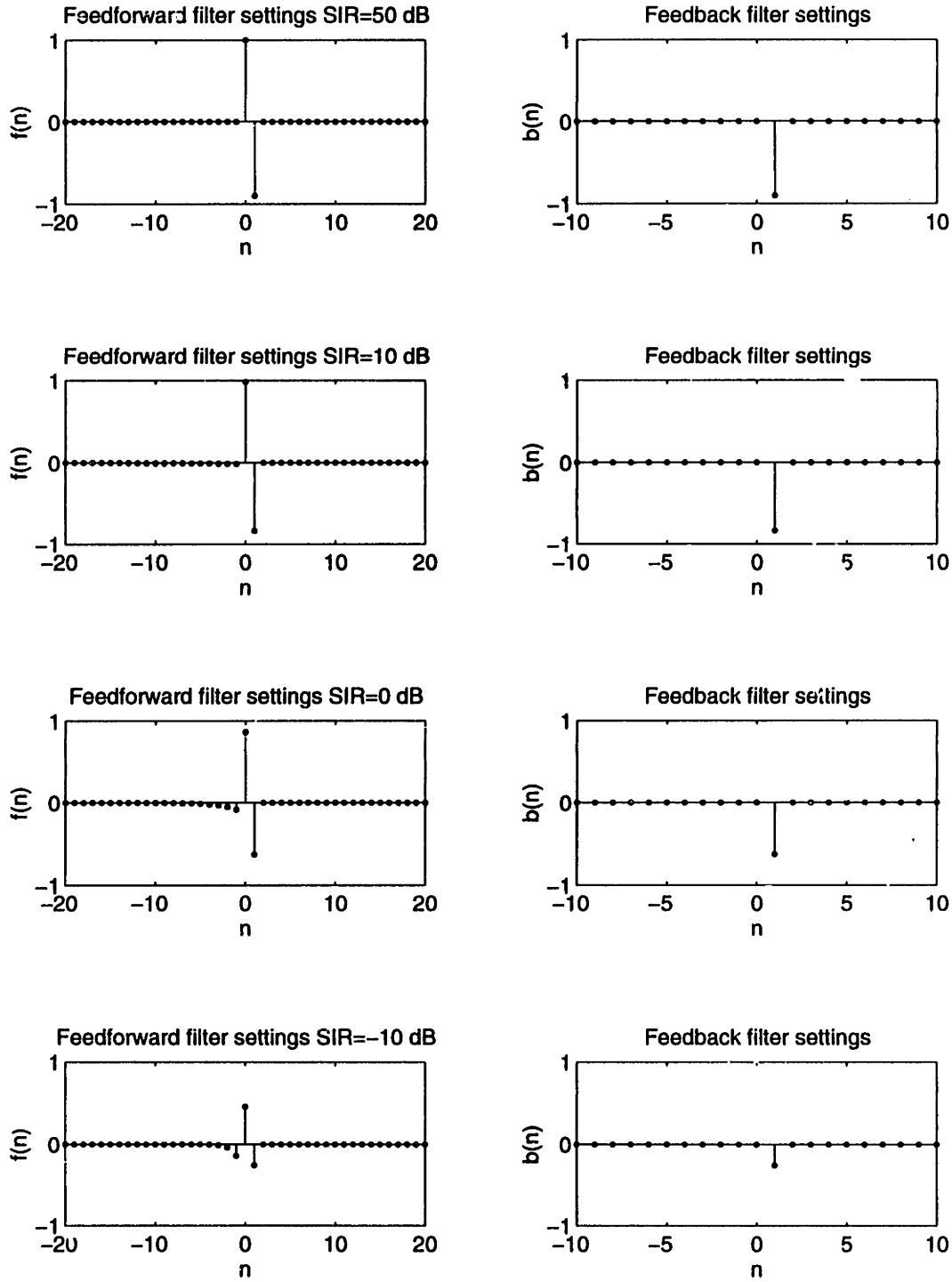

Figure 6-27: Evolution of the equalizer tap settings for the DFE-MSE as a function of SIR for a first-order autoregressive interference model with $\rho = 0.9$.

6.5.3.2 Third-order interference model

Let us now assume that the interference is described by the model of Section 3.5.3.4, i.e. an innovation process $\{n_k\}$ and a filter $H(z) = 1/A(z) = 1/(1 - \rho_1 z^{-1} - \rho_1 z^{-N} + \rho_1^2 z^{-N-1})$ where $A(z)$ is a monic polynomial. This is thought to model the NTSC interference reasonably accurately. The following results can be derived:

MFB

$$\gamma_{MF} = \frac{d_{min}^2}{\sigma_n^2} = \frac{x_{min}^2 \sigma_A^2 S_H}{\sigma_z^2} \tag{6.63}$$

where $\sigma_A^2 = 1 + 2\rho^2 + \rho^4$ is the energy of the received pulse for the equivalent channel and $S_H = \langle HH^* \rangle_A$. Thus, the MFB can be written

$$\gamma_{MF} = \sigma_A^2 S_H \gamma_0 \tag{6.64}$$

where $\gamma_0 = x_{min}^2/\sigma_z^2$.

Note: S_H may be calculated in closed form for this model. We have

$$HH^* = \frac{1}{(1 - \rho z)(1 - \rho z^{-1}) \prod_{k=1}^{N} (1 - \rho_k z)(1 - \rho_k z^{-1})} \tag{6.65}$$

where $\rho_k = \rho^{1/N} e^{j2\pi k/N}$ are the roots of $z^N = \rho$. Therefore

$$\langle HH^* \rangle_A = \frac{1}{2\pi j} \oint H(z) H^*(1/z^*) z^{-1} dz \tag{6.66}$$

can be evaluated using the residue theorem

$$\langle HH^* \rangle_A = \sum [\text{residues of } H(z)H^*(1/z^*)z^{-1} \text{ at the poles inside the unit circle}] \tag{6.67}$$

There is one pole at ρ and N poles at ρ_j, $j = 1, \cdots, N$. The residue at ρ is equal to

$$\text{Res}[H(z)H^*(1/z^*)z^{-1} \text{ at } z = \rho] = \frac{1}{(1 - \rho^2) \prod_k (1 - \rho_k \rho)(1 - \rho_k \rho^{-1})} \tag{6.68}$$

and the residues at ρ_j are given by

$$\text{Res}[H(z)H^*(1/z^*)z^{-1} \text{ at } z = \rho_j] = \frac{1}{(1 - \rho\rho_j)(1 - \rho_j^2) \prod_{k \neq j} (1 - \rho_k \rho_j)(1 - \rho_k \rho_j^{-1})} \tag{6.69}$$

It is possible to show that the residue at ρ vanishes as $N \to \infty$ while the sum of the residues at ρ_j, $j = 1, \cdots, N$ approaches $1/(1 - \rho^2)^2$. Thus, as $N \to \infty$,

$$\gamma_{MF} \to \frac{(1 + \rho^2)^2}{(1 - \rho^2)^2} \gamma_0 \tag{6.70}$$

In the following simulations, we have assumed a smaller value of N than would be used in an actual implementation. This was done to simplify the calculation of the optimum filters and to illustrate the main characteristics of the different schemes without having to worry about "edge" effects. The choice of a smaller value of N has a small effect on the error performance. For instance, the main effect in the previous formula is to change S_h by a very small amount.

MLSE The figure of merit of MLSE is given by

$$\gamma_{\text{MF}} = \frac{d^2_{\text{min}}}{\sigma_n^2} \tag{6.71}$$

In general, the minimum distance d_{min} will be smaller than for the MFB. As a result,

$$\gamma_{\text{MLSE}} < \gamma_{\text{MF}} \tag{6.72}$$

LE-ZF

$$\gamma_{\text{LE-ZF}} = \gamma_0 = \frac{1}{\sigma_A^2 S_H} \gamma_{\text{MF}} \tag{6.73}$$

LE-MSE The figure of merit is dependent on the SNR and is given by

$$\gamma_{\text{LE-MSE}} = \frac{x^2_{\text{min}}}{\sigma_n^2} \left\langle \frac{1}{AA^* + \sigma_n^2/\sigma_x^2} \right\rangle_A^{-1} \tag{6.74}$$

DFE-ZF Since $A(z)$ is causal, the figure of merit of the DFE-ZF is simply given by

$$\gamma_{\text{DFE-ZF}} = \frac{x^2_{\text{min}}}{\sigma_n^2} = \gamma_0 S_H = \frac{\gamma_{\text{MF}}}{\sigma_A^2} \tag{6.75}$$

DFE-MSE

$$\gamma_{\text{DFE-MSE}} = \frac{x^2_{\text{min}}}{\sigma^2} = \frac{x^2_{\text{min}}}{\left\langle \frac{\sigma_n^2}{AA^* + \frac{\sigma_n^2}{\sigma_x^2}} \right\rangle_G} = \gamma_{\text{DFE-ZF}} \left\langle \frac{1}{AA^* + \frac{\sigma_n^2}{\sigma_x^2}} \right\rangle_G^{-1} \tag{6.76}$$

Simulation results In general, there is a greater immunity to co-channel interference, if the interference follows a third-order model. The difference is all the more pronounced as the interference is more correlated, which is intuitively consistent. By comparing Figures 6-28 and 6-29 with Figures 6-24 and 6-25 respectively, one can see that the gain between first-order and third-order is approximately 0.5 dB for linear equalization and 1.5 dB for DFE when the interference is characterized by a correlation coefficient $\rho = 0.5$. This gain increases when the interference has a correlation coefficient $\rho = 0.9$. For DFE-ZF and DFE-MSE, the gain is approximately 7.2 dB whereas it is 8 dB for LE-MSE. These gains indicate that it should be possible to achieve a much greater immunity to co-channel interference than currently achieved, provided the equalizer is chosen appropriately. Further gains are possible if ML decoding is used since the previous relations indicate that figure of merit of MFB is 5.15 dB lower than DFE-ZF for this example.

Figures 6-30 and 6-31 show the evolution of the tap settings for a linear equalizer and a decision-feedback equalizer respectively, when the interference follows the same third-order model ($N = 50$).

It is instructive to compare these results with the corresponding results for the first-order interference model. The linear equalizer is strictly non-causal, and of much larger support than

in the first-order case. The minimization of the MSE is achieved by using distant precursor and postcursor samples as well as neighboring samples. The effect of the minimization is to create a filter with a comb-like frequency response. The nulls correspond to the peaks in the interference signal. These are all the more pronounced as the interference is stronger. Thus, for a linear equalizer to be effective against co-channel interference, the length of the equalizer must be very large. A bias is also evident in the LE-MSE, since there is a signal-dependent component in the error signal at the input of the decision device.

Figure 6-31 shows the evolution of the tap settings for the DFE-ZF (SIR=50 dB) and for the DFE-MSE. At SIR=50 dB, the forward section simply processes the received signal corrupted by the interference signal with a filter corresponding to the inverse of the minimum phase portion of the interference spectrum. The feedback filter removes the intersymbol interference introduced by the feedforward filter. Both the feedforward and feedback filters are causal and have a finite impulse response. At lower SIR, the feedforward filter is IIR, whereas the feedback filter is FIR. The forward filter can only be approximated, by an FIR filter and a sufficiently long delay. What is important to note is that the difference between the DFE-ZF and the DFE-MSE in terms of bit error performance is relatively small (approximately 1 dB), but the DFE-ZF has a simpler structure since both the feedforward and feedback filters have finite impulse responses.

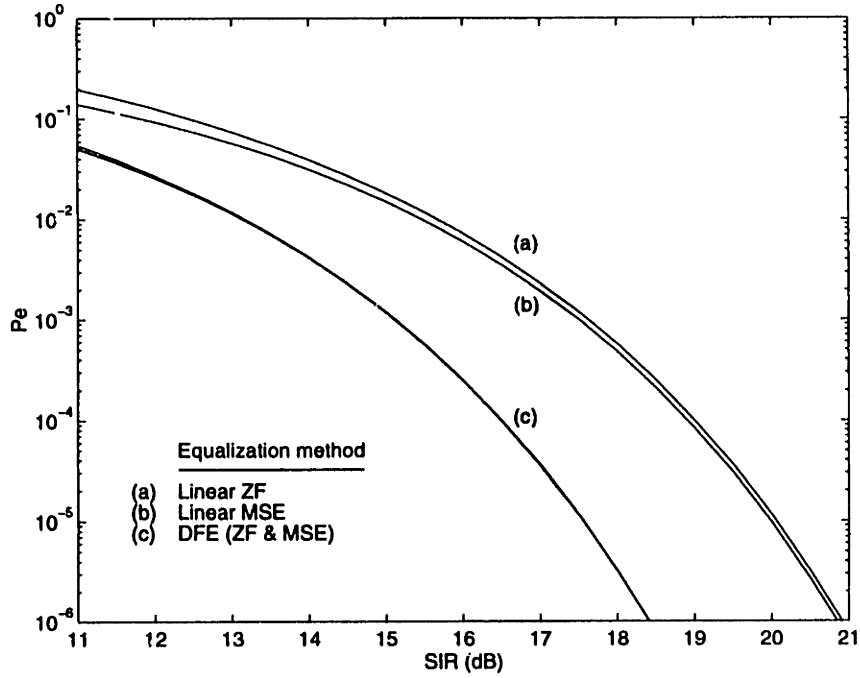

Figure 6-28: Performance of 16QAM with linear and decision-feedback equalization for an equivalent white noise channel of the form $A(z) = 1 - 0.5z^{-1} - 0.5z^{-N} + 0.25z^{-N-1}$ ($N = 50$).

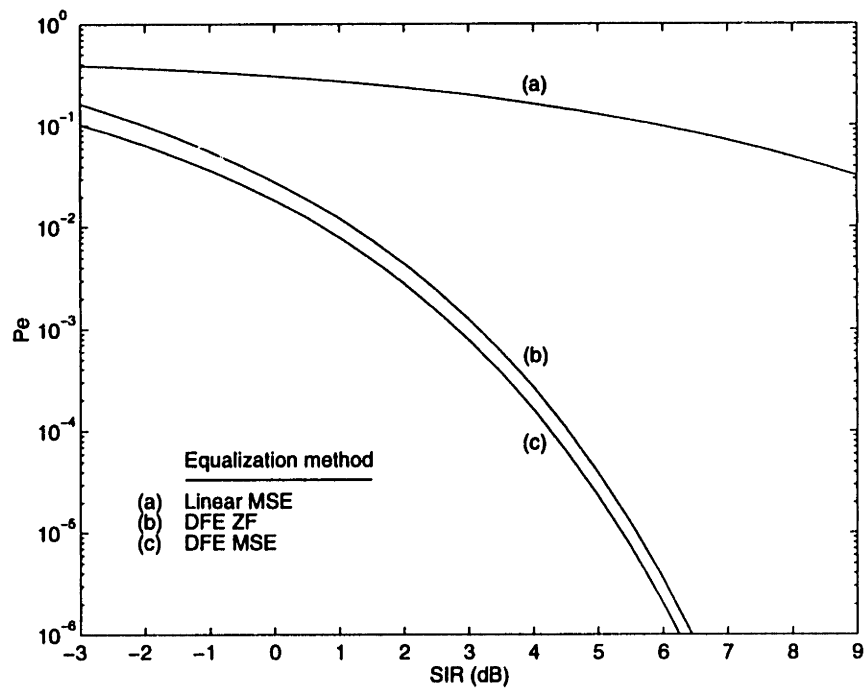

Figure 6-29: Performance of 16QAM with linear and decision-feedback equalization for an equivalent white noise channel of the form $A(z) = 1 - 0.9z^{-1} - 0.9z^{-N} + 0.81z^{-N-1}$ ($N = 50$).

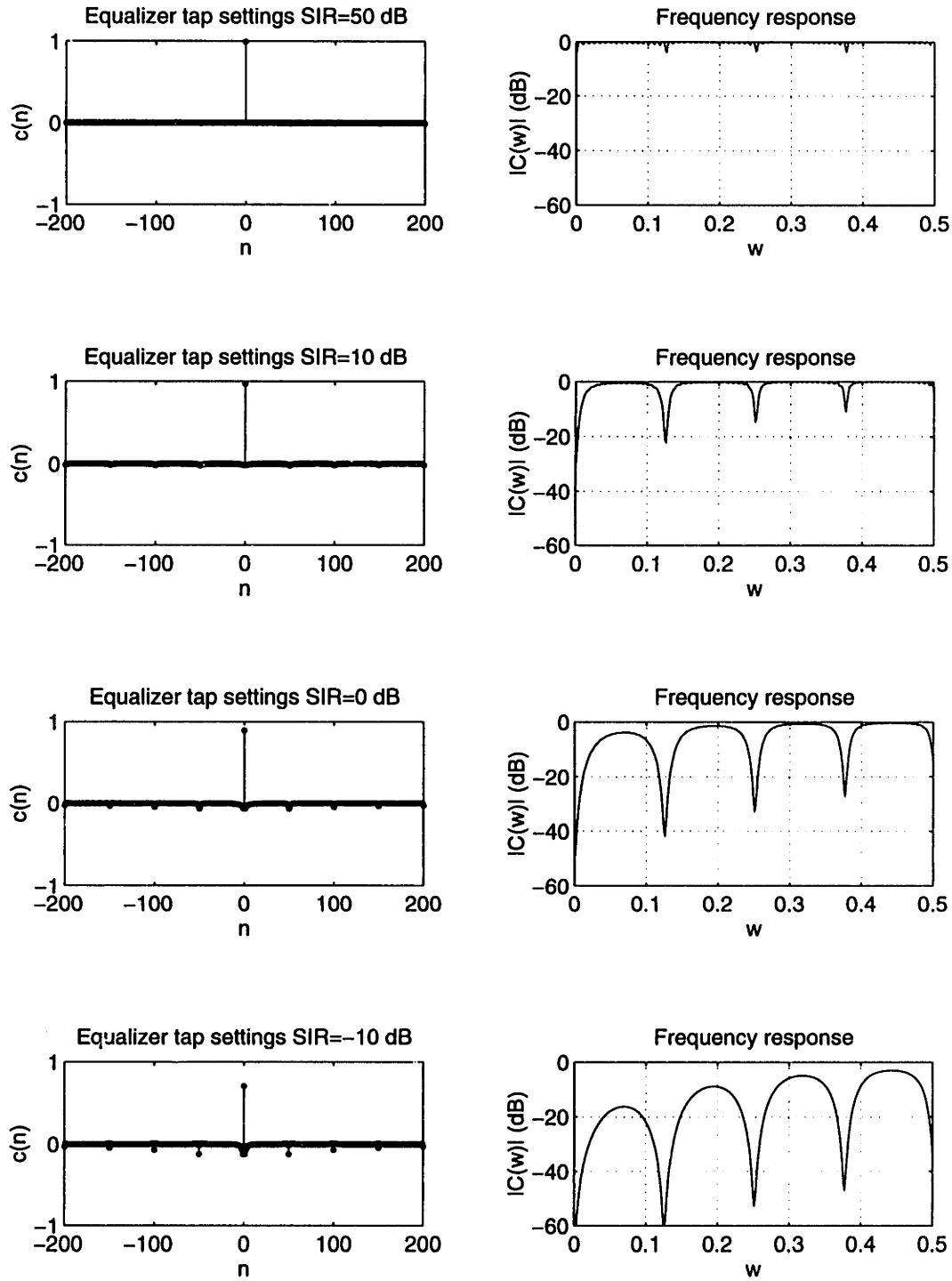

Figure 6-30: Evolution of the equalizer tap settings for the LE-MSE as a function of SIR for a third-order autoregressive interference model of the form $H(z) = 1 - \rho z^{-1} - \rho z^{-N} + \rho^2 z^{-N-1}$ ($\rho = 0.9$ and $N = 50$ in this example).

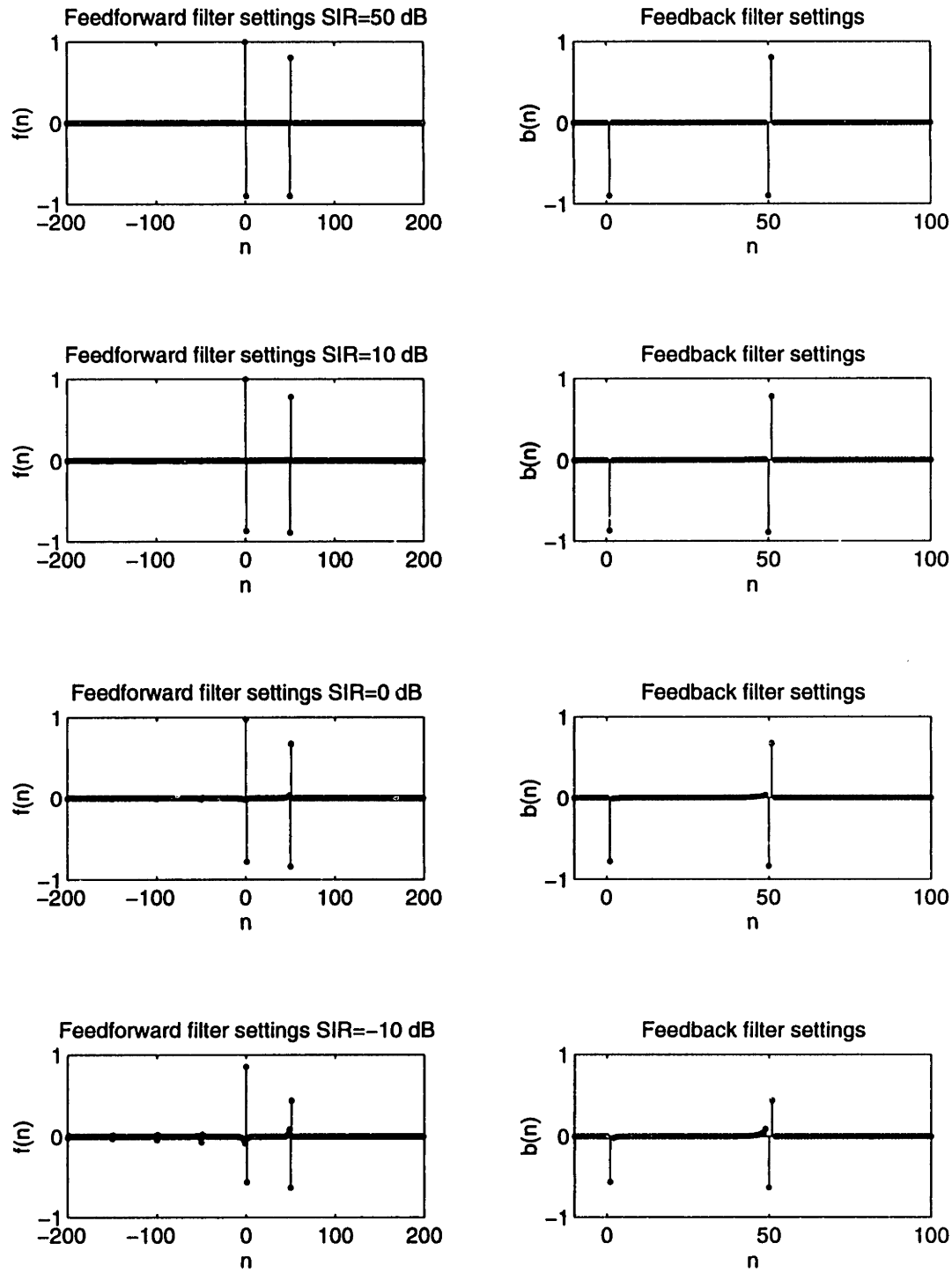

Figure 6-31: Evolution of the equalizer tap settings for the DFE-MSE as a function of SIR for a third-order autoregressive interference model of the form $H(z) = 1 - \rho z^{-1} - \rho z^{-N} + \rho^2 z^{-N-1}$ ($\rho = 0.9$ and $N = 50$ in this example).

6.5.3.3 Constrained-complexity interference rejection

In order to take advantage of the correlations between distant samples, the LE-MSE solution may require a very long filter. However, because of the nature of the interference, only a few taps are effectively used. The complexity of such an equalizer is more a function of the number of taps than of the length of the equalizer. Here we investigate 2 aspects. The first is the reduction in the figure of merit of the LE-MSE when the length of the equalizer is truncated. The second is the variation in the figure of merit as a function of the number of taps used. This second aspect is interesting to investigate because some of the characteristics of the interference are fixed and therefore reduced-complexity solutions may be found.

Let us formulate the traditional finite-length LE-MSE problem and outline its well-known solution. The extension to DFE is straightforward and is also provided.

Finite-length LE-MSE Let the vector of filter coefficients for the forward filter be

$$\mathbf{c}^t = [c_{-L}, \cdots, c_0, \cdots, c_L] \tag{6.77}$$

where $\mathbf{c}^t$ denotes the transpose of vector $\mathbf{c}$, $L = (N-1)/2$, and N is the number of equalizer taps. Also define a vector of past and future input samples to the equalizer,

$$\mathbf{w}_k^t = [w_{k+L}, \cdots, w_k, \cdots, w_{k-L}] \tag{6.78}$$

Assuming no decision errors, the error signal is given by

$$e_k = x_k - q_k = x_k - \mathbf{c}^t\mathbf{w}_k \tag{6.79}$$

We assume that all the random processes are stationary with known statistics and design the equalizer coefficients to minimize the MSE defined as $E[|e_k|^2]$. The MSE can be written

$$E[|e_k|^2] = E[|x_k|^2] - 2\,\mathrm{Re}[\mathbf{c}'\mathbf{R}_{wx}] + \mathbf{c}'\mathbf{R}_{ww}\mathbf{c} \tag{6.80}$$

where $\mathbf{c}'$ denotes the transpose conjugate of $\mathbf{c}$, $\mathbf{R}_{wx}$ is the cross-correlation vector defined by

$$\mathbf{R}_{wx} = E[\mathbf{w}_k^* x_k] \tag{6.81}$$

and $\mathbf{R}_{ww}$ is the autocorrelation matrix defined by

$$\mathbf{R}_{ww} = E[\mathbf{w}_k^* \mathbf{w}_k^t] \tag{6.82}$$

It is easy to verify that the matrix $\mathbf{R}_{ww}$ is Hermitian and Toeplitz. The matrix $\mathbf{R}_{ww}$ is also semi-definite; here we consider the cases where $\mathbf{R}_{ww}$ is positive definite. It is easy to show that the MSE is minimized for the following choice of the weight vector $\mathbf{c}$:

$$\tilde{\mathbf{c}} = \mathbf{R}_{ww}^{-1}\mathbf{R}_{wx} \tag{6.83}$$

The minimum MSE is then given by

$$\epsilon^2 = E[|x_k|^2] - \mathbf{R}'_{wx}\tilde{\mathbf{c}} \tag{6.84}$$

SNR gain of LE-MSE for third-order interference model The figure of merit of the finite-length LE-MSE is given by

$$\gamma_{\text{LE-MSE}} = \frac{2x_{\min}^2}{\epsilon^2} \tag{6.85}$$

We define the SNR gain by the ratio of $\gamma_{\text{LE-MSE}}$ to the signal-to-interference ratio, or

$$\text{SNR}_{\text{gain}} = \frac{E[|z_k|^2]}{\epsilon^2} \tag{6.86}$$

Figure 6-32 shows the evolution of the SNR gain as a function of filter length when the interference is of the form $1/A(z)$ with $A(z) = 1 - \rho z^{-1} - \rho z^{-N} + \rho^2 z^{-N-1}$ with $\rho = 0.9$ ($N = 50$ in this example), for 2 different values of the SIR. The SNR increases rapidly as a function of filter length, up to a length $N = 25$. The next increase occurs when the filter length is large enough to include samples that are strongly correlated with the current sample (i.e. around $N = 100$). The ultimate SNR gain is evidently obtained when the filter is unconstrained. In this case, the asymptotic gains are equal to 4.9 dB and 9.16 dB for SIR = 10 dB and SIR = 0 dB respectively. It is clear that only a small number of filter taps actually contribute to the gain. The SNR gain is within 0.5 dB of the maximum achievable gain with a linear equalizer for a filter length of 200 taps.

A reduced-complexity equalizer can be achieved by retaining only the coefficients that contribute most to the SNR gain and setting the other coefficients to zero. Figure 6-33 shows the variation of the SNR gain as a function of the number of taps chosen so as to provide the maximum increase in SNR gain. It is clear that most of the SNR gain can be achieved with only a few filter taps. At SIR = 0 dB, most of the gain can be achieved with 10 taps distributed around the multiples of N: the number of taps required to approach the asymptotic SNR gain increases as SIR increases, but this should not be an issue since the SIR is already high.

Finite-length DFE-MSE The optimal filter settings for the DFE can be obtained by considering the vector of filter coefficients $\mathbf{d}$ formed by concatenating the coefficients of the forward filter and those of the feedback filter $\mathbf{b}$:

$$\mathbf{d}^t = [\mathbf{c}^t, -\mathbf{b}^t] \tag{6.87}$$

We also define a vector $\mathbf{y_k}$ formed of the input samples to the forward equalizer $\mathbf{w_k}$ and the outputs from the decision device. Assuming no decision errors,

$$\mathbf{y}_k^t = [\mathbf{w}_k^t, \mathbf{x}_k^t] \tag{6.88}$$

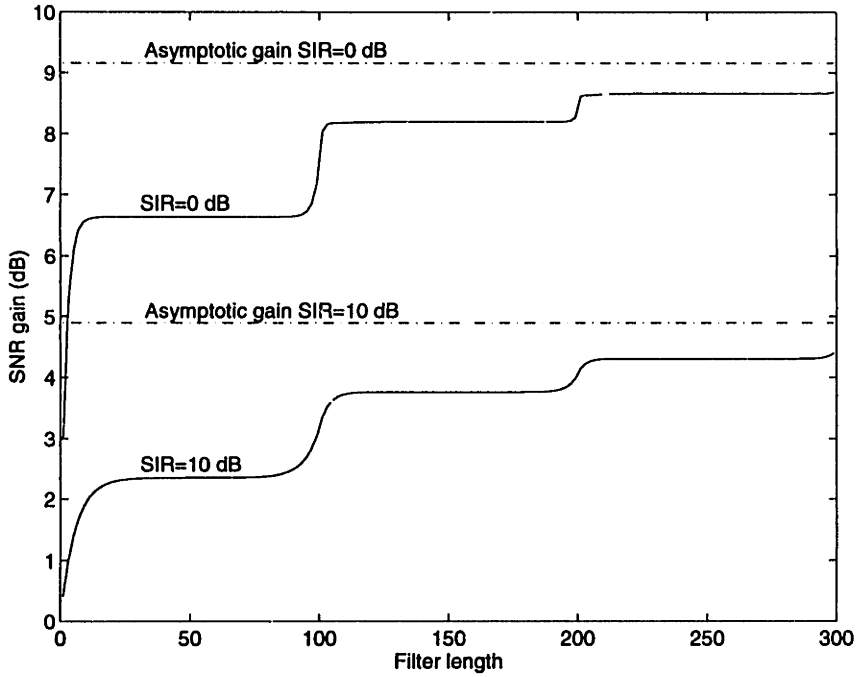

Figure 6-32: SNR gain vs. filter length for finite-length LE-MSE and interference model of the form $1/A(z)$ with $A(z) = 1-\rho z^{-1}-\rho z^{-N}+\rho^2 z^{-N-1}$ with $\rho = 0.9$ and $N = 50$.

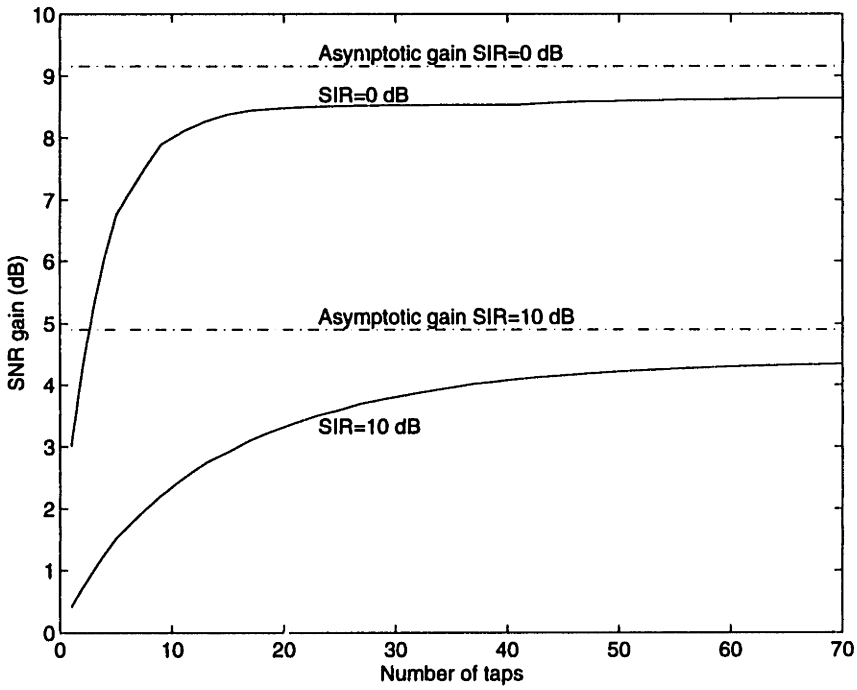

Figure 6-33: SNR gain vs. number of filter taps for finite-length LE-MSE and interference model of the form $1/A(z)$ with $A(z) = 1 - \rho z^{-1} - \rho z^{-N} + \rho^2 z^{-N-1}$ with $\rho = 0.9$ and $N = 50$.

where $\mathbf{x_k}$ is the vector of decisions starting at time $k-1$.

The error for the DFE-MSE is then given by

$$e_k = x_k - q_k = x_k - \mathbf{d}^t\mathbf{y_k} \tag{6.89}$$

which is minimized in a mean-square sense by the choice

$$\tilde{\mathbf{d}} = \mathbf{R}_{yy}^{-1}\mathbf{R}_{yx} \tag{6.90}$$

where $\mathbf{R}_{yy} = E[\mathbf{y}_k^*\mathbf{y}_k^t]$ and $\mathbf{R}_{yx} = E[\mathbf{y}_k^* x_k]$. The minimum MSE is then given by

$$\epsilon^2 = E[|x_k|^2] - \mathbf{R}'_{yx}\tilde{\mathbf{d}} \tag{6.91}$$

In the DFE-MSE, the forward and feedback filters are jointly optimized to produce the minimum MSE. It is therefore difficult to separate out the contributions of the two filters to the performance of the equalizer. To investigate the influence of the feedback filter, we use an alternative DFE structure sometimes called noise-predictive DFE.

Noise-predictive DFE Figure 6-34 shows two alternative decision-feedback structures which provide interesting interpretations. These forms are equivalent to the ones in Figure 6-22 in the case of infinite-length forward and feedback filters, but may be suboptimal in the case of finite-length forward filters. However, they present the advantage that the forward and backward filters can be adjusted independently.

An interpretation of Figure 6-34(a) is the following: the input to $B(z)$ is a sequence of interference samples formed by subtracting the decision $\hat{x}_k$ from the received sample w_k. Assuming decisions are correct, $w_k - \hat{x}_k$ does not contain any signal component. $B(z)$ then forms the optimal prediction of the current interference based on past interference samples. The prediction is then removed from the signal. Thus, the sequence q_k contains only white noise of minimum variance. Because the filter $B(z)$ forms the optimum prediction of the noise component, this structure is sometimes called noise-predictive DFE [3].

In Figure 6-34(b), a similar structure can be derived for the DFE-MSE. Here the forward filter is designed to minimize the MSE at its output. Thus, it is the same filter as for LE-MSE. The error term $e_k = w'_k - \hat{x}_k$ contains both a noise component and a signal-dependent component. The filter $B(z)$ is used to whiten the error sequence. However, as a result of the noise whitening, the error term at the input of the decision device contains a signal-dependent component (or residual intersymbol interference). By analogy, we call this structure the error-predictive DFE.

We now assume that the forward filter in Figure 6-34(b) is unconstrained, i.e. that it is equal to the unconstrained LE-MSE. In this case, the predictive form of the DFE is equivalent to the normal form of the DFE, even when the predictive filter is finite [76]. Therefore, the predictive

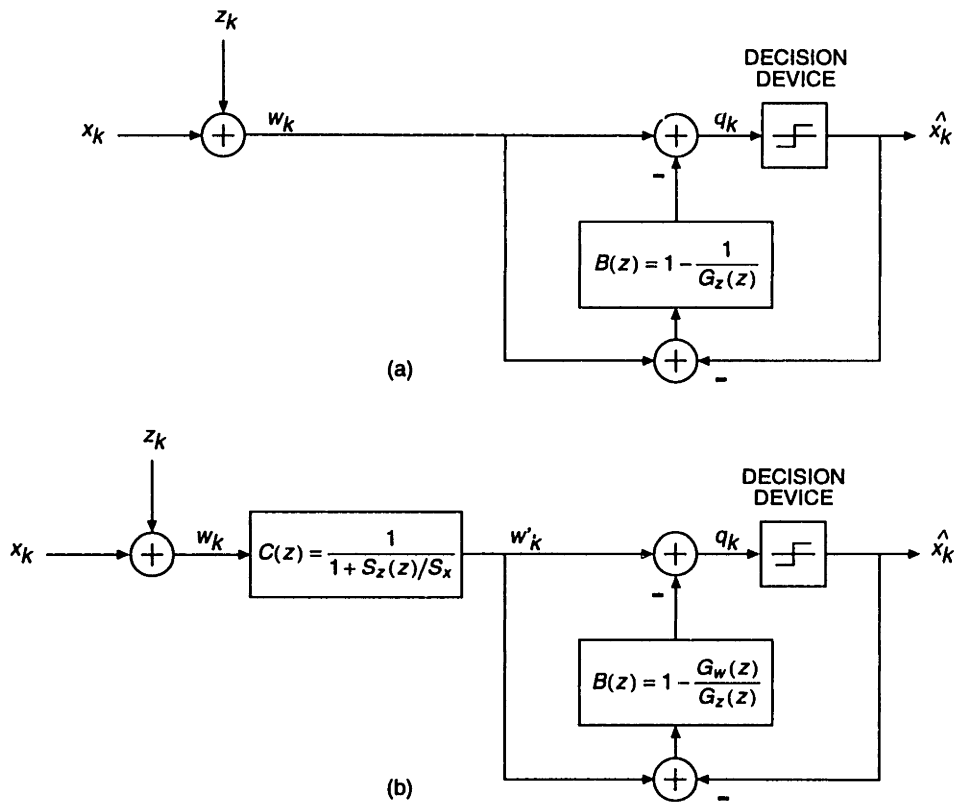

Figure 6-34: Interference rejection based on (a) Noise-predictive form of DFE-ZF (b) Error-predictive form of DFE-MSE.

filter $B(z)$ is assumed to consist of a finite number of taps and is again optimized to achieve the minimum MSE. We saw earlier that the spectrum of the error sequence e_k at the output of the LE-MSE was

$$S_E(z) = \frac{S_x S_z}{S_w} = \frac{S_x S_z}{S_x + S_z} \tag{6.92}$$

Let the vector of predictor coefficients be

$$\mathbf{b}^t = [b_1, \cdots, b_L] \tag{6.93}$$

and let $\mathbf{e}$ be the vector of past errors

$$\mathbf{e}_k^t = [e_{k-1}, \cdots, e_{k-L}] \tag{6.94}$$

The error at the output of the predictor is

$$e'_k = e_k - \mathbf{b}^t \mathbf{e}_k \tag{6.95}$$

which is minimized in the mean-square sense by the choice

$$\tilde{\mathbf{b}} = \mathbf{R}_{ee}^{-1} \alpha \tag{6.96}$$

where $\mathbf{R}_{ee} = E[\mathbf{e}_k^* \mathbf{e}_k^t]$ and $\alpha = E[\mathbf{e}_k^* e_k]$. The MSE is equal to

$$\epsilon^2 = E[|e_k|^2] - \alpha' \tilde{\mathbf{b}} \tag{6.97}$$

SNR gain of DFE-MSE for third-order interference model Let us now define the SNR gain as the decrease in error variance between the output of the LE-MSE and the input of the decision device. Therefore, this gain only relates to the performance of the predictor $B(z)$. To obtain the total SNR gain between the input to the forward filter and the input to the decision device, the LE-MSE gain must be added to the predictor gain.

Figure 6-35 shows the SNR gain for SIR = 0 dB and SIR = 10 dB. Also shown are the maximum achievable gains with an unconstrained predictor filter. The maximum gain is given by $E[|e_k|^2] / \langle S_{ee}(z) \rangle_G$. For this model of interference, all the SNR gain is achieved by ensuring that the feedback filter is of length of at least 51, which is consistent with the form of the unconstrained predictor filter $B(z) = 1 - G_w(z)/G_z(z)$. Therefore, the DFE-MSE is capable of achieving most of its gain by using very few non-zero coefficients in the feedback filter. This is important to control the propagation of errors, since the severity of the error propagation problem is more a function of the number of symbols that are fed back than the length of the feedback filter.

Although these results were derived for a few specific interference models, it is thought that real-world interference signals should have similar characteristics and therefore it should be possible to apply similar techniques in real-world cases.

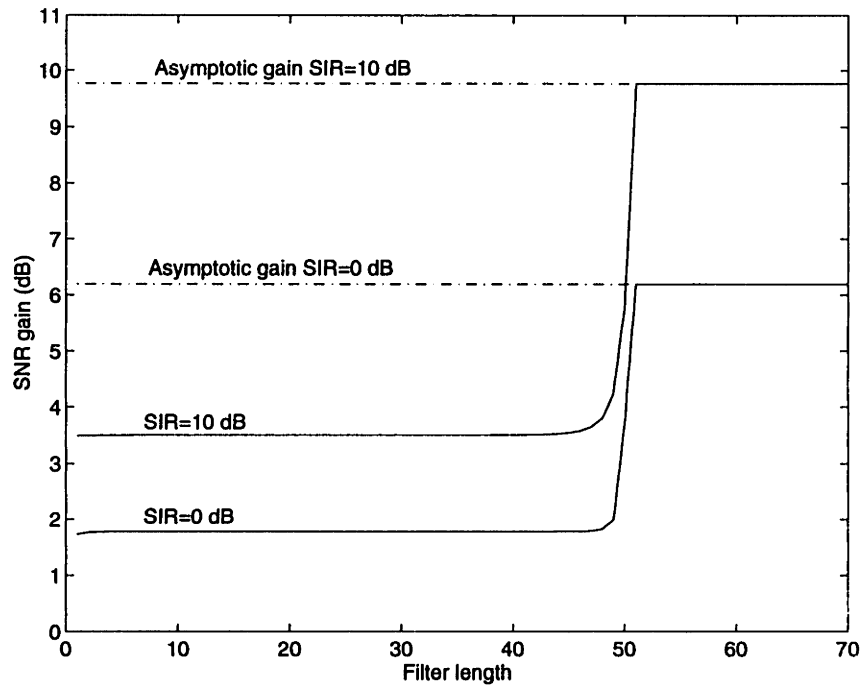

Figure 6-35: SNR gain vs. filter length for finite-length predictive DFE-MSE and interference model of the form $1/A(z)$ with $A(z) = 1 - \rho z^{-1} - \rho z^{-N} + \rho^2 z^{-N-1}$ with $\rho = 0.9$ and $N = 50$.

6.5.3.4 Effect of channel noise on interference rejection

As was seen previously, there is no difference in principle between the interference-only channel and the interference+noise channel. The equalization schemes shown in Figure 6-22 remain valid, provided the sequence z_k represents the interference+noise sequence rather than the interference-only sequence.

However, because of the different characteristics of white noise and strongly correlated interference, the value of the equalizer settings can be quite different from the interference-only case. The forward filter in the DFE-ZF $1/G_z(z)$ is no longer an FIR filter, since in general it will have both poles and zeros. In the interference-only case studied earlier, only a few coefficients had non-zero values (in the case of the AR noise model). In the interference+noise case, this is no longer the case. The feedback filter $B(z) = 1/G_z(z) - 1$ also has a large number of non-zero coefficients. While this is not a problem in principle, since this is the solution that minimizes the error variance at the input of the decision device, it is a problem in practice. Indeed, a large number of non-zero coefficients in the feedback path imply that the error propagation problem will be severe at low SNR. Thus we have conflicting requirements: we would like to minimize the error variance by using the more effective DFE approach, but the requirement for a long DFE filter implies that error propagation will be a problem.

One solution to this problem is to constrain the feedback filter to only have a few non-zero coefficients. As we have seen in Sec. 6.5.3.3, most of the performance gain can be achieved by using only a limited number of non-zero taps in the feedback path. It may also be desirable to limit the length of the forward filter in both LE-MSE and DFE-MSE cases. By doing this, we increase slightly the error variance at the input to the decision device, but we also reduce the probability of degradations due to error propagation. Such an approach is possible because the interference has several well defined characteristics, one of which is its fundamental frequency, and consequently, the number of samples between correlated interference samples is fixed. Such an approach would not be possible with the general interference signal or linear distortion, because the taps with significant coefficient values would be unknown a priori.

The constrained forward and feedback filters that minimize the MSE can be determined using a procedure similar to the one used for the determination of the finite-length DFE. Consider, for instance, an interference signal with power spectrum $S_z(z) = \sigma_n^2/AA^*$ with $A(z) = 1 - \rho z^{-1} - \rho z^{-N} + \rho^2 z^{-N-1}$. In addition to interference, the signal is degraded by white Gaussian noise. Let the signal-to-interference ratio be defined by

$$\text{SIR} = \frac{S_x}{\langle S_z \rangle_A} \tag{6.98}$$

and the signal-to-noise by

$$\text{SNR} = \frac{S_x}{N_0} \tag{6.99}$$

Let us define a vector $\mathbf{d}$ of forward and feedback coefficients

$$\mathbf{d}^t = [c_{-L}, \cdots, c_0, \cdots, c_L, -b_1, -b_N, -b_{N+1}] \tag{6.100}$$

and a vector $\mathbf{y_k}$ of input samples to the forward equalizer and past decisions from the decision device. Assuming no decision errors,

$$\mathbf{y_k^t} = [w_{k+L}, \cdots, w_k, \cdots, w_{k-L}, x_{k-1}, x_{k-N}, x_{k-(N+1)}] \tag{6.101}$$

The error for the DFE-MSE is then given by

$$e_k = x_k - q_k = x_k - \mathbf{d}^t\mathbf{y_k} \tag{6.102}$$

which is minimized in a mean-square sense by the choice

$$\tilde{\mathbf{d}} = \mathbf{R}_{yy}^{-1}\mathbf{R}_{yx} \tag{6.103}$$

where $\mathbf{R}_{yy} = E[\mathbf{y_k^*}\mathbf{y_k^t}]$ and $\mathbf{R}_{yx} = E[\mathbf{y_k^*}x_k]$. The minimum MSE for this constrained filter is then given by

$$\epsilon^2 = E[|x_k|^2] - \mathbf{R}'_{yx}\tilde{\mathbf{d}} \tag{6.104}$$

Figure 6-36 shows the performance of linear and decision-feedback equalization using a small number of forward and feedback filter coefficients. In the case of the DFE, a simple 3-tap feedback filter was used. As can be seen, there is little if no performance loss due to this restriction on the DFE filter. This is not unexpected, since it was found previously that little difference existed between DFE-ZF and DFE-MSE for this interference model, and the feedback filter for the DFE-ZF is a causal filter with 3 taps.

Figure 6-37 shows the performance of the reduced-complexity scheme in the presence of additive white Gaussian noise with SNR = 20 dB. As the SIR increases, the performance reaches an error floor corresponding to the error rate over the AWGN channel at that SNR. Since the channel is assumed ideal otherwise, the performance of the linear and decision-feedback equalizers converge at high SIR. At intermediate SIRs, the performance difference is about 6 dB at SNR = 20 dB, indicating the clear advantage of using a decision-feedback scheme.

Figures 6-38 and 6-39 further illustrate the behavior of the two schemes. In both cases, the error curves asymptotically converge to the corresponding error rates over the AWGN channel. However, the DFE curves converge more rapidly, as the DFE is able to reject the interference much more efficiently than the linear equalizer. Finally, it is clear that AWGN has a much more detrimental effect of performance than co-channel interference canceled via a DFE.

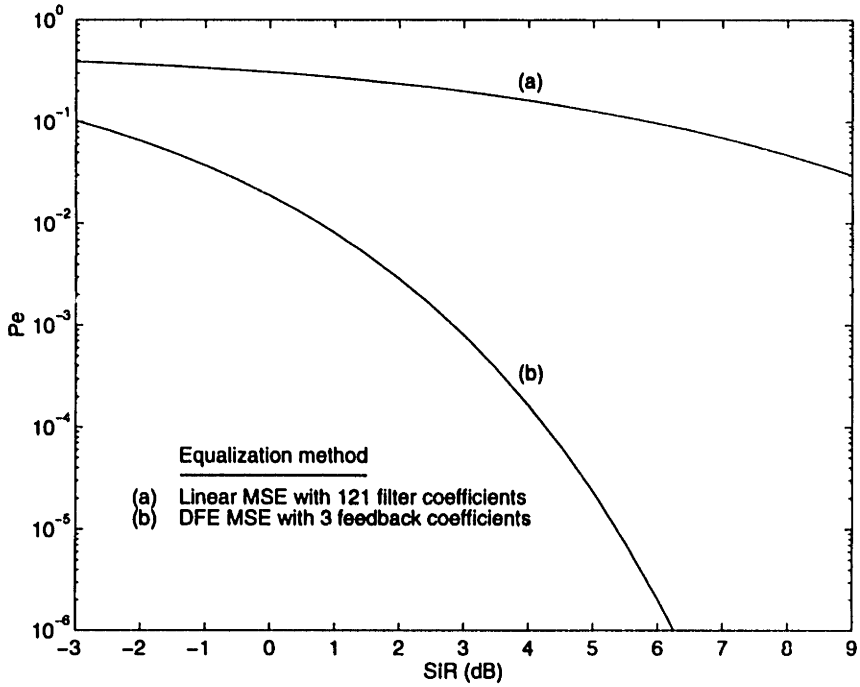

Figure 6-36: Performance of reduced-complexity linear and decision-feedback equalization for an interference model of the form $1/A(z) = 1 - 0.9z^{-1} - 0.9z^{-N} + 0.81z^{-N-1}$ ($N = 50$).

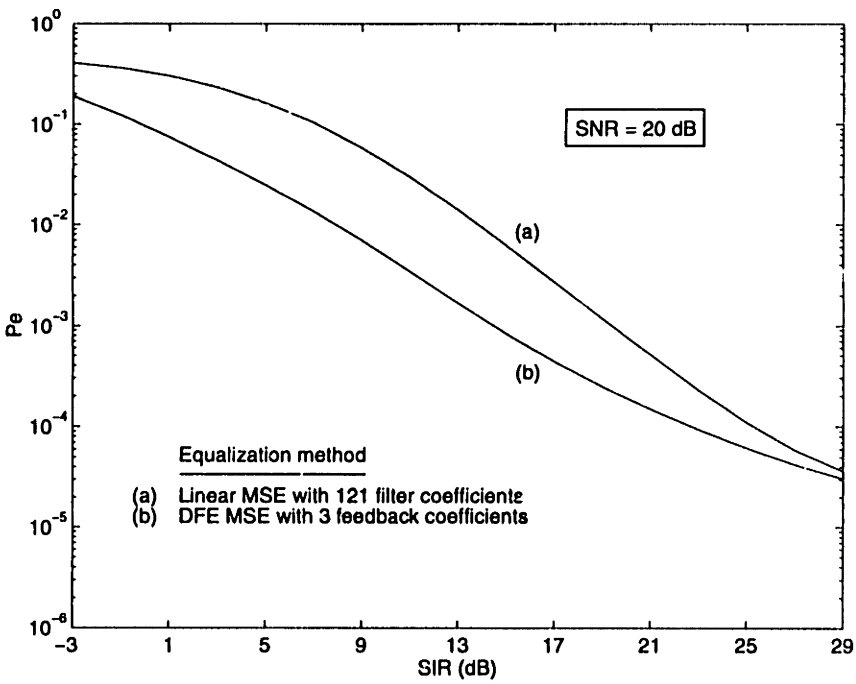

Figure 6-37: Performance of reduced-complexity linear and decision-feedback equalization at $SNR = 20$ dB for an interference model of the form $1/A(z) = 1-0.9z^{-1}-0.9z^{-N}+0.81z^{-N-1}$ ($N = 50$).

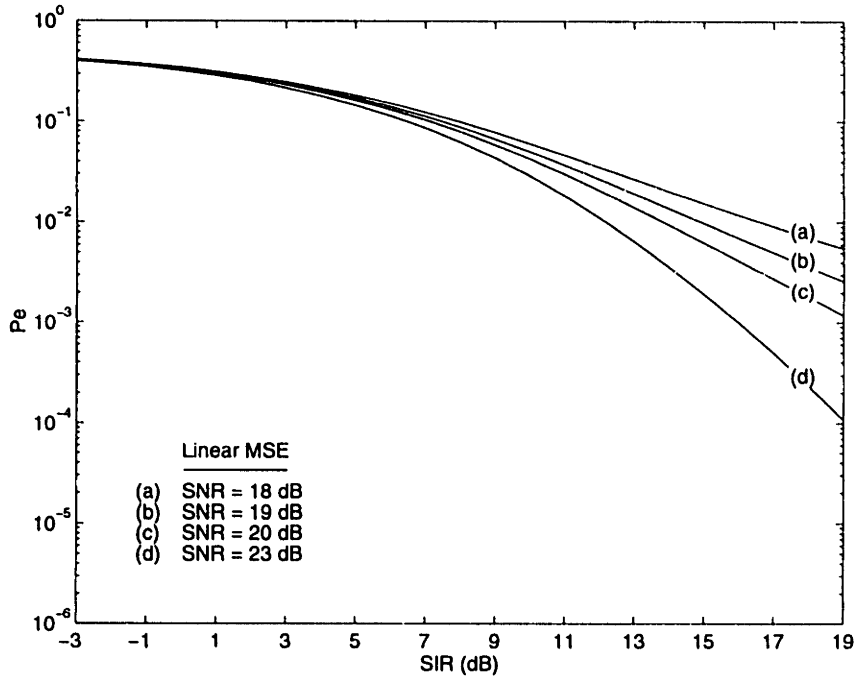

Figure 6-38: Performance of reduced-complexity linear equalization at several SNRs for an interference model of the form $1/A(z) = 1 - 0.9z^{-1} - 0.9z^{-N} + 0.81z^{-N-1}$ ($N = 50$).

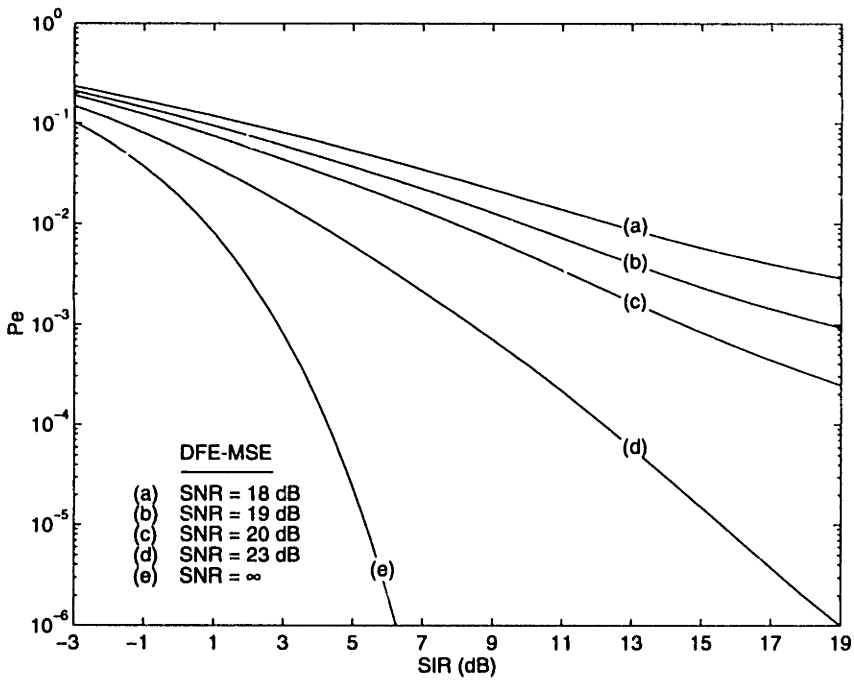

Figure 6-39: Performance of reduced-complexity decision-feedback equalization at several SNRs for an interference model of the form $1/A(z) = 1 - 0.9z^{-1} - 0.9z^{-N} + 0.81z^{-N-1}$ ($N = 50$).

6.5.3.5 Comparison with the precoding/comb filtering technique

It is difficult to provide an exact comparison between the TH precoding technique used in [97] and the equalization schemes described here without having a realistic interference signal. In this section, however, we provide some elements of comparison on the basis of a number of assumptions. In [97], the delay of 12 symbols was chosen so that the single coefficient for the receiver comb filter could be chosen as unity. This was an important consideration in that it allowed the resulting channel to be viewed as the partial response channel $H(z) = 1 - z^{-12}$ and the traditional techniques used for PR signaling could thus be applied[1]. With this delay, carrier frequency and sampling rate, the NTSC steady-state component of the interference falls near one of the nulls of the receiver comb filter. Such a filter is incapable of reducing the interference at frequencies other than those of the nulls, and in fact would amplify the interference signal if it happened to be concentrated at other frequencies.

Assuming the same interference model as earlier, the figure of merit of the receiver based on precoding and comb filtering with a filter $H(z)$ is given by

$$\gamma_{\text{PR}} = \frac{x_{\min}^2}{\sigma_n^2}\left\langle \frac{HH^*}{AA^*} \right\rangle_A^{-1} = \gamma_{\text{DFE-ZF}}\left\langle \frac{HH^*}{AA^*} \right\rangle_A^{-1} \tag{6.105}$$

If $A(z)$ is close to $H(z)$, the receiver comb filter will reduce the interference signal greatly, and the performance will be comparable to that of the DFE-ZF, which should not be surprising since this technique is essentially DFE implemented at the transmitter. There is no guarantee, however, that the filter $H(z)$ will correctly be matched to the interference source, since it is a fixed filter with single integer tag, whereas the DFE-ZF is designed to minimize the error at the input of the decision device.

Figures 6-40 and 6-41 show the performance of precoding compared to zero-forcing DFE for two different correlation coefficients of the interference. In Figure 6-40, the interference is modeled as an autoregressive process with correlation coefficient $|\rho| = 0.5$. The SNR difference between precoding and DFE-ZF is close to 4 dB at $P_e = 10^{-6}$. Figure 6-41 shows that this performance loss increases as the interference becomes more correlated. For $|\rho| = 0.9$, the loss is 7 dB at $P_e = 10^{-6}$. The difference is greater for a third-order interference model because more energy is present in the harmonics of the NTSC line frequency. Based on these results, it would seem desirable to implement more effective interference reduction schemes than the precoding and comb filtering with a single tap FIR filter scheme proposed in [97].

[1]The equivalent double-sideband QAM scheme would use a delay of 6 samples since the sampling rate is half that of single-sideband modulation.

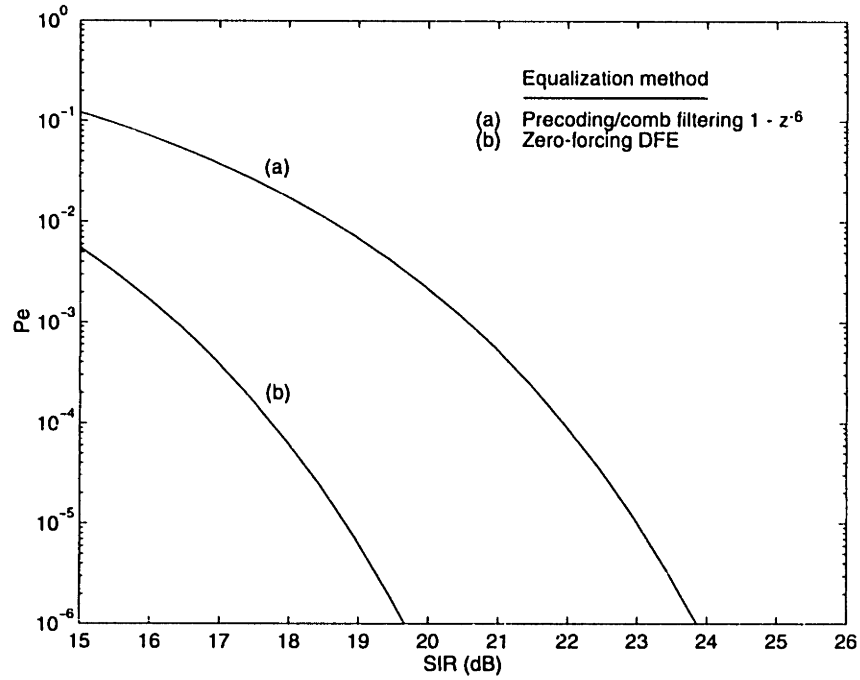

Figure 6-40: Performance of 16QAM with precoding/comb filtering by $1 - z^{-6}$ and zero-forcing DFE for an interference model of the form $1/A(z)$ with $A(z) = 1 - \rho z^{-1}$ and $\rho = 0.5e^{-j\pi/3}$.

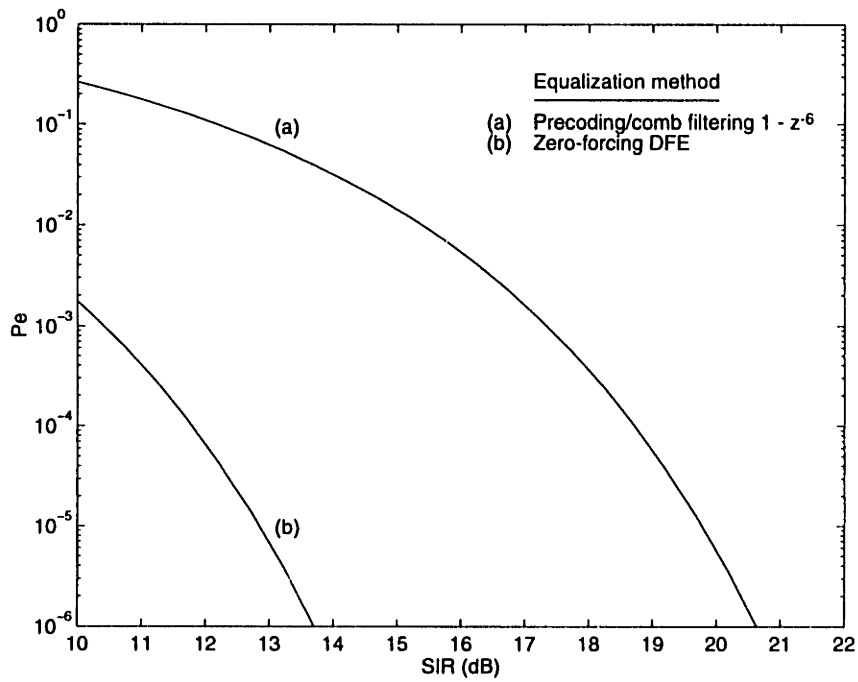

Figure 6-41: Performance of 16QAM with precoding/comb filtering by $1 - z^{-6}$ and zero-forcing DFE for an interference model of the form $1/A(z)$ with $A(z) = 1 - \rho z^{-1}$ and $\rho = 0.9e^{-j\pi/3}$.

6.5.3.6 Comparison with NTSC recursive cancellation technique

In the presence of strong interference, the effect of the LE-MSE equalizer is to create notches at the frequencies corresponding to the line rate harmonics. The NTSC recursive filter technique also seeks to create notches in the received signal's spectrum, but only at a limited and predetermined number of frequencies. It is difficult to carry out a rigorous comparison of the two schemes without having a representative sample of the NTSC interference and without knowledge of the exact filter settings. However, some estimates can be obtained.

Let us recall that the LE-MSE equalizer is given by

$$C(z) = \frac{1}{1 + S_z(z)/S_x(z)} \tag{6.106}$$

Let $G(z) = \sum_k G_{\omega_k}(z)$ be the combined filter corresponding to the bank of narrowband filters. The output q_k of the notch filter $C'(z) = 1 - G(z)$ has a Z-transform given by $Q(z) = X(z) - G(z)X(z) + Z(z) - G(z)Z(z)$. Thus, the error signal is $E(z) = X(z) - Q(z) = (G(z) - 1)Z(z) + G(z)X(z)$. The first term represents the remaining contribution from the interference, and the second term represents the intersymbol interference that has been introduced by the interference rejection filter. A tradeoff must be found between interference rejection and creation of intersymbol interference. Adding more filters reduces the NTSC interference but also increases the amount of ISI. A constrained optimal solution would consist of choosing $G(z)$ such that the error is minimized, subject to the constraint that the receive filter is of the form $C'(z) = 1 - G(z)$.

We now consider the case where the filter $C'(e^{j\omega T})$ is equal to $C(e^{j\omega T})$ over the range $|\omega| < \omega_k$, and unity outside. This corresponds to the case where the equalizer optimally cancels the first k harmonic peaks and leaves the other peaks unmodified. In practice, this is not possible with a constrained filter such as the recursive notch filter described in Sec. 6.5.1.3, but it represents an optimistic estimate of the interference reduction capability of the filter.

The spectrum of the error signal is then given by

$$S_e(z) = \begin{cases} S_x(z)S_z(z)/(S_x(z) + S_z(z)) & \text{for } |\omega| < \omega_k \\ S_z(z) & \text{elsewhere} \end{cases} \tag{6.107}$$

Thus the figure of merit of the receiver is given by

$$\gamma_{RC} = \frac{2x_{min}^2}{\langle S_e \rangle_A} \tag{6.108}$$

Figure 6-42 shows the performance of the recursive canceler when the interference is of the form $1/A(z)$ with $A(z) = 1 - \rho z^{-1} - \rho z^{-N} + \rho^2 z^{-N-1}$ with $\rho = 0.9$ ($N = 50$ in this example). The number of notches is varied from 1 to 5, as in [81], with a difference that here, the harmonic

peaks are linearly equalized whereas in [81] the notches had fixed depths and bandwidths, irrespective of the interference. The performance of a 5-notch canceler (center notch aligned on the video carrier frequency of the interference) approaches that of the LE-MSE . Even with a single notch centered at the video carrier frequency, the improvement over LE-ZF is close to 2 dB. However, it is important to remember that the performance of the linear equalizer is far worse than that of a decision-feedback equalizer.

Therefore, we conclude that a receiver front-end, consisting of a small number of notch filters, can improve the performance of the receiver, but that even with a filter optimally adjusted, the performance will be no better than that of the unconstrained MSE linear equalizer. In addition, the adaptation of a set of IIR filters can be problematic.

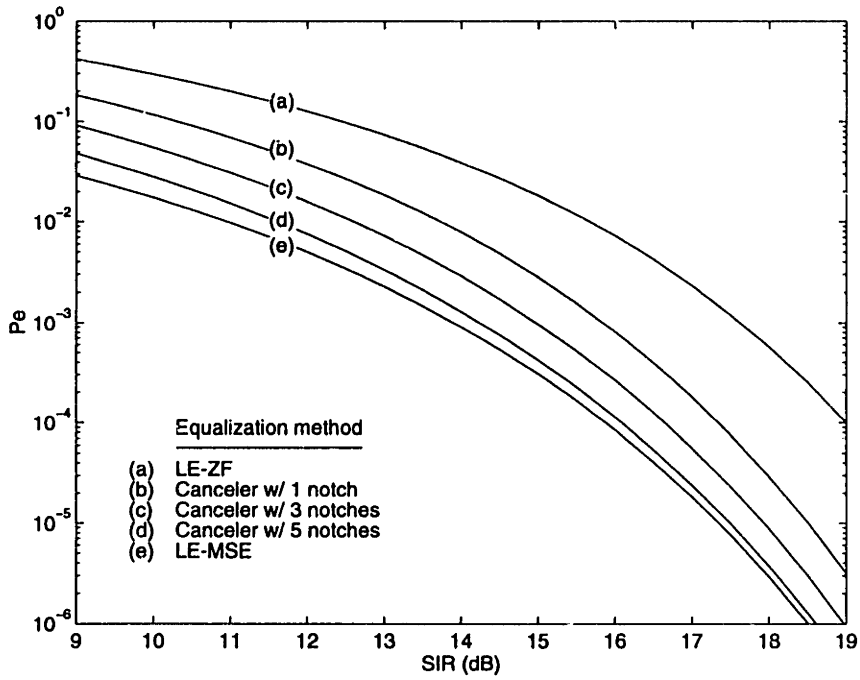

Figure 6-42: Performance of 16QAM with recursive cancellation for an interference model of the form $1/A(z)$ with $A(z) = 1 - \rho z^{-1} - \rho z^{-N} + \rho^2 z^{-N-1}$ with $\rho = 0.9$ and $N = 50$.

6.5.4 Improved interference rejection approach

So far we have restricted our attention to practical but suboptimal receiver structures. It is interesting to see how the performance of the receiver might be further improved. As we saw earlier, the optimum receiver for estimating the data sequence in the presence of linear distortions consists of a WMF followed by a Viterbi decoder that performs maximum-likelihood sequence estimation on the ISI trellis. Such an approach would also be optimal in the interference-only case. Unfortunately, the complexity of such a decoder would be considerable. As an example, consider the interference-only case. The equivalent channel for the third-order model we used in the simulations is of the form $H(z) = 1 - \rho z^{-1} - \rho z^{-N} + \rho^2 z^{-N-1}$. Thus the length of the impulse response of the channel is $K = N + 2$. Therefore ML decoding would require determining the best path in a trellis with M^{K-1} states, where M is the size of the signal set (e.g. 16 in the case of 16QAM).

There have been many efforts to find techniques for reducing the complexity of MLSE while retaining most of its performance. Some of the first techniques were based on channel truncation and prefiltering to shape the channel impulse response to a shorter one. In [36], Falconer and Magee adaptively optimized the prefilter and the desired channel impulse response, by minimizing the mean square error between the output of the equalizer and the desired response. Another approach consists of using a DFE to truncate the channel impulse response in order to reduce the system complexity and mitigate the effect of noise enhancement and then apply MLSE (Lee and Hill [64]). In general, these may be viewed as ad hoc techniques. A more general approach, the so-called Reduced State Sequence Estimation (RSSE) approach, has been recently suggested by Eyuboğlu and Qureshi [34, 35]. This approach provides an example of the possible tradeoffs between decoder complexity and receiver performance. For completeness, and because some use of these ideas will be made in the next chapter, we briefly outline the main concepts.

Let us consider the equivalent white noise channel model with channel filter $G_{h,n}(z)$ and input sequence $\{x_k\}$ described earlier. Let us assume that this channel filter can be approximated by an FIR filter characterized by the vector of coefficients $\mathbf{g} = [1, g_1, g_2, \ldots, g_K]$. In MLSE, the decoder operates over a trellis with states defined by the vector $[x_{n-1}, \ldots, x_{n-K}]$. As mentioned earlier, the decoding complexity is on the order of M^{K-1}, where M is the size of the alphabet from which the x_k are chosen. This, clearly, is a very large quantity when either K is large, or M is large. To reduce the decoding complexity, Eyuboğlu *et al.* defined a two-dimensional set-partitioning scheme using Ungerboeck-like set-partitioning principles. Let $\Omega(k)$ be a partition for the symbol x_{n-k}. Let J_k be the number of subsets in $\Omega(k)$, chosen to decrease from x_{n-1} to x_{n-K}. Thus, the total number of states is $J_1 \times \ldots \times J_K$. If $J_1 = \ldots = J_k = M$, the RSSE becomes equivalent to MLSE. If $J_1 = \ldots = J_k = 1$, RSSE becomes equivalent to DFE. Thus, RSSE may be

viewed as a flexible scheme for trading-off complexity and performance.

Figure 6-43 shows a possible implementation of an RSSE receiver for interference rejection. An equivalent structure can also be derived for the equivalent white noise channel. In order to reduce decoding complexity, the RSSE operates on the response $1 - \rho z^{-1}$, and decision-feedback is used for the cancellation of the higher-order terms. Alternatively, one may view the complete detector, including the feedback path, as an RSSE receiver with $J_2 = \ldots = J_{N+1} = 1$. The front-end $H(z)$ acts as an interference whitener, producing at its output a signal corrupted by intersymbol interference and white noise.

Figure 6-44 shows the performance of a simple 4-state RSSE decoder based on partitioning the 16QAM constellation into 4 subsets, using Ungerboeck set-partitioning principles. The performance, determined by Monte Carlo simulation, is clearly superior to that of the ideal DFE-MSE, achieving close to a 2 dB gain at $P_e = 10^{-6}$. Yet, this detector requires very little added complexity. Although it is unlikely this gain would be maintained in the presence of white noise and multipath distortions, it is interesting to see how simply the performance can be improved under strong interference conditions. The extension to a more complex interference and multipath situation is straightforward. It is also worth noting that the performance of this 4-state decoder is remarkably close to that of an MLSE decoder for the channel $1 - \rho z^{-1}$. Simulations have shown negligible loss at $SIR \gtrsim 0$ dB and a loss of a fraction of a dB below.

6.5.5 Joint multipath and interference reduction

Based on the first section of this chapter, it should be clear that the compensation of multipath distortions can be carried out using the same basic techniques as those used to reduce the impairments caused by NTSC co-channel interference. We have chosen, thus far, to focus our attention on the co-channel interference problem because the characteristics of the distortion appear to be more specific and therefore more amenable to original solutions. However, one should keep in mind that compensation of multipath distortions and rejection of co-channel interference are in fact part of a single receiver function: channel equalization. In practice, there may be reasons for performing the two tasks separately. One may be the desire to use interference rejection structures such as the ones described in the previous sections. For instance, it may be advantageous to perform decision-feedback on the interference only by restricting the non-zero taps to the ones expected to be important for canceling co-channel interference. In this case, the feedback structure becomes effective in the presence of strong co-channel interference but under normal conditions, the performance of the equalizer is essentially that of a linear equalizer. Since such an approach is a straightforward extension of the previous investigation, we will not develop it any further.

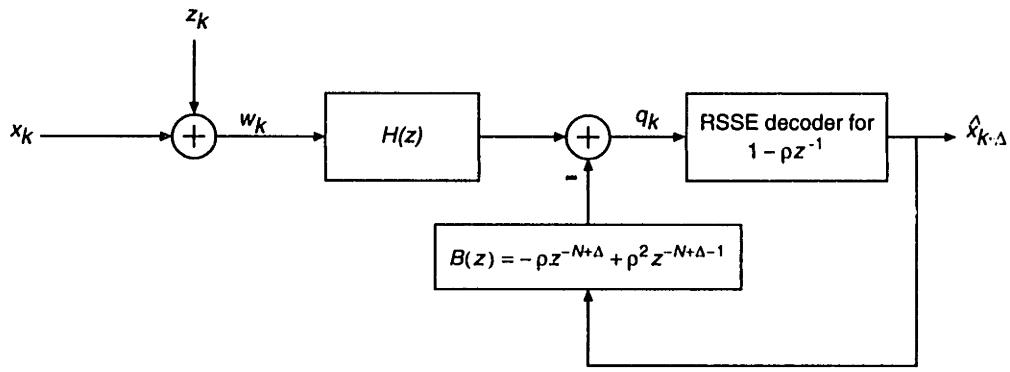

Figure 6-43: Interference rejection based on RSSE for an interference model of the form $1/H(z)$ with $H(z) = 1 - \rho z^{-1} - \rho z^{-N} + \rho^2 z^{-N-1}$.

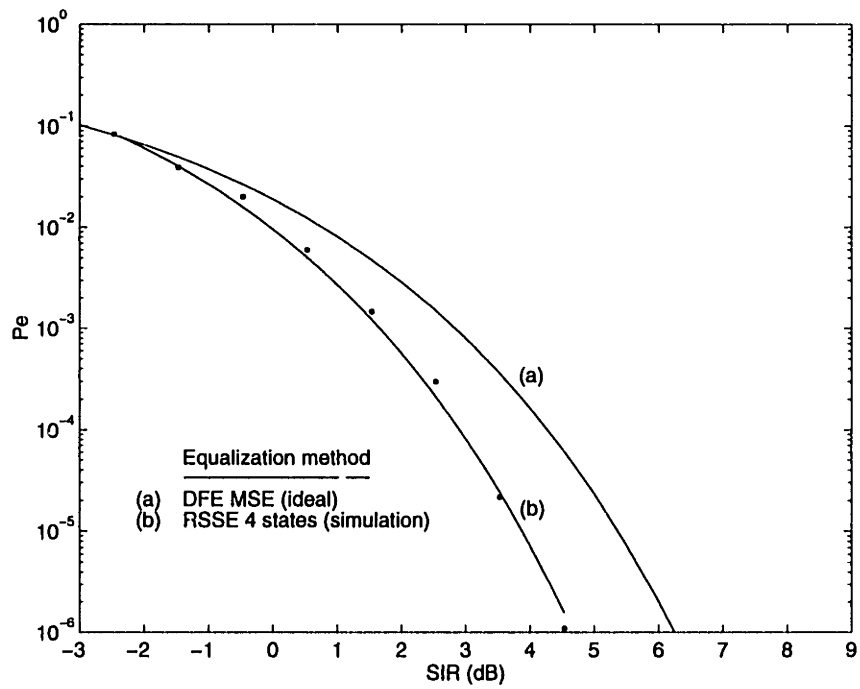

Figure 6-44: Performance of 16QAM with a simple 4-state RSSE decoder (interference model of the form $1/A(z)$ with $A(z) = 1 - \rho z^{-1} - \rho z^{-N} + \rho^2 z^{-N-1}$ with $\rho = 0.9$ and $N = 50$).

6.6 Conclusion

In this chapter, we have:

- Characterized the interference rejection problem as an equalization problem.
- Compared the performance of classical equalization structures in interference rejection schemes.
- Shown that DFE is in general far superior to LE for interference rejection.
- Taken advantage of some of the known characteristics of NTSC interference to achieve effective interference rejection at a very low added complexity cost.
- Proposed a scheme that uses a minimal total distortion criterion rather than a criterion based on an assumed level of interference.
- Compared the scheme with other interference rejection schemes and shown that the proposed scheme is much more effective at reducing interference.
- Investigated the impact of limiting the feedback path to only a few coefficients on error performance. The performance advantage of the DFE approach was shown to be retained, especially when co-channel interference is the dominant impairment.
- Proposed an improved interference rejection scheme based on a reduced-state sequence estimation (RSSE) approach. A gain of close to 2 dB at an error rate of 10^{-6} was demonstrated by simulation.

7

Equalization and interference rejection with coded modulation

7.1 Introduction

Equalization is only one function of the transmission system. The ultimate goal is to transmit data at as high a rate as possible through the channel, using the least possible bandwidth and power. It was shown in Chapter 4 that, at least for the point-to-point ideal bandlimited channel, schemes combining PAM modulation and coding could bring the minimum signal-to-noise ratio required to achieve an error rate of the order of 10^{-6} to within 2 to 6 dB of the capacity-achieving signal-to-noise ratio. One would like to achieve similar results on channels with linear distortions. In the case of digital HDTV broadcasting, the major impairments are co-channel interference, multipath distortions and receiver noise. Depending on the location of the receiver, one or several of these impairments may be dominant. However, as pointed out in Chapter 6, one can equate the digital transmission channel degraded by these impairments to a discrete-time channel with ISI and white Gaussian noise. Thus, techniques for combining equalization and coding for the Gaussian channel, although often developed in other areas of communications, should be applicable in the case of digital transmission of HDTV.

In Chapter 6, we showed that there is substantial benefit in using a decision-feedback filter to reduce co-channel interference, particularly when it is severe. This advantage comes from the fact that the interference is correlated, and therefore is predictable using appropriately designed prediction filters. Linear equalization, on the other hand, was shown to be ineffective in combatting strong NTSC interference. In addition to noise enhancement problems arising from linear processing of the received signal, the finite length of the filter limits the ability to appropriately attenuate the interference at those frequencies where it is the strongest.

Furthermore, because the frequency response of the equivalent white-noise channel has a number of in-band near-nulls, the convergence of adaptive equalizers can become problematic.

Using a decision-feedback equalizer as an effective way of combatting co-channel interference is interesting for HDTV because it has been shown by Price [74] that, by using an ideal decision-feedback equalizer, the SNR gap to capacity at low error rates can be closed to the same extent on channels with ISI as it can on ideal channels with only white Gaussian noise. Furthermore, it appears that this result even holds for relatively low signal-to-noise ratios provided the decision-feedback equalizer is operated at a suitably optimized sampling rate [58, 22]. Therefore, near-optimum utilization of channel resources can be achieved if a good way of combining decision-feedback equalization and coding can be found. There has been a lot of research into trying to solve this problem, some of which is discussed below.

The conventional method for combining equalization and coding, and the one which is the method of choice for the current generation of HDTV systems, is the concatenation of linear equalization and coding. This will be briefly examined in the next section. We will show why this is not in general an effective solution. The direct concatenation of decision-feedback equalization and trellis coded modulation, on the other hand, is in general not possible, because the signal set expansion required to provide redundancy for the coding process also reduces the minimum distance for a symbol-by-symbol decoder, thereby decreasing the reliability of the decisions. This mismatch between the equalizer and decoder essentially negates the gain achievable through bandwidth-efficient trellis coding. It is therefore necessary that more elaborate and practical ways of combining equalization and coding be found.

One suggestion to reduce the error propagation problem in a decision-feedback equalizer has been made by Eyuboğlu: to interleave the signal sequence in such a way that the slicer in the feedback loop of the DFE can be replaced by a maximum likelihood decoder [32]. In the periodic interleaving method proposed by Eyuboğlu, consecutive channel samples are separated after deinterleaving by a number of time increments equal to the decision delay of the decoder (or a delay such that the decoder provides reasonably reliable decisions). Unfortunately, it is not possible to ensure that all symbols be separated by a given minimum delay. At least one symbol per block must have zero delay. Therefore, this sample cannot be detected with the same reliability as the rest of the data. Another problem with this method is that, as a result of the variable delay between samples, the noise-prediction filter is time-varying. Although the implementation of a single-tap filter is straightforward, the implementation of a multi-tap filter is difficult, because processing is dependent on the location of the sample within the block. Furthermore, this scheme requires that the transmitter interleave the signal in such a way that the signal after deinterleaving is in the correct order (increasing time index). Such a technique does not appear to be easily applicable to the co-channel interference problem,

because the prediction filter used in this case calls for several widely-spaced taps, which would require a very large interleaver and a complicated control mechanism to select different filters depending on the index of the sample within each block of samples.

Another approach is to implement equalization at the transmitter. A variety of techniques for implementing transmitter-based equalization in combination with coding have been proposed in the literature. These can be divided into two sets. The first set is based on single carrier modulation and various forms of precoding compatible with coded modulation (e.g. Tomlinson-Harashima precoding, trellis precoding) [13, 44, 33]. The second set relies on multicarrier modulation and coding (block or trellis) to achieve information rates near channel capacity [98, 59, 58, 18, 79].

From the standpoint of HDTV broadcasting, these transmitter-based schemes suffer from a major handicap. Since HDTV broadcasting is a one-way multi-user channel, it is not possible to optimize the signaling rate and power and code rate assignments for all users simultaneously, as would be the case for multicarrier modulation. Nor is it possible to precode the signal for a specific channel impulse response, since the channel characteristics are highly variable across the coverage area. Therefore, while we can make worst-case assumptions as to the expected severity of the co-channel interference signal, for instance, this hardly seems like an optimal solution.

In this chapter, for the reasons stated above, we have chosen to restrict our attention to receiver-based schemes. The main emphasis of the chapter is on finding a good co-channel interference rejection scheme that is compatible with coded modulation. We first formulate the problem given the decoding constraints of the coded-modulation scheme, and then propose a scheme able to partially reduce co-channel interference by taking advantage of the correlation between distant samples of the interfering NTSC signal. Finally, we investigate ways of improving on the performance of the proposed scheme. To this end, we make use of the concept of reduced-state sequence estimation. The thread of this concept runs through the papers by Eyuboğlu *et al.* [34, 35], Chevillat *et al.* [17], Duel-Hallen *et al.* [28] and several others. The novelty here is to show how this concept can be applied to the problem of rejecting co-channel interference.

7.2 Conventional approach

A straightforward approach to equalizing bandwidth-efficient trellis-coded modulation is to apply a linear equalizer between the channel output and the trellis decoder. This arrangement is shown in Figure 7-1. Here, the slicer that was used in uncoded modulation is simply replaced

by a sequence detector. There is no fundamental difference between coded and uncoded modulation in this case, but there are some practical differences. A first difference is that decisions are produced by the detector with a delay Δ. A second difference arises when it becomes necessary to adapt the equalizer. Adaptive algorithms typically use an error signal derived from the difference between the input of the decision device and the estimated symbol. In this case, however, the input and output of the decision device correspond to symbols produced at different instants. It is therefore necessary to delay the input by an amount equal to the delay through the decoder in order to align the input and output sequences. As a result, the error signal is a delayed version of the error signal used in conventional linear equalizers operating with uncoded data. The implication is that, in order to retain convergence, the adaptation must proceed at a substantially reduced rate compared to the uncoded case. An alternative is to retain the slicer used in uncoded modulation and adapt the equalizer using tentative decisions. This has the advantage of speeding the adaptation process, but increases the risk of misconvergences [65]. In general, it is also necessary to insert a deinterleaver between the equalizer/interference-rejection circuit and the Viterbi decoder in order to reduce the correlation of the error sequence.

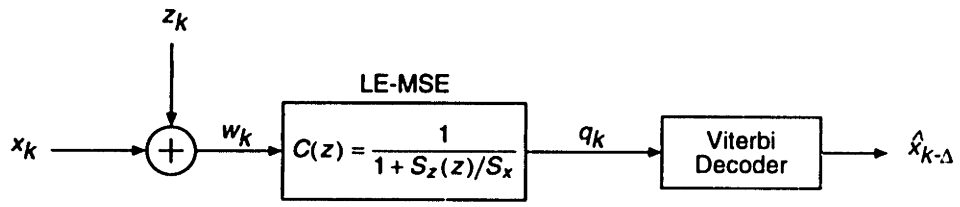

Figure 7-1: Combination of interference rejection and coding based on LE-MSE.

The error performance is approximately given by

$$\Pr(E) = K \cdot Q\left(\frac{d_{\min}}{2\sigma}\right) \tag{7.1}$$

where K is the average number of nearest neighbor signal sequences at the minimum distance, $d_{\min}$ is the minimum Euclidean distance of the code, and σ is the standard deviation of the error sequence at the output of the linear equalizer. Thus, in the case of a LE-MSE, we have

$$\sigma = \frac{1}{2}\left\langle \frac{S_z}{1 + S_z/S_x} \right\rangle_A^{1/2} \tag{7.2}$$

Simulation results of the performance of a linear interference rejection circuit concatenated with a 16-state 16QAM trellis code are shown in Figure 7-2, for two different signal-to-noise ratios. The LE-MSE is used to cancel interference in the presence of white noise. Block interleaving is used in the simulations to reduce error correlation. Although the performance is

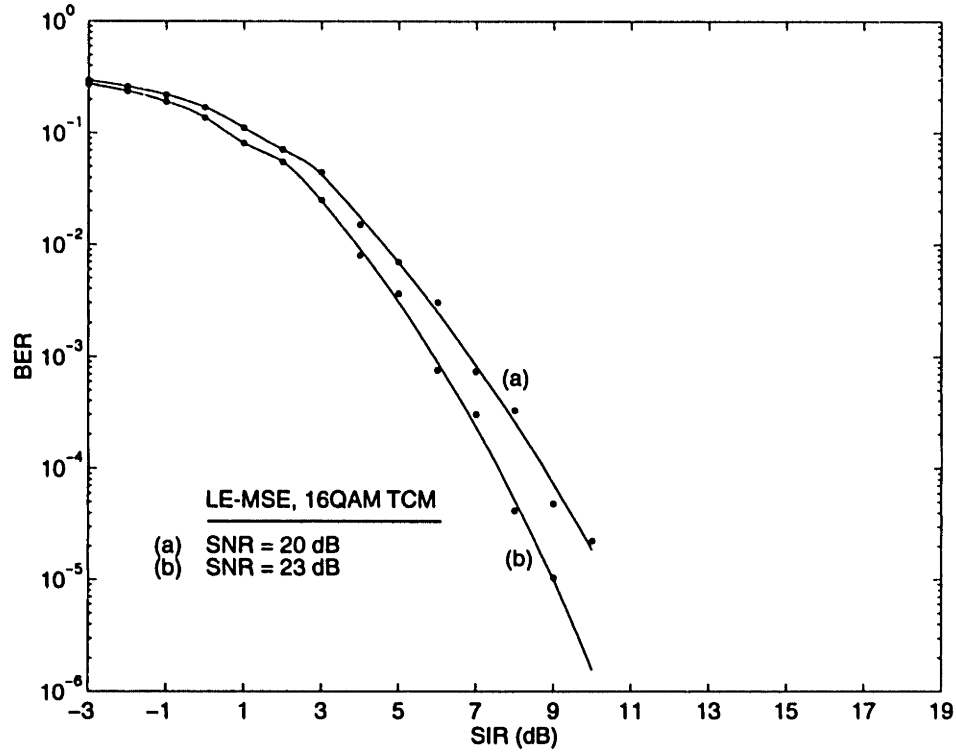

Figure 7-2: Performance of combined linear filtering and trellis coding approach, in the presence of co-channel interference. Trellis coding using a 2-dimensional 16-state 16QAM code. Interference model of the form $1/A(z) = 1 - 0.9z^{-1} - 0.9z^{-N} + 0.81z^{-N-1}$ ($N = 50$).

substantially better than in the uncoded case, the performance is limited by the inability of the equalizer to filter out the interference without causing excessive ISI.

7.3 Decision-feedback equalization with coded modulation

Linear equalization is in general unsatisfactory for channels with in-band nulls or near-nulls, such as the co-channel interference channel. It was shown in the previous chapter that decision-feedback equalization was in general far superior to linear equalization for such channels. The question then arises as to how to combine DFE and coding. DFE and coding cannot be simply concatenated because the signal-to-noise ratio at the input of the decision device is typically too low, as a consequence of the coding gain afforded by the trellis code. A natural idea is then to combine the decision-feedback equalization and the decoding stage into one, by replacing the decision device by a trellis decoder, or any other decoder capable of providing more reliable decisions than the simple slicer. Unfortunately, this is not possible in general, as decision-feedback equalization requires delay-free decisions to be fed back into the feedback filter. This is particularly true for linear channel distortions where the strongest ISI comes from the samples following the current sample.

In the case of co-channel interference, however, a distinctive characteristic is the existence of high correlations between distant samples (samples separated by a multiple of N, the number of samples in an NTSC scan line). A partial solution to the problem of combining DFE and coding in this case is therefore to cancel the co-channel interference on the current signal sample by forming a prediction based on interference samples from previous lines. The principle is illustrated in Figure 7-3 where, for clarity, the so-called noise-predictive form of the DFE has been used.

The error sequence at the input of the decision device for ideal DFE-ZF is white. This property is lost when the predictor is constrained. Thus, although the error sequence remains Gaussian, it is now correlated. Correlations between noise samples degrades the performance of the Viterbi decoder (i.e. the Viterbi decoder is maximum-likelihood under the assumption the noise samples are independent). To overcome this difficulty, we propose using interleaving to reduce the correlation between error samples. The overall block diagram of the new interference rejection scheme with coding and interleaving is shown in Figure 7-4. The arrangement of interleavers and deinterleavers is done is a way that is compatible with the decision-feedback equalizer. We exploit the fact that the number of samples N corresponding to one NTSC scan line is much larger than the decoding delay required by the trellis decoder. Thus, we can insert a short interleaver and deinterleaver at the output and input of the trellis decoder, respectively. Convolutional interleaving is preferable to block interleaving in this case because the total delay (interleaving+deinterleaving) is half of that required for a block interleaver [75]. The total delay for the feedback path must be smaller than N in order to use the N-step ahead predictor.

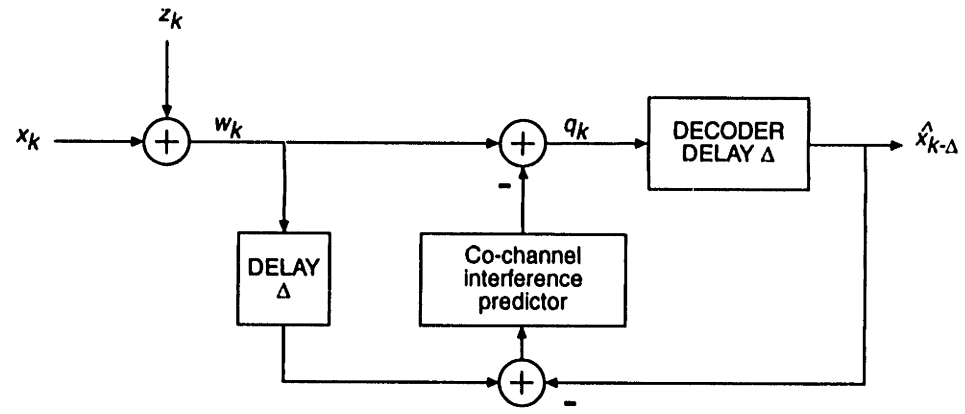

Figure 7-3: Combination of interference rejection and coding based on noise-predictive form of DFE, with decoding delay Δ.

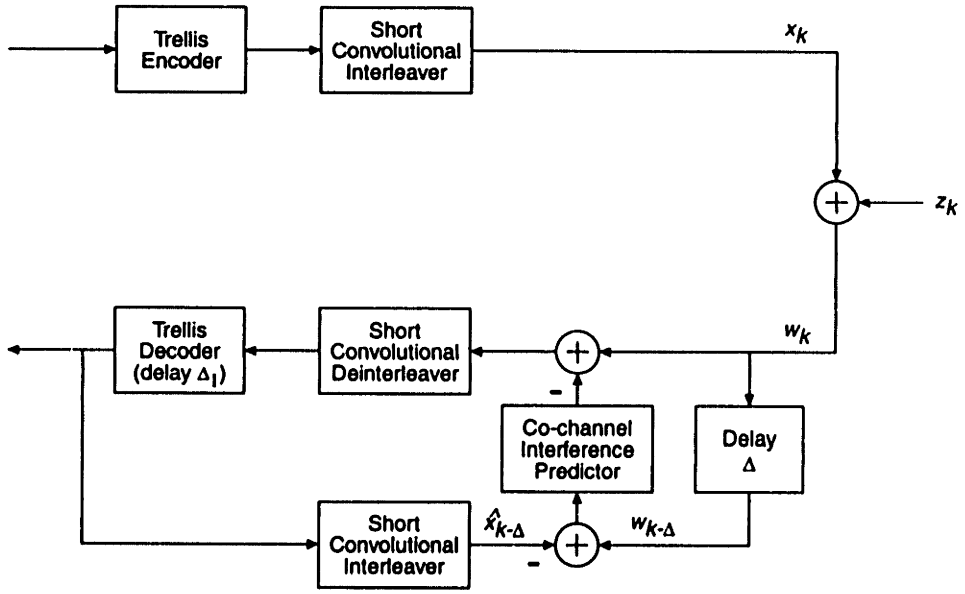

Figure 7-4: Combination of interference rejection and coding based on noise-predictive form of DFE with convolutional interleaving.

7.3.1 Decision-feedback equalization with a decoding delay

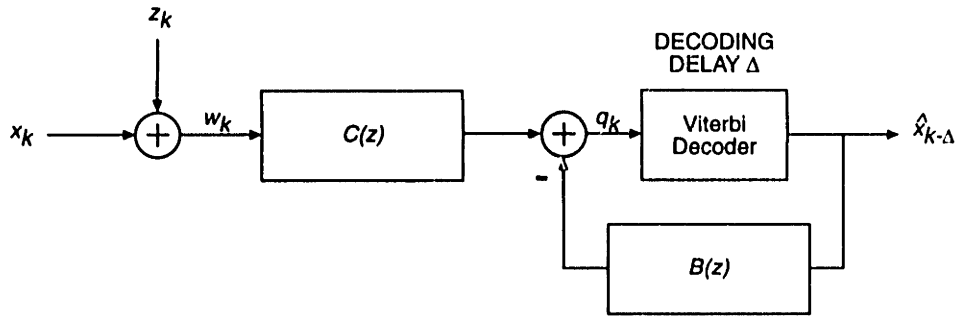

Figure 7-5: Combination of interference rejection and coding based on DFE with decoding delay Δ.

Minimum-MSE solution Here, we assume that decoder decisions are only available after a delay Δ.

The forward and feedback filters that minimize the MSE under this constraint can be determined using a procedure similar to the one used for the determination of the finite-length DFE.

Let us define a vector $\mathbf{d}$ of $2L + 1$ forward coefficients and N feedback coefficients

$$\mathbf{d}^t = [c_{-L}, \cdots, c_0, \cdots, c_L, -b_\Delta, -b_{\Delta+1}, -b_{\Delta+N-1}] \tag{7.3}$$

and a vector $\mathbf{y_k}$ of input samples to the forward equalizer and past decisions from the decision device. Assuming no decision errors,

$$\mathbf{y}_k^t = [w_{k+L}, \cdots, w_k, \cdots, w_{k-L}, x_{k-\Delta}, x_{k-\Delta-1}, \ldots, x_{k-\Delta-N+1}] \tag{7.4}$$

The error for the DFE-MSE is then given by

$$e_k = x_k - q_k = x_k - \mathbf{d}^t\mathbf{y_k} \tag{7.5}$$

which is minimized in a mean-square sense by the choice

$$\tilde{\mathbf{d}} = \mathbf{R}_{yy}^{-1}\mathbf{R}_{yx} \tag{7.6}$$

where $\mathbf{R}_{yy} = E[\mathbf{y}_k^*\mathbf{y}_k^t]$ and $\mathbf{R}_{yx} = E[\mathbf{y}_k^* x_k]$. The minimum MSE for this constrained filter is then given by

$$\epsilon^2 = E[|x_k|^2] - \mathbf{R}_{yx}'\tilde{\mathbf{d}} \tag{7.7}$$

Figure 7-6 shows the performance of decision-feedback equalization with $\Delta = 25$ and $N = 50$. A comparison with Figure 6-39 shows that there is a performance degradation of about

7 dB at $P_e = 10^{-6}$ when compared to the DFE with no constraint on the feedback loop delay, when the only source of impairment is co-channel interference. However, the performance is still much better than linear equalization. Furthermore, the difference between the delay-constrained and delay-unconstrained DFE is greatly reduced when the SNR decreases. At an SNR of 20 dB, the difference is very small.

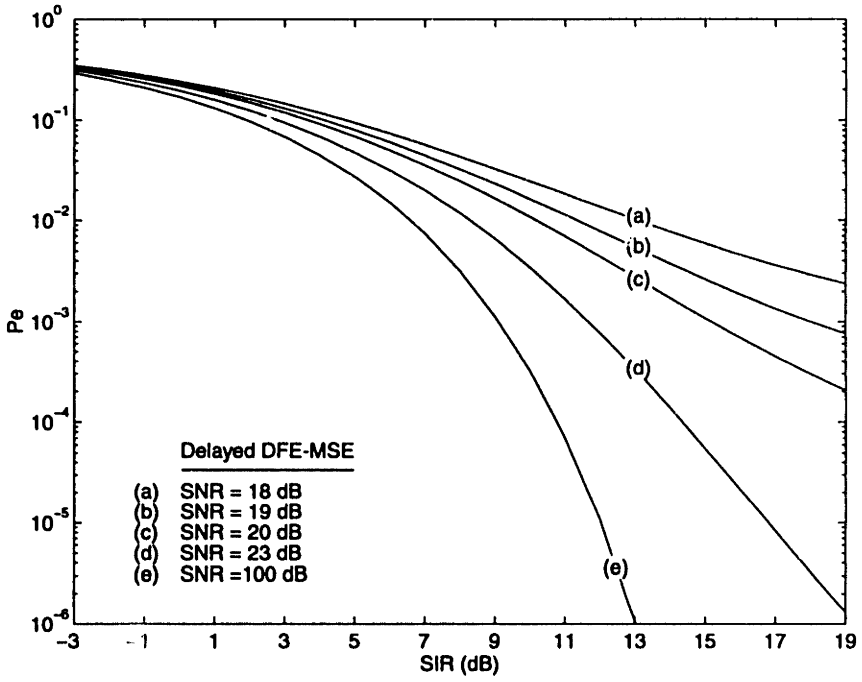

Figure 7-6: Performance of decision-feedback equalization with decoding delay $\Delta = 25$ at several SNRs for an interference model of the form $1/A(z) = 1 - 0.9z^{-1} - 0.9z^{-N} + 0.81z^{-N-1}$ ($N = 50$) and 16QAM.

7.4 Interference rejection scheme with improved performance

The scheme proposed in the previous section for combining interference rejection and trellis coded modulation uses interleaving to reduce the correlation of the error sequence at the input of the trellis decoder. We now consider an extension of this scheme, where the deinterleaver and trellis decoder are replaced by a filter to whiten the error sequence and a sequence estimator to estimate the sequence out of the whitening filter. We retain the noise-prediction filter (or feedback filter in the classical DFE) to form a prediction at time index k based on samples around time $k - N$. The prediction filter (or the feedback filter in the DFE) effectively enables us to reduce the complexity of the sequence estimator, as will later become apparent. The optimum decoding strategy for estimating the sequence out of the whitening filter $H(z)$ is maximum-likelihood sequence estimation (MLSE). The decoding complexity of an ML sequence detector is substantial, since the detector must determine the best sequence by searching a super-trellis constructed by combining the encoder states of the trellis code and the channel states created by filtering the co-channel interference. For a two-dimensional trellis code with S encoder states and a constellation expansion ratio of 2, and a channel memory of L symbols, the number of states in the super-trellis is $S' = S \times (W/2)^L$, where W is the size of the alphabet (size of the constellation). Therefore, in order to reduce the decoding complexity of MLSE, simplified, suboptimal procedures for estimating the best sequence in the ML super-trellis are needed.

In the next subsection, we outline briefly the concept of reduced-state sequence estimation. This technique was originally proposed for uncoded linear modulation systems but was recently extended to trellis coding [35, 17, 28][1].

We then show how an interference rejection structure with improved performance can be derived from the interference rejection structure proposed in the previous section, by applying a reduced-state sequence estimation algorithm on a filtered signal sequence. Simulation results are presented to demonstrate the performance of the new structure.

7.4.1 Reduced-state sequence estimation

Let us consider the problem of estimating a code sequence that has been processed through a canonical filter (channel) described by the vector of coefficients $\mathbf{g}' = [1, g_1, g_2, \ldots, g_L]$ and degraded by white Gaussian noise. Let the input to the filter be denoted by x_k and the output

[1] A comprehensive description of reduced-state sequence estimation can be found in [35], where it is shown how the concept of RSSE can be applied to the estimation of a coded sequence degraded by ISI.

by y_k. The channel output is therefore given by

$$r_k = y_k + w_k = x_k + \mathbf{g} \cdot \mathbf{x_k} + w_k \tag{7.8}$$

where "·" represents the scalar product of two vectors, $\mathbf{x_k} = [x_{k-1}, \ldots, x_{k-L}]$ represents the state vector of the filter (channel), $\mathbf{g} = [g_1, g_2, \ldots, g_L]$ represents the ISI coefficients introduced by the channel filter, and w_k is a complex white noise sequence with zero mean and variance $2\sigma^2$.

The optimum sequence decoder operating on the combined ISI and code trellis (MLSE) chooses the sequence of symbols x_k that minimizes the distance to the received sequence r_k and that corresponds to a path through the super-trellis. In this procedure, the super-trellis describes the state transitions of the combined code/channel state from time k to time $k+1$. Each state u_k at time k in the super-trellis is formed by concatenating the encoder state s_k and the channel state $\mathbf{x_k}$, i.e. $u_k = [s_k, \mathbf{x_k}]$. At each time step, the decoder computes the branch metrics $m(r_k; u_k; x_k) = |r_k - y_k|^2$, adds the branch metrics to the current path metrics in a manner consistent with the super-trellis state transitions, compares paths converging into a common state and retains only the path with the smallest path metric.

Even for moderate channel memories L, the decoding complexity, from a storage standpoint and from a computation standpoint, is in general far too large. The fact that the number of states in the super-trellis grows exponentially with the alphabet size means that even for relatively small constellations, the decoding complexity will be enormous. It is clear however that it should not be necessary to consider all transitions in the super-trellis to estimate the error performance, since some transitions are very unlikely and correspond to choosing points that are at large Euclidean distances from the received point.

In order to reduce the complexity of MLSE while still retaining most of its performance, Eyuboglu *et al.* introduced a set partitioning concept similar to that used in the construction of the trellis codes invented by Ungerboeck [34, 35]. In MLSE, the channel state is defined by $\mathbf{x_k} = [x_{k-1}, \ldots, x_{k-L}]$. We saw that x_{k-j} multiplied by the filter coefficient g_j defines the j-th ISI term. Suppose that instead of considering x_{k-j} in the channel state $\mathbf{x_k}$, we partition the constellation for the signal point corresponding to the j-th ISI term into J_j subsets, and consider the label $a(x_{k-j})$ of the subset to which x_{k-j} belongs. Let us also designate the partition for x_{k-j} by $\Omega(j)$ and the order of the partition by $J_j = 2^{l_j}$. We can now form a special type of state, which Eyuboglu calls a "super-state", which consists of the concatenation of the code state (as previously) and a "coset state" $\mathbf{t_k} = [a(x_{k-1}), \cdots, a(x_{k-L})]$, where $a(x_{k-j})$ is the coset label in the partition $\Omega(j)$ for the symbol x_{k-j}. Thus,

$$v_k = [s_k, \mathbf{t_k}] = [s_k, a(x_{k-1}), \cdots, a(x_{k-L})] \tag{7.9}$$

With this definition of a super-state, it can be seen that the complexity of the resulting super trellis can be made to range from that of the MLSE super-trellis (when $J_j = W$ for all j) to that of the code trellis (when $J_j = 1$ for $j > 1$).

By imposing a nested structure on the partitions $\Omega(j), \quad j = 1, \ldots, L$, it is possible to ensure that the current super-state ν_k and the input x_k uniquely define the next super-state ν_{k+1}. However, since the super-state ν_k does not completely specify the channel state $\mathbf{g_k}$, it is not possible to uniquely label the trellis branches with an output symbol. The branch metric computation is therefore computed differently than in MLSE. Here,

$$m(r_k; \hat{\mathbf{x}}_\mathbf{k}(\nu_k); x_k) = |r_k - \hat{\mathbf{x}}_\mathbf{k} \cdot \mathbf{g} - x_k|^2 \tag{7.10}$$

where $\hat{\mathbf{x}}_\mathbf{k} = [\hat{x}_{k-1}, \ldots, \hat{x}_{k-L}]$ is an estimate of the channel state formed by taking the signal point estimates stored in the path history for the super-state ν_k.

A special case of RSSE is PDFD or parallel decision-feedback decoding, where the number of states is the number of encoder states. In contrast to DFE where the same feedback decision is used for all contending paths, in PDFD each path uses decision-feedback based on its own history. In this fashion, the decoder avoids using a single unreliable decision for feedback. It is still suboptimum compared to MLSE because it uses a reduced trellis where paths merge earlier than in the ML super-trellis. Therefore the VA does not exploit the differences between sequences and its decisions may be somewhat premature. Also, as a result of the decision-feedback mechanism, error propagation may occur. However, the performance of PDFD is vastly superior to that of linear equalization with coding.

RSSE also makes it possible to trade off complexity for performance by increasing the order of the partitions corresponding to the different ISI terms. The performance improvement depends on the specific channel impulse response and trellis code used. In general, performance increases rapidly with the partition order, until the performance of MLSE is approached. Past this point, further increases in the partition order only serve to increase the decoder complexity.

7.4.2 New interference rejection scheme with improved performance

Figure 7-7 shows the structure of a new interference scheme with improved performance. This scheme combines the advantages of the decision-feedback/noise-predictive structure described in the previous section with the power of RSSE. The basic principle is the following: for illustration purposes, the received signal is assumed to consist of the transmitted signal + NTSC interference (i.e. the channel is otherwise ideal). The received signal is delayed by an amount Δ equal to the delay through the sequence estimator and combined with the output

from the sequence estimator in order to form a delayed sequence of noise estimates. These noise estimates are then weighted with a prediction filter to produce a prediction of the current distortion based on these past samples. The prediction is then subtracted from the received sequence, thereby canceling that part of the interference that was predictable based on interference samples at times prior to time $k - \Delta$. The remaining portion of the interference is whitened by a whitening filter $H(z)$ which, in the process, introduces intersymbol interference. A reduced-state sequence estimator is then used to estimate the resulting coded sequence.

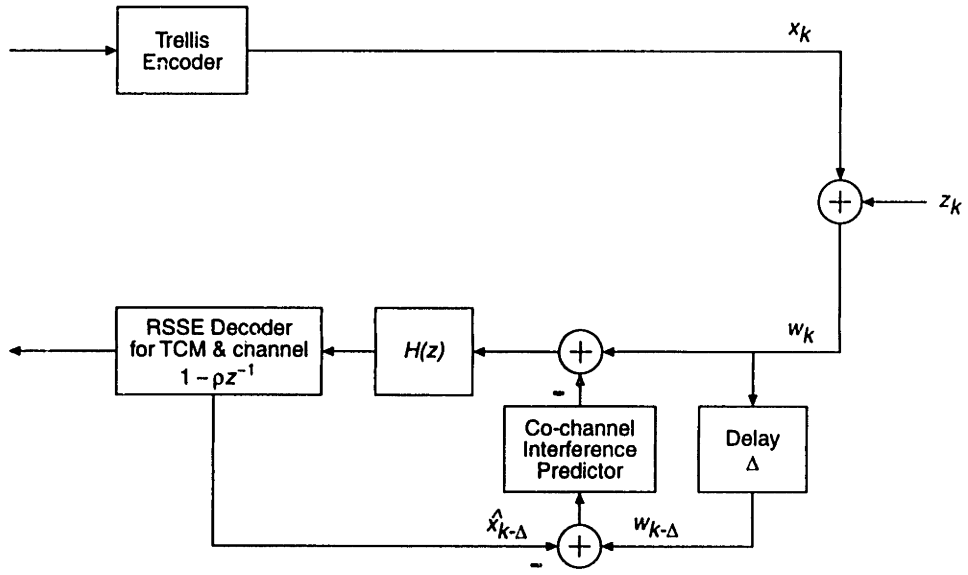

Figure 7-7: Combination of interference rejection and trellis coded modulation using DFE and RSSE.

Simulation results for this new structure are shown in Figures 7-8 and 7-9 for two different trellis codes. In Figure 7-8, the trellis code is a 16-state 16QAM Ungerboeck trellis code. The reduced-state trellis decoder operates over a super-trellis constructed from the concatenation of the trellis encoder states and the channel $1 - \rho z^{-1}$, with $\rho = .9$. We show the performance (obtained by Monte Carlo averaging) of three different estimation techniques with different degrees of complexity. The least complex is the PDFD structure. For PDFD, the number of states is equal to the number of states in the trellis. However, decoding complexity is greater than that of the trellis code alone because of the more complex branch metric computations. Compared to DFE, the performance is improved, which may be attributed to the fact that PDFD implements decision-feedback on an individual path basis. Therefore, the decisions, although premature, tend to be more reliable than in the case of DFE where a single unreliable decision is used for all paths. The second performance curve shows the performance of a RSSE using a partition order of 4 and a memory order of 1. The state complexity of the decoder is 32.

Compared to the PDFD scheme, the performance is improved by more than 2 dB at $P_e = 10^{-6}$. This appears to be a very worthwhile tradeoff of complexity versus performance. A further 1 dB of improvement can be obtained by decoding the true MLSE trellis at a substantial complexity increase. For this simple trellis, full MLSE is still possible and does provide a large performance gain. However, the complexity is substantially larger than PDFD.

Figure 7-9 shows the performance of a 32QAM trellis code, again with 16 states. The performance of PDFD is far superior to that of the interference rejection system based on LE-MSE. The second curve corresponds to a sequence estimator with a partition order of 8. Simulation results show that the performance of this RSSE decoder is equal to that of the MLSE for 1/4 of the complexity. It is difficult to say how the complexity-performance trade-off should be made. However, an interesting possibility with the scheme is the ability to improve the performance of individual receivers. No cooperation with the transmitter is necessary, in contrast to many of the schemes proposed to date.

7.5 Conclusion

In this chapter, we have investigated the problem of combining coding and equalization from the point of view of reducing NTSC co-channel interference in HDTV broadcasting. The peculiar nature of the interference signal offers the possibility of developing efficient rejection structures compatible with coded modulation. The first structure that was proposed used decision-feedback equalization with trellis decoding implemented in the feedback path of the equalizer. The inclusion of the decoder in the feedback path allows for more reliable decisions to be made, and therefore allows operation of the combined decoder/interference-rejection system at substantially lower signal-to-interference ratios than would be possible with the more conventional linear equalizer. A second structure, which is an extension of the first one, replaces the trellis decoder and convolutional interleaver with a reduced-state sequence detector. The performance of this RSSE-based interference rejection scheme was simulated to show the trade-offs between performance and complexity. Even with a relatively simple PDFD structure, the performance was significantly superior to LE-MSE based interference rejection schemes. The structures presented here were derived assuming a simple interference model and should only be used as illustrative examples. It is thought, however, that the general structure of the proposed schemes could be retained in a real-world implementation.

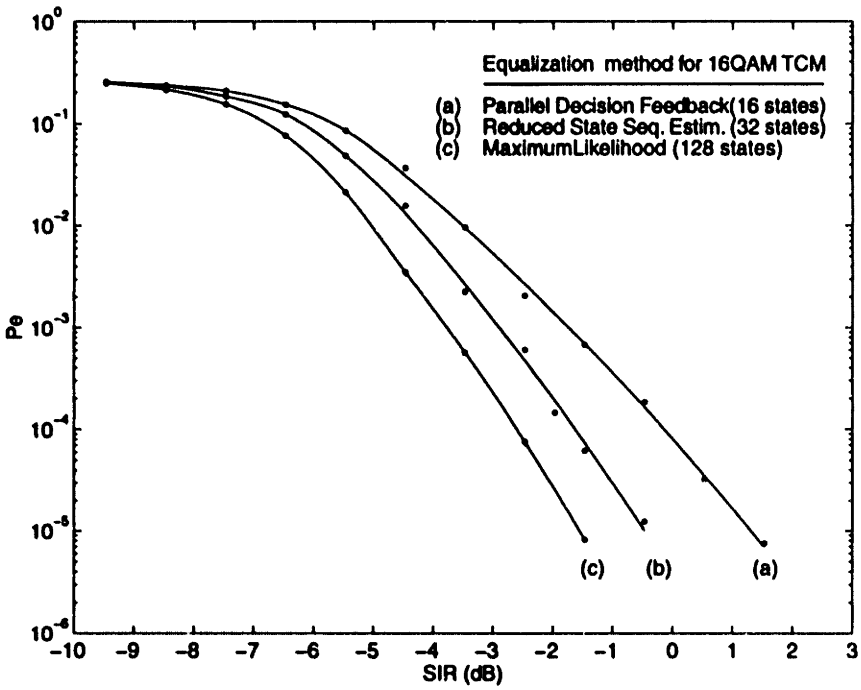

Figure 7-8: Interference reduction for 16-state 16QAM Ungerboeck trellis code using parallel decision-feedback decoding, reduced-state sequence estimation, and maximum-likelihood decoding on $1-\rho z^{-1}$ channel with tail cancellation of higher order terms. Interference model of the form $1/A(z) = 1-0.9z^{-1}-0.9z^{-N}+0.81z^{-N-1}$ ($N = 50$).

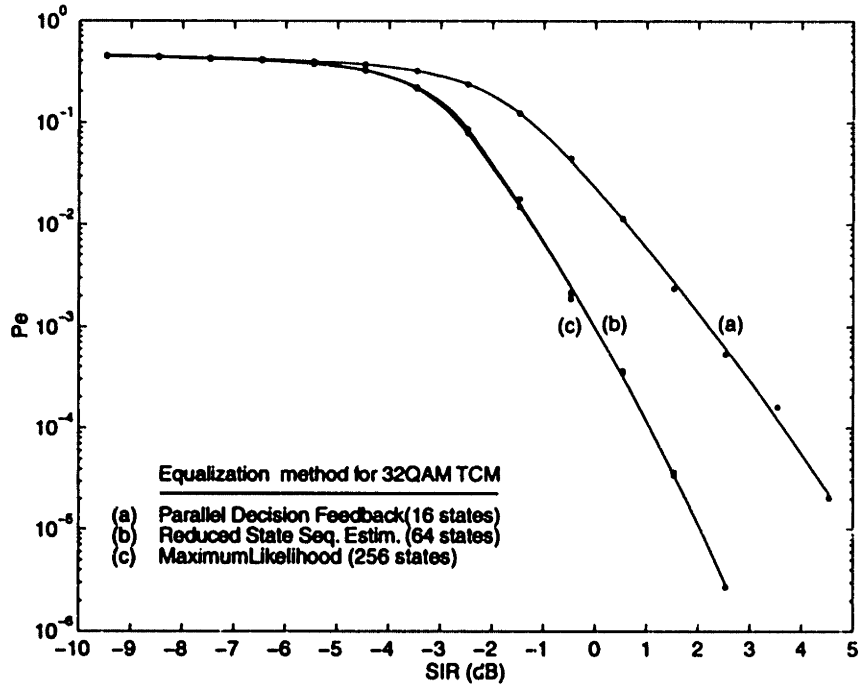

Figure 7-9: Interference reduction for 16-state 32QAM Ungerboeck trellis code using parallel decision-feedback decoding, reduced-state sequence estimation, and maximum-likelihood decoding on $1-\rho z^{-1}$ channel with tail cancellation of higher order terms. Interference model of the form $1/A(z) = 1-0.9z^{-1}-0.9z^{-N}+0.81z^{-N-1}$ ($N = 50$).

8

Equalization and multicarrier modulation

8.1 Introduction

In Chapter 6, we examined a number of methods for mitigating linear channel distortion, including linear and decision-feedback equalization. In Chapter 7, we mentioned the interesting result due to Price that the SNR gap between uncoded modulation and the Shannon capacity limit could be closed to the same extent on channels with ISI as it could on ideal Gaussian noise channels, if ideal decision-feedback equalization is employed to cancel postcursor intersymbol interference [74]. This suggests that the decision-feedback equalizer is in some sense a canonical receiver structure for channels with linear distortion.

A different approach to compensating linear channel distortion can be derived by dividing the transmission bandwidth into a large number of independent smaller channels (subchannels), and optimizing the transmission power and data rate of each subchannel such that the overall data rate is maximized for a given transmission power. This approach is often called multicarrier modulation (MCM)[1] and has been successfully used on severely distorted channels for which there is a reverse path to the transmitter.

In this chapter, we do not consider the problem of using MCM to optimize data transmission on such two-way channels, since these are not representative of HDTV broadcast channels. Rather, we seek to investigate a different aspect of MCM that applies to broadcasting applications: that of receiver-based channel equalization for multipath channels. A persistent claim

[1] A variety of terms are used to describe the technique of transmitting data over a set of parallel channels: Orthogonally Multiplexed QAM [52, 53], Orthogonal Frequency Division Multiplexing (OFDM) [21, 2], Multitone Quadrature Amplitude Modulation [57], Discrete Multitone Modulation (DMT) [18], etc. Here, we use the generic term Multicarrier Modulation (MCM) [8].

in the HDTV community has been that systems based on multicarrier modulation, particularly those that combine coding and multicarrier modulation, are better able to cope with strong multipath echoes and co-channel interference than the more traditional systems that use a single carrier to transmit information (which we refer to as single carrier modulation (SCM) systems). In order to investigate this claim, we formulate the equalization problem for MCM and provide an analysis of the performance of MCM over the ISI channel (static multipath) and over a multipath fading channel. We show through analysis and simulation that the performance depends critically on whether the multipath is static or time-varying. For the static multipath channel, which is thought to represent most cases of UHF HDTV transmission, the performance is found to be comparable to that of linearly equalized single carrier systems and is therefore inferior to that of the improved single-carrier equalization schemes.

8.2 Overview of MCM

8.2.1 MCM for the Gaussian channel

The concept of multichannel modulation for optimal transmission over ISI channels can be traced to Shannon's original work on channel capacity. Referring back to Eq. (4.5) in Section 4.2.2, we see that the channel capacity of a Gaussian channel is in fact defined in terms of a multichannel decomposition into parallel independent subchannels, each with a power assignment specified by Eq. (4.3) (the so-called water-pouring theorem of information theory). This fact has been the theoretical basis for developing a variety of multichannel modulation schemes potentially capable of approaching the channel capacity limit.

As was shown in Chapter 4, in order to approach capacity on Gaussian channels, coding must be used. Several of the recent discrete multitone schemes combine coded modulation and block DFT based MCM in novel ways. In [79], Ruiz *et al.* combine high gain coset codes and MCM to achieve high spectral efficiency. The design of the energy distribution and coded information allocation over the subchannels is optimized for the finite block size of the DFT and for the size of the coset code, leading to an implementable coding system with good performance. It is argued that this coding technique is more powerful than the trellis codes with spectral nulls proposed by Calderbank [12]. An important conclusion of this work was that, for channels with severe ISI, only a fraction of the subchannels should be used, and that an equal power allocation over that fraction is optimum.

Recently, several methods have been proposed that create independent subchannels in the "code" domain rather than in the frequency domain. The technique known as Vector Coding [58] is a method to combine channel coding with channel equalization in an optimal

way, creating orthogonal vector channels at the receiver. The subchannels do not necessarily occupy disjoint frequency bands, but because they are code-orthogonal, they form the desired parallel independent subchannels inherent in the multichannel approach. One interesting conclusion is that the optimal vectors, under certain constraints, are the eigenvectors of the channel autocorrelation matrix.

Another MCM technique that uses frequency overlapping but code-orthogonal subchannels is the "Structured Channel-Signaling" approach described in [61]. This method is used in the presence of noise with known correlation and requires multiple co-located transmitters and receivers that use coordinated transmission, generating interference-free independent subchannels.

A number of practical systems based on the concept of MCM have been developed. Perhaps one of the first practical applications of the concept was in the Kineplex and Kathryn systems in the early 1960's [21]. Since then, multicarrier modulation has been proposed as a possible scheme for the transmission of data over a variety of channels, including voiceband data channels (Telebit modems) [8] and high-speed digital subscriber lines (HDSL and ADSL) [18, 19]. In these applications, a reverse channel between receiver and transmitter is required to achieve high channel efficiency.

Since MCM is capable of achieving the same performance as SCM, a natural question arises as to which scheme is best, from a cost or complexity standpoint. A clear-cut answer to this question is difficult to give. On a general level, the advantages of multicarrier modulation for point-to-point communication include: the possibility of assigning different powers and spectral efficiencies to different carriers so as to avoid the noise or interference enhancement that occurs with linear equalization of single carrier modulation schemes (carrier loading); and, a greater robustness to impulsive noise and short flat non-frequency-selective fading. A significant disadvantage of multicarrier modulation for point-to-point communication is the increased delay compared to single carrier schemes and susceptibility to rapidly-varying frequency-dependent disturbances. Few modem manufacturers have adopted multicarrier modulation schemes (with the notable exception of Telebit), apparently because the increased delay was considered a serious disadvantage while the advantages were not considered overriding: Tomlinson-Harashima precoding, for instance, can achieve much the same results for single carrier systems as adaptive carrier loading for MCM. It appears that the choice between MCM and SCM is often dictated more by practical considerations of secondary importance rather than by a definitive superiority of one scheme over the other.

8.2.2 MCM for the broadcast channel

MCM-like schemes have also been used in the broadcasting of digital audio (DAB) to mobile receivers, for different reasons [2, 60]. The design of a VHF/UHF broadcast system for mobile receivers is particularly challenging. The transmission channels for these applications are relatively broadband (1.5 MHz and above) and are subject to multipath degradations, interference and frequency-selective fading. Multipath causes the received signal strength to vary rapidly when the receiver is moving. Moreover there is typically no direct line-of-sight path between the transmitter and the receiver, inducing a phenomenon known as Rayleigh fading.

On these channels, since no reverse channel is available to optimize the transmission parameters, the advantage of MCM over linearly equalized PAM partially disappears. However, because of the time variations of the channel (temporal fading) and of the frequency selectivity of the channel, it is not possible for single carrier systems to achieve the same performance as on Gaussian channels. Rather, various time, frequency and even spatial diversity techniques must be used in order to transmit data over these channels. Spread spectrum techniques, for instance, are well suited for communication over these channels. MCM-based techniques are also well suited for these applications because they effectively divide the frequency-selective channel into subchannels which are frequency-nonselective and yet are still varying sufficiently slowly with respect to the signaling rate that the channel characteristics can be correctly estimated. Techniques developed for narrowband frequency-nonselective channels (low data rate transmission to mobile receivers) can then be used over each of the subchannels. These techniques include specially designed bandwidth-efficient trellis codes for fading channels, as studied by Biglieri *et al.* [7], Divsalar [27] and others. In addition, the multicarrier structure allows for more control over the time-frequency tradeoffs than would be possible with a narrowband fading channel. It is possible to provide redundancy and diversity, both in time and frequency, through a careful choice of the coding and interleaving procedures.

Another potential area of application of multicarrier modulation, and one that is discussed here, is for the terrestrial broadcast of high-rate television, including HDTV. DAB channels and digital HDTV broadcasting channels share a number of characteristics: for instance, multipath propagation and co-channel interference are issues common to digital DAB and HDTV broadcasting. However, there are substantial differences. Although the HDTV broadcast channel is time-varying and frequency-selective (see for example [54, 10]), the severity of the fading is much less than for the DAB channel. In addition, the required spectral efficiency for digital HDTV must typically be much higher than DAB.

This chapter investigates the claim that multicarrier modulation is both better able to cope with strong multipath echoes than single carrier systems and is able to take *advantage* of

echoes originating from on-channel repeaters [51]. This issue is important because some have proposed to design a broadcasting system based on single-frequency networks, thus taking advantage of the claimed multipath immunity to gain a large increase in the spectrum efficiency of terrestrial broadcasting. We provide an analysis of the performance of multicarrier modulation for the two different cases of multipath propagation. We support the analysis by Monte Carlo simulations. We show that for stationary receivers, the claim is not valid, and therefore, that there is no clear advantage to using multicarrier modulation for the purpose of broadcasting to fixed receivers. On the other hand, we confirm that MCM is an interesting technique for frequency-selective fading channels.

By comparison the problem of designing a broadcast system for digital HDTV is more simple (stationary receivers) but the required spectral efficiency for digital HDTV must typically be much higher. The current HDTV prototype systems achieve spectral efficiencies of approximately 4 bits/s/Hz whereas the proposals for digital broadcast over fading multipath channels have spectral efficiencies below 1 bit/s/Hz. Multipath propagation and co-channel interference are issues common to digital audio broadcast (DAB) and HDTV broadcast.

8.3 General principles of MCM

Let us assume that we have at our disposal a data stream of rate R bits/sec. In single-carrier PAM modulation, these data are used to select points from a signal set (QAM, MPSK, etc.) which determines the phase and amplitude of the carrier over a symbol interval.

With multicarrier modulation, the basic idea is to split the data into many parallel, low-bit-rate data streams. These are subsequently mapped onto their own signal sets and modulated onto carriers spaced $1/T_s$ apart, where T_s is the symbol time on each of the subchannels. Figure 8-1 illustrates the basic idea. Each channel k is characterized in terms of an elementary prototype waveform :

$$g_k(t) = \begin{cases} e^{j2\pi f_k t} & 0 \le t < T_s \\ 0 & \text{otherwise} \end{cases} \tag{8.1}$$

where $\{f_k\}$ is the set of N carrier frequencies under consideration, i.e:

$$f_k = f_0 + k/T_s, \quad k = 0 \text{ to } N-1 \tag{8.2}$$

The basic pulse shape used here is a rectangular window modulated at frequency f_k, but this is only one of a family of possible windows.

The MCM signal (more precisely its complex envelope) can equivalently be written as a linear

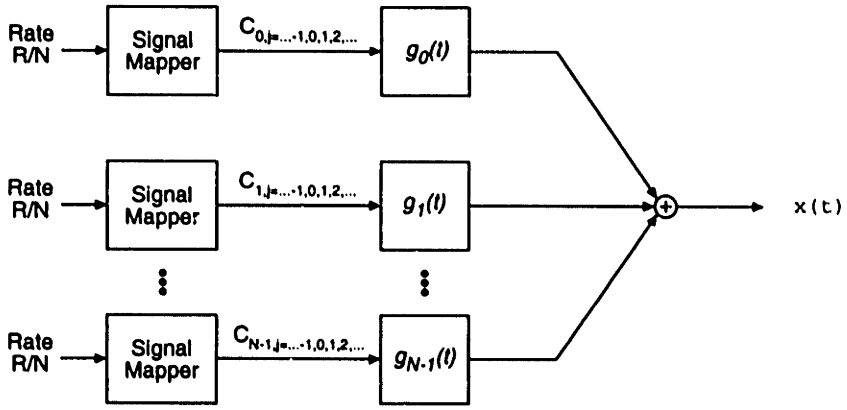

Figure 8-1: MCM signal synthesis using a bank of bandpass filters.

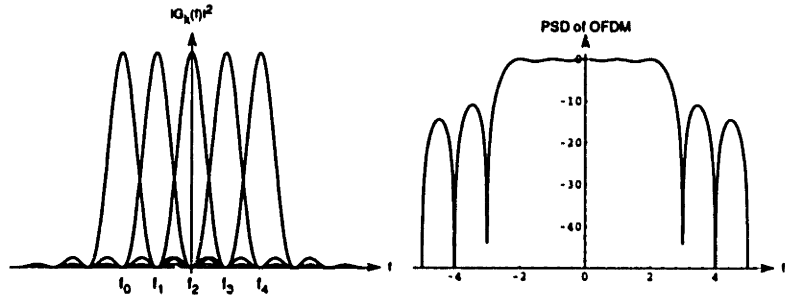

Figure 8-2: Spectrum of the pulses $g_k(t)$ and example of power spectral density of MCM signal.

combination of the elementary functions $\psi_{j,k}(t) = g_k(t - jT_s)$ in the form:

$$x(t) = \sum_{j=-\infty}^{+\infty} \sum_{k=0}^{N-1} C_{j,k}\psi_{j,k}(t) \tag{8.3}$$

where $C_{j,k}$ are a set of signal points representing the source data (see Figure 8-1). We will assume for the moment that the input bit rate for each of the signal mappers is the same, and that the signal constellations are identical, although this does not have to be the case. It is easy to see that the set of functions $\psi_{j,k}(t)$ satisfy orthogonality conditions:

$$\int_{-\infty}^{+\infty} \psi_{j,k}\psi^*_{j',k'}(t)dt = \begin{cases} T_s & \text{if } j = j' \text{ and } k = k' \\ 0 & \text{otherwise} \end{cases} \tag{8.4}$$

In contrast to conventional FDM, it is also clear that the channels overlap in the frequency domain, as is illustrated in Figure 8-2. At the receiver, the multicarrier signal is demodulated using a bank of N correlators performing the following decoding:

$$C_{j,k} = \frac{1}{T_s}\int_{-\infty}^{+\infty} x(t)g^*_k(t - jT_s)dt \tag{8.5}$$

Figure 8-3 shows such a receiver.

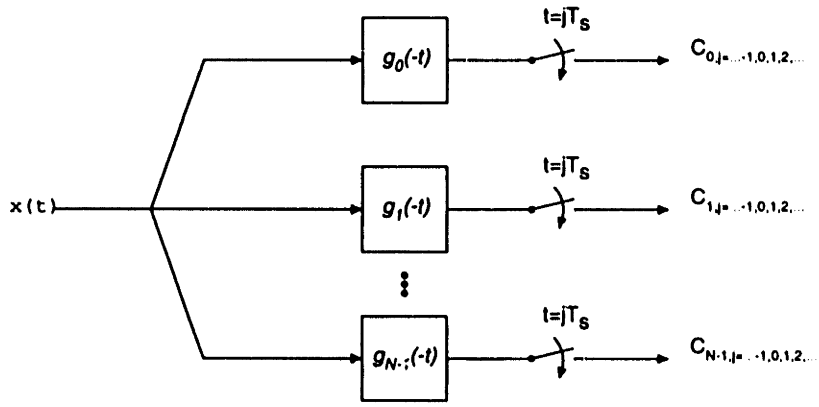

Figure 8-3: Demodulation of an MCM signal using a bank of correlators.

Of course this is not how the actual transmitter/receiver pair would be implemented. It is easy to see that, in the absence of channel noise and other channel distortions, an equivalent structure can be derived. This is achieved by first translating to baseband and sampling $x(t)$ at rate $1/T$, where $T = T_s/N$, and then taking the DFT of the sampled signal [92]:

$$C_{k,j} = \mathrm{DFT}_j \left\{ \frac{1}{N} x(t) e^{-j2\pi f_0 t} |_{t=(jN+n)T} \right\} \tag{8.6}$$

This result holds for the general case: it can be shown that the signal samples form a set of sufficient statistics. A more practical implementation of an MCM transmission system using FFT blocks is shown in Figure 8-4.

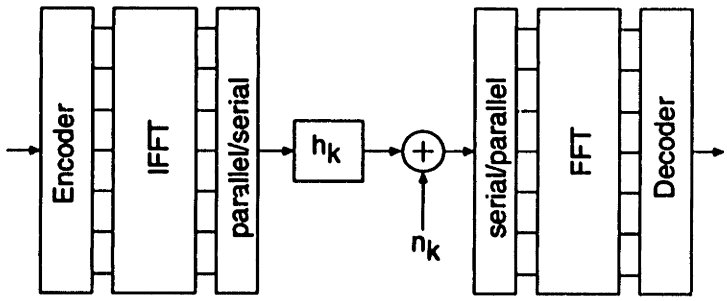

Figure 8-4: Discrete-time multicarrier transmission.

8.4 Performance of MCM in the presence of multipath

8.4.1 Guard interval

In the case of single carrier systems, the effect of multipath is to introduce intersymbol interference (ISI). In the case of MCM, the effects of multipath are twofold: first, the orthogonality conditions (8.4) are no longer maintained, and second, subcarriers suffer different attenuations.

Let the received signal $y(t)$ be

$$y(t) = x(t) * h(t) + n(t) \tag{8.7}$$

where $h(t)$ is the impulse response of the channel, and $n(t)$ is the aggregate of Gaussian noise and interference. The output of the correlators in Fig 8-1 is now:

$$Y_{j,k} = H_{j,k}C_{j,k} + N_{j,k} \tag{8.8}$$

where $H_{j,k} = \rho_k e^{j\phi_k}$ is the frequency response of the channel at frequency f_k and time frame j, and $N_{j,k}$ is a complex term representing the power of the noise at frequency f_k and time frame j.

The problem of loss of orthogonality is solved very simply by augmenting the symbol time T_s to include a guard period Δ.

$$T_s' = T_s + \Delta \tag{8.9}$$

The MCM signal becomes:

$$x(t) = \sum_{j=-\infty}^{+\infty} \sum_{k=0}^{N-1} C_{j,k}\psi_{j,k}'(t) \tag{8.10}$$

where $\psi_{j,k}'(t) = g_k'(t - jT_s')$ and

$$g_k'(t) = \begin{cases} e^{j2\pi f_k t} & -\Delta \le t < T_s \\ 0 & \text{otherwise} \end{cases} \tag{8.11}$$

At the receiver, the multicarrier signal is demodulated using a bank of N correlators performing the following decoding:

$$C_{j,k} = \frac{1}{T_s}\int_{-\infty}^{+\infty} x(t)g_k^*(t - jT_s')dt \tag{8.12}$$

The integration at the receiver is still over an interval of duration T_s starting at time 0 after the intersymbol interference from the previous symbol has ended. The penalty for inserting a guard period is a reduction of the information rate. The resulting SNR loss is $10\log(1 + \Delta/T_s)$.

The effect of channel selectivity (attenuation and phase delay) can be approximately modeled by the quantities $\rho_{j,k}$ and $\phi_{j,k}$ in each subchannel. If the channel is time-invariant, these can be assumed to be constants and precomputed before the start of the data transmission, by sending a known sequence and measuring attenuation and phase delay in each band. Each received symbol $Y_{j,k}$ is then multiplied by $1/\rho_{j,k}e^{-j\phi_{j,k}}$. If the channel is not time invariant, the channel characteristics must be estimated by other means. In one system, the channel characteristics are obtained as a by-product of the carrier recovery procedure [2].

8.4.2 Discrete-time models for the HDTV channel

In the analysis carried out in the next section, the performance of MCM is investigated using two multipath models. The "static multipath" model assumes that temporal variations of the channel characteristics are slow compared to the signaling rate, so that the channel may be considered as essentially time-invariant. The number of paths to the receiver is assumed to be small. The effect of the transmit filter $g(t)$, the channel impulse response $f(t)$ and the sampled whitened matched filter (MF and WF) front-end is described in discrete time by a time-invariant FIR filter h_k (cf. Fig. 8-5). This model is thought to describe most HDTV channels.

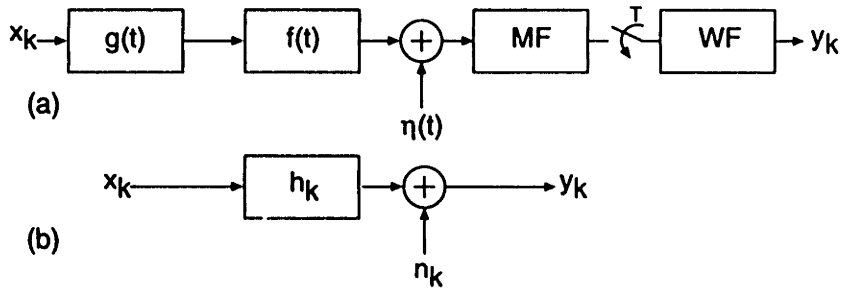

Figure 8-5: (a) Baseband channel model. (b) Equivalent discrete-time channel model.

The second model assumes a time-variant impulse response of the form described in Section 3.4. The number of paths is assumed sufficiently large so that the impulse response becomes a complex-valued Gaussian random variable. As a consequence, the samples of the channel frequency response are also complex-valued Gaussian random variables. The time scale of the temporal variations of the channel characteristics is assumed to be of the order of a few MCM symbols. Since we assume in the remainder that perfect interleaving is used to decorrelate the signal samples, we may disregard the precise time scale of the variations of the channel gain. We call this model the "dynamic multipath" model.

8.4.3 Performance analysis

In the following section, we analyze the performance of MCM for the static multipath channel and for the dynamic multipath channel. The case of coded MCM is explored, of which uncoded MCM is a particular case.

Let C denote the set of all possible coded signal sequences $\{\mathbf{Z}_L\}$, where $\mathbf{Z}_L$ is a coded symbol sequence of length L. Let us suppose that $\mathbf{X}_L$, an element of C, is the transmitted sequence. Then X_i represents the ith transmitted symbol, corresponding to some time frame j and some subchannel k. The corresponding received sequence at the input of the decoder is denoted $\mathbf{Y}_L$. The received symbol Y_i is related to the transmitted symbol X_i by

$$Y_i = H_i X_i + N_i \tag{8.13}$$

where H_i is a complex value corresponding to the channel gain at time index j and subchannel index k, and N_i is a sample of a zero-mean complex additive white Gaussian noise process.

The ML (Viterbi) algorithm searches the set C for the sequence $\mathbf{Z}_L$ with the minimum path metric from the received sequence $\mathbf{Y}_L$. For computational reasons, the path metric is chosen with an additive property, that is, the path metric $m(\mathbf{Y}_L, \mathbf{Z}_L)$ is the sum of the branch metrics $m(\mathbf{Y}_L, \mathbf{Z}_L) = \sum_{j=1}^{L} m(Y_i, Z_i)$. In the remainder, we assume that the channel gains H_i have been estimated and are known. The ML metric for this problem is then

$$m(Y_i, Z_i) = |Y_i - H_i Z_i|^2 \tag{8.14}$$

The pairwise error probability of choosing the path $\mathbf{Z}_L$ instead of $\mathbf{X}_L$ (first error event probability) is equal to

$$P(\mathbf{X}_L \rightarrow \mathbf{Z}_L) = Pr\{m(\mathbf{Y}_L, \mathbf{Z}_L) < m(\mathbf{Y}_L, \mathbf{X}_L)\} \tag{8.15}$$

Using the union bound technique, the bit error probability can be upper-bounded by

$$P_b \leq \frac{1}{k} \sum_{\mathbf{Z}_L, \mathbf{X}_L} B(\mathbf{Z}_L, \mathbf{X}_L) P(\mathbf{X}_L \rightarrow \mathbf{Z}_L) \tag{8.16}$$

where $B(\mathbf{Z}_L, \mathbf{X}_L)$ is the number of erroneous information bits on the path $\mathbf{Z}_L$ and k is the number of information bits in a symbol. $B(\mathbf{Z}_L, \mathbf{X}_L)$ can be found by using a suitable path enumerating function for the code considered.

The pairwise probability conditioned on $\mathbf{H}_L$ is

$$P(\mathbf{X}_L \rightarrow \mathbf{Z}_L | \mathbf{H}_L) = Q\left(\frac{d'}{2\sigma}\right) \tag{8.17}$$

where $Q(.)$ is the Gaussian error integral, $d'^2 = \sum_{i=1}^{L} |H_i|^2 d_i^2$ and $d_i = |Z_i - X_i|$.

Using the approximation $Q(x+y) \leq \exp(-x^2/2)Q(y)$ and $Q(x) \leq \frac{1}{2}\exp(-x^2/2)$ for $x, y \gg 1$ (we could equally well have used the Chernoff bound) we can write

$$P(\mathbf{X}_L \to \mathbf{Z}_L|\mathbf{H}_L) \leq \frac{1}{2}\exp\left(-\frac{1}{8\sigma^2}\sum_{i\in\eta} d_i^2 H_i^2\right) \tag{8.18}$$

where η is the set of all i such that $m(Y_i, Z_i) \neq 0$. The average pairwise probability is computed by integrating over all values of the channel gains. We now assume that the channel gain terms are independent and identically distributed, which may be achieved by proper symbol interleaving/deinterleaving. Therefore

$$P(\mathbf{X}_L \to \mathbf{Z}_L) \leq \frac{1}{2}\prod_{i\in\eta}\int_{H_i}\exp\left(-\frac{1}{8\sigma^2}d_i^2|H_i|^2\right)p(|H_i|)d|H_i| \tag{8.19}$$

8.4.3.1 Static multipath

Let us consider a simple case, albeit important in practice, of an echo of magnitude a ($0 \leq a \leq 1$). The frequency response of the discrete-time channel (up to and including the whitened matched filter) is of the form

$$H(e^{-j\omega}) = 1 - ae^{-j(n\omega+\phi_0)} \tag{8.20}$$

where ϕ_0 is some arbitrary phase. Interleaving ensures that ω is uniformly distributed within the interval of definition and therefore we can write

$$P(\mathbf{X}_L \to \mathbf{Z}_L) \leq \frac{1}{2}\prod_{i\in\eta}\frac{e^{-\kappa_i(1+a^2)}}{2\pi}\int_0^{2\pi} e^{-\kappa_i 2a\cos\omega_i}d\omega_i \tag{8.21}$$

where $\kappa_i = d_i^2/8\sigma^2$. The integral is recognized as the zero-order modified Bessel function of the first kind, denoted $I_0(.)$. We finally obtain

$$P(\mathbf{X}_L \to \mathbf{Z}_L) \leq \frac{1}{2}\exp(-\frac{d^2}{8\sigma^2}(1+a^2))\prod_{i\in\eta} I_0(2a\kappa_i) \tag{8.22}$$

where $d^2 = \sum_{i\in\eta} d_i^2$ is the usual squared Euclidean distance along the error path. The dominant terms in Eq. (8.16) correspond to paths with the largest pairwise error probabilities. At high SNR, these are the terms for which $\prod_{i\in\eta} I_0(2a\kappa_i)$ is large. The first term of the asymptotic expansion of $I_0(x)$ for large x is equal to $I_0(x) \approx e^x/\sqrt{2\pi x}$, so that the pairwise error probability becomes

$$P(\mathbf{X}_L \to \mathbf{Z}_L) \leq \frac{1}{2}\exp(-\frac{d^2}{8\sigma^2}(1-a^2))\prod_{i\in\eta}(4\pi a\kappa_i)^{-1/2} \tag{8.23}$$

From (8.23), it is clear that, when $a = 1$, the pairwise error probability displays a characteristic dependence on the SNR to the power $L_\eta/2$, where L_η is the size of the set η and is called the effective constraint length (ECL) of the code [7]. Although this result is derived for a single echo, it can be shown that this result holds for any number of equal strength echoes for which

the zeros of the channel response are located on the unit circle. In particular, this result holds for $h_k = 1 + z^{-1} + z^{-2}$. A strikingly different result may be achieved with an impulse response $h_k = 1 + z^{-1} - z^{-2}$ with zeros at $(-1 + \sqrt{5})/2$ and $(-1 - \sqrt{5})/2$. The equivalent equal energy, minimum-phase response is $h_k = K_0(1 + (1 - \sqrt{5})/(1 + \sqrt{5})z^{-2})$ where $K_0 = \sqrt{(3 + \sqrt{5})/2}$. This implies that the error rate now decreases exponentially fast, and that the SNR is multiplied by an additional factor $K_0^{L_\eta/2}$.

It is clear that, as the number of echoes is increased and echoes are added with random phases, the distribution of H_l will approach a Gaussian distribution.

8.4.3.2 Dynamic multipath

In the dynamic multipath channel model, the terms H_l are Gaussian distributed, and therefore the amplitudes $|H_l|$ are distributed according to a Rician distribution. Eq.(8.18) can be written

$$P(\mathbf{X}_L \to \mathbf{Z}_L) \leq \frac{1}{2} \prod_{l \in \eta} \frac{1 + K}{1 + K + \kappa_l} \exp\left(-\frac{K\kappa_l}{1 + K + \kappa_l}\right) \tag{8.24}$$

where K is the ratio of the direct power to the power in the echoes. In the case of strong echoes, $K \ll 1$, and for reasonably large SNR values,

$$P(\mathbf{X}_L \to \mathbf{Z}_L) \leq \frac{1}{2} \prod_{l \in \eta} \frac{1}{\kappa_l} \tag{8.25}$$

that is, the pairwise error probability is inversely proportional to the product of the squared Euclidean distances along the error event path and displays a characteristic dependence on SNR to the power L_η, a well-known result for SCM nonfrequency selective fading. When L_η is large, the performance is not very different from the Gaussian case.

8.4.4 Simulation results

For the purpose of investigating the performance of MCM on the described channels, we have used a rate 1/2, constraint-length 7 (64 states) code with an ECL=6, similar to one used in [51], associated with a 16QAM modulation format. The large ECL ensures that sufficient diversity is provided over dynamic multipath channels. At this point, it is worthwhile noting that conventional trellis codes with large Euclidean distances may perform very poorly over such channels because of the existence of parallel transitions at the minimum distance ($L_\eta = 1$). The Monte Carlo simulations were carried out using 512 carriers, a 20% guard interval, and assuming infinite interleaving. We have plotted the bit error rate against an SNR defined as the ratio between the power of the reference signal (direct signal) and the noise power. While the custom for fading channels is to include both direct and diffuse powers in the signal power,

our definition has the merit of showing clearly and intuitively how the performance is affected by a varying number of echoes or scatterers.

Fig. 8-6 shows the expected poor performance of uncoded MCM on a highly frequency selective channel. Fig. 8-7 shows the performance of uncoded MCM on a dynamic multipath channel with a delay spread equivalent to the static channel. As can be seen, the error rate decreases only inversely proportionally to the SNR, but additional echo power improves the performance. Fig. 8-8 shows the performance of coded MCM on the same channels as in Fig. 8-6. The dependence on the SNR is clearly inversely proportional to the third power of the SNR, as predicted for channels with zeros near the unit circle, and additional echoes *degrade* the performance. Curve (e) illustrates the performance for $h_k = 1 + z^{-1} - z^{-2}$. Fig. 8-9 shows the performance of coded MCM on the same channels as in Fig. 8-7. The error rate decreases as the sixth power of the 1/SNR for a large number of scatterers, which is the predicted result. The decrease is even faster for a small number of scatterers. The powers of the direct and indirect signals combine additively.

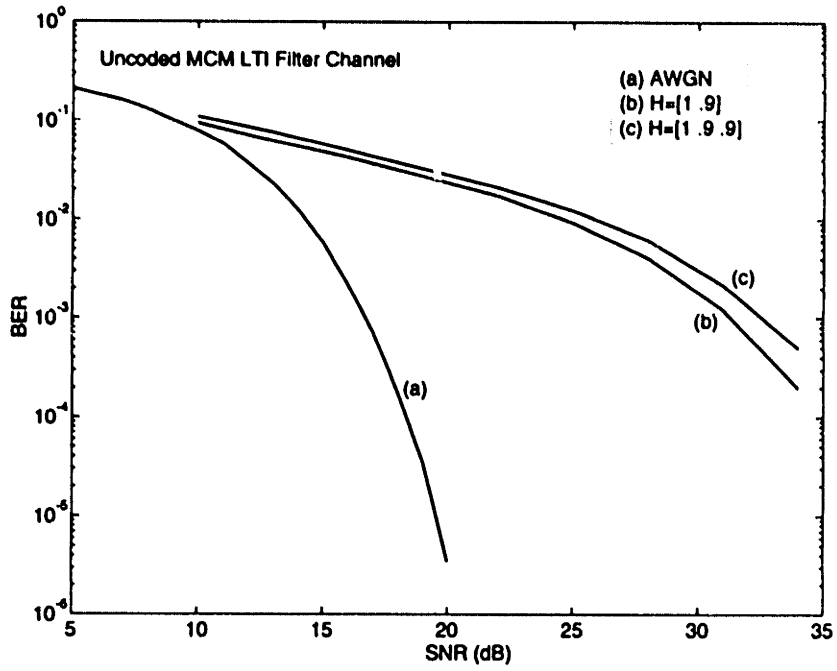

Figure 8-6: Simulation results for uncoded MCM over static multipath channel.

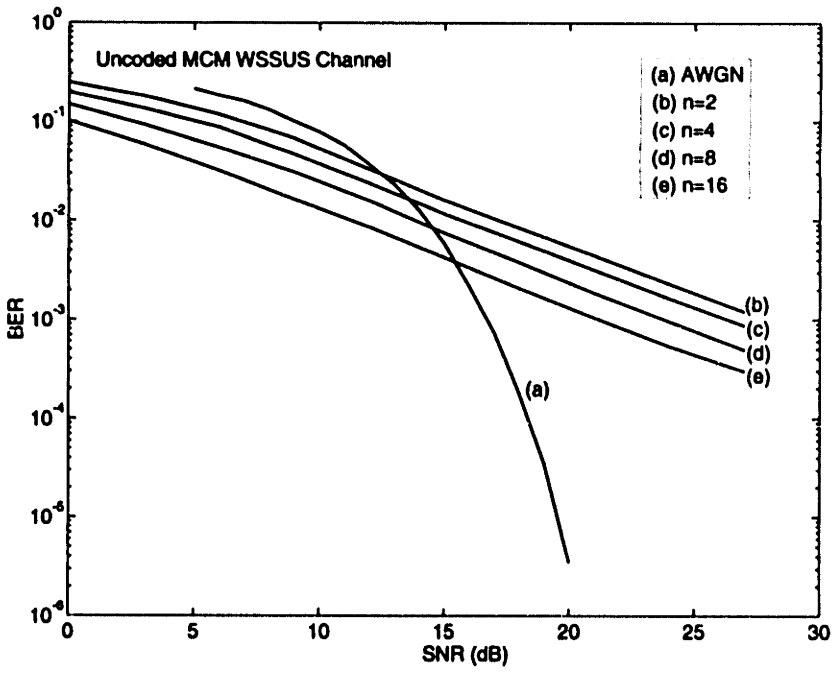

Figure 8-7: Simulation results for uncoded MCM over dynamic multipath channel.

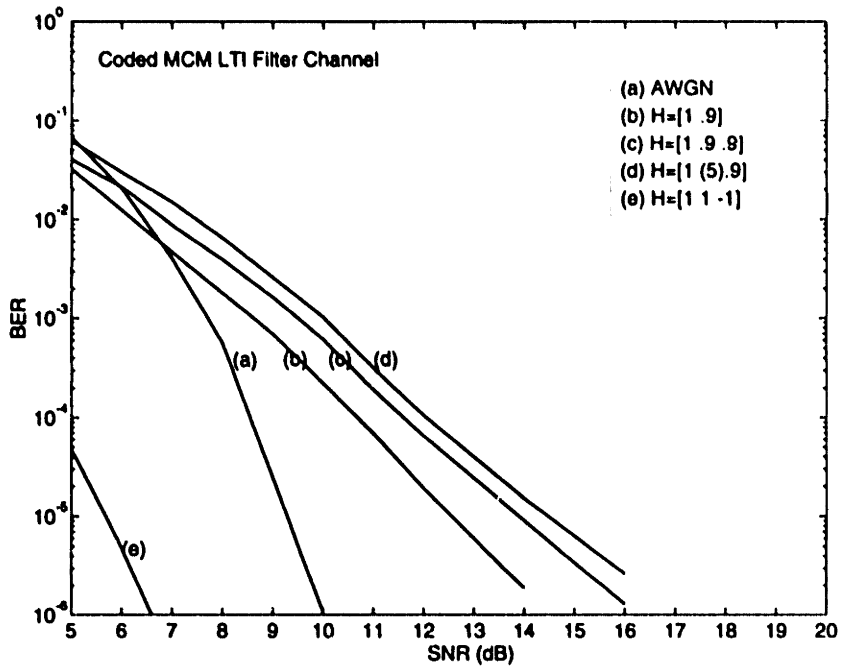

Figure 8-8: Simulation results for coded MCM over static multipath channel.

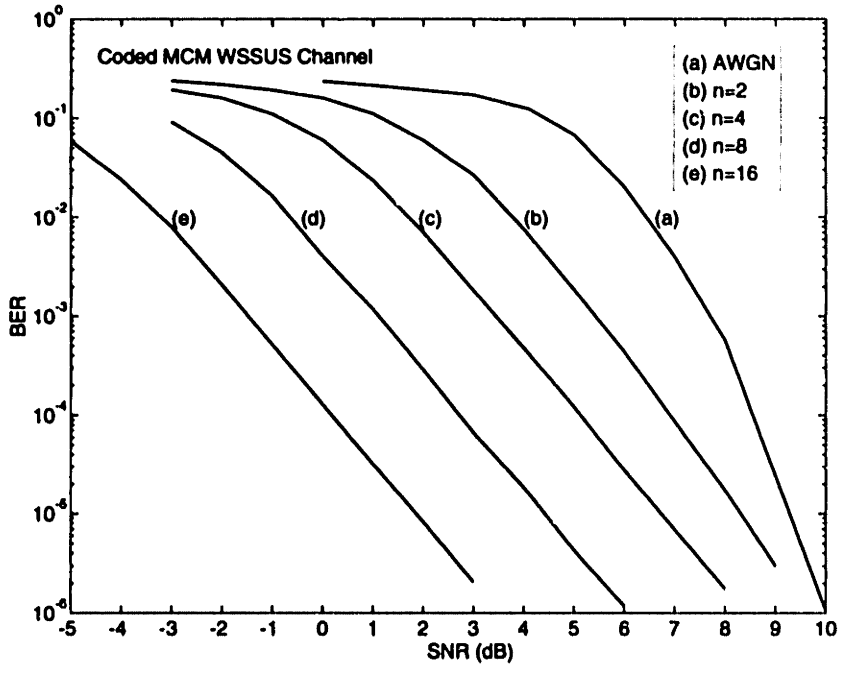

Figure 8-9: Simulation results for coded MCM over dynamic multipath channel.

8.5 Comparison with single-carrier modulation

Eqs. (8.16), (8.17) and (8.19) show that the average error rate is obtained by averaging the Gaussian error function over the distribution of the channel gains. We showed that for the simple case of a single echo of magnitude equal to that of the desired signal, the error rate decreases inversely proportionally to the signal-to-noise ratio.

In Chapter 6, we provided several figures of merit for single carrier equalization schemes. In particular, we showed that for LE-MSE, when the receiver front end is a WMF, the MSE is given by

$$2\sigma^2 = N_0\langle 1/(S_{h,n} + N_0/S_x)\rangle_A, \tag{8.26}$$

yielding a figure of merit

$$\gamma_{\text{LE-MSE}} = \frac{x_{\min}^2}{N_0/2} \frac{1}{\langle 1/(S_{h,n} + N_0/S_x)\rangle_A} \tag{8.27}$$

and an error probability

$$P_e = K\,Q\left(\frac{1}{2}\sqrt{\gamma_{\text{LE-MSE}}}\right) \tag{8.28}$$

where K is the number of nearest neighbors. The performance of LE-MSE may be poor when the channel has a near null, but in general, the error rate decreases exponentially fast with increasing SNR, due to the mitigating term N_0/S_x in the expression of the variance of the error signal. We therefore conclude that the LE-MSE has a better performance than MCM, in the absence of coding. Furthermore, decision-feedback equalization would be far superior to MCM in the case of strong multipath.

In the case of coding, we found that the performance of MCM depended critically on the ECL of the code. While it was found that a large ECL could be used to increase the diversity factor of the system, it still seems that the performance of a combined equalization and coded modulation scheme for single-carrier modulation can outperform an MCM scheme.

8.6 Conclusion

In this chapter, we have investigated the performance of multicarrier modulation over static and dynamic multipath channels. Both analysis and simulations show that the performance of MCM over the dynamic multipath channel improves as the number of echoes or scatterers increases. Moreover, the combination of coding and MCM makes it possible to approach the performance over the AWGN channel by exploiting the diversity introduced by the code. As such, MCM appears to be a good solution for dynamic multipath channels. The performance of MCM over static multipath channels, however, is not nearly as good. We have derived the performance of MCM for a simple case, and found that, for the same code, the pairwise error

rate decreases at only half the rate achieved in the dynamic multipath case. This behavior is largely due to the non-Gaussian distribution of the channel gains. It may appear that the solution would be to increase the built-in diversity of the code, but in a broadcasting environment, this would mean an overall rate penalty for all receivers. It should also be noted that single carrier equalization schemes, such as DFE or even LE-MSE are able to outperform MCM, though perhaps at a substantial implementation cost.

9

Conclusion

In this thesis, we have explored issues related to the transmission of digital data by terrestrial broadcasting means and proposed some potentially important ways of improving the existing methods of HDTV transmission. Three areas were investigated in depth: efficient coding techniques for HDTV; equalization/interference rejection techniques for HDTV, and the relevance of multicarrier modulation in the HDTV environment.

The first part of the thesis investigated efficient coding techniques which ensure the optimal use of the limited bandwidth and power available to transmit HDTV signals. The problem was explored along two paths. The first consisted in examining the performance of coded modulation and concatenated coded-modulation schemes for the Gaussian channel. We reviewed several concepts central to coded modulation on high-rate channels, and proceeded to perform a detailed evaluation of a number of trellis-coded modulation schemes, those of most interest in HDTV terrestrial broadcasting applications. The second explored the problem of matching the data rate to the variable channel capacity of a degraded broadcast channel. The notion of multiresolution constellations was reviewed, and an analysis of the trade-offs involved in providing a multiplicity of data rates and signal-to-noise ratio was carried out.

In the second part of the thesis, issues related to the rejection of co-channel interference were investigated. The problem was examined in two stages. In the first instance, the problem was characterized as an equalization problem and a number of receiver structures were proposed. A number of comparisons were made with existing and proposed interference rejection schemes. It was shown how all of these schemes could be viewed as special cases of the general equalization structures introduced at the beginning of Chapter 6. In the second instance, the problem of combining bandwidth-efficient coding with the interference schemes proposed in Chapter 6 was examined. The peculiar characteristics of the NTSC interference were exploited in order to derive efficient and cost-effective interference rejection schemes. In particular, a

scheme based on a combination of decision-feedback equalization and reduced-state sequence estimation was shown to perform very well in combination with trellis-coded modulation.

The final part of the thesis further developed the idea of using multicarrier modulation on a digital television broadcast channel. It has been argued that multicarrier modulation is particularly well suited to networks of transmitters because its performance is dependent on the total power received from multiple transmitters. Whether multicarrier modulation is capable of taking advantage of echoes is a contentious issue. An analysis of the problem was carried out based on a number of simplifying assumptions. We did not find any evidence to support this argument for either a time-invariant or a slowly time-varying multipath channel, which are thought to describe UHF HDTV channels.

Future directions: There are a number of opportunities for further research related to the transmission of television signals over the terrestrial broadcast channel. It would be useful to have a more detailed model of the HDTV transmission channel, in order to match the channel coding more closely to the characteristics of the channel. For instance, while it appears that the television channel can, in many cases, be reasonably well modeled as a multipath channel with interference, it seems likely that the propagation process is far more complicated near the fringes of the service area, or when a line-of-sight signal is not available. A clear understanding of the tradeoffs involved in providing a multiplicity of data rates and degrees of robustness would be helpful.

The existing structure of the television network based on the use of a small number of central transmitters is undeniably inefficient, since much power is wasted precisely in those areas where bandwidth and power are most in demand for other services. It would appear that it would be very desirable to provide a service with a more uniform spatial distribution of power. This observation has motivated attempts to develop so-called single-frequency networks. It seems clear, at the time of this writing, that an adequate, cost effective solution is yet to be found. An understanding of the complex issues involved in developing such a network would be the basis for important future research.

NTSC planning factors

A.1 NTSC service contours

Television grade A and grade B contours are defined by the NTSC Planning Factors in terms of field strengths (in dB above $1\mu V/m$, often abbreviated dBu) and indicate the approximate extent of coverage over average terrain in the absence of interference from other stations. Specifically, NTSC Grade B service is intended to provide service to rural areas for at least 50 percent of the locations for 90 percent of the time and Grade A service is intended to provide service in an urban environment to at least 70 percent of the locations for 90 percent of the time. A third contour, the so-called city grade, is also sometimes used. The city grade service contour is intended to provide service in an urban environment for at least 90 percent of the locations for 90 percent or more of the time [71]. The numerical value of this contour is 6 dB higher than the grade A contour value.

In order to facilitate the determination of these contours, the FCC has issued a series of field-strength charts, known as the $F(50,50)$ and $F(50,10)$ charts, which are intended to be used for coverage area predictions. The 50 percent field strength is defined as that value exceeded for 50 percent of the time (median field strength). The $F(50,50)$ and $F(50,10)$ charts give the estimated 50 percent field strength exceeded at 50 percent and 10 percent of the locations respectively. More generally, an $F(x,y)$ curve defines the field strength exceeded at x percent of the locations at least y percent of the time as a function of the distance from the transmitter. Grade A and grade B contours are determined, respectively, from the $F(70,90)$ and $F(50,90)$ field strength charts, which are related to the $F(50,50)$ curves through a simple equation which incorporates a time-fading factor ΔT and a location probability factor ΔL. These factors reflect the fact that field strengths vary with time and location, even between points relatively close together (it has been suggested that the received field strength follows

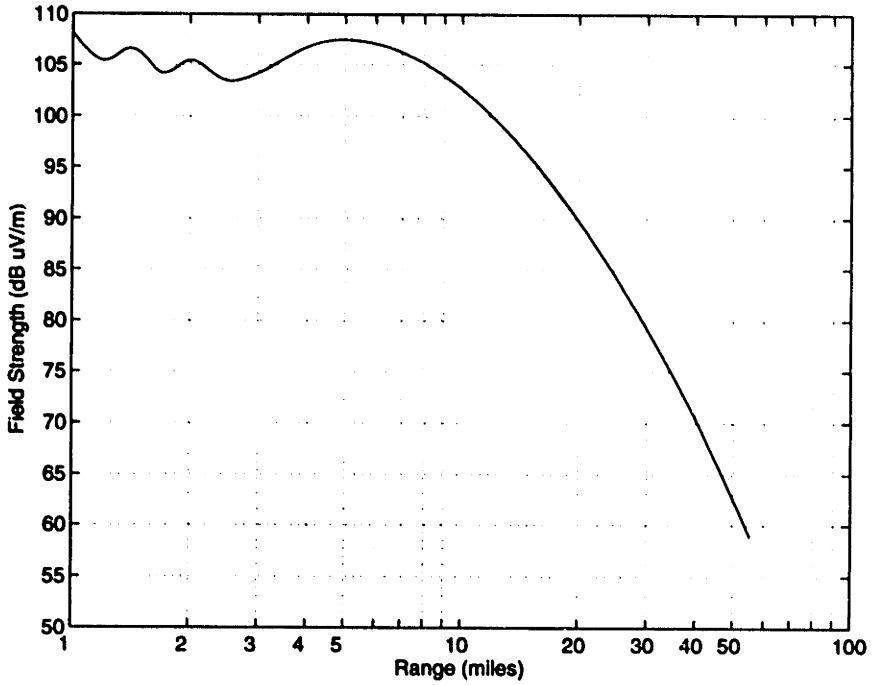

Figure A-1: Typical NTSC field strength as a function of distance at UHF (based on data in a note by O. Bendov).

a log-normal distribution as a function of location at any given distance from the transmitter). The various $F(x, y)$ curves attempt to describe the statistical characteristics of these variations but cannot predict the *exact* value of the field strength at a particular location at a given time. The requirements are summarized in table A.1.

A fairly typical $F(50, 50)$ UHF propagation curve is shown in Figure A-1 for a 55 kW transmitter with an antenna gain of 20. It is interesting to note that the field strength decreases by 8-10 dB per 10 miles, past 20 miles.

It is important to note that the $F(x, y)$ curves are statistical in nature and represent an average over a large number of measurements; they do not clearly distinguish how specific impairments have been weighted. Clearly, since the numerical values associated with the service contours are in terms of field strengths, some assumptions had to be made with respect to the receiver (antenna height, antenna gain, line loss, receiver noise figure). This is because it is ultimately the voltage at the receiver terminals, together with the noise and interference impairments, which determine whether or not a picture of any given quality will be produced. Picture quality itself is a subjective parameter, which implies that assumptions had to be made about the nature of the typical viewer.

A.2 NTSC receiver SNR

Given a field strength value E obtained from an $F(50,50)$ curve, it is thus possible to obtain the receiver SNR through the following equation

$$\text{SNR} = E + K_d + G - N_I - N_R - L - \Delta T - \Delta L \quad (\text{dB}) \tag{A.1}$$

where K_d is the so-called dipole factor (proportionality constant relating the voltage across a given receiver impedance R to the ambient electric field for a half-wave dipole, in dB/m), defined as

$$V = K_d \cdot E, \quad \text{where} \quad K_d = \frac{\lambda}{2\pi}\sqrt{\frac{R}{R_0}}, \quad \text{and} \quad R_0 = 73.5\Omega \tag{A.2}$$

where λ is the wavelength, G is the receiver antenna gain, N_I is the receiver noise temperature, N_R is the receiver noise figure (figure of merit indicating how much greater the actual receiver noise voltage is compared to the noise voltage in an ideal receiver), L is the downlead line loss, and ΔT and ΔL are the time and location factors respectively. Typical values at mid-UHF are given in table A.2

A.3 NTSC channel separations

Table A.3 summarizes the most important sources of interference and the required channel separations.

Service Contour	Probability of service	F(50,50) in dBμV/m		
		Low VHF	High VHF	UHF
City Grade	90% locations for 90% time	74	77	80
Grade A	70% locations for 90% time	68	71	74
Grade B	50% locations for 90% time	47	56	64

Table A.1: Service contours. *Source:* Part 73.610, Table IV, 73.698, FCC Rules and Regulations.

Parameter	Level
Grade B SNR (6 MHz)	28.5 dB
Dipole Factor K_d (75Ω, 609 MHz)	-22 dB/m
Antenna Gain G	13 dB
Thermal noise N_I (75Ω, 6 MHz)	2.6 dBμV
Noise Figure N_R	10 dB
Downlead Loss L	5 dB
90% Time Factor at 56 mi ΔT	8.7 dB
Field Strength E	63.8 dBμV/m

Table A.2: Typical values for NTSC parameters.

Interference type	Channel numbers and separations	Required separation mi (km)
Co-channel	0	155(249)
Adjacent channel	±1 (6 MHz)	55(89)
Sound image	±14 (84 MHz)	60(97)
Picture image	±15 (90 MHz)	75(121)
Local Oscillator	±7 (42 MHz)	20(32)
IF beat	±8 (48 MHz)	20(32)
Intermodulation	±2 through ±5	20(32)

Table A.3: Channel separations for channel 14-69 (UHF). *Source:* Part 73.610, Table IV, 73.698, FCC Rules and Regulations.

B

Symbol, bit and block error rate calculations

Error performance is a natural figure of merit for a digital communication system. There are, however, several ways of measuring this error performance, depending on the use intended for the detected data. A natural measure for communication systems such as those discussed in this dissertation is the symbol error probability, since it is often the one that is the easiest to determine, based on the physical characteristics of the channel and the modulation scheme. When the transmission system uses more complex schemes that combine modulation and coding, sequence error rates are often more easy to estimate. Another quantity that is often of interest is the bit error rate, or bit error probability. Indeed, it is often the case that we wish to make a clear distinction between the source and channel coding portions of the communication system, and a bit stream is a natural interface between the two. In digital television systems, however, the interface is usually based on a block structure, and it is thus natural to express the performance of the system in terms of block error rate. These various performance measures differ, and it is often desirable to convert between them. We summarize in this section the formulas used to convert between symbol, bit and block error rate.

Bit error rate Here we assume that a symbol error rate has been determined for the modulation scheme under consideration, which we denote by P_{bit}. Let M be the number of bits per symbol. Equivalently, we may say that M is the number such that 2^M is the size of the signal set. In general, it is necessary to know the detail of the modulation scheme in order to relate the symbol error rate and the resulting bit error rate at the output of the decision device. However, a reasonable approximation, for high SNR, consists in assuming that the most probable symbol errors correspond to the selection of one of the nearest neighbors of the correct signal point. Assuming Gray coding of the signal set, in which nearest neighbors correspond to groups of bits that differ by 1 bit, we can write

$$P_{\text{bit}} \approx \frac{1}{M} P_{\text{sym}} \tag{B.1}$$

It is important to note, however, that the probability of bit error can often be computed exactly without resorting to this approximation. A number of textbooks provide detailed determinations of the bit and symbol error rates for the most traditional PSK and QAM modulation schemes [75, 62].

Probability of block error It is often the case that transmission systems need to operate on blocks of bits rather than on the binary information itself. For instance, a modem may be embedded in a system that formats bits into blocks, transmits the blocks and performs some form of error checking on the blocks to decide which blocks to repeat. In such a case, the block error rate is a more meaningful parameter. Another example is the conversion from bit error rate at the output of one decoding unit to block (or non-binary symbols) error rates at the input of a succeeding decoding unit.

Let B denote the number of bits in a block, so that B/M is the number of symbols in a block. Then,

$$P_{\text{block}} = 1 - (1 - P_{\text{sym}})^{B/M} \approx \frac{B}{M} P_{\text{sym}} \tag{B.2}$$

Clearly, this relation does not apply to block codes, which insert redundancy in the data stream in order to correct errors due to the noisy channel conditions.

Block codes We are particularly interested in determining bounds on the performance of Reed-Solomon (RS) codes when used in concatenation with convolutional codes, since these have proven to offer good performance for reasonable complexity [38, 45]. RS codes are a natural choice as outer codes in a concatenated coding scheme because they are maximum distance separable codes (that is, the minimum distance of an (n, k) code is $d_{\min} = n - k + 1$, one greater than the number of parity symbols) and because cost effective decoding algorithms are now well established.

Accordingly, let us consider the case of a RS code $[n, k, t]$ over GF(2^l) where the block length is $n \leq q + 1$, with $q = 2^l$, $k = n - 2t$, and the error-correction capability is t errors. If the symbol error probability is P_{in}, an upper bound on the block error rate at the output of the RS decoder is given by

$$P_{\text{block}} \leq \sum_{i=t+1}^{n} \binom{n}{i} P_{\text{in}}^{i} (1 - P_{\text{in}})^{n-i} \tag{B.3}$$

This result follows directly from the fact that the code is guaranteed to correct error patterns with up to t errors (the error correcting capability of the code). The number of guaranteed correctable error patterns is therefore $N_t = \sum_{i=0}^{t} \binom{n}{i}$. In general, N_t represents only a small fraction of the 2^{n-k} error patterns that are correctable with syndrome decoding, but for large $n - k$, a decoder capable of correcting all the correctable error patterns would be very complex and expensive. Most of the standard decoding algorithms for the class of BCH codes, of which

RS codes are a subclass, are designed to correct the error patterns which are guaranteed by the error-correcting capability t of the code, and to raise a flag to other detected but uncorrected errors. This type of decoding is called bounded distance decoding. Fortunately, bounded distance decoding is easy to analyze.

The block error rate for bounded distance decoding becomes

$$P_{\text{block}} = \sum_{i=t+1}^{n} \binom{n}{i} P_{\text{in}}^{i} (1 - P_{\text{in}})^{n-i} \tag{B.4}$$

A bound on the decoded symbol error probability can be determined in the following way. As previously, the probability of i errors is $\binom{n}{i} P_{\text{in}}^{i} (1 - P_{\text{in}})^{n-i}$. The number of extra errors introduced due to an incorrect decoding is smaller or equal to t. Thus, the average number of "byte" errors is upper-bounded by $(i + t)\binom{n}{i} P_{\text{in}}^{i} (1 - P_{\text{in}})^{n-i}$. The byte or symbol error rate is upper-bounded by

$$P_{\text{out}} \leq \frac{1}{n} \sum_{i=t+1}^{n} (i + t) \binom{n}{i} P_{\text{in}}^{i} (1 - P_{\text{in}})^{n-i} \tag{B.5}$$

In order to derive the bit error rate at the output of the decoder, additional assumptions must be made. One reasonable assumption is to assume that all symbol errors are equally probable and occur with probability $P_{\text{out}}/(2^l - 1)$, since $2^l - 1$ is the number of symbols other than the correct symbol. For each symbol error, there are $\binom{l}{k}$ ways in which k bits out of l may be in error. Hence, the average number of bit errors per l-bit symbol is

$$\sum_{k=1}^{l} k \binom{l}{k} \frac{P_{\text{out}}}{2^l - 1} = l \frac{2^{l-1}}{2^l - 1} P_{\text{out}} \tag{B.6}$$

and the average bit error rate is the result in Eq. (B.6) divided by l, the number of bits per symbol. Therefore

$$P_{\text{bit}} \approx P_{\text{out}} \frac{2^{l-1}}{2^l - 1} \tag{B.7}$$

which is upper-bounded by

$$P_{\text{bit}} \lesssim \frac{2^{l-1}}{2^l - 1} \frac{1}{n} \sum_{i=t+1}^{n} (i + t) \binom{n}{i} P_{\text{in}}^{i} (1 - P_{\text{in}})^{n-i} \tag{B.8}$$

In most cases, for reasonably small P_{in} (on the order of 10^{-2}), the first term dominates, and we can write,

$$P_{\text{bit}} \lesssim \frac{2^{l-1}}{2^l - 1} \frac{2t + 1}{n} \binom{n}{t + 1} P_{\text{in}}^{t+1} (1 - P_{\text{in}})^{n-t-1} \tag{B.9}$$

If the l-bit symbols of the RS code are composed of smaller, m-bit symbols (e.g. the decoded symbols of a inner trellis code) then the input error rate is

$$P_{\text{in}} = 1 - (1 - P_{\text{sym}})^{l/m} \tag{B.10}$$

where P_{sym} is the m-bit channel symbol error rate, since there are l/m channel symbols in each RS symbol, and an RS symbol will be correct iff all constituent channel symbols are correct. For example, for $m = 4$ (16-QAM) and $l = 8$ (GF(2^8)), $P_{ln} \approx 2Psym$, since there are 2 channel symbols in each RS symbol.

To illustrate, let us consider a specific example: let the block code be a RS code [208,188,10] over GF(2^8). It is generally agreed that the threshold of visibility for impairments of the HDTV signal is around 1 block error per second. Let us assume an overall data rate of 20 Mb/s. The resulting block error rate is therefore $P_{block} = 1/(20 \times 10^6/(188 \times 8)) = 7.5 \times 10^{-5}$. The corresponding bit error rate is

$$P_{bit} \leq \frac{2^7}{2^8 - 1}\frac{21}{208}P_{block} = 3.6 \times 10^{-6} \tag{B.11}$$

C

Estimating the probability of error by the Monte Carlo method

For a digital system, the relevant measure of performance is always related to the system's error producing behavior. Different aspects of that behavior can be of interest. A common one is the probability of error. Let us assume that a system transmits symbols from an alphabet of size M, where usually $M = 2^k$, and where the average production of errors in an indefinitely long sequence is the measure of interest. Let N be the number of transmitted symbols and $n(N)$ be the corresponding number of observed errors. The probability of error P is obtained as the limit, as $N \to \infty$, of the ratio $n(N)/N$. For $M = 2$, P is called the bit error rate, or bit error probability. For $M > 2$, p is conventionally called the symbol error probability.

An obvious method of estimating the error probability P is to observe the system's output over a finite time and count the number of errors that occurred over that time. This is known as the Monte Carlo method. Other methods, such as importance sampling, tail extrapolation, and extreme-value theory can be used to estimate quantities such as the probability of error, but they are less general and therefore will not be considered here. Information concerning these latter methods can be found in [56].

In the Monte Carlo method, an important issue is then to know how accurate or reliable results are. In other words, we would like to provide a confidence interval together with the estimated error probability. In this appendix, we derive some simple bounds, which justify the rule of thumb used in the simulations of waiting until 100 errors have occurred before estimating the error probability.

To fix ideas, let us consider a generic system such as shown in Figure C-1. Let us assume that all transmitted symbols are equally likely, so that we do not need to characterize the

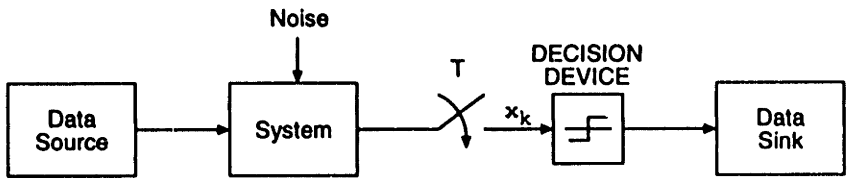

Figure C-1: Generic system model.

probability of error on a symbol basis. The output of the sampler consists of a discrete-time sequence of noisy symbols $\{x_k\}$. We further assume, to keep the discussion simple, that the samples are independent, identically distributed (i.i.d.).

Let the unbiased estimator of P be $\hat{P}$, defined as

$$\hat{P} = \frac{n(N)}{N} \tag{C.1}$$

For a given N, $N\hat{P}$ is binomially distributed, and thus, one can, in theory, obtain an exact, closed-form expression for the confidence interval in terms of the cumulative beta distribution. However, this is not the approach taken here, since the problem of determining the confidence interval has a simpler solution in the case of interest in digital communications, namely large N and small P. Indeed, as $N \to \infty$, the estimator $\hat{P}$ converges to P, almost surely, by the strong law of large numbers. Specifically, the estimator $\hat{P}$ converges to a normal distribution with mean P and variance $P(1-P)/N$, which are always verified in practice. Hence, one can construct a confidence interval of the form

$$\Pr\left[\left|P - \frac{N}{N+d_\alpha^2}\left(\hat{P} + \frac{d_\alpha^2}{2N}\right)\right|^2 < d_\alpha^2\left(\frac{\hat{P}(1-\hat{P})}{N} + \frac{d_\alpha^2}{4N^2}\right)\right] = 1-\alpha \tag{C.2}$$

where d_α is chosen so that

$$\frac{1}{\sqrt{2\pi}}\int_{-d_\alpha}^{d_\alpha} e^{-t^2/2}dt = 1-\alpha \tag{C.3}$$

Heuristically, we can see that the normal approximation will be reasonably good if at least $P \geq d_\alpha[P(1-P)/N]^{1/2}$, which means the standard deviation is smaller than P by a factor of d_α, a small number.

The absolute value of the confidence interval is not as informative as the confidence interval normalized to the probability of error itself. Let us consider the case of small error probabilities and set $\hat{P} = 10^{-\nu}$ and $N = \eta \cdot 10^{\nu}$. We further make the approximations $N/(N+d_\alpha^2) \simeq 1$ and $\hat{P}(1-\hat{P}) \simeq \hat{P}$. We can then express Eq. (C.2) as

$$\Pr[P_- \leq P \leq P_+] = 1-\alpha \tag{C.4}$$

where the confidence interval $[P_-, P_+]$ is given by

$$P_\pm = 10^{-\nu}\left(1 + \frac{d_\alpha^2}{2\eta}\right)\left(1 \pm \left(\frac{4\eta}{d_\alpha^2} + 1\right)^{1/2}\right) \tag{C.5}$$

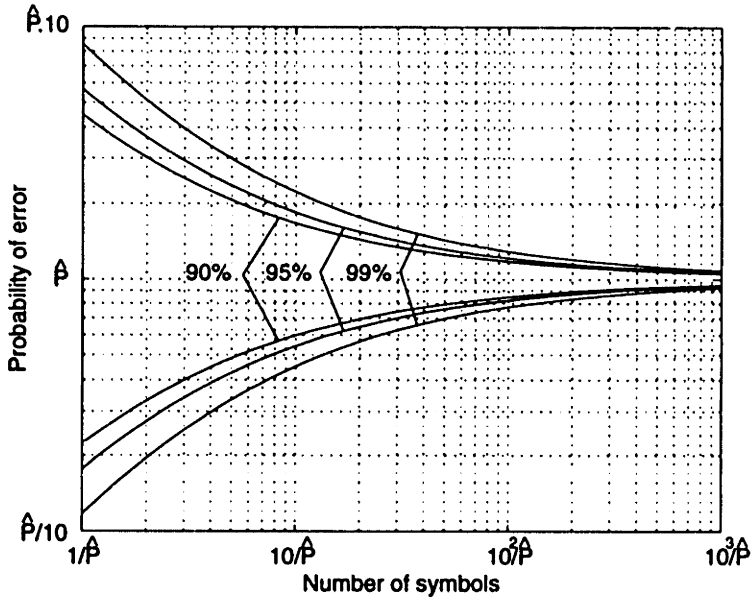

Figure C-2: Confidence intervals on the probability of error when the observed value is $\hat{P}$, based on the normal approximation.

This interval is plotted in Figure C-2 for 90%, 95%, and 99% confidence intervals. From this figure, one sees that if $N = 10/\hat{P}$, the 95% confidence interval is $[1.8\hat{P}, 0.55\hat{P}]$, i.e. a factor of 2 on the probability of error, which is normally considered sufficient. If we increase N by a factor of 10, i.e. $N = 100/\hat{P}$, the 95% confidence interval becomes $[1.25\hat{P}, 0.8\hat{P}]$. As we expect, the confidence interval narrows relatively slowly since it decreases only as $1/\sqrt{N}$. In general, the simulation results in this thesis were obtained with $N = 100/\hat{P}$. There is little point going beyond this, since the statistical variability would only decrease by a small amount for a large increase in simulation runtime.

Bibliography

[1] Advanced Television Research Consortium, *Advanced Digital Television: Prototype Hardware Description*, February 1992.

[2] M. Alard and R. Lassalle, "Principles of modulation and channel coding for digital broadcasting for mobile receivers", *EBU review*, vol. 224, August 1987.

[3] C. A. Belfiore and J. H. Parks, "Decision-feedback equalization", *Proceedings of the IEEE*, vol. 67, pp. 1143-1156, August 1979.

[4] P. A. Bello, "Characterization of randomly time-variant channels", *IEEE Trans. Commun. Syst.*, vol. 11, pp. 360-393, 1963.

[5] A. J. Bennett, "New modulation techniques for increased efficiency in UHF-TV transmitters", *Proceedings of the IEEE*, vol. 70, no. 11, pp. 1312-1318, November 1982.

[6] P. Bergmans, "Random coding theorem for broadcast channels with degraded components", *IEEE Trans. Inform. Theory*, vol. 19, pp. 197-207, 1973.

[7] E. Biglieri, D. Divsalar, P. J. McLane, and M. K. Simon, *Introduction to trellis-coded modulation with applications*, Macmillan Publishing Company, 1991.

[8] J. A. C. Bingham, "Multicarrier modulation for data transmission: an idea whose time has come", *IEEE Commun. Mag.*, vol. 28, pp. 5-14, May 1990.

[9] R. E. Blahut, *Digital Transmission of Information*, Addison-Wesley, 1990.

[10] M. L. Bucher, "Simulation of multipath fading/ghosting for analog and digital television transmission in broadcast channels", *IEEE Trans. Broadcasting*, vol. 38, no. 4, pp. 256-262, December 1992.

[11] A. R. Calderbank, "Multilevel codes and multistage decoding", *IEEE Trans. on Commun.*, vol. 37, no. 3, pp. 222-229, March 1989.

[12] A. R. Calderbank, T. A. Lee, and J. E. Mazo, "Baseband trellis codes with a spectral null at zero", *IEEE Trans. Inform. Theory*, vol. 34, no. 6, pp. 425-434, 1988.

[13] A. R. Calderbank and J. E. Mazo, "Spectral nulls and coding with large alphabets", *IEEE Commun. Mag.*, vol. 29, no. 12, pp. 58-67, December 1991.

[14] A. R. Calderbank and N. Seshadri, "Multilevel codes for unequal error protection", *IEEE Trans. Inform. Theory*, vol. 39, no. 4, pp. 1234-1248, July 1993.

[15] A. R. Calderbank and N. J. A. Sloane, "New trellis codes based on lattices and cosets", *IEEE Trans. Inform. Theory*, vol. 33, no. 2, pp. 177-195, March 1987.

[16] R. W. Chang, "High-speed multichannel data transmission with bandlimited orthogonal signals", *Bell Syst. Techn. J.*, pp. 1775-1796, December 1966.

[17] P. R. Chevillat and E. Eleftheriou, "Decoding of trellis-encoded signals in the presence of intersymbol interference and noise", *IEEE Trans. on Commun.*, vol. 37, no. 7, pp. 669-676, July 1989.

[18] J. S. Chow, J. C. Tu, and J. M. Cioffi, "A discrete multitone transceiver system for HDSL applications", *IEEE J. Select. Areas Commun.*, vol. 9, no. 6, pp. 895-908, August 1991.

[19] J. S. Chow, J. C. Tu, and J. M. Cioffi, "Performance evaluation of a multichannel transceiver system for ADSL and VHDSL services", *IEEE J. Select. Areas Commun.*, vol. 9, no. 6, pp. 909-919, August 1991.

[20] H. Y. Chung, "Unequal error protection of data using trellis-coded modulation", in *GLOBECOM '92. IEEE Global Telecommunications Conference.*, Orlando, FL, USA, December 1992, vol. 3, pp. 1759-1763.

[21] L. J. Cimini, Jr., "Analysis and simulation of a digital mobile channel using orthogonal frequency division multiplexing", *IEEE Trans. on Commun.*, vol. COM-33, no. 7, pp. 665-675, July 1985.

[22] J. M. Cioffi, G. P. Dudevoir, M. V. Eyuboğlu, and G. D. Forney, "MMSE decision-feedback equalizers and coding - Part I: General results", Preprint, 1992.

[23] Consultative Committee for Space Data Systems, *Recommendations for space data systems standards: Telemetry channel coding*, Blue Book, CCITT, 1984.

[24] T. M. Cover, "Broadcast channels", *IEEE Trans. Inform. Theory*, vol. IT-18, pp. 2-14, January 1972.

[25] T. M. Cover and J. A. Thomas, *Elements of Information Theory*, Wiley-Interscience, New York, NY, 1991.

[26] P. G. M. de Bot, "Multiresolution transmission over the AWGN channel", Memo RWR-546-PDB-92057-pdb, Philips Research Laboratories, June 1992.

[27] D. Divsalar and M. K. Simon, "Trellis coded modulation for 4800-9600 bps transmission over a fading mobile satellite channel", *IEEE J. Select. Areas Commun.*, vol. SAC-5, no. 2, pp. 162-175, February 1987.

[28] A. Duel-Hallen and C. Heegard, "Delayed decision-feedback sequence estimation", *IEEE Trans. on Commun.*, vol. COM-37, pp. 428-436, May 1989.

[29] C. Eilers, G. Sgrignoli, and D. Felland, "A 70-mile long-distance experimental broadcast of digital spectrum compatible high definition television", *IEEE Trans. Broadcasting*, vol. 38, pp. 202-218, December 1992.

[30] C. Eilers and P. Fockens, "The DSC-HDTV interference rejection system", *IEEE Trans. Consum. Electron.*, vol. 38, pp. 101-107, June 1992.

[31] A. El Gamal and T. M. Cover, "The capacity region of a class of broadcast channels", *IEEE Trans. Inform. Theory*, vol. IT-25, pp. 166-169, 1979.

[32] M. V. Eyuboğlu, "Detection of coded modulation signals on linear, severely distorted channels using decision-feedback noise prediction with interleaving", *IEEE Trans. on Commun.*, vol. 36, no. 1, pp. 13-20, January 1988.

[33] M. V. Eyuboğlu and G. D. Forney, "Trellis precoding: combined coding, precoding and shaping for intersymbol interference channels", *IEEE Trans. Inform. Theory*, vol. 38, no. 2, pp. 301-314, March 1992.

[34] M. V. Eyuboğlu and S. U. H. Qureshi, "Reduced state sequence estimation with set partitioning and decision feedback", *IEEE Trans. on Commun.*, vol. 36, no. 1, pp. 13-20, January 1988.

[35] M. V. Eyuboğlu and S. U. H. Qureshi, "Reduced state sequence estimation for coded modulation on intersymbol interference channels", *IEEE J. Select. Areas Commun.*, vol. 7, no. 6, pp. 989-995, August 1989.

[36] D. D. Falconer and F. R. Magee, "Adaptive channel memory truncation for maximum likelihood sequence estimation", *Bell Syst. Techn. J.*, vol. 52, pp. 1541-1562, November 1973.

[37] K. Fazel and J. J. Lhuillier, "Application of unequal error protection codes on combined source-channel coding of images", in *IEEE International Conference on Communications ICC '90*, Atlanta, GA, USA, April 1990, vol. 3, pp. 898-903.

[38] G. D. Forney, *Concatenated Codes*, MIT Press, 1966.

[39] G. D. Forney, "Maximum likelihood sequence detection in the presence of intersymbol interference", *IEEE Trans. Inform. Theory*, vol. 18, no. 3, pp. 363-378, May 1972.

[40] G. D. Forney, "Coset codes - part I: Introduction and geometrical classification", *IEEE Trans. Inform. Theory*, vol. 34, no. 5, pp. 1123-1151, September 1988.

[41] G. D. Forney, "Coset codes - part II: Binary lattices and related codes", *IEEE Trans. Inform. Theory*, vol. 34, no. 5, pp. 1152-1187, September 1988.

[42] G. D. Forney, "Trellises and lattices: Theory of high-rate data transmission and quantization - course notes", Course notes, M.I.T, 1991.

[43] G. D. Forney, R. G. Gallager, G. R. Lang, F. M. Longstaff, and S. U. Qureshi, "Efficient modulation for band-limited channels", *IEEE J. Select. Areas Commun.*, vol. SAC-2, no. 5, pp. 632-647, September 1984.

[44] G. D. Forney and M. V. Eyuboğlu, "Combined equalization and coding using precoding", *IEEE Commun. Mag.*, vol. 29, no. 12, pp. 25-34, December 1991.

[45] J. G. C. Clark and J. B. Cain, *Error-Correction Coding for Digital Communications*, Plenum Press, 1981.

[46] R. G. Gallager, "Capacity and coding for degraded broadcast channels", *Problemy Peredachi Informaccii*, vol. 10, no. 3, pp. 3-14, 1974.

[47] R. G. Gallager, *Information Theory and Reliable Communication*, John Wiley and Sons, Inc., 1968.

[48] General Instrument Corp., *DigiCipher HDTV - System Description*, American Television Alliance, August 1991.

[49] S. Haykin, *Adaptive Filter Theory*, Prentice Hall, 1986.

[50] C. Heegard, S. A. Lery, and W. H. Paik, "Practical coding for QAM transmission of HDTV", *IEEE J. Select. Areas Commun.*, vol. 11, no. 1, pp. 111-118, January 1993.

[51] J. F. Helard and B. Le Floch, "Trellis coded orthogonal frequency division multiplexing for digital video transmission", in *IEEE Global Telecommunications Conference. GLOBECOM '91*, Phoenix, Ariz., USA, December 1991, vol. 2, pp. 785-791.

[52] B. Hirosaki, "An orthogonally multiplexed QAM system using the Discrete Fourier Transform", *IEEE Trans. on Commun.*, vol. COM-29, no. 7, pp. 982-989, July 1981.

[53] B. Hirosaki, S. Hasegawa, and A. Sabato, "Advanced groupband data modem using orthogonally multiplexed QAM technique", *IEEE Trans. on Commun.*, vol. COM-34, no. 6, pp. 587-592, June 1986.

[54] G. Hufford, "A characterization of the multipath in the HDTV channel", *IEEE Trans. Broadcasting*, vol. 38, no. 4, pp. 252-255, December 1992.

[55] N. S. Jayant and P. Noll, *Digital Coding of Waveforms*, Prentice-Hall, 1984.

[56] M. C. Jeruchim, "Techniques for estimating the bit error rate in the simulation of digital communication systems", *IEEE J. Select. Areas Commun.*, vol. 2, no. 1, pp. 153-170, January 1984.

[57] I. Kalet, "The multitone channel", *IEEE Trans. on Commun.*, vol. 37, no. 2, pp. 119-124, February 1989.

[58] S. Kasturia, J. Aslanis, and J. M. Cioffi, "Vector coding for partial-response channels", *IEEE Trans. Inform. Theory*, vol. 36, no. 4, pp. 742-762, July 1990.

[59] S. Kasturia and J. M. Cioffi, "Precoding for block signaling and shaped signal sets", in *Proceedings ICC'89*, Boston, Mass., USA, June 1989, vol. 2, pp. 1086-1090.

[60] B. Le Floch, R. Halbert-Lassalle, and D. Castelain, "Digital sound broadcasting to mobile receivers", *IEEE Trans. Consum. Electron.*, vol. 35, no. 3, pp. 493-503, August 1989.

[61] J. Lechleider, "The feasibility of using adaptive transmitters to suppress crosstalk", in *Proceedings ICC'89*, Boston, Mass., USA, June 1989, vol. 1, pp. 548-551.

[62] E. A. Lee and D. G. Messerschmitt, *Digital Communication*, Kluwer Academic Publishers, Boston, MA, 1988.

[63] E. A. Lee and D. G. Messerschmitt, *Digital Communication*, (second edition) Kluwer Academic Publishers, 1994.

[64] W. U. Lee and F. S. Hill, "A maximum likelihood sequence estimator with decision-feedback equalization", *IEEE Trans. on Commun.*, vol. 25, no. 9, pp. 971-979, 1977.

[65] G. Long, F. Ling, and J. G. Proakis, "The LMS algorithm with delayed coefficient adaptation", *IEEE Trans. on Acoust., Speech and Sig. Proc.*, vol. 37, no. 9, pp. 1397-1405, 1989.

[66] Mass. Inst. of Tech., *Channel-Compatible DigiCipher HDTV System*, American Television Alliance, April 1992.

[67] H. Miyakawa and H. Harashima, "A method of code conversion for a digital communication channel with intersymbol interference", *Trans. Inst. Electron. Commun. Eng. Japan*, vol. 52-A, pp. 272-273, June 1969.

[68] A. N. Netravali and B. G. Haskell, *Digital Pictures: Representation and Compression*, Plenum Press, New York, NY, 1988.

[69] J. J. Nicolas and J. S. Lim, "Equalization and interference rejection for the terrestrial broadcast of digital HDTV", in *Proceedings ICASSP 93*, Minneapolis, Min., USA, April 1993.

[70] J. J. Nicolas and J. S. Lim, "On the performance of multicarrier modulation in a broadcast multipath environment", in *Proceedings ICASSP 94*, Adelaide, Australia, April 1994.

[71] R. O'Connor, "Understanding television's grade A and grade B service contours", *IEEE Trans. on Broadcasting*, vol. 14, no. 4, December 1968.

[72] W. Paik, "DigiCipher - All digital, channel compatible, HDTV broadcast system", *IEEE Trans. on Broadcasting*, vol. 36, no. 4, December 1990.

[73] W. K. Pratt, *Digital Image Processing*, John Wiley & Sor ;, Inc., New York, NY, 1992.

[74] R. Price, "Nonlinearly feedback equalized PAM versus capacity for noisy filter channels", in *Proceedings ICC'72*, Philadelphia, Penn. , USA, June 1972, vol. 1, pp. 22.12-22.17.

[75] J. G. Proakis, *Digital Communications*, McGraw-Hill Book Company, New York, NY, 1989.

[76] S. U. H. Qureshi, "Adaptive equalization", *Proceedings of the IEEE*, vol. 73, no. 9, pp. 1349-1387, September 1985.

[77] K. Ramchandran, A. Ortega, K. M. Uz, and M. Vetterli, "Multiresolution broadcast for digital HDTV using joint source/channel coding", *IEEE J. Select. Areas Commun.*, vol. 11, no. 1, pp. 6-23, January 1993.

[78] M. Rouanne, "An algorithm for computing the distance spectrum of trellis codes", *IEEE J. Select. Areas Commun.*, vol. 7, no. 6, pp. 929-940, August 1989.

[79] A. Ruiz, J. Cioffi, and S. Kasturia, "Discrete multiple tone modulation with coset coding for the spectrally shaped channel", *IEEE Trans. on Commun.*, vol. 40, no. 6, pp. 1012-1029, Jun. 1992.

[80] B. R. Saltzberg, "Performance of an efficient parallel data transmission system", *IEEE Trans. on Commun. Tech.*, vol. 15, pp. 805-811, December 1967.

[81] C. Scarpa, "A recursive NTSC canceler to reduce co-channel interference into HDTV broadcasts", *IEEE Trans. Consum. Electron.*, vol. 39, no. 3, pp. 696-703, August 1993.

[82] W. F. Schreiber, "Considerations in the design of HDTV systems for terrestrial broadcasting", in *Electronic Imaging '90*, Boston, Mass., October 1990.

[83] W. F. Schreiber and A. B. Lippman, "Single-channel HDTV systems, compatible and non-compatible", in *Visual Communications and Image Processing '88*, Cambridge, Mass., 1988, SPIE - The International Society for Optical Engineering, vol. 1001, pp. 787-795.

[84] C. Shannon and W. Weaver, *The Mathematical Theory of Communication*, University of Illinois Press, Urbana, Illinois, 1963.

[85] M. Tomlinson, "New automatic equalizer employing modulo arithmetic", *Electron. Lett.*, vol. 7, no. 7, pp. 138-139, March 1971.

[86] G. Ungerboeck, "Channel coding with multi-level/phase signals", *IEEE Trans. Inform. Theory*, vol. 28, pp. 55-67, January 1982.

[87] G. Ungerboeck, "Trellis-coded modulation with redundant signal sets, part I and II", *IEEE Commun. Mag.*, vol. 25, no. 3, pp. 5-21, February 1987.

[88] K. M. Uz, K. Ramchandran, and M. Vetterli, "Multiresolution source and channel coding for digital broadcast of HDTV", in *Proc. 4th International Workshop on HDTV, Torino, Italy*, September 1991.

[89] A. J. Viterbi and J. K. Omura, *Principles of Digital Communication and Coding*, McGraw-Hill, New York, NY, 1979.

[90] L. F. Wei, "Trellis-coded modulation with multidimensional constellations", *IEEE Trans. Inform. Theory*, vol. 33, no. 4, pp. 483-501, July 1987.

[91] L. F. Wei, "Coded modulation with unequal error protection", *IEEE Trans. on Commun.*, vol. 41, no. 10, pp. 1439-1449, October 1993.

[92] S. B. Weinstein and P. M. Ebert, "Data transmission by frequency-division multiplexing using the discrete Fourier transform", *IEEE Trans. on Commun.*, vol. 19, no. 5, pp. 628-634, October 1971.

[93] K. Wesolowski, "An efficient DFE and ML suboptimum receiver for data transmission over dispersive channels uinsg two-dimentional signal constellations", *IEEE Trans. on Commun.*, vol. 19, no. 3, pp. 336-339, March 1987.

[94] K. Yao, "On the minimum average probability of error expression for binary pulse communication systems with intersymbol interference", *IEEE Trans. Inform. Theory*, vol. 17, pp. 528-531, May 1971.

[95] Y. Yasuda, K. Kashiki, and Y. Hirata, "High-rate punctured convolutional codes for soft decision Viterbi decoding", *IEEE Trans. on Commun.*, vol. 32, pp. 315-319, Mar 1984.

[96] E. Zehavi and J. K. Wolf, "On the performance evaluation of trellis codes", *IEEE Trans. Inform. Theory*, vol. 33, no. 2, pp. 196-202, March 1987.

[97] Zenith and AT&T, *Digital Spectrum Compatible Television - System Description*, September 1991.

[98] N. Zervos and I. Kalet, "Optimized decision feedback equalization versus optimized orthogonal frequency division multiplexing for high-speed data transmission over the local cable network", in *IEEE Int. Conf. Commun. ICC'89*, 1989.

[99] K. Zhou, J. Proakis, and F. Ling, "Decision-feedback equalization of time-dispersive channels with coded modulation", *IEEE Trans. on Commun.*, vol. 38, no. 1, pp. 18–24, January 1990.